Deliverable 7.2: UPDATED STATE-OF-THE-ART ON THM BEHAVIOUR OF I) BUFFER CLAY MATERIALS AND OF II) HOST CLAY FORMATIONS

Work Package 7

The project leading to this application has received funding from the European Union's Horizon 2020 research and innovation programme under grant agreement No 847593.

Document information

Project Acronym	**EURAD**
Project Title	**European Joint Programme on Radioactive Waste Management**
Project Type	**European Joint Programme (EJP)**
EC grant agreement No.	**847593**
Project starting / end date	**1st June 2019 – 30 May 2024**
Work Package No.	**7**
Work Package Title	**Influence of Temperature on Clay-based Material Behaviour**
Work Package Acronym	**HITEC**
Deliverable No.	**7.2**
Deliverable Title	**Updated State-Of-The-Art on THM Behaviour of I) Buffer Clay Materials and of II) Host Clay Materials**
Lead Beneficiary	**CIEMAT**
Contractual Delivery Date	**May 2024**
Actual Delivery Date	**June 2024**
Type	**Report**
Dissemination level	**Public**
Authors	**María Victoria Villar (CIEMAT), Pierre Besuelle (UGrenoble), Katerina Cernochova CTU), Frédéric Collin (ULiege), Jaime Cuevas (UAM), Robert Cuss (BGS), Christophe de Lesquen (ANDRA), Arnaud Dizier (EURIDICE), Ginger El Tabbal (EDF), Antonio Gens (UPC), Natalia Gimeno (CIEMAT), Caroline Graham (BGS), Dragan Grgic (ULorraine), Jon Harrington (BGS), Christophe Imbert (CEA), Vlastislav Kašpar (ÚJV), Stephan Kaufhold (BGR), Olivier Leupin (NAGRA), Séverine Levasseur (ONDRAF/ NIRAS), David Mašín (CU), Jan Najser (CU), Asta Narkūnienė (LEI), Markus Ollin (VTT), Heini Reijonen (GTK), Šárka Šachlová (ÚJV), Sergey Sayenko (KIPT), Eric Simo (BGE), Daniel Svensson (SKB), Jiri Svoboda (CTU), Alexandru-Bogdan Tatomir (BGE), Gianni Vettese (UH), Janne Yliharju (JYU), Borys Zoblenko (SIIGNASU)**

To be cited as:

Villar, M.V.; Besuelle, P.; Cernochova, K.; Collin, F.; Cuevas, J.; Cuss, R.; de Lesquen, C.; Dizier, A.; El Tabbal, G.; Gens, A.; Gimeno, N.; Graham, C.; Grgic, D.; Harrington, J.; Imbert, C.; Kašpar, V.; Kaufhold, S.; Leupin, O.; Levasseur, S.; Mašín, D.; Najser, J.; Narkūnienė, A.; Ollin, M.; Reijonen, H.; Šachlová, Š.; Sayenko, S.; Simo, E.; Svensson, D.; Svoboda, J.; Tatomir, A.; Vettese, G.; Yliharju, J.; Zoblenko, B. (2023). D7.2 HITEC. Updated State-of-the-Art on THM behaviour of i)

Buffer clay materials and of ii) Host clay formations. Deliverable D7.2 HITEC. EURAD Project, Horizon 2020 No 847593. 129 pp.

Disclaimer

Acknowledgement

This document is a deliverable of the European Joint Programme on Radioactive Waste Management (EURAD). EURAD has received funding from the European Union's Horizon 2020 research and innovation programme under grant agreement No 847593.

Status of deliverable		
	By	**Date**
Delivered (Lead Beneficiary)	CIEMAT	10/05 2024
Verified (WP Leader)	VTT	10/06/2024
Reviewed (Reviewers)	Patrik Sellin (SKB)	16/05/2024
Reviewed (Reviewers)	Gilles Armand (ANDRA)	10/06/2024
Approved (PMO)	Bharti Reddy (RWM)	12/06/2024
Submitted to EC	Andra (Coordinator)	12/06/2024

Executive summary

Most safety cases for radioactive waste disposal concepts that involve clay consider a temperature limit of 100°C in the buffer and 90°C in the clay host rock. Being able to tolerate higher temperature would have significant advantages for the repository optimisation. To reduce conceptual and modelling uncertainties associated to this higher temperature, EURAD-HITEC aimed at determining the influence of temperatures above those limits on buffer and clay host rock properties, trying to establish if the buffer safety functions are unacceptably impaired, as well as the possible extent of elevated temperature damage in the near and far field of clay host rock formations and the consequences of any such damage.

Three clay formations considered to host radioactive waste repositories in Europe were analysed in the EURAD-HITEC Project: the Boom Clay, the Callovo-Oxfordian claystone and the Opalinus Clay. As buffer material, Wyoming-type bentonites and predominantly-divalent bentonites were studied. An overview of what is known about these clay materials is given in this report, including the effect of temperature on the materials' behaviour. As well, large-scale tests relevant in terms of the temperatures involved are described, including those that have been used as benchmark exercises during the Project. Experimental and modelling activities carried out in the framework of the project concerning these materials are synthesized herein.

The study of the effect of temperature on bentonite properties was tackled both by analysing the change of properties of preheated material and by determining the hydro-mechanical properties of the bentonite at high temperatures. To cover the first instance, bentonite was heated at 150°C in dry and wet conditions for different periods of time up to 2 years. Clay mineralogy was remarkably preserved. The slight changes observed in other properties were opposite depending on the heating conditions: if evaporation was allowed, decreases in cation exchange capacity, specific surface area, sorption coefficients and swelling pressure (only in high-density samples) were observed. It is presumed that the changes were caused not by the temperature itself, but by the strong drying induced by the elevated temperature. Bentonite was also subjected to hydration under thermal gradient in field and laboratory tests and then analysed. No structural modifications of the smectite were observed, but dissolution and precipitation of species occurred and were conditioned by the kind of bentonite and hydration water. These processes were accompanied by modification of the exchangeable cation complex.

The determination of hydro-mechanical properties of expansive clay at elevated temperatures is challenging, because of the experimental and interpretation issues. The results were not conclusive concerning the impact of high temperature on swelling pressure, although in most cases a reduced swelling pressure was obtained when temperature increased, and the impact was more significant for the higher dry densities. The results may be affected by the experimental protocols, the use of bentonite or purified smectite, and the exchangeable cations. In any case, even at the highest temperatures the bentonite had the ability to fill voids and was able to develop large swelling pressures at high densities.

Three thermo-hydro-mechanical models were developed or upgraded during the project to include thermal phenomena and dependencies, and they were applied to the simulation of new laboratory thermo-hydraulic tests in cells.

The laboratory tests with host rock materials analysed two aspects: the impact of temperature on the short- and long-term behaviour of the clay host rock and the self-sealing processes. In the first case the focus was on the thermal pressurisation and the risk of damage if the effective vertical stress becomes tensile. Important hydro-mechanical couplings between peak pore water pressure, temperature, permeability and confining stress were identified. The triaxial tests showed that the thermal loading rates applied and the particular stress conditions during the tests significantly condition the behaviour observed (formation of microcracks, strength reduction). Nevertheless, the results confirmed that the

claystone keeps its good mechanical and retention properties, even when heated at high temperature (up to 100°C). Provided that the clay content of the samples was high enough, self-sealing was an efficient mechanism whatever the experimental conditions, although temperature may have a slight delaying effect on the process.

The benchmarks selected for the modelling activities comprised the modelling of generic cases of a high-level waste repository, two large-scale in situ tests experiments and triaxial laboratory tests. The benchmarks selected were the PRACLAY and ALC1605 heating tests, performed in the HADES (Belgium) and Bure (France) underground research laboratories, respectively. Consistent results were obtained on the generic cases by the different codes and teams, which increases the confidence one can have in these poro-elastic models and shows the robustness of the modelling approach used to design the repositories. Some models were improved to reproduce in-situ observations and predict the development of the excavated-damaged zone. The modelling of laboratory experiments showed the importance of a good understanding of the tests setup and of the boundary conditions. For both in-situ experiments, the teams successfully managed to reproduce the anisotropic response of the clay host rocks to excavation and heating. The evolutions of temperature and pore pressure were well modelled in the far-field with a poro-elastic approach, but more advanced models are needed to take into account the processes occurring around the tunnels (e.g., modification of hydraulic properties within the EDZ, creep).

Acronyms and symbols

ORGANIZATIONS

ANDRA	Agence Nationale pour la Gestion des Déchets Radioactifs (France)
BGE	Bundesgesellschaft für Endlagerung (Germany)
BGR	Bundesanstalt für Geowissenschaften und Rohstoffe (Germany)
BGS	British Geological Survey (United Kingdom)
CEA	Commisariat à l'Energie Atomique (France)
CIEMAT	Centro de Investigaciones Energéticas, Medioambientales y Tecnológicas (Spain)
CTU	Czech Technical University (Czech Republic)
CU	Charles University (Czech Republic)
EC	European Commission
EDF	Electricité de France
ENRESA	Empresa Nacional de Residuos Radiactivos (Spain)
EURIDICE	European Underground Research Infrastructure for Disposal of nuclear waste in a Clay Environment (Belgium)
GRS	Gesellschaft für Anlagen und Reaktorsicherheit (Germany)
GTK	Geological Survey of Finland
SIIG NASU	Institute of Environmental Geochemistry of National Academy of Sciences of Ukrainia (Ukrainia)
JYU	University of Jyväskylä (Finland)
KIPT	Kharkov Institute of Physics and Technology (Ukrainia)
LEI	Lithuanian Energy Institute (Lithuania)
NAGRA	Nationale Genossenschaft für die Lagerung radioaktiver Abfälle (Switzerland)
NWMO	Nuclear Waste Management Organization (United Kingdom)
ONDRAF/NIRAS	Organisme national des déchets radioactifs et des matières fissiles enrichies / Nationale instelling voor radioactief afval en verrijkte Splijtstoffen (Belgium)
POSIVA	Expert organisation responsible for the final disposal of spent nuclear fuel of the owners (Finland)
RWM	Radioactive Waste Management (United Kingdom)
SCK•CEN	Studiecentrum voor Kernenergie / Centre d'Étude de l'énergie Nucléaire (Belgium)
SKB	Svensk Kärnbränslehantering (Sweden)
SÚRAO	Správa Úložišť Radioaktivních Odpadú (Czech Republic)
UGrenoble	Université de Grenoble (France)
UH	University of Helsinki (Finland)
ÚJV	ÚJV Řež (Czech Republic)
ULiege	Université de Liège (Belgium)
ULorraine	Université de Lorraine (France)
UPC	Universitat Politècnica de Catalunya (Spain)
VTT	Technical Research Centre of Finland (Finland)

PROJECTS/FACILITIES

ABM	Alternative Buffer Materials
ALC	Alvéoles HA et chemisage – HLW cell and lining

CRQ	Comportement THM Représentatif d'un Quartier HA – Representative THM Behaviour of a HLW disposal section
EB	Engineered Barrier Emplacement
ESDRED	Engineering Studies and Demonstration of Repository Designs
FE	Full-scale Emplacement Experiment
FEBEX	Full-scale Engineered Barriers Experiment
HADES	High-Activity Disposal Experimental Site
HE	Heating Experiment Series
LOT	Long term test of buffer material
LUCOEX	Large Underground Concept Experiments
MHM URL	Meuse/Haute-Marne Underground Research Laboratory
TED	experimentation T(h)Ermique Deux – Thermal Experiment #2
TER	experimentation T(h)ERmique - (T(h)ERmal experiment
TFW	
TIMODAZ	Thermal Impact on the Damaged Zone around a Radioactive Waste Disposal in Clay Host Rocks

SPECIFIC VOCABULARY

µCT	Microcomputerized Tomography
CD	Consolidated-Drained
COx	Callovo-Oxfordian Clay
CPM	Continuous Porous Media
CRZ	Containment-providing rock zone
CU	Consolidated Undrained Test
DFN	Discrete Fracture Network
DGR	Deep Geological Repository
DZ	Damaged zone
EBS	Engineered Barrier System
EDZ	Excavation Disturbed Zone
GBM	Granulated Bentonite Mixture
HHGW	High Heat Generating Wastes
HLW	High-Level Waste
HLW-LL	High-Level Waste, Long Life
ILW	Intermediate-Level Waste
ILW-LL	Intermediate Level Waste, Long Life
L/ILW	Low/Intermediate Level Waste
NCL	Normal Compression Line
OCR	Overconsolidation Ratio
OPA	Opalinus Clay
PA	Performance Assessment
RD&D	Research, Development and Demonstration
SF/SNF	Spent (Nuclear) Fuel
THM	Thermo-Hydro-Mechanical
THMC	Thermo-Hydro-Mechanical and Chemical

UCS	Uniaxial Compressive Strength
URF	Underground Research Facility
URL	Underground Research Laboratory
WP	Work Package
WRC	Water Retention Curve
ZFC	Connected Fractured Zone
ZFD	Discrete Fractured Zone

SYMBOLS

B	hardening parameter
c, c'	cohesion, effective cohesion
c_p	solid phase specific heat
C_α	secondary consolidation coefficient
C_p	volumetric heat capacity
C_s	swelling index
e	void ratio
E, E'	Young modulus, effective Young modulus
$E_\perp$, $E_{//}$	Young modulus perpendicular and parallel to bedding
G, G_v	shear modulus
k_i k_{iv} k_{ih}	intrinsic permeability, vertical, horizontal
k_w	Hydraulic conductivity (saturated water permeability)
M	critical state parameter
m, S	fitting parameters (as defined by Hoek & Brown)
n	porosity
N	parameter of the Cam-clay model defining the position of normal compression line
p p^m p^M	mean effective stress, microstructural, macrostructural
p_r p_e	reference stress, Hvorslev equivalent pressure
P_s, P_c	swelling pressure, confining pressure
P_w	pore water pressure
S_r S_{rl}	degree of saturation, liquid residual degree of saturation
T	temperature
w	water content
α α_s α_u	linear thermal expansion coefficient, of solid, undrained
ε ε^m ε^M	strain, micro, macro
ϕ'	effective friction angle
φ_c	critical state friction angle
κ κ^*	elastic compressibility, parameter controlling the slope of the isotropic unloading line
λ λ_h λ_v λ_0	thermal conductivity, horizontal, vertical, initial
λ_1 λ_2	parameters of the water retention curve
λ^*	parameter of the Cam-clay model defining the slope of normal compression line
Λ	thermal pressurisation coefficient

ν $\nu_{//}$ $\nu_{\perp}$	Poisson's ratio, paralel, perpendicular to bedding
ν' $\nu'_{//}$ $\nu'_{\perp}$	Effective Poisson's ratio, paralel, perpendicular to bedding
ρ_d ρ_s	dry density, solid density
σ, σ^m σ^M	stress, micro, macro
σ_1, σ_3	maximum and minimum principal stress at failure
σ'_3	
σ_H/σ_h	maximum and minimum horizontal stresses
σ_v	vertical stress
σ_c	uniaxial compressive strength of the intact rock
τ	shear stress
ψ	dilation angle

Table of contents

1 Introduction 12
2 WMO conceptualisation 13
2.1 ANDRA (France) 15
2.2 BGE (Germany) 16
2.3 ENRESA (Spain) 17
2.4 NAGRA (Switzerland) 18
2.5 ONDRAF/NIRAS (Belgium) 18
2.6 SKB (Sweden) and POSIVA (Finland) 20
2.7 RWM (United Kingdom) 20
2.8 SÚRAO (Czech Republic) 21
3 Buffer materials 21
3.1 Materials used in HITEC 22
3.1.1 Wyoming-type bentonite 24
3.1.2 FEBEX bentonite 24
3.1.3 BCV bentonite 25
3.1.4 Other bentonites 26
3.2 Relevant large-scale tests 27
3.2.1 Alternative Buffer Materials (ABM, Äspö) 27
3.2.2 Long term test of buffer material (LOT, Äspö) 30
3.2.3 Heating Experiment (HE-E, Mont Terri) 31
3.2.4 Full-Scale Emplacement experiment (FE, Mont Terri) 32
3.2.5 Ophelie mock-up 33
3.3 Effect of high temperature on buffer 33
3.3.1 Preheated material 36
3.3.2 Determination of properties at high temperature 46
3.3.3 Small-scale simulation experiments 55
3.3.4 Summary and conclusions 57
3.4 State of THM models' development 59
4 Clay host rock 61
4.1 Materials considered in HITEC: properties and temperature impact 62
4.1.1 Boom Clay 64
4.1.2 Callovo-Oxfordian claystone 69
4.1.3 Opalinus clay 74

4.2 Relevant large-scale tests 77
4.2.1 Large-scale in situ PRACLAY heater test 77
4.2.2 ALC 1605 HLW cell test 78
4.3 Effect of temperature on clay host rocks 81
4.3.1 Background 81
4.3.2 Progress made during HITEC 86
4.4 Modelling tools and approaches 93
4.4.1 Callovo-Oxfordian Clay 93
4.4.2 Boom Clay 94
4.4.3 Opalinus Clay 96
4.4.4 Modelling work done during HITEC 97
5 Conclusions 102
6 References 104

1 Introduction

The WP7 "Influence of Temperature on Clay-based Material Behaviour" of the EURAD Project aimed to develop and document improved thermo-hydro-mechanical (THM) understanding of clay-based materials (host rocks and buffers) exposed at high temperatures or having experienced high temperature transients for extended durations. The WP's raison d'être was to evaluate whether or not elevated temperature limits (up to 150°C for the clay buffer and ~90°C for the host rock) are feasible for a variety of geological disposal concepts for high heat generating wastes (HHGW). For the disposal of HHGW it is important to understand the consequences of the heat produced on the properties and long-term performance of the natural and engineered clay barriers. Most safety cases for disposal concepts that involve clay currently consider a temperature limit of 100°C. Being able to tolerate higher temperature, whilst still ensuring an appropriate performance, would have significant advantages (e.g. shorter above-ground cooling times, more efficient packaging, fewer disposal containers, fewer transport operations, smaller facility footprints, etc.). Consequently, HITEC is a step toward optimization of the architecture of the deep geological disposal. HITEC looked at bentonite buffers and determined the temperature influence on buffer physical properties, swelling pressure, hydraulic conductivity, water adsorption, mineralogy and geochemistry trying to establish if the buffer safety functions are unacceptably impaired. The WP also studied the possible extent of elevated temperature damage in the near and far field of clay host rock formations (e.g. from over-pressurisation) and indicated the likely consequences of any such damage.

Previous and ongoing national and Community-supported research programmes led to detailed understanding of the various key thermo-hydro-mechanical and chemical (THM-C) processes taking place in the buffer material up to 100°C (e.g. FEBEX, PROTOTYPE, BACCHUS, PEBS) and in host claystone (e.g. SELFRAC, TIMODAZ, NF-PRO). Namely, within the PEBS project (Long-term Performance of the Engineered Barrier System, 7th European FP 2007-2011) the conclusion was reached that the characterisation of bentonite performance and THM properties below 100°C was largely established (Johnson et al. 2014). Overall, the observed effects of temperature on the hydro-mechanical properties (decrease of swelling pressure, increase of permeability, decrease of water retention capacity) can be qualitatively explained by considering the transfer of high-density interlayer water to the macropores that is triggered by the increase in temperature. The different behaviour of smectites exchanged with monovalent versus divalent ions can be explained by taking into account the different interlayer/diffuse-double-layer water ratio in both. However, the literature survey performed during the PEBS project confirmed that the information regarding bentonite at higher temperatures was less abundant. Lack of information was identified in particular:

- for granular bentonite material (manufactured bentonite as grains or pellets);
- with respect to the water retention curve;
- concerning the effect of degree of saturation on thermal conductivity (low thermal conductivity would lead to higher temperature) and water permeability; and
- regarding the effect of temperature on swelling capacity depending on exchangeable cations.

The TIMODAZ project analysed the evolution of the excavation damaged zone (EDZ) during the thermal transient in the context of a geological repository for heat-emitting waste in plastic and indurated clay host rocks. The project focused on the possible additional damage created by the thermal load. The knowledge gathered during the project indicated that an increase in temperature due to the presence of heat-emitting wastes will induce strong and anisotropic THM coupled responses within the clay (Yu et al. 2010). The thermal expansion of pore water and the thermal-induced decrease of clay strength may pose a risk of additional mechanical damage. However, no evidence was found throughout the TIMODAZ experimental programme showing temperature-induced additional opening of fractures or

a significant permeability increase of the EDZ. The project also concluded that, with the current knowledge, the capacity of the repository host rock to perform its intended role as a barrier and to maintain the long-term safety functions of the system will be still preserved in spite of the combined effect of the inevitable EDZ and the thermal output from the waste (Yu et al. 2010). All the favourable properties of the clay host rock that guarantee the effectiveness of the safety functions of the repository system are expected to be maintained after the heating-cooling cycle. Those basic assumptions used in performance assessment calculations still remain valid when considering the thermal impact on the evolution of the EDZ around a radioactive waste repository in clay host rock.

In the following sections syntheses of the state of knowledge on the THM behaviour of different buffer materials and clay host rocks at different temperatures are presented separately. In this sense, this document is an update of the State of the Art report by Villar et al. (2020). The progress made during HITEC has also been included. For a better contextualization of this information, the national geological waste disposal concepts of the participant organisations are initially summarised. The characteristics of the clay materials analysed during the project, bentonites and host rocks, are described and their thermal, hydraulic and mechanical properties are summarised. Experimental procedures, processes, parameters and models available at low or high temperature for the various buffer materials and host rocks are summarised. Large-scale in situ experiments, some of which have been modelled during the project, are briefly described.

2 WMO conceptualisation

The following sections give background information on different national concepts for disposal of HHGW (e.g. spent fuel, SF and/or high-level waste, HLW), identifying the role assigned to each component of the multiple barrier system and the way in which temperature may affect their performance.

There are several common features to all concepts. Indeed, radioactive substances will be contained within several overlapping protective barriers so that no deficiency in one barrier and no predictable geological or other change will endanger the isolation. The barriers include the physical state of the fuel, the disposal canister, the bentonite-based buffer, the backfilling of the tunnels and the surrounding rock (Figure 2-1) and other sealing elements such as plugs.

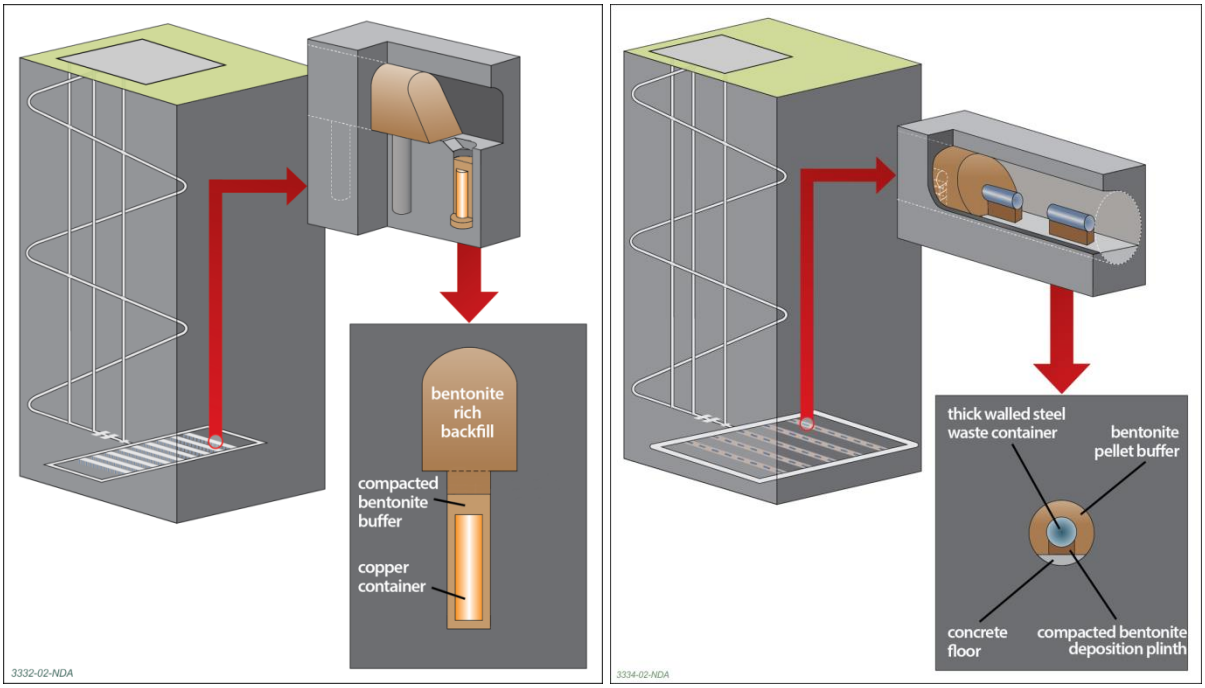

Figure 2-1. Illustrative designs for a higher strength rock (based upon KBS-3V, left) and lower strength sedimentary rock type (based upon NAGRA concept, right) after RWM (2016)

Table 2-1 summarises some characteristics of the different national concepts presented. Their stage of development is diverse, and whereas some have a selected lithology and a defined architecture, others are still considering desgins for different potential host rocks. There are two concepts which do not consider the use of a clay buffer between the canister and the host rock, ANDRA and ONDRAF/NIRAS, both designed for clay host rock. In contrast, NAGRA, whose concept is also designed for clay host rock, does consider the use of a clay buffer around the canisters. The concepts of the rest of agencies are based on crystalline host rock (except for ENRESA). Among them only ENRESA and SÚRAO use bentonites with a predominance of divalent cations in the interlayer of the smectite, whereas the others consider the use of sodium bentonite (Wyoming-type).

Regarding temperature constraints, all the concepts presented assume that the temperature at any part of the buffer or host rock should be below 100°C, except for NAGRA, which allows a temperature of 130°C at the canister/buffer interface. Predictions of the thermal evolution of the repository are also sketched in the following sections. They are based in modelling exercises of generic repositories, and have been used to optimise the repository design in order to reduce its thermal impact.

Table 2-1. Summary of characteristics of repository concepts

WMO	CONCEPT	CLAY BUFFER TYPE	THERMAL ASPECTS
ANDRA	Cigéo	No clay buffer	T<90°C in COx No formation damage
BGE	ANSICHT	Sodium bentonite	Preliminary cask surface T <100°C
ENRESA	2004-concept clayrock	Divalent bentonite	T <100°C in bentonite ΔT<5°C upper aquifer ΔT<0.5°C land surface

WMO	CONCEPT	CLAY BUFFER TYPE	THERMAL ASPECTS
NAGRA	HLW	Sodium bentonite	130°C canister/buffer <90°C rock
ONDRAF /NIRAS	Monoliths B and Supercontainer	No clay buffer	<100°C overpack <25°C top clay formation
POSIVA	KBS-3V	Sodium bentonite	T <100°C in buffer
RWM	preliminary	Sodium bentonite	
SKB	KBS-3V	Bentonite	T <100°C in buffer
SÚRAO	preliminary	Divalent bentonite	T <100°C in bentonite

2.1 ANDRA (France)

In the 1990s, the French National Radioactive Waste Management Agency (ANDRA) started a study on the Callovo-Oxfordian (COx) claystone as a possible host rock for radioactive waste disposal.

In the Cigéo, the industrial geological disposal facility (ANDRA 2005), the main underground disposal area will be divided into two sections depending on the type of radioactive waste (intermediate level long life (ILW-LL) or high-level long life (HLW-LL)). The HLW-LL containers will be emplaced in dead-end, horizontal micro-tunnels of 0.9 m in diameter favourably aligned with respect to the stress field. To prevent rock deformation and enable potential retrieval of waste containers during the reversibility period, the micro-tunnels will have a non-alloy steel casing. If no retrieval operation is decided, the final closure of Cigéo will come about a century after the start of its operation. The drifts leading to the disposal sections as well as the shafts and ramps will then be backfilled and sealed. The closure structures will consist of seals, HLW cell plugs and backfill. The seals are designed to prevent the water flows between the underground facility and the overlying formations and to limit the water circulation in the drifts, whereas the backill function is to limit the development of the fractured zone after the rupture of the lining, strengthening the sides and roofs of the drifts in the underground facility. None of these will be subjected to very high temperatures and hence they have not been considered in HITEC.

The disposal system is designed to robustly fulfil the following post-closure safety functions (ANDRA 2016):

- to isolate the waste from humans and from the biosphere so that the safety of the disposal facility is not significantly affected by climatic erosion or normal human activities,
- to prevent water circulation in the waste disposal facility,
- to limit the release of radionuclides and toxic chemicals and immobilise them in the repository,
- to delay and reduce the migration of radionuclides and toxic chemicals released.

The last three safety functions rely primarily on the favourable characteristics of the Cox formation. The packages and the repository's engineered components, specifically the underground facility's architecture on completion and closure structures, also contribute to containment of the waste and to maintaining the conditions for flows of water through the facility to be very slow.

During operation the temperature will increase rapidly near the disposal cell to reach a maximum around 80°C between 10 and 15 years after the waste packages are set. Further away, the temperature peaks will be lower and reached later. Half-way between two HLW cells, it will be reached between 400 and 500 years with a magnitude of 40 to 50°C depending on the package type and their location in the HLW repository zone. At the top and base of the COx formation, the 40°C peak will be reached after approximately 1000 years. The increase in temperature will result in 1) an increase in the overall

stress levels and 2) an increase in pore pressure. Namely, and considering the repository design, the following will result:

- a significant increase in the effective vertical stress (the tensile stress is considered to be positive) due to thermal pressurisation that may cause effective tensile stresses;
- a decrease in total horizontal stresses due to thermo-mechanical compression stresses;
- an increase in the deviatoric stress (decrease in horizontal stresses and increase in vertical stress).

This load pathway may result in a rupture from cracks/fractures, in theory sub-horizontal (perpendicular to the tensile stress direction) in case of tensile failure. In cases where the deviatoric stress is sufficiently high, shear failure may also occur. Therefore, the thermo-hydro-mechanical (THM) behaviour of the COx claystone is important in the rational design of an underground nuclear waste disposal facility, because no formation damage should be caused by thermal loading. Hence, the purpose of the thermal design is to prevent the appearance of any damage in this zone, located far away from the cells (“far-field"). Increasing the distance between the cells (centre-to-centre distance) will attenuate the interaction between the cells and reduce the amplitude of the maximum stresses. On the other hand, reducing the spacing between two HLW cells would have a major impact on the size of the HLW repository zone and consequently on the cost of the project.

2.2 BGE (Germany)

The Federal Company for Radioactive Waste Disposal mbH (Bundesgesellschaft für Endlagerung mbH, BGE) started a Site Selection Procedure aiming to ensure the best possible safety for storing high-level radioactive waste in Germany for the duration of one million years. The areas initially identified (BGE 2020a, b) included both plastic clays and claystones, including the Opalinus clay formation (in the south of Germany). In case of selection of a crystalline host rock, the safe confinement has to be ensured by means of higher requirements for the engineered barriers, i.e. the technical barriers (disposal waste packages) and geotechnical barriers (e.g. bentonite buffer and sealing of mine openings). Until the siting region is not selected, only schematic descriptions of the repository, adapted to the subarea, will be used for the preliminary safety investigations. Hence, based on generic reference models, Pöhler et al. (2010) developed concepts for vertical borehole disposal and horizontal gallery disposal in claystone for the first time. Both concepts served as basis for further development of the ANSICHT project, where a safety assessment methodology for the two repository concepts in two generic reference formations was carried out. The clay formations serve as geological barrier. The repository is located at a depth between 700 and 900 m, and in order to ensure the mechanical stability of the tunnels, a concrete liner is foreseen in all mine openings. The tunnels are backfilled with expansive clay buffer like bentonite after the disposal of the waste packages. The function of the buffer is to retard possible fluid migrations from and to the waste packages and to ensure the retention of the radionuclides due to its sorption capacity. The clay formation in combination with the engineering barrier system guarantee the long-time confinement of the radioactive waste. It is expected that the remaining voids in the repository will be progressively closed due to the healing and sealing properties of claystone. Meanwhile the buffer will progressively saturate with water coming from the surrounding saturated rock and the swelling process will take place. Both phenomena lead to the closure of the gallery and therefore to the confinement of the disposed waste packages, although the closure of the excavated area in the repository will take some time to complete. Therefore, plugs and seals are installed at several locations with redundant and diverse sealing elements in the repository to ensure the sealing of the repository in the early stage.

As the maximum possible temperatures in the respective host rocks have not yet been determined, a temperature of 100°C at the outer surface of the waste packages can be assumed for precautionary reasons. Scientific investigation of thermal effect up to temperatures of 150°C was initiated in Jobmann

et al. (2017). Based on thermal analyses, the spacings between the waste packages with heat-generating radioactive waste in an emplacement tunnel and between the tunnels were optimized in order to limit the temperature peak in the repository.

2.3 ENRESA (Spain)

The Spanish repository concept in plastic clay rock is based on the disposal of spent fuel in carbon steel canisters in long horizontal disposal galleries. Canisters are disposed of in cylindrical disposal cells constructed with pre-compacted bentonite blocks of 1,700 kg/m^3 dry density (in order to achieve a final dry density of 1,600 kg/m^3). The blocks are initially non-saturated (degree of saturation of 66%). The disposal galleries of 580 m in length and 2.4 m in diameter are located at a depth of 250 m in the host formation. A 0.3 m thick concrete liner is required to deal with the plastic nature of the clay host rock. The separation between canisters is determined mainly by thermal constraints. Separations of 1 m between canisters and 50 m between disposal galleries have been established, in order not to exceed a temperature of 100°C in the bentonite. Actual separation is a function of the properties of the host rock. Once a disposal gallery is completed, it is sealed with a 6-m long seal made of bentonite blocks and closed with a concrete plug at its entry. After completion of all the disposal galleries, the main drifts, ramp, shafts and other remaining rock cavities will be backfilled with compacted clay from the excavation of the repository, and subsequent projection of clay pellets in the remaining openings.

The bentonite buffer is required to maintain a large diversity of safety functions, which can only be fulfilled once the bentonite saturates and swells, tightly closing the construction gaps between the bentonite blocks and the liner or the canister wall on the one hand and between the blocks themselves on the other. Nevertheless, there are no safety functional requirements applicable during the time when the canister provides absolute containment. During the re-saturation of the buffer, the main concern is the preservation of the favourable properties of the buffer material: low hydraulic conductivity (which makes radionuclide transport by advection negligible); sorption of many radionuclides (especially actinides); and filtration of colloids and large complex molecules because of the small size of the pores. As the safety functions assured by the buffer are assumed for the full duration of the quantitative safety assessment (on the scale of a million years), its properties have to be preserved at a sufficient level for commensurate periods of time. Namely the long-term safety functions of the bentonite buffer are:

- Isolate the waste package from the geosphere by limiting advective transport of corroding agents to the canister.
- Avoid canister sinking in the disposal drift that could result in direct contact of the canister with the rock, hence short-circuiting the buffer.
- Avoid excessive swelling pressures that could contribute to total pressures that the canister cannot withstand.
- Avoid excessive temperatures (>100°C) that could result in chemical alteration of the bentonite and jeopardize its safety functions.
- Avoid the build-up of excessive gas pressure in the near-field, without undue impairment of the safety functions.
- Reduce microbial activity to minimize microbial corrosion of the canister.

The geometry of the repository, i.e. separations between canisters and between galleries, is determined, mainly, by limitations of thermal order and aspects of security and economy. A thermal analysis was carried out to define the geometry of the disposal area, optimizing its size as small as possible (for safety and economy) without exceeding thermal restrictions, namely the maximum permissible temperature increases in the upper aquifer (5°C) and on the land surface (0.5°C), and the maximum permissible temperature in the bentonite buffer (100°C).

Based on the established repository geological data (including a thermal conductivity value of the clay rock of 1.5 W/m·K), on the depth selected for the repository (250 m), and on the initial thermal power of 1,200 W per canister, the already mentioned separations of 1 m between canisters and 50 m between disposal galleries were established in order to comply with the thermal restrictions imposed.

2.4 NAGRA (Switzerland)

The disposal canisters, placed in up to 700-m long drifts with a 2.8 m inner diameter, are centrally arranged, necessitating a pedestal of compacted bentonite blocks (Na-bentonite from Wyoming, dry density 1,450 kg m^{-3}) for initial support. Remaining spaces are filled with highly compacted bentonite granules (about 80% dense granules at 2,100–2,200 kg m^{-3} and 20% powder), forming a protective buffer around the canisters. Spacing of approximately 3 m between canisters limits temperature rise in the buffer and rock due to radioactive decay. The repository concept (NAGRA 2022) utilizes a cementitious liner for emplacement room and tunnel wall support, resistant to mechanical loads. To prevent hydraulic shortcuts and ensure compartmentalization, sealing sections of granular and preformed brick buffer material (1,650-1,750 kg·m^{-3}) are placed at regular intervals along the drifts, about one for every 10 canisters, creating a hydraulic barrier (NAGRA 2014a). No liner is present where sealing sections are placed, allowing direct watertight contact between bentonite and Opalinus Clay.

For high-level radioactive waste disposal, key requirements for a buffer material, irrespective of the host rock, include low hydraulic permeability, self-sealing ability, and long-term durability. Bentonite's safety-relevant properties encompass swelling capacity for mechanical stabilization, chemical retention of radionuclides, low hydraulic conductivity, high viscosity for canister support, adequate gas transport capacity, minimized microbial corrosion, resistance to mineral transformation, and suitable heat conduction. A smectite content of 75% to 90% is generally accepted, with the Swedish concept specifying 80% to 85% (SKB 2010), supported by Leupin & Johnson (2013).

SF canisters emit an average initial heat output of 1,500 W, resulting in a canister-buffer interface temperature of about 130°C within ten years (Senger et al. 2014). The rock temperature at the drift boundary peaks at about 90°C after 100 years. Thermal conductivity of bentonite significantly influences buffer peak temperatures, particularly in relation to buffer saturation (NAGRA 2015). Limited thermal pulse ensures rock temperatures stay below the Opalinus Clay's reconstructed maximum paleotemperature (NAGRA 2008).

Increasing near-field rock temperature causes thermal stresses, rock heave, and a slight rise in hydraulic conductivity due to reduced viscosity. Thermal expansion of groundwater/pore water, coupled with low hydraulic conductivity in the rock and buffer, results in increased pore water pressure; within 20 m of the drifts, pressure may reach 70% of lithostatic pressure after the first hudreds of years. Potential mechanical impacts are expected to be minor, with thermally-induced pressures driving increased water flow into the EDZ and buffer, promoting self-sealing of the EDZ and increased buffer saturation (Lanyon 2019a, b).

2.5 ONDRAF/NIRAS (Belgium)

The current Belgian concept for long-term radioactive waste management foresees Monoliths B and Supercontainers to be emplaced in the geological disposal facility (GDF) constructed in Boom Clay or Ypresian clays (Figure 2-2). The supercontainer is a prefabricated concrete container that surrounds the Primary Waste Packages (PWPs) for category C waste (Leonard 2017). The C wastes (high level and long lived radioactive waste) emit large amount of heat. The supercontainer packages will be disposed in disposal galleries with a concrete lining to guarantee stability. A cement backfill will fill the gap between the concrete lining and the supercontainer. The disposal galleries will be perpendicular to the

access galleries and have an inner diameter of 3.5 m. The spacing between each supercontainer in a gallery is 10 cm and the inter-axis distance between the disposal galleries in the C-zone will be 50 or 120 m, depending on the waste (vitrified, SF).

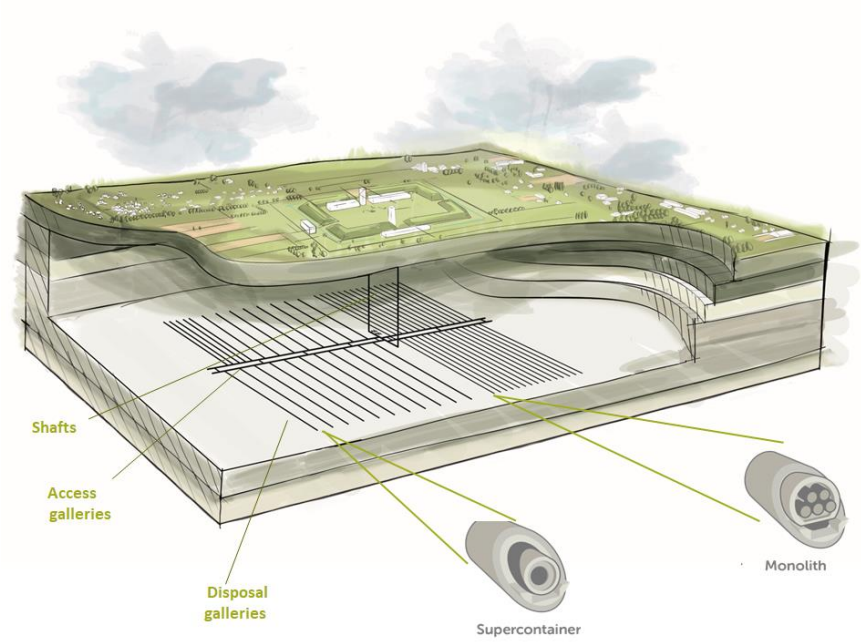

Figure 2-2. Schema of the Belgian concept of geological disposal facility in poorly indurated clay (ONDRAF/NIRAS 2020)

A multi-barrier system is defined in the geological disposal facility design:

1. The engineered barriers system (EBS), which is made up of the supercontainer (or monoliths B), the backfill of the disposal gallery and the concrete lining of the galleries (disposal and access galleries)
2. The natural barrier system, which is the host rock formation, i.e. the clay (Boom or Ypresian clays).

Each component has a chemical or/and mechanical function. The geological disposal facility has been designed in order to limit the evolution of the temperature at the overpack, in the supercontainer, and the clay formation – upper aquifer interface. Several parameters may be modified to accommodate the heat output: the number of primary packages in the supercontainer (the number of vitrified waste canister or the number of spent fuel assemblies), the spacing between supercontainers within a disposal gallery, the period of cooling prior to the disposal and the distance between the disposal galleries. The three first parameters control the near-field temperature while the last one the far-field temperature. The temperature at the overpack is limited to remain below 100°C while the temperature at the top of the host clay formation is restricted to be lower or equal to 25°C. The restriction at the overpack is driven by chemical reasons, in particular corrosion issues, while at the interface with the aquifer, the limitation is guided by drinkability of the upper aquifer.

The disposal system has to provide three main safety functions (ONDRAF/NIRAS 2013): engineered containment (only for category C waste) during the thermal phase, delay and attenuation of the releases in order to retain the contaminants for as long as required within the disposal system; isolation of the waste from people and the environment for as long as required. The primary component of the disposal system from the point of view of long-term safety is the host formation. The properties of the poorly indurated clays studied in Belgium make of them efficient natural barriers to the migration of radionuclides and chemical contaminants towards the surface environment: very low permeability, strong retention capacity and capacity of self-sealing.

The increased temperature in the clay induces strongly coupled hydro-mechanical perturbations: volumetric expansion of both the pore water and the rock minerals and thus an increase in pore water pressures and mean stresses. This may cause a decrease in effective stress in the clay. Numerical predictions of the THM impact of a GDF on the clay host formation showed that the temperature will increase quickly around the disposal gallery before rising slowly into the clay massif thanks to the heat dissipation. A maximum of 60°C will be reached at the wall of the gallery. The distance between the disposal galleries is sufficient to not have a mutual interaction, i.e. the temperature evolution around one gallery will not affect the peak temperature in the neighbouring one. The temperature variation at the interface Boom Clay – lining has a maximum value of 50°C, the peak of the temperature is reached after one or two decades. At this interface, the pore water pressure will increase because of the significant discrepancy between the thermal expansion coefficient of the solid and the one of the liquid phase. The pore water pressure will quickly rise to a value close the undisturbed value of the pore pressure which pointed to 4 MPa in the case of a repository at 400 m depth. The analysis of the variation of the state of mechanical stress shows that the excavation process will generate plastic strain. The variation of temperature will affect the mechanical state of stress by accumulating additional plastic strain around the gallery. This additional irreversible strain may modify the EDZ by extending the initial cracks, increasing the permeability or generating irreversible changes in the EDZ, affecting the favourable properties of the clay. There are other uncertainties on the large-scale hydromechanical response of the Boom Clay to heat, particularly regarding the role of anisotropies in the THM properties and in-situ stresses.

The heating of the clay can also induce changes in the mineralogy and geochemistry of the Boom Clay. Until now no significant changes in the clay mineralogy or geochemistry were observed, but research is still on-going, mainly on the effect of a combined thermal and alkaline perturbation. Furthermore the thermal reactivity of the Boom Clay kerogen constitutes a factor of uncertainty. Because the kerogen in the Boom Clay is thermally immature, significant amounts of CO_2 and organic acids will be released during heating. This release may affect the mobility of radionuclides by complexation, while the dissolution of CO_2 in water, leading to pH reduction, may modify the near-field chemistry of the clay.

2.6 SKB (Sweden) and POSIVA (Finland)

In Sweden, used nuclear fuel will be emplaced in the Forsmark bedrock at a depth of approximately 500 metres. The final disposal plans are based on the KBS-3V concept, developed by SKB, also to be used by Posiva. In Finland, spent nuclear fuel will be embedded in Olkiluoto bedrock at a depth of 400-450 metres. The bentonite buffer that surrounds the vertically installed copper canisters is composed of Wyoming Na-bentonite in form of compacted bentonite blocks (dry density 1650-1800 kg/m^3) and bentonite pellet filled gaps (dry density 880-960 kg/m^3) between canister and the compacted blocks as well as between the compacted blocks and host rock. Performance target of maximum 100°C temperature for buffer has been set to ensure favourable early evolution of the engineered barriers. This target is taken into account in the thermal dimensioning of the repository (Ikonen et al. 2018) that analyses allowed distance between disposal canisters and disposal tunnels and is basis for designing the repository layout.

2.7 RWM (United Kingdom)

No disposal site or geology has been selected so far in the UK, and therefore illustrative designs have been adopted for suitable generic rock types (Figure 2-1). For lower strength sedimentary host rocks (e.g. clay) and higher strength host rocks (e.g. granite), a bentonite engineered barrier system is adopted, to surround high heat generating waste containers (RWM 2016). For illustrative purposes

before a repository site is chosen, RWM has broadly adopted the NAGRA concept for a lower-strength sedimentary rock type, and the KBS-3V system developed by SKB for a higher strength rock type, for the disposal of high heat generating waste. Both disposal concepts assume the use of Na montmorillonite bentonite such as the Wyoming type for the buffer surrounding the waste container.

Thermal dimensioning work by RWM has highlighted that significant repository footprint and waste cooling time reductions can be achieved through thermal optimisation (Amec 2016). This work is a key driver for RWM to better understand the thermal limits of the bentonite buffer, since this component of the disposal system currently limits thermal loading in the proposed facility.

2.8 SÚRAO (Czech Republic)

The Czech DGR concept considers only crystalline rock environments, i.e. igneous or metamorphic rock (granites, gneisses) massifs at depths of approximately 500 metres below surface. The repository will serve for the disposal of spent nuclear fuel (SF) and other high- and intermediate-level radioactive waste that cannot be disposed of in existing repositories. The two sections of the DGR (SF and HLW/ILW) will be separated by a natural rock partition of sufficient thickness.

The final technical design of the repository has not yet been decided. Preliminary project design studies concerning DGR construction that have been compiled for each of the 9 potential sites consider four SF disposal options, i.e. combinations of vertical and horizontal disposal and the fully-mechanised and conventional excavation of the underground complex. The vertical system involves the drilling of vertical disposal wells from horizontal disposal tunnels. The wells will have a diameter of 1.8 m and a length of around 5.5 m or 7.2 m depending on the type of containers. The horizontal disposal system considers the drilling of horizontal tunnels with a diameter of 2.2 m and maximum lengths of 300 m (e.g. Špinka et al. 2018).

The basic buffer concept involves a combination of compacted bentonite blocks and pellets, while the backfill concept is based on a bentonite material only; however, the option of the use of a mixture of bentonite and crushed rock has not been rejected. Currently, it is planned that Czech bentonite of the Ca-Mg type with enhanced iron content in its octahedral positions (Hausmannová et al. 2018), will be used as the buffer and backfill material.

3 Buffer materials

This chapter is devoted to the buffer material, namely bentonite. This would be the clay material submitted to a higher temperature in the repository, because it will be in direct contact with the canisters. HITEC aimed to develop improved understanding of buffer clay-based materials exposed to temperatures above 100°C for extended durations and evaluate whether or not elevated temperature limits of 100–150°C are safe for a variety of geological disposal concepts (described in chapter 2).

In the framework of HITEC, both Wyoming-type bentonites (i.e. sodic montmorillonites) and predominantly-divalent bentonites were analysed. Most of these bentonites have been studied as engineered barrier materials for decades, and a summary of their main mineralogical, geochemical and hydro-mechanical characteristics, based on a literature search and on the participant's input, is given in the first part of this chapter. Then, large-scale tests, relevant in terms of the temperatures involved or performed using some of those bentonites, are described.

The main part of the chapter summarises the experimental (subchapter 3.3) and modelling (subchapter 3.4) activities carried out in the framework of the Project. Both subchapters start with an overview of what was known about the effect of elevated temperature on the bentonite properties and performance prior to HITEC. The description of the results obtained during the Project is based on

deliverables D7.7 (Svensson et al. 2023), D7.8 (Graham et al. 2023), D7.9 (Villar et al. 2023) and D7.10 (Vasconcelos et al. 2023). In particular, the analyses on buffer material carried out in Task 3 of the Project determined the impact of temperature on bentonite swelling pressure, hydraulic conductivity, strength, water retention and transport properties. Additionally, mineralogical and geochemical aspects were also considered, and a literature review on this topic is presented at the beginning of subchapter 3.3. For each activity, context of knowledge and advances made outside the project is also given.

3.1 Materials used in HITEC

Three main bentonites were identified as those better characterised and to be used by more participants in the HITEC project and in a wider variety of tests, including the large-scale ones (section 3.2). These are MX-80, FEBEX and BCV, although several other bentonites were also used in the project, such as Bara-Kade, Kunipia-G, PBA-22 Extra, PBC. In addition, some of the materials used in the ABM large-scale test (e.g. DepCAN, Asha505, Calcigel) are also briefly described below.

The following tables show summaries of the main properties of the buffer materials considered in HITEC. All of them have a high smectite content (>72%) and CEC (>64 meq/100 g), with sodium as main exchangeable cation in MX-80, Bara-Kade and Asha505. In some cases the range of values is broad because they correspond to different batches.

Table 3-1. Basic properties of some bentonite materials

Bentonite	**MX-80**[a]	**FEBEX** [b]	**BCV** [c]	**Kunipia-G** [d]	**PBA-22 Extra** [e]
Liquid limit (%)	350-570 (490)	102±4	140±2		119
Plastic limit (%)	46-70 (50)	53±3			42
Grain density (g/cm^3)	2.76-2.82 (2.78)	2.70±0.04	2.76±0.02	2.71	
Hygroscopic water content (%)	(12.3±0.1)	13.7±1.3	11		12
Total specific surface area (m^2/g)	(624)	725	432-482	524-660	375-400
BET specific surface area (m^2/g)		32±3		42	90-120

[a] range of values from literature, in parenthesis values for Posiva batches (Kiviranta & Kumpulainen, 2011; Kiviranta et al. 2018); [b] ENRESA, 2006; [c] Červinka et al. 2018; [d] Massat et al. 2016, Chaaya et al. 2023; [d] Zoblenko et al. 2023

Table 3-2. Mineralogy of some bentonite materials (Tr=traces)

Bentonite	**MX-80** [a]	**FEBEX** [b]	**BCV** [c]	**PBA-22 Extra** [d]
Smectite	61-95 (88±3)	92±4 [e]	72 [e]	>90%
K-feldspars	4-15 (2±2)	Tr	-	Tr
Quartz	4-15 (4±0)	2±1	10-11	3-5
Cristobalite	Tr	2±1	-	
Tridymite	Tr (-)			
Calcite	Tr	1±1	1-4	2-5
Pyrite	(1±0)		-	
Plagioclase	4-15 (3±1)	3±1	-	

Bentonite	MX-80 [a]	FEBEX [b]	BCV [c]	PBA-22 Extra [d]
Goethite	-	-	3	
Gypsum	Tr (-)			
Ankerite + siderite	-	-	1	
Illite	Tr (-)	-	2-3	
Kaolinite	-	-	4-6	
Anatase	-	-	2-3	

[a] range of values from literature, in parenthesis values for Posiva batches (Kiviranta & Kumpulainen, 2011; Kiviranta et al. 2018); [b] ENRESA, 2006; [c] Červinka et al. 2018; [d] Zoblenko et al. 2023; [e] smectite-illite mixed-layer

Table 3-3. Exchangeable cations and cation exchange capacity (CEC) for some bentonite materials

Bentonite	Na^+	Ca^{2+}	Mg^{2+}	K^+	Sum cations	CEC
MX-80 [a]	50-74 (58)	10-30 (24)	3-8 (9)	(2)	(93)	(86)
FEBEX [b]	28	33	33	3	98	98
BCV [c]	6-14	13-26	41-58	1-3	58-71	57-66
DepCAN [d]	21-22	35-40	21-29	1-2	79-94	82-79
Asha505 [d]	62	19-17	12-16	1	94-90	89-88
Calcigel [d]	2-3	52-54	12-17	1-9	68-75	66-70
Kunipia-G [e]	83	12	5	1	115	109
PBA-22 Extra [f]	x	xxx				93

[a] range of values from literature, in parenthesis values for Posiva batches (Kiviranta & Kumpulainen, 2011; Kiviranta et al. 2018); [b] ENRESA, 2006; [c] Červinka et al. 2018; [d] Svensson et al. 2011; [e] Chaaya, 2023; [f] Zoblenko et al. 2023

Table 3-4. Chemical composition of some bentonite materials

Element (wt.%)	MX-80 [a]	FEBEX [b]	BCV [c]	DepCAN [d]	Asha505 [d]	Calcigel [d]	PBA-22 [e]
SiO_2	61.55±0.29	57.89±1.55	47.86±0.68	52.01	46.48	54.67	54.7
Al_2O_3	20.55±0.25	17.95±0.71	14.11±0.03	17.54	20.64	17.54	16.3
MgO	2.53±0.01	4.21±0.21	2.60±0.03	3.11	2.01	3.37	3.2
Fe_2O_3	3.89±0.04	3.12±0.22	10.42±0.05	4.64	12.16	5.05	5.7
CaO	1.32±0.05	1.83±0.10	2.58±0.01	5.07	0.84	2.94	2.1
Na_2O	2.41±0.01	1.31±0.09	0.30±0.04	0.78	1.97	0.47	0.1
K_2O	0.78±0.02	1.04±0.05	0.92±0.02	0.90	0.14	1.16	0.7
TiO_2	0.17±0.00	0.23±0.01	2.12±0.01	0.71	1.01	0.41	
MnO	2.53±0.01	0.04±0.00	0.18±0.00	0.07	0.05	0.03	
SO_3	0.15±0.01	0.04	N.D.	N.D.	N.D.	N.D.	
P_2O_5		0.03±0.01	0.48±0.01	0.143	0.091	0.096	

Element (wt.%)	MX-80 [a]	FEBEX [b]	BCV [c]	DepCAN [d]	Asha505 [d]	Calcigel [d]	PBA-22 [e]
LoI	6.26±0.01	13.8±2.6	N.D.	14.5	14.4	14.1	

[a] values for Posiva batches (Kiviranta & Kumpulainen, 2011; Kiviranta et al. 2018); [b] ENRESA, 2006; [c] Červinka et al. 2018; [d] Svensson et al. (2011); [e] Zoblenko et al. 2023

3.1.1 Wyoming-type bentonite

The MX-80 bentonite comes from Wyoming (USA) and is produced by American Colloid Co. It is a bentonite of volcanic origin, powdered and Na-homogenised. The deposit has been mined for decades, for which reason the characteristics of the bentonite found in the literature vary over time and also depending on the batches. Some of the initial characterisations of the material in the context of radioactive waste disposal were performed by Müller-Vonmoos & Kahr (1983), Borgesson et al. (1988), Madsen (1998) or Pusch (2001). Dixon et al. (2023) present a recent database of properties determined by various authors, including thermal conductivity, hydraulic conductivity and swelling pressure, highlighting their variability.

The material with commercial name 'Bara-Kade' is Wyoming sodium bentonite similar to MX-80. The as-received water content was 8.2%.

In the HE-E and FE tests the MX-80 was used in the form of irregular pellets of size <10 mm, dry density ~2.1 g/cm^3 and water content 6% (see de Book et al. 2009 and Gaus et al. 2014) for manufacturing process). The Volclay used by BGS has a grain size from 16 to 200 µm and was characterised by Svensson et al. (2017).

The water retention capacity of MX-80 bentonite has been checked by different authors, and the effects on the water retention curve (WRC) of dry density (e.g. Pintado et al. 2013, Seiphoori et al. 2014) and temperature have also been analysed (e.g. Jacinto et al. 2009). Jacinto et al. (2009) found that the influence of dry density on the water retention capacity depends on the suction range, the limiting value being around 30 MPa. For suctions above this threshold value the retention capacity in terms of water content is slightly higher as the dry density is higher, whereas for lower suctions, the lower the dry density of the bentonite the higher its water content. The retention capacity decreases with temperature, more than predicted by the change in surface tension, especially for the high temperatures and the low suctions. Villar & Gómez-Espina (2008) reported some suction measurements on compacted MX-80 bentonite with different water contents at temperatures of up to 120°C.

The dependence of swelling pressure and hydraulic conductivity on dry density was already systematically studied by Villar (2005) and Karnland et al. (2008).

The increase of thermal conductivity of the MX-80 bentonite with dry density, water content and temperature has been shown by Tang et al. (2008a) and Xu et al. (2019), with values measured between 0.2 and 1.2 W/m·K, for ranges of dry density 1.0-1.8 g/cm^3, water content 0-25% and temperature 5-90°C.

3.1.2 FEBEX bentonite

The FEBEX bentonite is a 900-t batch of bentonite that was extracted from the Cortijo de Archidona deposit and processed in 1996 for the FEBEX project. The processing consisted in homogenisation, air-drying and manual removal of volcanic pebbles on site and, at the factory, crumbling, drying in a rotary oven at temperatures between 50 and 60°C and sieving through a 5-mm mess. The initial characterisation can be found in the final report of the project (Enresa 2006) and in Villar (2002) and

Fernández (2004). This material was also used for the NF-PRO and PEBS projects (Villar & Gómez-Espina 2009) and was distributed over the years to different laboratories to be used in different projects (e.g. ABM [Svensson et al. 2011], ESDRED [Alonso et al. 2008]).

The smectite content of the FEBEX bentonite is above 90 wt.%. The smectitic phases are actually made up of a montmorillonite-illite mixed layer, with 10-15 wt.% of illite layers. It also contains variable quantities of other minerals, as detailed in Table 3-2. Although it predominantly contains divalent exchangeable cations, the sodium amount in the interlayer is also relevant (Table 3-3). The predominant soluble ions are chloride, sulphate, bicarbonate and sodium. Other basic properties can be found in Table 3-1.

The retention curve of the bentonite was determined in samples compacted to different dry densities at different temperatures (Lloret *et al*. 2004, Villar & Lloret 2004, Villar & Gómez-Espina 2009). The volume of the samples remained constant during the determinations, since they were confined in constant volume cells. An empirical fitting relating water content to suction, degree of saturation, porosity and temperature was presented in Villar & Gómez-Espina (2009).

The saturated hydraulic conductivity of compacted bentonite samples is exponentially related to their dry density (Villar 2002). For a dry density of 1.6 g/cm^3 the saturated permeability of the bentonite is approximately $5 \cdot 10^{-14}$ m/s at room temperature, either with diluted granitic or deionised water used as percolating fluid. The temperature increase tends to increase permeability (Villar & Gómez-Espina 2009). Some isothermal infiltration tests and heat flow tests at constant overall water content were performed during FEBEX I project and they were backanalysed using CODEBRIGHT (Lloret *et al*. 2002, Pintado *et al*. 2002). It is possible to fit the experimental data using a cubic law for the relative permeability and a value of 0.8 for the tortuosity factor.

The swelling pressure of compacted samples is also exponentially related to the bentonite dry density (Villar 2002). The bentonite compacted at dry density of 1.6 g/cm^3 and saturated with deionised water at room temperature develops a swelling pressure of about 6 MPa. Saturation with a Spanish diluted granitic water gives similar values, whereas temperature causes a decrease of them (Villar & Gómez-Espina 2009).

The thermal conductivity measured in samples compacted in the range of water content 0-25% and dry density 1.49-1.75 g/cm^3 expands between 0.45 and 1.30 W/m·K, with a dependence on degree of saturation that could be fit to a sigmoidal relation (Villar 2002).

3.1.3 BCV bentonite

Bentonite BCV is a typical Czech bentonite that formed via the in-situ alteration of Fe-rich tuffs and augite-biotite-type tuffites. The contribution of Fe to the system occurred as a consequence of the activity of the Krušnohorsko-ohárecká tectonic zone (Franče 1992). Because Fe erosion did not take place during the argillisation phase, the smectites in these bentonites remained enriched with iron (especially in the octahedral positions). Moreover, the accessory minerals also contain a significant proportion of Fe, i.e. Fe carbonates and oxohydroxides.

BCV is produced industrially by Keramost Ltd at their Obrnice plant. The bentonite treatment process commences with the sieving of the coarse material employing a sieve with a 20x20 cm mesh. The bentonite is then homogenised in a wheeled mill from where it is transferred to a rotary oven where the material is dried (average temperature of 110°C) for 45 minutes. The drying process ensures a water content of around 10% and results in the preparation of the material for final milling and air sieving. The processing of the BCV material leads to a mixture where 1% of the total weight of the grains can be larger than 0.315 mm and at least 70% of the grains are smaller than 0.063 mm. The BCV material was first tested in 2017, and the characteristics of the material have been reported by Červinka et al. (2018), Hausmannová, et al. (2018), Svoboda (2019).

Some basic properties of this material and its mineralogy are given in Table 3-1 and Table 3-2. The content of amorfous phases can be as high as 10 wt.% (Červinka et al. 2018). Its main exchangeable cations are magnesium and calcium (Table 3-3).

The retention curves of the bentonite were determined at ambient temperature for samples compacted to various dry densities. The volume of the samples remained constant during the whole test. In the range of dry densities between 1.4 and 1.8 g/cm^3 no differences of gravimetric water content for a given suction were observed (Červinka et al. 2018).

The saturated hydraulic conductivity of compacted BCV bentonite samples decreases exponentially with the dry density (Hausmannová et al. 2018). For a dry density of 1.6 g/cm^3, the saturated hydraulic conductivity of the bentonite is approximately $1.14 \cdot 10^{-13}$ m/s at room temperature with deionised water as the percolating fluid.

The swelling pressure of compacted samples is also related exponentially to the dry density of the bentonite (Hausmannová et al. 2018). The material develops a swelling pressure of around 8 MPa when compacted at a dry density of 1.6 g/cm^3 and saturated with deionised water at room temperature.

The thermal conductivity of BCV bentonite compacted at a dry density of 1.6 g/cm^3 is ~0.6 W/m·K for w = 12% and 1.4 W/m·K for the almost fully saturated sample (Červinka et al. 2018).

3.1.4 Other bentonites

The in situ large-scale test ABM (Alternative Buffer Material), conducted by SKB at Äspö Hard Rock Laboratory (described in section 3.2.1), tested a variety of bentonites. They are all high-grade bentonites with smectite content of around 80 wt%, with high swelling pressures at high densities, and regarded as possible buffer or backfill candidates. They are described in detail in Svensson et al. (2011). Upon dismantling of the test parcel ABM5 some of these bentonites were analysed and the results presented in the context of HITEC, namely:

- DepCAN is from Milos (Greece), and is a calcium dominated bentonite. The smectite is regarded as montmorillonite.
- Asha505 is from Kutch (India), is sodium dominated and is high in iron (~13 wt% Fe_2O_3), hence its colour is brown. The smectite is regarded as montmorillonite/beidellite with somewhat higher charge.
- Calcigel is a calcium Bavarian bentonite (Germany). The smectite is regarded as montmorillonite. The Calcigel bentonite often changes in colour in experiments, and there are indications that the smectite structural iron is more sensitive to redox reactions than most others of the bentonites studied.

Ukrainian bentonite was used in research conducted at KIPT, provided by Dashukovskiy bentonites. The material is referred to as PBC (Powder Bentonite from Cherkasy region of Ukraine). It is a natural bentonite containing Na-montmorillonite up to 60% and Ca, Mg-montmorillonite up to 20%, along with quartz and calcite. The bentonite was received ground to a grain size <0.16 mm and with a water content of 7.4%.

Bentonite from the Ukrainian deposit of Cherkasy was studied by SIIGNASU, in particular the industrially milled powder called bentonite PBA-22 «Extra» delivered by Dashukovskiy (Zoblenko et al. 2023). It is a commercial calcium bentonite with a content of montmorillonite of 70-85%, along with variable quantities of quartz (5–20%), and calcite (2–5%), accessory minerals (zircon, rutile) and feldspar. It has a BET external specific surface area of 90-120 m^2/g, a CEC of 93 meq/100 g, liquid limit of 119%, plastic limit of 42% and a hygroscopic water content of 12%. The structural formula based on the chemical analyses shown in Table 3-4 is $(Al_{1.21}Fe^{3+}_{0.49}Mg_{0.30})[Al_{0.18}Si_{3.82}]O_{10}(OH)_2 + (Ca_{0.17}Na_{0.03})$.

The Kunipia-G, used in the studies by BRGM, is a highly pure montmorillonite (>95%), with traces of quartz and carbonates, provided by Kunimine Industries and issued from the purification of the natural bentonite Kunigel-V1. The structural formula of this montmorillonite $Na_{0.41}K_{0.01}Ca_{0.04}(Si_{3.92}Al_{0.08})(Al_{1.51}Mg_{0.37}Fe_{0.12})0_{10}(OH)_2,nH_2O$ with a negative layer charge of 0.5 per half unit-cell was determined by Massat et al. (2016). Other properties can be found in Table 3-1 to Table 3-3. For the investigation carried out in HITEC the smectite was washed and homo-ionized in Na^+ and Ca^{2+} exchanged-form. Details about the preparation and characteristics of these samples can be found in Chaaya (2023) and Chaaya et al. (2023).

3.2 Relevant large-scale tests

Some large-scale tests performed in underground laboratories (Äspö in Sweden, Mont Terri and Grimsel in Switzerland) and also a mock-up are briefly described in the following sections. In all of them a bentonite buffer was used and a heater(s) simulating the waste canister. In the in situ tests hydration was natural and in some cases with an additional artificial contribution. They have been selected because of the relevance of the temperatures on the heater surface (>100°C). However, this is not an exhaustive compilation, and only those tests proposed by the contributors have been included. For example, the Temperature Buffer Tests (TBT) ran in Äspö for seven years with a heater temperature of 140°C using MX-80 bentonite as buffer material (Äkesson et al. 2012).

A summary of the main characteristics of these large-scale tests is given in Table 3-5. Different host rocks, buffers, spatial configurations and temperatures are represented. Some of the tests are still running and providing online information. The others have already being dismantled (some parcels of the ABM and LOT tests, Ophelie), and information on the postmortem state and modification of properties is available. In fact material coming from the ABM test has been analysed in the context of HITEC, and this is why this test is described in more detail.

Table 3-5. Summary of relevant large-scale tests characteristics

Test	Host Rock	Duration	Characteristics	Temperature	Buffer
ABM SKB	Granite (Äspö)	1, 3, 5 years	Reduced scale, vertical pit	130°C (250°C)	11 different clays
LOT SKB	Granite (Äspö)	1, 6, (20) years	Reduced scale, vertical pit	Up to 130°C	MX-80 (Na bentonite)
HE-E NAGRA	Opalinus (Mont Terri)	>12 years	Reduced scale, gallery	140°C	Sand/MX80 mixture MX80 pellets
FE NAGRA	Opalinus (Mont Terri)	>9 years	Real scale, gallery	140°C	MX80 blocks MX80 pellets
Ophelie	Mock-up (Mol)	4.5 years	1:1 scale	170°C	FoCa/sand/graphite (60/35/5)

3.2.1 Alternative Buffer Materials (ABM, Äspö)

The ABM test parcels exposed different clay materials to conditions similar to a storage place and to adverse conditions with respect to temperature. The first ABM experiments (1-3) were installed in 2006 (Eng et al. 2007), and three additional ones were installed within the ABM45 project in 2012

(Sandén et al. 2018). Each of these parcels is a vertical borehole with a depth of 3.2-3.7 m and a diameter of 0.3 m excavated in the Äspö HRL. For the experiments in general the target temperature was 130°C (the only exception was ABM5), the heater was made of steel and different compacted bentonites were installed in direct contact with each other surrounding the central heater (Figure 3-1). The clays used are Asha 505, Calcigel, Callovo-Oxfordian (COx), IBECO, Deponit CA-N (Dep CAN), FEBEX, Friedland, Ikosorb Ca White, Ibeco Seal M-90, Kunigel VI, Wyoming bentonite MX-80 and Rokle. A water saturation system together with a sand filter allowed rapid water saturation. A summary of the characteristics of the tests performed is shown in Table 3-6.

ABM1 was excavated in 2009 (e.g. Svensson et al. 2011, Svensson and Hansen 2013) and ABM2 was excavated in 2013 (e.g. Svensson 2015). Upon dismantling these tests showed locally precipitates and iron corrosion products. The montmorillonites was typically fairly intact, with a minor formation of saponite. However, no impact on the buffer performance was found (Svensson 2015). The temperature in ABM5 was initially kept low at around 50°C (Figure 3-2), because it was impossible to get the water pressure to the target level. In 2016 the temperature was increased stepwise to very high temperatures of up to 250°C at the heater interface. ABM5 was excavated in 2017, and some blocks looked rather intact while others were highly fractured and very fragile due to the high temperature.

Table 3-6: Characteristics and duration of the ABM tests

Test	Duration	Characteristics
ABM1	28 months (2006-2009)	Artificial wetting
ABM2	6.5 years (2006-2013)	Artificial wetting for 2.5 years, heating to 141°C afterwards
ABM3	(2006-present)	Artificial wetting
ABM4	(2012-present)	Artificial wetting
ABM5	5 years (2012-2017)	Temperature at 50°C until 2016, then gradually increased up to 250°C, artificial wetting
ABM6	(2012-present)	Artificial wetting

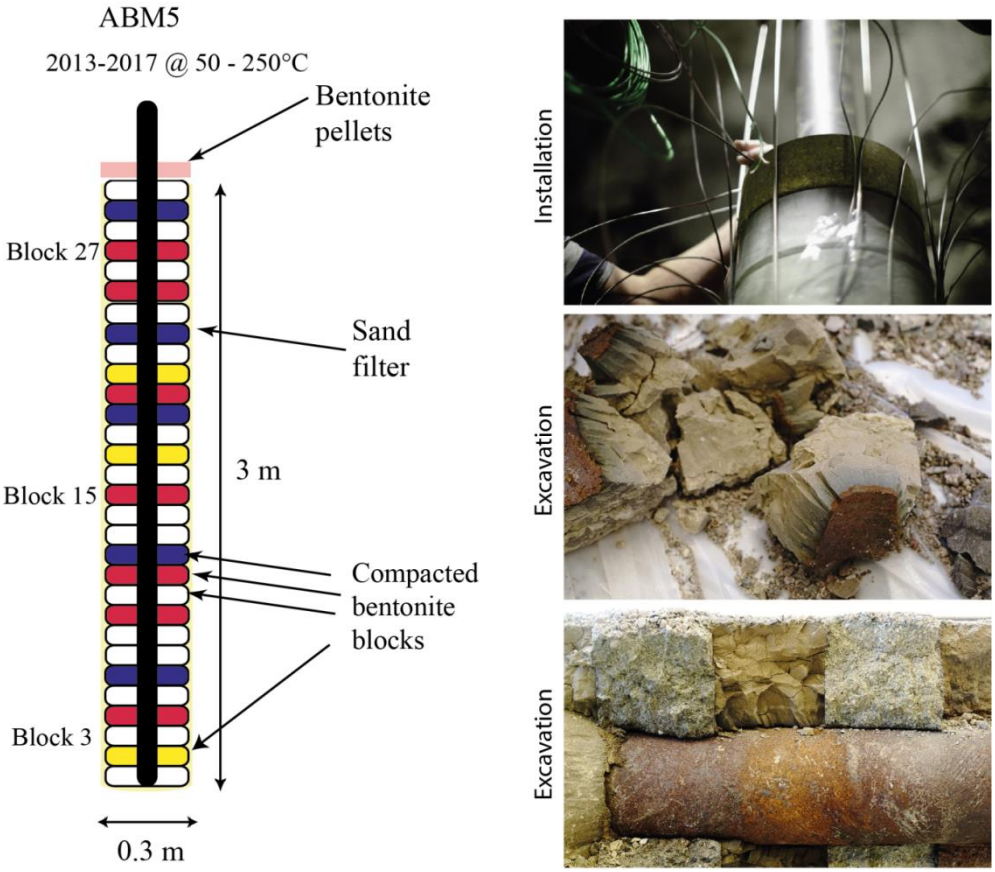

Figure 3-1. Schematic illustration of the ABM5 experiment and pictures from installation and excavation of the ABM5 experiment

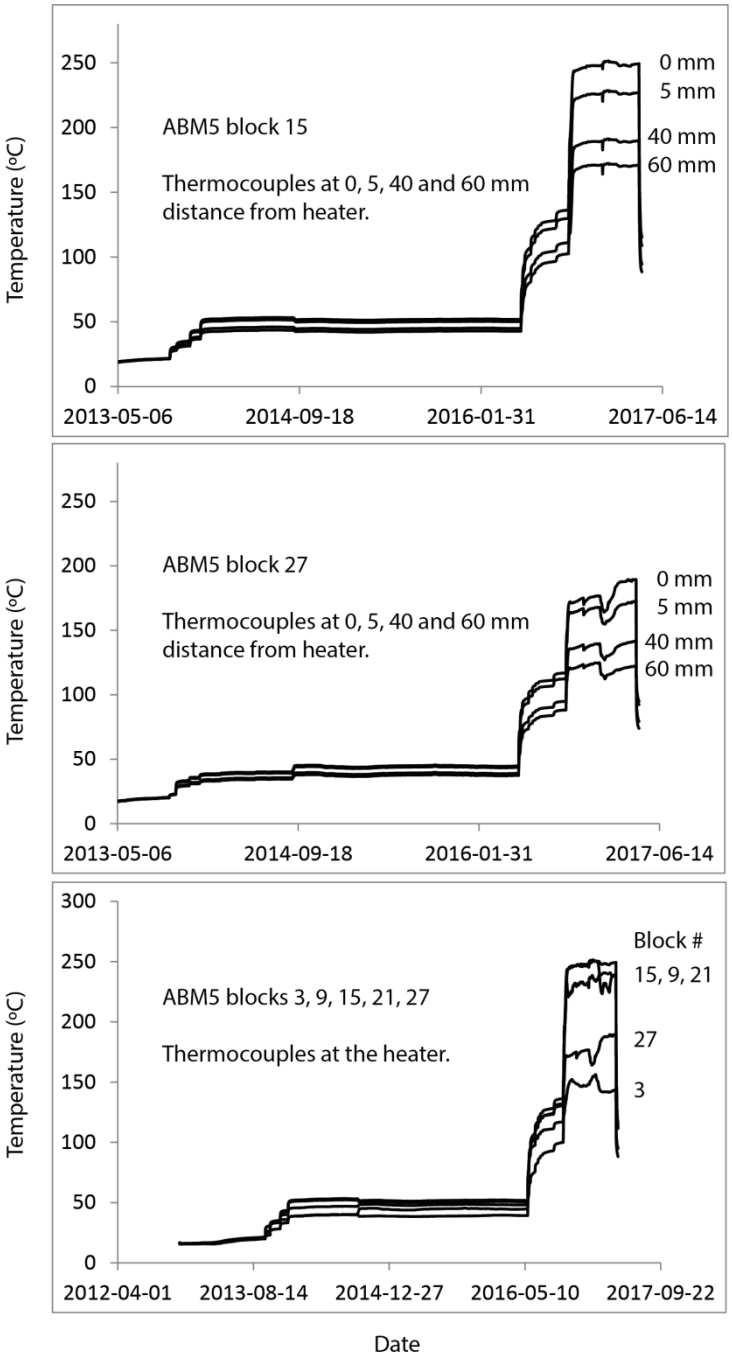

Figure 3-2. Overview of the thermal evolution of the ABM5 experiment

3.2.2 Long term test of buffer material (LOT, Äspö)

The LOT experiments were created mainly to study the long-term stability of the bentonite, the mineral composition and the impact on important properties such as swelling pressure and hydraulic conductivity. The overall design of LOT is almost identical to the ABM experiment (Figure 3-1), however ABM uses many different bentonites and steel instead of copper. The LOT experiments (7 installed, 6 retrieved, Table 3-7) use copper heaters and Wyoming bentonite (MX-80) naturally saturated with groundwater, and run at 90°C (S-series) and 130°C (A-series). The copper heaters were not designed for corrosion studies; however, separate copper coupons were installed in the bentonite for that purpose. The LOT experiments are ~4 m high; 0.3 m in diameter and the central copper heaters are

0.1 m in diameter. The reports of the uptake of the experimental packages A1 (adverse 130°C, 1 year), A2 (adverse 130°C, 6 years) and A0 (adverse 130°C, 1.5 year) are in Karnland et al. (2000, 2009 and 2011), respectively, and SKB TR-09-31.

The LOT S2 and A3 were excavated in September 2019. Chemical analysis of block 15 in the A3 experiment showed maxima of Ca and S at the heater and at about 20 mm from it. The elevated levels of Ca and S were attributed to local accumulation of anhydrite, also detected by XRD. However, in the neighbour block 16, Ca and S only showed one maximum. The reason is currently not understood; however, most likely local variations in e.g. temperature, water saturation history or fractures in the rock possibly may give rise to minor local variations, demonstrating the importance of analysing several different profiles. Anhydrite accumulation was however expected, and has previously been seen in other field experiments. A minor increase in Mg was observed towards the heater, which was expected from earlier field experiments, however, no corresponding new phase was observed in the XRD data.

Table 3-7: Characteristics and duration of the LOT tests

Test	Duration	Characteristics
A0	1.5 year (1999-2001)	Heater temperature at 130°C
A1	1 year (1996-1998)	Heater temperature at 120 -150°C with a heater of 1000 W
A2	6 years (1999-2006)	Heater temperature at 120 -150°C
A3	~10 years (retrieved in 2019)	Heater temperature at 120 -150°C
S1	1 year (1996-1998)	Heater temperature at 90°C with a heater of 600 W
S2	~9 years (retrieved in 2019)	Heater temperature at 90°C
S3	>10 years (ongoing)	Heater temperature at 90°C

3.2.3 Heating Experiment (HE-E, Mont Terri)

The HE-E Experiment is a 1:2 scale heating experiment considering natural re-saturation of the EBS at a maximum heater surface temperature of 140°C (Gaus (Ed.) 2011, Teodori & Gaus (Eds.) 2012). It is part of a series of heater experiments, identified by the HE code, that have been undertaken in the Mont Terri underground research laboratory (URL) with the broad aim of investigating the THM processes occurring in the Opalinus Clay and the bentonite buffer (NAGRA 2019). The experiment was constructed between December 2010 and June 2011 and operation is ongoing. It is conducted in a 50-m-long tunnel of 1.3 m diameter (Gaus et al. 2014). The test section of the micro-tunnel has a length of 10 m and was characterised in detail during a ventilation experiment, which took place in the same test section (Mayor et al. 2007). The aims of the HE-E Experiment are focused on the early non-isothermal re-saturation period and its impact on the THM behaviour of the EBS, namely:

- to provide the experimental data required for the calibration and validation of existing THM models of the early re-saturation phase
- to upscale thermal conductivity of the partially saturated EBS from laboratory to field scale for pure bentonite and bentonite-sand mixtures

The experiment consists of two independently heated sections, each with a length of 4 m. The heaters were placed in a steel liner supported by MX-80 bentonite blocks with a dry density of 1.81 g/cm^3 and a water content of 10.3%. The dimensions and materials of the two sections were the same apart from the granular filling material: Section One was filled with a 65:35 granular mixture of sand and bentonite

(Bentosund WH2), and Section Two was filled with pure MX-80 bentonite pellets. For the sand/bentonite mixture, the grain spectrum was 0.5-1.8 mm, the water content was 13% for the bentonite and 0.05% for the sand (giving a total water content of the mixture of approximately 4%) and a dry density of 1.38 g/cm^3 (and an emplaced dry density of 1.48-1.50 g/cm^3). The pellets were the same as used for the ESDRED emplacement test (de Book et al. 2009). Use of two types of granular filling material allowed comparison of the THM behaviour of the two EBS materials under almost identical conditions.

The heating started in June 2011, and the maximum temperature was reached in June 2012. Since then, the temperature has been held constant. The results from the HE-E to date have been consistent with the previous heater experiments conducted in Mont Terri and have allowed further development of the capability to predict the early-stage performance of the EBS and near-field rock. The EBS is characterised by a high temperature gradient owing to its low thermal conductivity in response to drying from the introduction of the heaters. The temperature at the interface of the Opalinus Clay and the EBS is ~50°C.

3.2.4 Full-Scale Emplacement experiment (FE, Mont Terri)

The main aim of the FE experiment is the investigation of SF/HLW repository-induced THM coupled effects on the host rock at this scale and the validation of existing coupled THM models (NAGRA 2019). Further experimental aims were 1) the verification of the technical feasibility of constructing a disposal tunnel using standard industrial equipment, 2) the optimisation of the bentonite buffer material production and 3) the investigation of (horizontal) canister and bentonite buffer emplacement procedures for underground conditions.

The layout of the FE experiment was designed to simulate the Swiss repository concept for SF/HLW conditions in one single tunnel at the Mont Terri URL (Müller et al. 2015). First, a 50-m long experimental tunnel was constructed. At the deep end of the FE tunnel an ISS (interjacent sealing section) was built using only steel arches for rock support, while the rest of the tunnel is supported by shotcrete. A 'bentonite block wall' was erected manually in a section of the ISS. In the FE tunnel, 3 heaters with dimensions similar to those of waste canisters were emplaced on top of 'bentonite block pedestals'. The first heater emplaced at the deep end of the FE tunnel was named H1, the middle one H2 and the most 'shallow' heater (close to the plug) H3. The remaining space was backfilled with a highly compacted 'granulated bentonite mixture' (GBM). Finally, the experiment was sealed off (towards the FE cavern) with a concrete plug holding the bentonite buffer in place and reducing air and water fluxes. The heating phase started in December 2014, with the heaters' surface temperature at values between 120 and 130°C, although it is expected they eventually reach 130-150°C at the surface of the middle heater and approximately 60-80°C at the rock interface.

Even though in the case of the FE-Experiment the swelling potential of the bentonite does not apply directly to the FE as full saturation is not likely to happen within the 10-15 years planned for the experiments duration, the emplaced material had to comply with the safety related requirements (Leupin & Johnson 2013). The reason for this is that in the FE the focus was set on the THM behaviour of the buffer, which should be as close as possible to the one expected for real disposal conditions.

In the context of the FE experiment, several modelling exercises have been carried out (e.g. Senger 2015, Garitte et al. 2014). A set of scoping calculations aimed at bracketing the main parameters and independent variables associated with the FE experiment (e.g. temperature at the different components, pore water pressure and strain in OPA, etc.) was carried out by Ewing & Senger (2012). Such exercise supported the design of the FE experiment and its monitoring system. Second, a calibration and validation exercise, which included uncertainty analysis was carried out by different modelling teams.

The experience and data from previous experiments, especially HE-E, were used to develop scoping estimates of key parameters and variables of the FE experiment, including 1) the evolution of temperature on the heater surface, in the bentonite and in the Opalinus Clay, 2) the degree of saturation and relative humidity in the bentonite and Opalinus Clay, 3) the pore water pressure in the Opalinus Clay, and 4) the strain in the Opalinus Clay.

3.2.5 Ophelie mock-up

The OPHELIE mock-up simulated (full-scale with respect to the diameter, and with a length of 5 m) a section of a disposal gallery of the SAFIR-2 reference design (valid in the 90s) as far as the buffer material and the disposal tube were concerned. The initial objective of the mock-up was to verify some practical aspects like the robustness and performance of the sensors in harsh conditions over a period of several years, the specification, manufacture and placement procedures for the buffer material and the hydration process for this material (Van Humbeeck et al. 2009). The mock-up also served as a preliminary investigation into the buffer material's thermo-hydro-mechanical behaviour and an observation of its evolution, during 4.5 years (1997-2002) of hydration and heating, through the monitoring and post-mortem analysis programme.

The mock-up's metallic structure was composed of a main jacket, two covers and the central tube simulating the disposal tube. The hydration system was fixed at 1 MPa to saturate the buffer. The buffer material consisted of pre-fabricated blocks of a mixture of 60% FoCa clay, 35% sand and 5% graphite uniaxially compacted at 61 MPa. A complete buffer section consisted of three concentric rings.

The operational stage of the mock-up consisted of the following phases: hydration at ambient temperature, heating with continuing hydration and cooling phase. The heating phase, at 170°C, started six months after the start of hydration (when the buffer was mostly saturated and a high thermal conductivity was measured) and lasted 4.5 years. The mock-up was then cooled down rapidly by switching off all heating elements six weeks before dismantling began.

Mineralogical changes observed on the exposed buffer material after 4.5 years of hydration and heating were very limited. The main modifications concerned the presence of gypsum where the buffer made contact with the central tube, at the interface with the stainless steel liner at the periphery and in the joints between blocks. An enrichment of chemical species towards the central tube (chlorides…) was identified, combined with an impoverishment of chemical species like bicarbonate or sulphate towards the tube.

Overall, from a thermo-hydro-mechanical point of view, the buffer material fulfilled its role: it retained a low hydraulic conductivity/permeability and a high thermal conductivity. However, the hydraulic conductivity of the exposed material was slightly higher than that for the initial material. All technological gaps were filled by swelling. However, the swelling process was not homogeneous. The swelling mainly occurred close to the liner and the joints between blocks, although closed, remained visible.

3.3 Effect of high temperature on buffer

Background

Mineralogical, geochemical and microstructural alteration of the bentonite buffer due to thermal, hydraulic, and chemical gradients may impair the safety functions of the engineered barrier, particularly its swelling and retention capacity (see chapter 2). These alteration processes may include loss of montmorillonite mass, cementation due to the precipitation of secondary minerals, alteration

of cation exchange capacity (CEC), and dissolution of accessory minerals). A summary by Villar et al. (2023) indicates that the most commonly reported alteration processes of bentonite are illitisation via potassium fixation in the interlayer, increase in smectite layer charge, and release of silicon (see Leupin et al. 2014, for a review). Among the main parameters triggering this transformation are temperature and potassium availability, whereas the presence of divalent cations in the interlayer and the unsaturated conditions would suppress conversion. Transformation to chlorite and saponite has also been reported (Kumpulainen et al. 2016). In addition, the accessory minerals in bentonite (sulphates, carbonates) will also be affected by the thermal gradient; their dissolution, transport, and reprecipitation could lead to significant salt accumulation close to the canisters (Fernández & Villar, 2010; Kober et al. 2021) and silica precipitation (Svensson & Hansen, 2013; Wersin et al. 2007).

Wersin et al. (2007) reviewed work assessing the performance of the bentonite barrier beyond 100°C. No significant changes of hydraulic and mechanical properties had been reported for bentonite materials exposed to temperatures of at least 120°C under wet conditions, but the data suggested significant cementation and perhaps also illitisation at 150°C and beyond. Natural analogue bentonite samples that showed substantial cementation and illitisation effects still displayed rather favourable hydraulic properties. Under dry conditions, bentonite was found to be stable to higher temperatures, maybe as high as 350°C. Hence, the mineralogical transformation of bentonite minerals that are likely to occur at temperatures of relevance (between 100°C and 150°C) seem to be limited even over very long times. The fact that in repository relevant conditions, temperatures above 100°C coincide with low water saturation (because of the slow groundwater inflow towards the engineered barrier and the existence of a thermal gradient across it) might further reduce the already slow reaction rates.

For example, in the safety assessment of SKB, the montmorillonite transformation in a KBS-3 repository is assumed to be small based on the following observations and arguments:

1. The time scale for significant montmorillonite transformation at repository temperatures in natural sediments is orders of magnitude longer than the period of elevated temperature in a KBS-3 repository (e.g. Velde & Vasseur, 1992).

2. The bentonite material is close to mineralogical equilibrium to start with (e.g. Fritz et al. 1984).

3. Transformation is limited by low transport capacity, principally regarding potassium (Hökmark et al. 1997) and silica (Karnland & Birgersson, 2006).

4. All published kinetic models, based both on natural analogues and laboratory experiments indicate that the transformation rate is very slow under repository conditions (e.g. Huang et al. 1993).

The montmorillonite transformation process can also be quantified by modelling. Based on the above description, no mineral transformation is expected to be faster than illitization as a result of elevated temperature. Consequently, the maximum temperature effect is modelled in the safety assessment of SKB by the kinetic expression for illitisation proposed by Huang et al. (1993) and by use of different but realistic potassium concentrations. As long as the maximum temperature is below 100°C the montmorillonite in the buffer is assumed to be stable for the timescale of the repository.

However, prior to HITEC, a fully coupled THMC 1000-year simulation of a nuclear waste repository in a clay formation with a bentonite buffer and a temperature close to the waste canister of 200°C, showed some degree of illitisation in both the bentonite buffer and the surrounding clay formation (Zheng et al. 2015). Other chemical alterations detected were the dissolution of K-feldspar and calcite, and precipitation of quartz, chlorite, and kaolinite. In general, illitisation in the bentonite and the clay formation was enhanced at higher temperature, but was affected by many chemical factors, mainly the concentration of K in the pore water as well as the abundance and dissolution rate of K-feldspar; less important ones are the concentration of sodium and the quartz precipitation rate.

Concerning the geochemical evolution, Sena et al. (2010) developed a numerical model with the purpose of simulating 1) the thermo-hydraulic, 2) transport and 3) geochemical processes that were observed in the LOT A2 test parcel (section 3.2.2). The numerical model developed was a 1D axisymmetric model that simulates the water saturation of the bentonite under a constant thermal gradient, the transport of solutes and the geochemical reactions observed in the bentonite blocks. A case was modelled considering the highest temperature reached by the bentonite, 130 and 85°C near the copper tube and near the granitic host rock, respectively. The transport of solutes during the bentonite water saturation stage is believed to be controlled by water uptake from the surrounding groundwater to the wetting front and, additionally, by a cyclic evaporation/condensation process (Karnland et al. 2009a). Once bentonite is water saturated, the transport of solutes is driven by diffusion. However, the transport of chloride was modelled taking into account advective, dispersive and diffusive fluxes that are believed to have occurred under the high temperature in the LOT A2 test. The computed evolution of the bentonite saturation and the simulated transport of chloride were in good agreement with data measured at the end of the test, reflecting the reliability of the conceptual model defined. The main geochemical processes that are believed to have developed during the LOT A2 test are (Arcos et al. 2006): 1) precipitation/dissolution of carbonate, sulphate and silica minerals and, 2) cation exchange in the montmorillonite interlayer. Numerical results predict the dissolution/precipitation of anhydrite, calcite and silica in the heated bentonite in agreement with data measured at the end of the LOT A2 test.

Sellin & Leupin (2013) identified as a safety-relevant issue the effects on bentonite of long periods of unsaturated conditions with elevated temperatures. In particular, the question of how this may influence the subsequent swelling properties after full saturation was discussed in Johnson et al. (2014) from a literature review perspective. The evidence found was not completely consistent, but showed that significant reduction in swelling pressure can occur in some cases above 110-120°C, although in most cases in which swelling pressure was measured, values of more than 50% of initial values were observed. It was noted that if fully saturated samples were exposed to short-term laboratory heating as high as 150°C and swelling pressure and hydraulic conductivity were measured after cool-down, property changes were small compared to reference untreated samples (Dueck, 2014). Furthermore no significant changes were found after the six-year duration LOT study, performed at Äspö (section 3.2.2), in which the bentonite experienced temperatures up to 130°C (Karnland et al. 2009a).

Experimental work performed during HITEC

The study of the effect of temperature on bentonite properties can be tackled either by analysing the change of properties of preheated material or the properties of the bentonite at high temperatures. Both cases were dealt with in HITEC because they are complementary.

In the first instance, the material can be heated in the laboratory (usually in powder form) or come from the dismantling of a TH cell or an in situ test, where samples for postmortem analyses are obtained. The determination of characteristics and properties of preheated material intends to ascertain if they have permanently changed as a result of the treatment at high temperature. The thermal phase of the repository will be transient, and there is a need to ascertain if the drying and heating that the buffer will experience during this period entail irreversible consequences on its properties. The properties of these preheated materials are usually tested at laboratory temperature and compared with those obtained in non-heated material to assess the changes during operation (section 3.3.1).

In contrast, the aim of the THM tests that are performed in non-treated material at high temperature is to determine the parameters that define the behaviour of the buffer while in operation, i.e. under high temperature. These in turn could be divided into those intended to determine specific

parameters, such as swelling pressure, permeability or the water retention curves (reported in 3.3.2) and those that try to simulate the conditions of the barrier in the repository with respect to the hydraulic and thermal gradients, while following the evolution of the buffer behaviour (reported in 3.3.3). As indicated above, the latter provide also, upon dismantling, preheated material to analyse the potential changes in buffer characteristics or properties.

The following subsections summarise relevant results taken from recent literature and the advances made during the HITEC project and reported in the project deliverables connected to Task 3 D7.7, D7.8 and D7.9 (Svensson et al. 2023a; Graham et al. 2023; Villar et al. 2023a, respectively), grouped according to the classification detailed in the previous paragraphs.

3.3.1 Preheated material

The preheated material used in HITEC came from field and laboratory experiments. Consequently, there were significant differences in the spatial and time scales considered. Furthermore, even among the laboratory tests there can be a large variety of scales and actual conditions of treatment. For example, in the studies reported below, the bentonite was treated under thermo-hydraulic gradient (field and laboratory cell tests) or just heated without simultaneous hydration. Among the latter, some treatments were performed with dry bentonite and others with wet bentonite, either allowing evaporation during heating or not. These experimental conditions may have an effect on the changes observed and should be considered when assessing the results.

3.3.1.1 Laboratory treatment at constant temperature

Tests in which the material is preheated are usually carried out with powder materials in dry state or mixed with water at different solid:liquid ratios. Tests of this kind concerning montmorillonite mineralogical stability were reviewed by Leupin et al. (2014), who classified them as:

- smectite-to-illite hydrothermal experiments with MX-80 bentonite at temperature of 270°C that reveal no evidence of any illitisation even with variable potassium activity conditions;
- experiments on thermal stability of montmorillonite at 90-150°C, showing montmorillonite dissolving and releasing silica, altering the montmorillonite towards beidellite;
- experiments on the effect of steam on the swelling capacity of bentonite at temperatures up to 200°C showing that high-temperature water vapour and unsaturated conditions do not cause significant reduction of the water uptake capacity of montmorillonite.

Steam heating is in fact an extreme treatment, carried out in high-pressure vessels (autoclaves, made out of stainless steel, titanium, PEEK) at temperatures much higher than those currently considered in repository concepts (Leupin et al. 2014, Heuser et al. 2014), usually carried out using low solid:liquid ratios and with materials previously purified. The studies are designed to analyse illitisation process (that needs high temperature and potassium content in the system), cementation (silica precipitation) and loss of swelling capacity (in terms of water uptake or interlayer changes). The results obtained in this kind of tests depend on solid:liquid ratio, time, temperature, potassium concentration in pore water, layer charge of smectite or interlayer cation. Perhaps because of the variety of factors that may impact the results, there is no general agreement on the effect of steam on bentonite properties, although none of the "new" studies point to drastic changes, but to slow changes in the smectite character (from montmorillonite to beidellite) or layer charge (Wersin, 2007; Leupin et al. 2014).

In the framework of the Safe Barriers project (RWM 2017), the impacts of corrosion products, ionic solutions and heating on the behaviour of bentonite were explored (Davies et al. 2017). Experiments were conducted using 1:10 bentonite suspensions in NaCl, $CaCl_2$ and KCl solutions (up to 1 M) with steel coupons, and in constant volume test cells with compacted bentonite. Data for heated (up to 150°C) samples, and those exposed to iron corrosion products, yielded low reductions in swelling

indices, compared to those exposed to saline solutions (Davies et al. 2019). These data do not, however, reflect impacts upon the swelling pressure of highly compacted bentonites, which is arguably a more safety relevant property than free-swelling index.

The tests mentioned above generally refered to materials with low solid/liquid ratio that may not be fully representative of the actual repository conditions. Tests using compacted bentonite with much higher solid:liquid ratios (up to 1:50) were performed by Valter & Plötze (2013), with MX-80 bentonite with different degrees of saturation stored at different temperatures in a closed system. They showed a high mineralogical stability but considerable changes in physicochemical properties, particularly above the critical temperature of 120°C. The cation exchange capacity decreased during heating at 150°C by approximately 10%. The specific surface area dropped by more than 50%. The water vapour adsorption ability dropped by 25% already within three months at 120°C. These changes were mostly related to the variations in the interlayer cation composition (a slight conversion from the sodium to an earthalkali form of the bentonite) and to smectite aggregation processes.

In the context of HITEC several laboratories carried out preheating of bentonite under different conditions detailed in Table 3-8 and analysed the changes occurred. A summary of the findings for the different bentonites analysed reported in deliverable D7.7 (Svensson et al. 2023a) is given below.

Table 3-8: Summary of experiments with powder preheated bentonite carried out in HITEC

Organisation	Bentonite	Solid:liquid ratio	Temperature (°C)	Duration (months)
UH	Bara-Kade	1:20	150	8-36
VTT	Bara-Kade	Dry (open)	105, 150	6
KIPT	PBC	Dry (airtight)	150	6, 12
SIIGNASU	PBA-22 Extra	Dry (open)	150	3, 6, 18
SIIGNASU	PBA-22 Extra	1:2.2	150	18
ÚJV-CEG CTU	BCV	Dry (open)	150	6-24
ÚJV-CEG CTU	BCV	1:2	150	6-24
CU	BCV	Dry (open)	150	12

Wyoming-type bentonite

The University of Helsinki studied the impacts of increasing heat load (150°C, up to 3 years) on a Na-Wyoming bentonite buffer material (Bara-Kade, used as supplied), heating vessels with solid:liquid ratio 1:20 and using reference water for the Onkalo site in Finland (Vuorinen & Snellman, 1998). To provide a quantitative and mechanistic description of the effects of elevated temperature on bentonite/radionuclide interactions combined Sr sorption isotherm experiments and extended X-ray absorption fine structure (EXAFS) analyses were used. Visible bentonite alterations with increasing heat treatment time were seen in the XRD patterns (Figure 3-3, left), namely an increase in the basal reflection from 10.05 Å to 12.13 Å over 30 months, which is consistent with a decrease in exchangeable Na^+ and an increase in Ca^{2+}. The cation exchange capacity increased after 22 months of heat treatment (from 91 to 98 meq/100 g), which is contrasting to literature (e.g. Kaufhold & Dohrmann 2010). In Sr-90 sorption isotherm experiments (Figure 3-3, right), a large difference in Sr uptake in neutral, pH 8, (approx. 40%) vs. alkaline, pH 13, (approx. 90%) regimes, with slightly lower uptake on heat-treated bentonite than fresh.

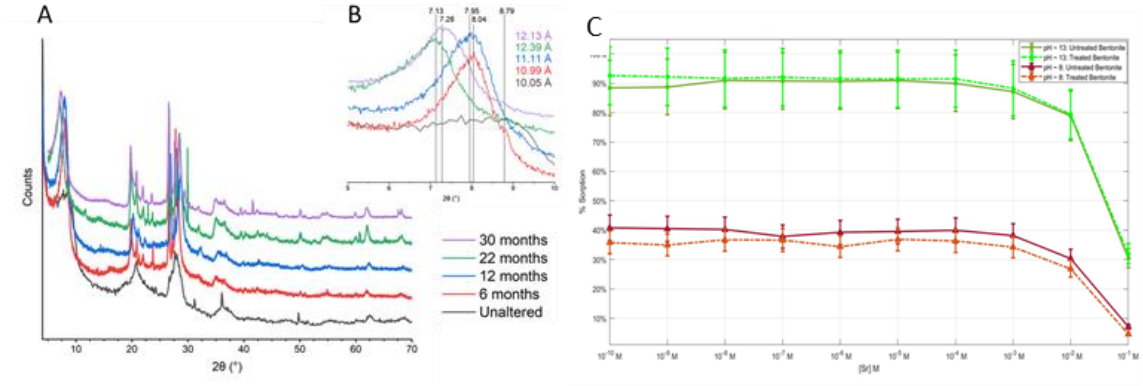

Figure 3-3. A. Changes in XRD patterns for unaltered bentonite (black) vs. 150 °C heat treated systems (coloured lines); B. changes in the basal reflection (marked with vertical lines), values in Å given in colours; C. Sr isotherms for treated (22 months, 150 °C) and untreated bentonite at pH 8 and 13

The same kind of bentonite was used by VTT to perform volumetric, isotropic compression and shear tests in powder samples preheated at 105 and 150°C for 6 months. The treated samples were wetted either by water vapour equilibrium (to minimise dissolution of minerals and cation exchange) or by mixing with liquid water (much faster) to water content of 17%, which is the bentonite average installation moisture in the Posiva's disposal concept (see section 2.6). Afterwards the samples were isotropically compacted to a dry density of 1.6 g/cm^3 following compression-decompression cycles (ranging from 0 to 12 MPa) with simultaneous measurement of volume changes. This procedure provided data on volumetric elastoplastic behaviour. It was concluded that heat treatment of the powder did not affect the volumetric compression properties of bentonite.

Ukrainian bentonites

The Ukrainian sodic bentonite PBC was heated at 150°C for 12 months in the delivery state, i.e. with no water addition and under airtight conditions, for which reason the water content of the clay remained equal to the initial one during heating (7.4%). Comparison of XRD data for the initial bentonite and after heat treatment showed that no phase transformations occurred during heat treatment, the weight ratios of the mineralogical phases (quartz, calcite and montmorillonite) remained. The powder material was compacted after treatment to different dry densities with the water content of 7.5% and the swelling pressure was measured at room temperature. A reduction of swelling pressure in the samples preheated was observed, particularly for those heated for longer time (Figure 3-4).

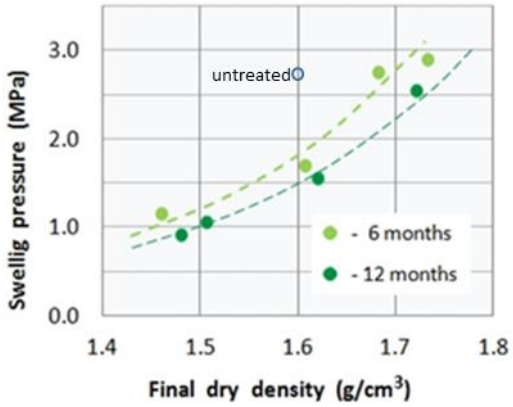

Figure 3-4. Swelling pressure of PBC bentonite compacted to different dry densities after treatment at 150°C in dry conditions for different periods of time

Another Ukranian bentonite, of reference PBA-22 Extra, was also submitted to heating at 150°C under dry and wet conditions (Zoblenko et al. 2023). The samples heated at dry conditions lost the interlayer water (decrease of the (00l) reflections with heating time), but restored it when montmorillonite was saturated with water. The *d* spacing of the (060) reflections increased with time of heating from the original 1.504 Å value to 1.505 and 1.506 after 6 and 12 months, respectively. After 3 and 6 months of heating the CEC decreased to 79 and 73 meq/100 g, respectively, whereas the BET specific surface area decreased to values of 90-100 m^2/g and 75-80 m^2/g, respectively. The influence of temperature on the swelling pressure and hydraulic conductivity of Ca-bentonite after dry processing was shown to be negligible within the limits of measurement errors.

Czech bentonite

The Czech bentonite BCV was heated in powder form at 150°C for periods of time between 6 and 24 months under dry (with evaporation allowed) and wet (1:2 solid:liquid ratio in a hermetic vessel) conditions. This preheated material was subsequently analysed by CTU and ÚJV at room temperature. The dry material was simply allowed to cool down before being tested, whereas the wet material was dried at 60°C for two weeks, ground into powder similar to the dry material and tested.

No significant changes in mineralogical composition were detected by ÚJV using XRD, the percentage of smectite in the illite/smectite mixed-layer remained the same (80±5 %) in all samples. After heating under wet conditions the basal reflection changed from 14.63 to 15.19 Å. A slight decrease of cation exchange capacity in dry samples and a slight increase in wet samples was detected, well correlated with the slight decrease of specific surface area observed in the samples treated in dry conditions and the increase observed in the samples treated in wet conditions (Table 3-9). While in dry samples Mg^{2+} prevailed as exchangeable cation over Ca^{2+}, the opposite occurred in wet samples. Given that the mineralogical composition and illite/smectite ratio did not significantly change, it can be presumed that these decreases were given by the changes within montmorillonite layer structure, probably the collapse of some of the montmorillonite interlayer spaces. Lower Cs distribution coefficients were found for dry heated samples as the treatment time was longer, which was attributed to an actual reduction of the sorption sites.

Swelling pressure and hydraulic conductivity were measured in samples compacted at different dry densities (from 1.4 to 1.8 g/cm^3) by CTU, CU and ÚJV. The swelling pressure of the dry treated bentonite was not affected by elevated temperature in the low dry density range, but lower swelling pressure was observed at dry densities higher than 1.6 g/cm^3, although possibly within the variability range (Figure 3-5). In contrast, the values measured in wet-treated samples were in the upper range

of the expected values. No decrease of swelling potential due to thermal treatment was observed in samples dry heated for 12 months. Regarding hydraulic conductivity, it was shown to increase with respect to the reference values for all dry densities in samples treated under dry conditions irrespective of the treatment time and remain approximately the same (or even lower) for the wet treated samples (Figure 3-6). Consistently with these results, the liquid limit, specific surface area, cation exchange capacity and swell index of the dry treated bentonites were lower than the values measured in the untreated bentonite, whereas they were close or slightly higher for the wet treated samples (Table 3-9).

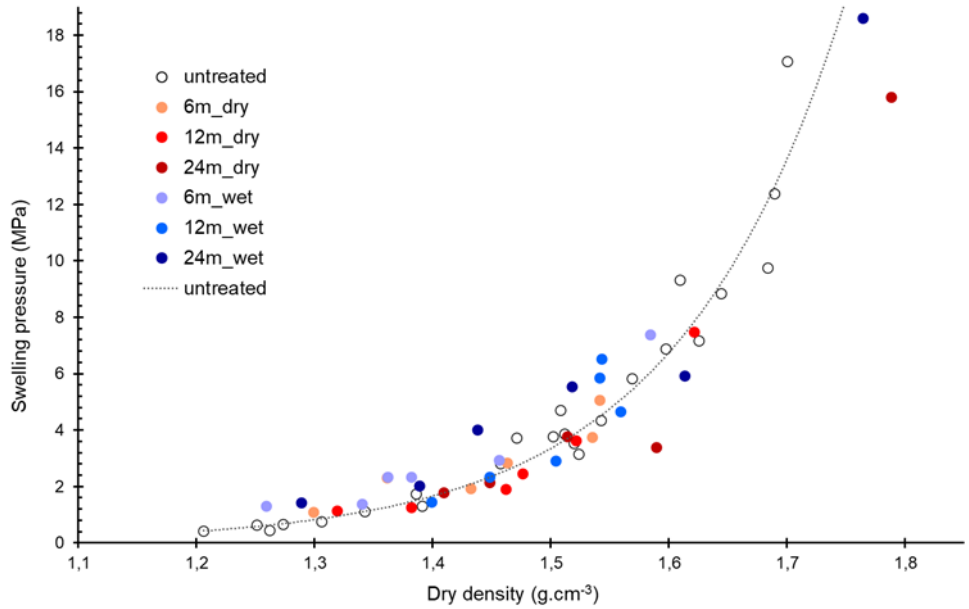

Figure 3-5. Swelling pressure of BCV bentonite preheated for 6, 12 and 24 months in dry and wet state

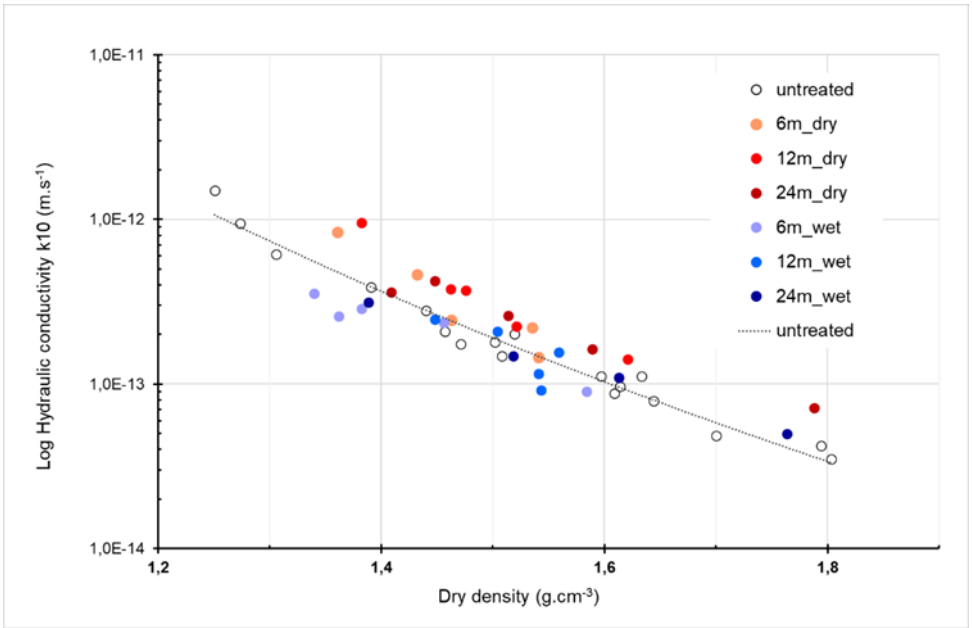

Figure 3-6. Hydraulic conductivity of BCV bentonite preheated for 6, 12 and 24 months in dry and wet state

Table 3-9. Physico-chemical properties of BCV bentonite after preheating

Material	Liquid limit (%)	Swell index (mL/2g)	CEC (meq/100g)	Sum of EC (meq/100g)	SSA (m^2/g)	Exchang. Ca^{2+}	Exchang. Mg^{2+}	Exchang. Na^{+}
BCV ref	141	8.3	59.9±2.6	62.0±3.9	478±4	26.0	57.7	13.5
6 m dry	130		55.0±2.4	59.1±2.1	437±4	36.5	47.2	11.8
12 m dry	125	6.9	50.9±1.3	58.5±1.9	423±3	38.5	45.0	11.7
24 m dry	120	6.4	53.7±0.1	57.9±0.9	416±2	40.3	43.8	10.5
6 m wet	143		60.4±1.3	65.0±0.9	487±8	53.4	31.1	11.8
12 m wet	134	10.1	64.8±0.5	64.8±6.3	500±7	58.9	27.6	9.6
24 m wet	127	8.8	69.8±0.1	63.0±0.1	500±5	74.0	11.3	10.8

The water retention curve was determined in preheated samples compacted to dry densities of 1.4, 1.6 and 1.8 g/cm^3 in cells with perforated lids (30 mm diameter, 15 mm height) that were placed in a high relative humidity atmosphere. A RH/T sensor placed inside the sample allowed to check the suction variation as the sample hydrated, and couple it to the water content estimated from the cell weight changes. A drying path was followed afterwards by placing the samples in a desiccator with silica gel. Figure 3-7 shows the results obtained. The samples heated under dry conditions had lower water retention capacity than those heated under wet conditions, particularly for the higher suctions. Additionally they also presented larger hysteresis between the wetting and the drying paths. Thermal loading time seems to have only a minor impact.

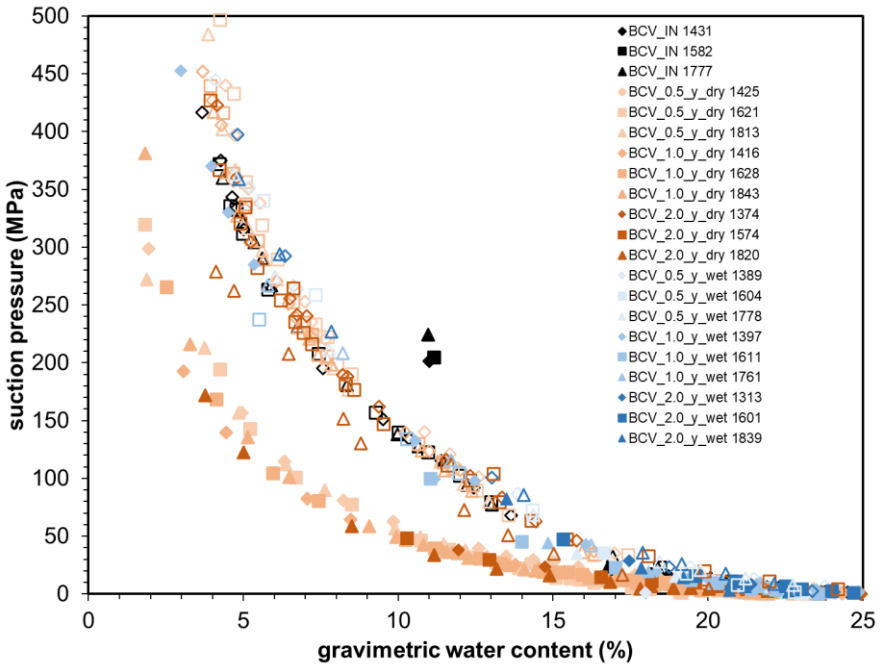

Figure 3-7. Water retention curves of the reference BCV bentonite (INPUT) and of the bentonite preheated at 150°C under dry conditions for 6 and 12 months (0.5_y and 1_y) compacted at different dry density (indicated in the legend in kg/m^3) (modified from Kašpar et al. 2021)

3.3.1.2 Material subjected to thermal gradient in laboratory cells

In thermo-hydraulic tests in cells the buffer material is subjected simultaneously to heating and hydration in opposite directions in order to simulate the conditions of the clay barrier in the repository, i.e. the interaction of the water coming from the host rock and the thermal gradient generated by the heat emitted by the wastes in the canisters. Upon dismantling of this kind of tests, the postmortem analyses of the treated buffer materials allow to observe changes in their properties and performance. In the framework of HITEC, TH tests were performed using Wyoming-type and BCV bentonites and heater temperatures above 140°C (see section 3.3.3 for a more detailed description). The modifications detected in the bentonite as a result of the TH treatment are summarised below.

Two sets of thermo-hydraulic tests were analysed by CIEMAT and UAM. The tests consisted in heating a bentonite column through the base while water was injected on top for 2.5 and ~9 years. In one set of tests, blocks of compacted MX-80 powder (10x10 cm) were used and the heater was set at 110°C. The cells were hydrated using saline and dilute water (tests C4 and C5, respectively) (Villar et al. 2021). In the other set of TH tests (consisting just of test HEE-B, Villar et al. 2022, 2023) the height of the column was 50 cm and the heater was set at 140°C. It was saturated with saline water and MX-80 pellets were used.

In tests C4-C5 no significant montmorillonite structural modifications took place during operation. Octahedral Mg relatively increased near the heater and in all the samples the layer charge decreased with respect to the values of the reference samples. Mineralogical changes were only observed in areas where the temperatures were higher than ~60°C and particularly in the few millimetres closest to the heater. Calcium sulphate (probably anhydrite) was detected in areas at less than 4 cm from the heater. Total consumption of oxygen seems to have occurred in both experiments, explaining the presence close to the heater of pyrite and oxides in different oxidation states in the case of C4. As a result of the hydration with saline water in cell C4, carbonates and sulphates precipitated at various locations, NaCl-spotted areas were observed close to the heater and corrosion occurred at the contact with the steel elements. None of these features were observed in cell C5, hydrated with glacial water. In this cell, close to the hydration surface calcium carbonates precipitated.

The changes in the pore water composition inferred from the aqueous extracts were affected by 1) the composition of the incoming water, 2) the dissolution of mineral species present in the initial bentonite as a result of the water content increase, 3) cation exchange processes. The ions coming with the hydration water and those coming from the dissolution of minerals were transported by advection and accumulated in the lower half of the columns at the bottom, precipitating closer to the heater. The overall concentration of the ions in the samples increased significantly with respect to the initial one. The maxima in sulphate concentration were accompanied by increases in the soluble sodium and calcium contents, possibly indicating the precipitation of anhydrite at less than 4 cm from the heater. The precipitation of carbonates close to the heater was reflected in the decrease in bicarbonate content from the hydration surface towards the heater.

Also at the end of the HEE-B test all the samples continued to consist predominantly of a dioctahedral smectite, with no significant differences from the original with respect to the distribution of structural cations and layer charge. Sodium continued to predominate in the exchangeable cation complex, probably as a consequence of the hydration with a predominantly sodic solution. However, some contribution of divalent cations toward the hydration surface could be detected. Despite the lack of montmorillonite alteration at the structural level, the drier samples, those that were submitted to temperatures >60°C, remarkably had a significant resistance to rehydration under room relative humidity conditions. However, this was not an irreversible process, as the samples hydrated normally when the relative humidity was high (97%) and expanded as expected when suspended in water.

Although hydration took place with a highly saline water –which seems to have inhibited the formation of colloids– the overall increase in water content allowed the dissolution of some species and the solubilised ions were transported towards the heater and precipitated at two distinct areas: sulphate, sodium, and calcium peaked at ~18 cm from the heater whereas chloride moved closer to the heater (accompanied by sodium and calcium), concentrating at 9 cm from it, coinciding with a vapour leak area. This leak started at some undetermined moment during the test through a sensor inlet. This experimental artefact seems to have conditioned the processes around it, such as the movement of solubilised ions. The liquid-water availability was probably affected also in the areas of temperatures higher than 60°C, which would limit the reactivity there. Nevertheless, evidence of precipitation of calcite and calcium sulphates and dissolution of cristobalite and quartz were observed in the areas where the temperature was higher than 100°C (Villar et al. 2023).

Around this sensor inlet the specific surface area of the bentonite was lowest, indicating aggregation of particles likely caused by shrinkage when water evaporated from bentonite whose water content was higher prior to the start of the leak. From this point towards the heater the bentonite was disaggregated, with specific surface areas smaller than the initial one. Lower BET specific surface areas have been systematically observed in TH tests towards the heater. Values as low as 5 m^2/g were measured in a test performed with Bara-Kade bentonite performed under the same conditions and duration of test C4 (Wyoming-type bentonite, hydration with saline water, 2.5 years) but with higher heater temperature (150 vs. 110°C).

The swelling pressure and hydraulic conductivity of the samples at the end of the TH tests were related to dry density following the trend expected for the untreated bentonite, irrespective of the kind of hydration water or duration of the TH test (Villar et al. 2021, 2022). The slightly lower swelling pressure after the TH treatment was justified by the higher initial water content of the samples. The hydraulic conductivity values after the TH treatment were below the ones obtained for the untreated bentonite, which could be explained by the "maturation" of the microstructure during the thermo-hydraulic treatment, with the average pore size becoming smaller and more homogeneous over time. However, these observations only apply to samples that reached a high degree of saturation at the end of the TH treatment and were subjected to a maximum temperature of ~100°C (cells C4 and C5) and even lower (~34°C) for cell HEE-B. The BCV samples treated by CTU for much shorter times (<1 year) at temperatures of up to 150°C showed no changes in hydraulic conductivity, permeability and liquid limit with respect to the untreated bentonite, provided the postmortem degree of saturation was high. In contrast, the samples that remained with a low degree of saturation during the TH treatment period showed higher postmortem hydraulic conductivity and lower liquid limit, in agreement with the results obtained in samples that were oven dried (section 3.3.1.1). No alteration of swelling pressure was observed though.

3.3.1.3 Material subjected to thermal gradient in large-scale tests

Large-scale in situ tests are performed in underground laboratories with demonstration purposes and to reproduce representative conditions of the buffer for long periods of time. Their dismantling provides relevant postmortem information about the modifications experienced by the barrier material and the processes that took place during operation. In the SKB field experiments at Äspö using various bentonites (some of them described in section 3.2), at least the following mineralogical and geochemical processes related to the thermal gradient were identified:

- Stiffening of the buffer (LOT, Karnland et al. 2009).
- Accumulation of non exchangeable magnesium towards the heater (LOT, ABM, Prototype, e.g. Karnland et al. 2009, Olsson et al. 2013, Svensson 2015).
- Dissolution of cristobalite close to the heater (e.g. Svensson & Hansen, 2013).

- Formation of oxygen-sensitive Fe(II) phases at steel/bentonite interface (Svensson & Hansen, 2013).
- Formation of ferrosaponite/saponite associated with a high increase in Mg (ABM2 with FEBEX bentonite, Svensson 2015).
- Accumulation of $CaSO_4$ (gypsum/anhydrite) (LOT, Prototype and ABM).
- Local accumulation of NaCl (halite) (ABM2).
- Physical disintegration of bentonite blocks, in some parts along with halite accumulation (ABM2).

In particular, the ABM experiment (described in section 3.2.1) performed at the Äspö URL offered valuable insights into iron-bentonite interactions and temperature impact on a diversity of bentonites in repository-like conditions (e.g. compacted clay, non-powdered metallic iron, swelling pressure from the clay, large scale, in situ placement at repository depth, and natural water sourced from the bedrock). The ABM5 parcel was retrieved in 2017 after 4.5 years of heating. The temperature in the buffer was initially below 100°C, and then it was increased stepwise to values 100-150°C (depending on the location) and finally to values 150-250°C for almost a year (Figure 3-2).

The changes in the mineralogy, geochemistry and hydro-mechanical properties of four different bentonites (section 3.1.4) were analysed by various laboratories. SKB made the following observations (Svensson et al. 2023b):

- No general significant alteration of smectite in the bentonite was observed.
- Minor changes were detected in the cation exchange capacity (CEC). Cation exchange reactions made the distribution of Na and Ca more homogenous after the experiment. However, these changes did not seem to be correlated with smectite transformation or any significant impact on important properties of the bentonite, such as swelling pressure or hydraulic conductivity.
- In fact, swelling pressure and hydraulic conductivity were unaffected by the extremely high temperatures in the ABM5 experiment. Figure 3-8 shows examples for some of the samples retrieved after Ca-homoionisation.
- Corrosion products were observed at the iron/heater interface. Dissolution-precipitation of sulphate was observed, as well as cation exchange reactions.
- Minor magnesium redistribution was occasionally observed, however no or very small amounts of trioctahedral smectites were found.
- Unexpected extensive physical breakdown of some of the bentonite blocks occurred, attributed to the extremely high temperature conditions during the experiment (Figure 3-1).

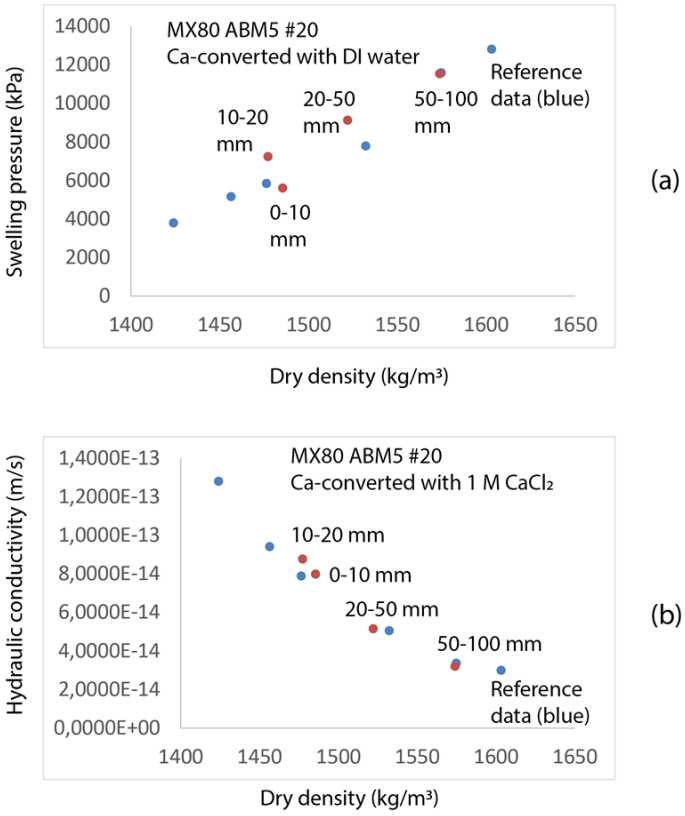

Figure 3-8. Swelling pressure and hydraulic conductivity of MX80 samples of the ABM5 #20 (red symbols, distances to the heater indicated in mm) and of the reference bentonite (blue symbols). The samples were first Ca-exchanged in 1 M $CaCl_2$ solution and then a) tested with DI for swelling pressure, b) tested with 1 M $CaCl_2$ for hydraulic conductivity (Svensson et al. 2023a)

The samples coming from the ABM5 were also analysed by BGR. Elemental profiles were produced (Kaufhold et al. 2021) and discussed by comparing them with previously measured results. Most of the blocks of ABM5 showed a slight increase of the S content in the central part and some dissolution at the inner and outer parts. This behaviour was similar to the results found in the LOT A2 experiment (Karnland et al. 2009) but much less pronounced. The redistribution of S- and C-phases, probably caused by dissolution and precipitation, did not depend on the type of bentonite. The same bentonites installed in different depths showed different profiles which indicates that the local conditions were more important than the material properties. No general trend, however, was detected when comparing dry density, water content, and degree of saturation with the chemical and mineralogical changes. On average, more Cl^- was found in the more saturated lowermost part. Most of the bentonites showed an initial Cl^- content of < 0.1 mass% and an increase in the reacted blocks which can only be explained by Cl^- derived from the rock water which migrated into the blocks. Expectedly Fe increased at the contact to the heater due to corrosion. The Fe increase, however, was smaller compared to previous tests, although this could be partially explained by the differences in the sampling depths among different tests (the sampling depth was larger in the samples from ABM5 because of the relatively small area close to the heater). Magnesium enrichment was observed close to the heater, as was also the case in many other large-scale tests, regardless of whether an iron or a copper heater was used. For the first time a clay containing trioctahedral smectite (saponite) was used in a large-scale test, and it showed a Mg decrease at the heater. The Mg enrichment and depletion may result from dissolution/precipitation processes but this phenomenon has to be investigated further. In previous tests the Mg enrichment was observed along with formation of trioctahedral domains which can be detected based on the intensity of the d_{060} XRD-reflection of the smectite. In

the ABM5 test, however, no sign of trioctahedralisation was found. Simultaneous thermal analysis (STA) proved that calcite can be involved in corrosion, leading to the formation of siderite at the expense of calcite. STA also showed that pyrite was sometimes preserved and sometimes oxidised, likely depending both on local conditions and on the characteristics of pyrite.

In summary, based on the chemical and mineralogical analyses performed on the ABM5 material and the comparison with other tests it was not possible to detect any specific high temperature reaction. In other words, none of the changes observed in the present study could be attributed to high temperature. Moreover, most of the changes, e.g. Mg enrichment, corrosion, trioctahedralisation were less pronounced compared to other tests conducted at lower temperature but for longer times with higher water contents.

3.3.2 Determination of properties at high temperature

The determination of thermo-hydro-mechanical properties (permeability, swelling/consolidation, water retention capacity, strength, etc.) at high temperature generally involves technical challenges that may come from, among others:

- the materials used in the testing cells and their reaction upon heating, which involves calibration issues;
- sourcing of seals that are not compromised at high temperatures;
- the adequacy of the sensors used, which have to be suitable not only for high temperatures, but also in most cases to harsh, aggressive environments that are boosted by heat;
- undesirable behaviours of the testing systems, such as vapour leaking.

Probably because of these concerns, testing thermo-hydro-mechanical properties at temperatures higher than 100°C is rarely done or reported in literature, as section 0 already put forward. In fact, newly developed oedometers for testing soils are designed to work at temperatures of up to just 70°C (e.g. Kirkham et al. 2020). Daniels et al. (2017a, b) identified limitations for assessing gas flow at temperatures above 150°C, and concluded that further development of apparatus is required to ensure robust data collection at high temperatures.

Nevertheless, Yoon et al. (2023) recently reported measurements of thermal conductivity of a Ca-type compacted bentonite (Gyeongju, South Korea) with different water contents at temperatures of up to 150°C. The values obtained at this temperature were similar to those obtained at room temperature.

Other hydro-mechanical properties are discussed in the following subsections, stressing particularly the advances made in the framework of HITEC (Graham et al. 2023), which have been significant both in terms of equipment development and processes understanding.

3.3.2.1 Permeability and swelling

The effect of temperature on permeability, swelling capacity and swelling pressure of compacted bentonite has been tested for many years (see for example Villar & Lloret (2004) for an initial review and Chaaya (2023) for a recent one), and it is acknowledged that this effect may differ depending on the type of material, and even on the type of cations in the exchange complex. As for the reasons behind the behaviours observed, temperature-induced transfers between intra-aggregate adsorbed water —of density higher than that of free water— and inter-aggregate free water have been invoked (see also Johnson et al. 2014).

Although most experimental evidence (including that obtained in HITEC and summarised below) reported decreases of swelling pressure with temperature, molecular dynamics simulations of the effect of temperature on swelling pressure of sodium smectite showed a gradual increase in swelling pressure with increasing temperature from 27 to 327°C, which was attributed to the increase in the

thermal motion of water molecules (Akinwunmi et al. 2019). In these simulations, the increase of the swelling pressure was higher at high dry densities in the whole temperature range.

Jadda & Bag (2020) determined the swelling pressure of two Indian bentonites at elevated temperatures (up to 95°C) using three different procedures (isothermal, incremental and decremental), and found that the effect of temperature on swelling depended on the methodology followed: in isothermal conditions the swelling pressure was found to increase for divalent bentonite with increase in temperature, whereas it was noted to decrease for the Na-bentonite. The measured swelling pressure was found to increase for both bentonites during incremental temperature condition, whereas a signifcant decrease in swelling pressure was observed in decremental temperature condition. According to these authors, the major exchangeable cations present in bentonite are responsible for the differences in measured swelling pressure of the two bentonites.

Ruan et al. (2022) discussed different factors that may affect the swelling pressure values obtained at high temperature: liquid injection rate, system compliance, side of water injection (from sample top or bottom). They tested various bentonites compacted at a range of dry densities between 1.1 and 1.85 g/cm^3 at temperatures of up to 80°C. The swelling pressure evolution curves obtained followed the usual pattern observed by many authors both at room and higher temperatures: an initial quick development followed by a decrease that is recovered and eventually ends in the equilibrium swelling pressure value, giving place to peak, valley and equilibrium swelling pressure values. They observed that the effect of temperature on the swelling behaviour depended on the fabric of the clay. For powder bentonite, the swelling pressure values at the end of the different stages increased with temperature, whereas for granular bentonite these values decreased. The authors consider that these observations resulted from the competition of interlayer swelling, inter-particle swelling, free water expansion and mineral thermal expansion.

It is clear that temperature increases the hydraulic conductivity, although this increase cannot be explained in most cases solely by the increase in water kinematic viscosity, and other reasons, such as microstructural or pore fluid chemistry changes, have been invoked (e.g. Villar and Lloret, 2004).

In a suite of isotropic and constant volume tests in custom-made cells at temperatures up to 200°C researchers at BGS found a trend for decreasing intrinsic permeability of up to an order of magnitude with increasing temperature up to ~150°C (Zihms & Harrington, 2015). Intrinsic permeability still remained below 10^{-20} m^2 for temperatures up to 150°C. Above 150°C, large increases in permeability were seen which were attributed to sample thermal contraction enabling flow along the sides, but uncertainties remained in the expected amount of vessel expansion and steam generation (Daniels et al. 2017a). Buiding on this work, during HITEC constant volume cells allowed the observation of radial and axial swelling pressures evolution at multiple locations when compacted bentonite was subject to high temperature. Testing began with samples very close to or fully saturated and constrained by the apparatus either under a constant volume condition, or with radial constraint and a limited degree of axial expansion permitted (to explore the impact of heat on density and water content homogenisation). Deioinised water was used both to prepare the samples and to saturate them during the tests. Two types of tests were conducted: 1) swelling pressure tests, where a constant water pressure of 4.5 MPa was applied to the sample for a period of between 50 and 100 days, and 2) combined hydraulic permeability and swelling pressure tests, where the sample was subjected to applied water pressure gradient of 2 MPa (with 4 MPa injection pressure and 2 MPa downstream pressure) and subjected to a series of thermal cycles. Key findings from swelling pressure tests were as follows:

– Even at high temperature (90-100°C), the bentonite was able to swell and completely fill the void space when axial strain was allowed, exerting a measurable swelling pressure (Daniels et al. 2021), which was observed to be lower towards the lower density end and at higher temperature (Figure

3-9, left). Significant heterogeneity remained in most of the observed swelling pressure distributions, which was greater in those samples allowed to swell axially. In agreement with this observation, no homogeneous state in terms of dry density or water content was reached by the end of testing.

- Measured swelling pressure was found to reduce with increasing temperature (100-200°C) for dry densities higher than 1.6 g/cm^3, irrespective of the axial constraint conditions, but for low dry densities (1.3 g/cm^3) swelling pressure was relatively insensitive to temperature. Furthermore, where swelling pressure was seen to reduce (T>100°C and higher dry densities), a notable temporal degradation was also apparent (Figure 3-9, right). Whlist both axial and radial stresses were still measurable at temperature as high as 200°C, a substantial reduction was still apparent, for example reducing by ~5 MPa between 100 and 175°C (for a dry density of 1.7 g/cm^3).
- During the thermal cycling tests, the observed reduction in swelling pressure was hysteretic and not completely recovered on returning to the initial temperature of 100°C.

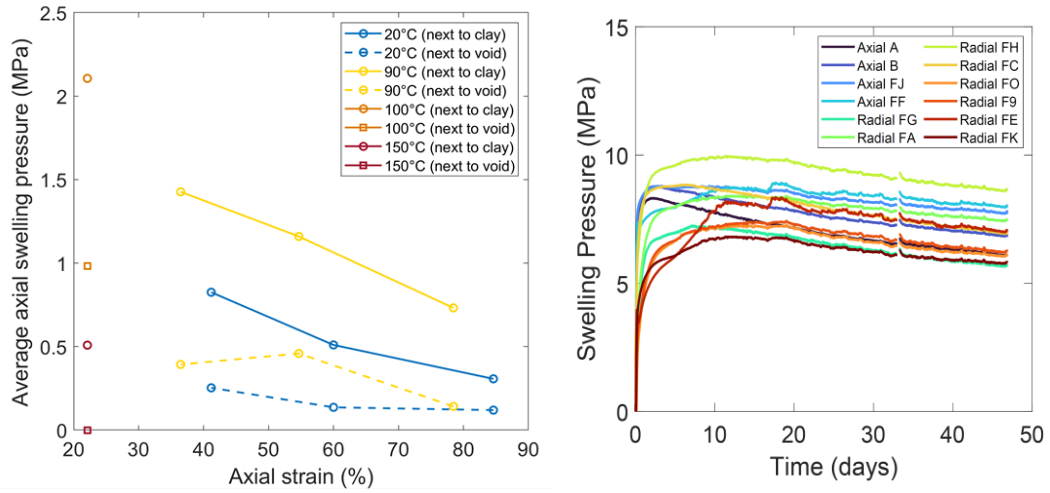

Figure 3-9. Average swelling pressure after 100 days, as a function of axial strain resulting from swelling into remaining void of MX-80 samples initially compacted at 1.7 g/cm³ (left) and swelling pressure evolution of MX-80 bentonite compacted to dry density 1.7 g/cm³ and tested at T=175°C with a water injection pressure of 4 MPa as measured by sensors located at different sample locations (right) (results of BGS in Graham et al. 2023)

Permeability tests were performed in samples that had a relatively high saturation before being allowed to fully hydrate once exposed to a temperature of 100°C. Permeabilities were then measured at increasing temperature up to 200°C. Minimal change in hydraulic conductivity was found to occur with increasing temperature, despite measured impacts on swelling pressure.

BGS proposed as one possible explanation for the observed reduction in swelling pressure at higher dry densities the thermally-induced yield of the sample between temperatures of 100-200°C (Graham et al. 2023). Contraction of the bentonite, as a result, would result in a drop in stresses under a constant volume condition and is consistent with only a minimal increase in hydraulic permeability that can be explained by flow of water along the sides of the sample. Nevertheless, they suggest that additional testing is necessary to explore this process further, as well as the observation of swelling pressure reduction with time.

X-ray tomography was used at the University of Jyväskylä and the Geological Survey of Finland to monitor wetting and swelling of temperature-controlled Bara-Kade bentonite samples (from 20 to 130°C). The samples were held in a constant cylindrical volume while wetted with simulated Olkiluoto groundwater (Vuorinen & Snellman 1998) coming from a container in the upper part of the cell. The

water was not pressurised, but for the test at 130°C the container was sealed, which would make the pressure in it increase to 270 kPa. The sample diameter was 42 mm and height 21 mm. For the saturation of the sample it was found that if venting was allowed when the temperature was higher than 100°C, water evaporated through the venting valve and the samples did not saturate. So the valve was closed during the tests at 130°C and only occasionally opened. During the wetting process swelling pressure was monitored with force sensors and X-ray imaging and/or X-ray tomography were used to monitor water transport and deformation, allowing obtaining the 3D spatial and time evolution of local partial densities of dry bentonite and water.

The X-ray tomographic method is based on the measurements of the changes in the local values of the linear X-ray attenuation coefficients. A key part of the analysis is the measurement of the internal displacements based on digital image correlations, more accurately this measurement is done using a block-matching method which is based on phase correlation (Harjupatana et al. 2015). In practise, the displacement field computations were done with the pi2 software (available at https://github.com/arttumiettinen/pi2). In order to determine an accurate quantitative estimate, a careful calibration procedure must be performed based on the known values for the initial and final average water contents of the samples. These initial and final average water contents are determined gravimetrically.

Water transport was faster the higher the temperature, so the saturation level was attained significantly faster when temperature increased. Figure 3-10 shows an approximate spatial distribution of water content inside the samples (some artefacts caused by the analysis method cannot be ruled out). The temporal evolution of the profiles of the degree of saturation suggested that diffusion may have a role in the transport process in addition to advection, because there was no clear waterfront visible in the profiles. In fact, effective diffusion coefficients were computed from the average degree of saturation, and the values obtained allowed to reproduce reasonably well the estimated profiles of degree of saturation using a simple 1D diffusion model. Nevertheless, it is acknowledged that these coefficients should depend on water content and that the role of advection and water vapour diffusion should also be taken into account.

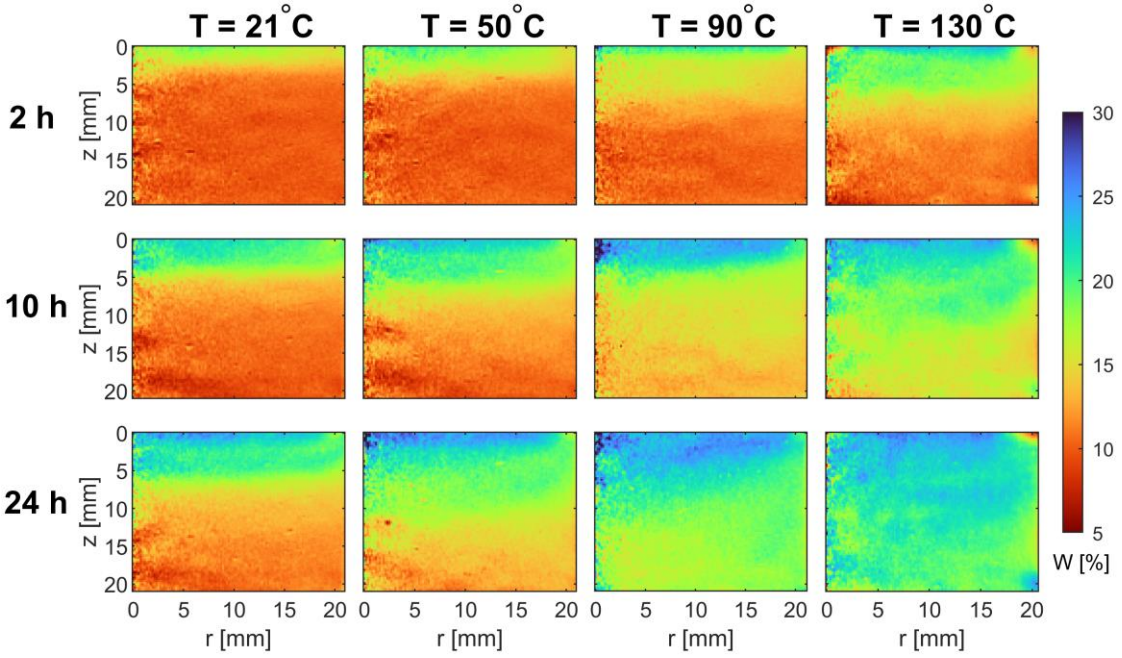

Figure 3-10. Azimuthally averaged water content at four temperatures and 3 times after the start of wetting of a Bara-Kade sample compacted at dry density 1.65 g/cm³ (results of JYU in D7.8, Graham et al. 2023)

The development of axial pressure both on top and bottom of the samples was quicker the higher the temperature, and presented the non-monotonous pattern usually observed in bentonite: an initial increase followed by a decrease that eventually leads to the final steady values. The initial peak was sharper the higher the temperature. Preliminary results seem to indicate that the effect of temperature is more significant for the higher dry densities.

The swelling pressure and hydraulic conductivity of the Czech bentonite BCV was tested by CTU and CU. In the first case the compacted samples were 30 mm in diameter and 20 mm in height. They were initially saturated with distilled water injected at a pressure of 1 MPa, permeability was measured once steady flow was reached, and after releasing the water injection pressure, swelling pressure was measured. Afterwards the temperature was gradually raised up to 130°C and the measurement of permeability and swelling pressure was repeated for each temperature step. When the temperature increased from 20 to 130°C, total pressure decreased from 1.5 to 0.8 MPa for a bentonite dry density of 1.39 g/cm^3, from 1.8 to 0.7 MPa for a bentonite dry density of 1.45 g/cm^3 and from 4.6 to 3.1 MPa for a bentonite dry density of 1.54 g/cm^3. In all cases the decrease was more significant as the temperature was higher. Remarkably, for each temperature, the axial pressure did not reach a stable value, but decreased continuously, particularly for the highest temperature. After cooling the swelling pressure did not reach the original value. As expected, the hydraulic conductivity increased with temperature.

CU performed oedometric loading tests at 20, 100 and 150°C on samples compacted to 1.6 g/cm^3. The samples were saturated with distilled water at room temperature and then backpressure was increased to 0.5 MPa, temperature was set to the target value and the samples were incrementally loaded. The slopes of the compression lines determined at different temperatures were similar. However, the position of compression lines shifted towards lower porosities with increasing temperature (Figure 3-11). Furthermore, the vertical strain of a sample saturated at room temperature under free swelling conditions was barely affected by the increase of temperature to 100°C.

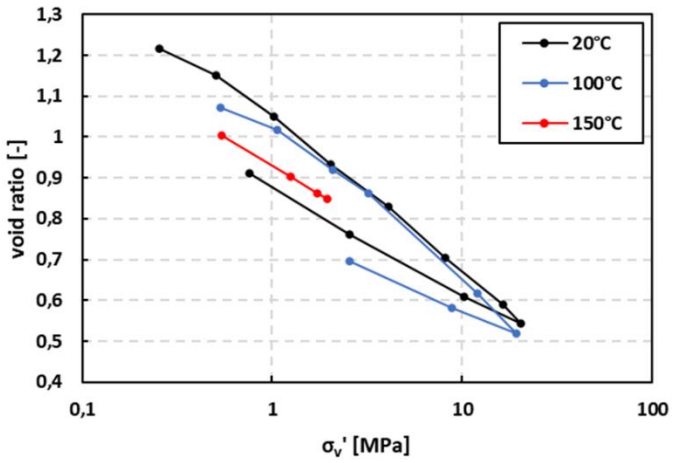

Figure 3-11. Oedometric tests performed with BCV bentonite compacted at dry density 1.6 g/cm^3 at different temperatures (results of CU in D7.8, Graham et al. 2023)

In contrast to the observations of CTU, no significant influence of temperature on swelling pressure was identified for temperatures of up to 150°C by CU in samples that had been previously saturated at room temperature. Only small variations were measured, and these could be attributed to the effect of the apparatus and the rate of thermal loading. The reason for the qualitatively different results obtained by the two laboratories is the different method of evaluation. Swelling pressure at CU was

determined shortly after heating (in the order of hours), whereas at CTU it was measured weeks after temperature application and includes the reduction in swelling pressure due to long-term high temperature exposure. In both laboratories the pressure response after heating exhibited qualitatively similar trends.

The effect of a cyclic temperature change was investigated on samples compacted at 1.6 g/cm^3 saturated at 20°C and later submitted to heating-cooling cycles up to 150°C both by CU. The final swelling pressures measured in both the heating and cooling stages gradually decreased with the number of cycles (Figure 3-12). Furthermore, for temperature higher than 50°C a continuous decrease in swelling pressure during 30 days was observed for each temperature step. This decrease was more significant as the temperature was higher. Indeed, no cyclic temperature changes will take place in a repository, but these results show that, under the conditions tested, the decrease in swelling pressure resulting from heating would be permanent, which was demonstrated by comparing the swelling pressure measured before and after the heating period.

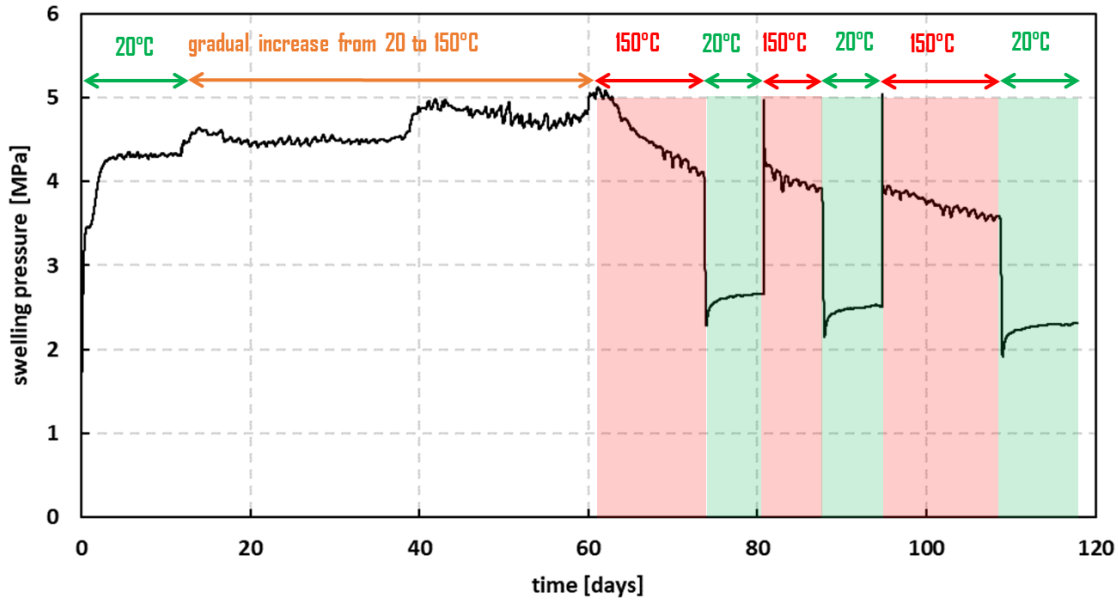

Figure 3-12. Evolution of axial stress measured during saturation and thermal cycles in a BCV sample compacted at dry density 1.6 g/cm³ (results of JYU in D7.8, Graham et al. 2023)

A miniaturized oedometer set up (9x9 mm) made out of PEEK was developed at BRGM to perform tests at high temperature with Kunipia smectite. The cell was equilibrated for 24 hours at the chosen temperature (inside an oven or using a heating jacket) before hydration through the lower piston. For tests performed at 100°C, the solution was injected with a pressure of 1.5 bar to avoid evaporation of the solution. The swelling tests were performed on Na^+ or Ca^{2+}-exchanged smectite at dry densities of 1.4, 1.5 and 1.8 g/cm^3 using solutions of NaCl or $CaCl_2$, respectively, of ionic strength 0.0001 and 0.1 M (Chaaya, 2023). Temperature speeded the saturation process (Figure 3-13), likely because of the hydraulic conductivity increase with temperature, and also decreased the final swelling pressure value of the Na-exchanged smectite, more significantly as the density was higher. In contrast, the final swelling pressure value of the Ca-exchanged samples was not affected by temperature (Figure 3-14). Hence, it seems that, in confined conditions, the temperature only affected the crystalline swelling of sodic smectite, likely because of the different affinity to water of Na^+ and Ca^{2+}. The tests performed at 150°C showed a scarce influence of the sample density and very low values with respect to those

measured at 100°C: 1.3-1.6 MPa for the Na-exchanged samples and 4.2-4.4 MPa for the Ca-exchanged ones.

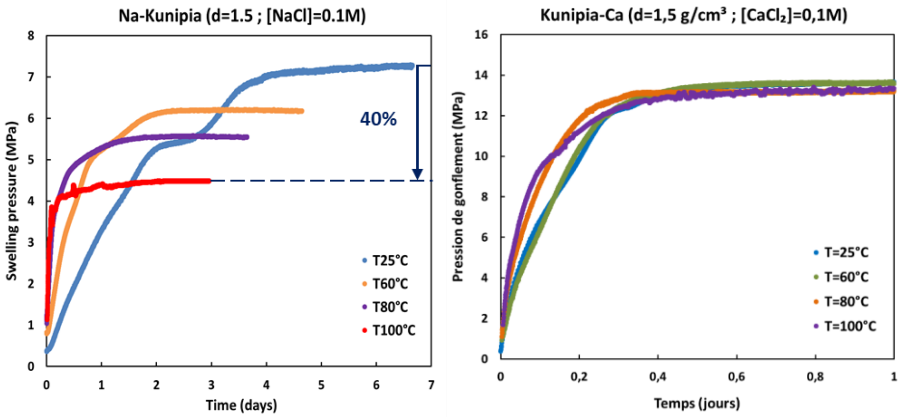

Figure 3-13. Swelling pressure evolution of Na and Ca-exchanged Kunipia smectite compacted at a dry density of 1.5 g/cm3 and saturated with solutions 0.1 M (NaCl and $CaCl_2$, respectively) under different temperatures (Chaaya, 2023)

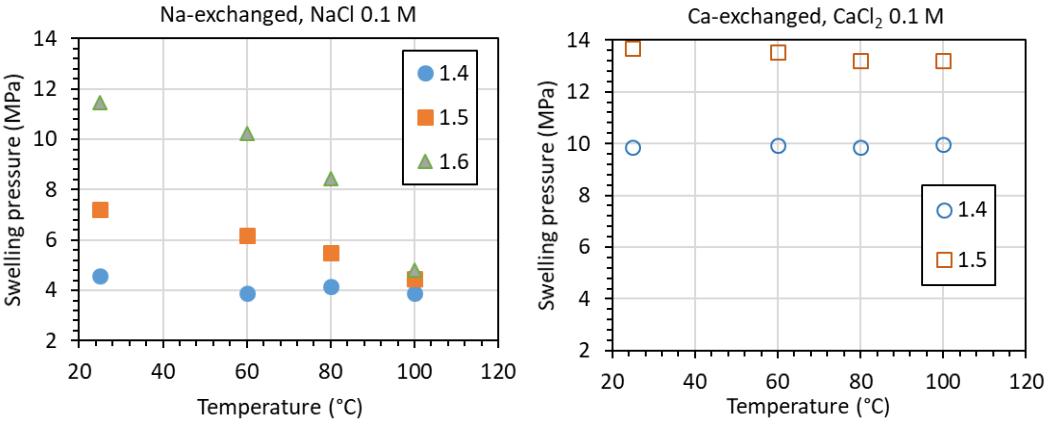

Figure 3-14. Final swelling pressure measured in homoionised samples of Kunipia smectite compacted to different dry densities (indicated in the legend in g/cm³) and saturated with 0.1 M solutions under different temperatures (data from Chaaya, 2023)

3.3.2.2 Water retention curves: adsorption processes

The methodology most frequently used to determine water retention curves is to subject the samples to different relative humidities (suctions) for periods of time sufficiently long for the material to reach an equilibrium water content. This is usually known as the water transfer technique, which is equivalent to the determination of vapour sorption isotherms. Using this technique Sun et al. (2020) determined the water retention curves of the Czech bentonite B75 compacted at dry densities between 1.3 and 1.9 g/cm^3 at temperatures of up to 80°C. The water retention capacity significantly decreased at high temperature, especially at high relative humidity (low suction). The authors were able to predict this dependence using a combination of the thermodynamic Clausius-Clapeyron equation and the Guggenheim–Anderson–de Boer model, which was also able to reproduce the independence of water retention from soil compaction (dry density) under high total suction. Ni et al. (2022) determined the water retention curves of the Chinese GMZ bentonite also using the vapour transfer technique for temperatures up to 80°C, and were able to fit the results obtained by

considering a double-porosity structure in which the microstructural deformation depends lineally on temperature.

In the framework of HITEC the sorption isotherms of homogenised Kunipia smectite at free and constant volume conditions (dry density from 1.2 to 1.9 g/cm^3) were determined in a temperature and humidity controlled chamber. Because of vapour condensation issues, the tests for RH higher than 70% could not be performed when the temperature was above 42°C. For higher temperature the limitations of this procedure became more significant. The results obtained under constant volume in samples compacted at dry densities ~1.5 g/cm^3 under 25 and 42°C are shown in Figure 3-15. For the two materials the water retention capacity decreased with temperature, but much more significantly in the case of the Na-exchanged smectite.

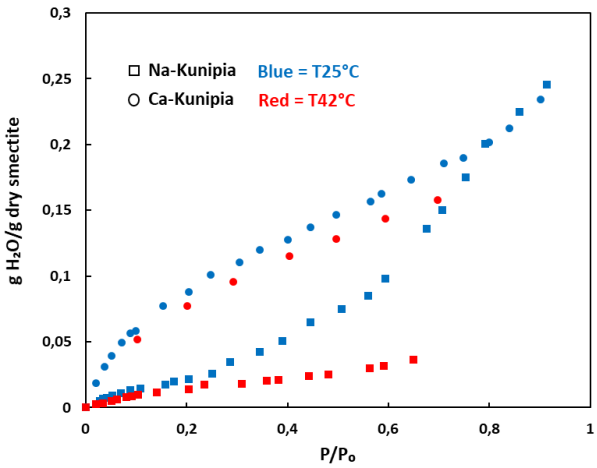

Figure 3-15. Water sorption isotherms of Na-exchanged and Ca-exchanged Kunipia smectite obtained under constant volume (dry density 1.5 g/cm^3) and two temperatures (Chaaya, 2023)

Chaaya (2023) also monitored the apparent basal spacing of Na and Ca-Kunipia using XRD analyses on unconfined oriented powder slides at 25°C and 80°C while increasing the relative humidity. Divalent smectites hydrated more rapidly than monovalent smectites at both temperatures, given their higher ionic potential (Ferrage et al. 2005). Temperature increase from 25°C to 80°C had a very negligible effect on the interlayer water retention capacity, and hence the basal spacing at 80°C was only slightly lower than at 25°C (Figure 3-16).

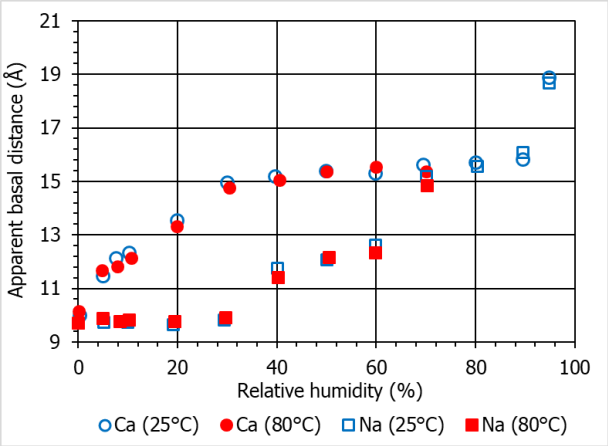

Figure 3-16. Change with relative humidity increase of the apparent basal spacings of Kunipia smectite measured in oriented aggregates (modified from Chaaya, 2023)

Another procedure to determine the water retention curve of compacted bentonite at high temperature consists in measuring the suction of samples of different water content while the temperature is kept at the desired value. For that, the compacted bentonite is kept in a stainless-steel hermetic cell that is heated on the outside. The relative humidity and temperature inside the bentonite are measured (and converted into suction) with capacitive sensors (for the high suction range) or psychrometers (suction <6 MPa). However, the determination of water retention curves in the low suction range at high temperature using thermocouple psychrometers presents the setback that they do not reach the equilibrium necessary for the measurement for temperatures higher than 60°C, which did not allow to define the curves in the low suction range as it had been foreseen (Villar et al. 2020). The measurements performed showed the usual decrease of suction as temperature increased, but the accuracy of the measurement worsened as the temperature increased, as a result of the higher uncertainty in the relative humidity measurement for the higher values. It was also concluded that the suctions measured with the capacitive sensors tended to be overestimated.

The water retention curves obtained at temperatures between 20 and 100°C showed a sharper decrease of suction with water content as the temperature was higher, particularly above 60°C (Figure 3-17). The comparison with results obtained in previous investigations for water contents <20% confirms the same trends. Suction reached 0 values for lower temperatures as the bentonite degree of saturation was higher, what is explained because the increase in temperature triggers the transfer of water from the microstructure to the macrostructure, where it behaves as free water (Lloret and Villar 2007). For temperatures above 40°C and in the range of water contents analysed, the water retention capacity of the FEBEX bentonite tended to be higher than that of MX-80, consistent with the results by Chaaya (2023) reported above concerning Na and Ca-exchanged smectite.

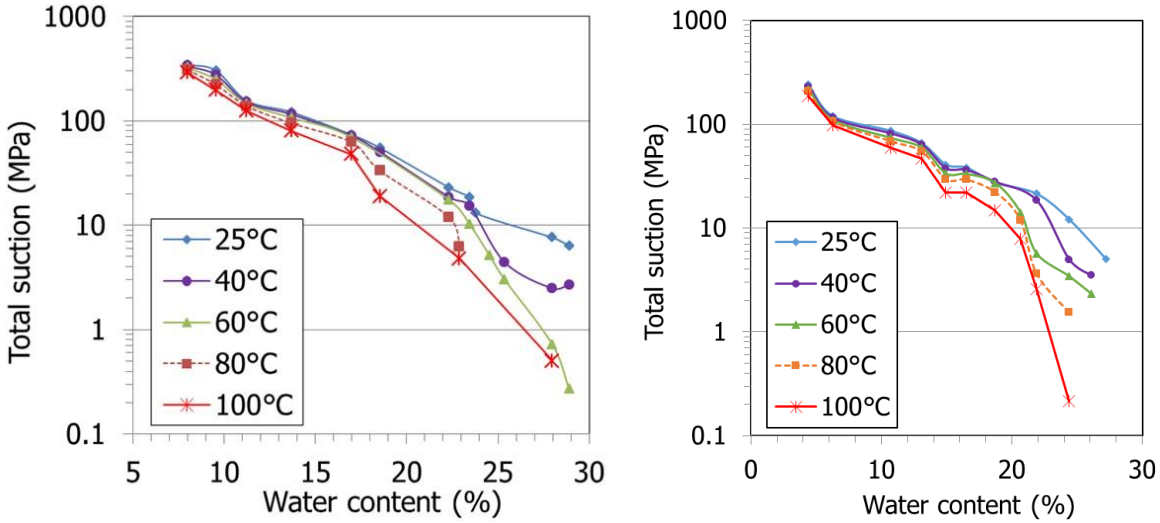

Figure 3-17. Water retention curves at different temperatures for FEBEX (left) and MX-80 (right) bentonites compacted at dry density 1.6 g/cm³, obtained during HITEC and in previous projects (*w*<20%) (results of CIEMAT in D7.8, Graham et al. 2023)

3.3.3 Small-scale simulation experiments

Laboratory tests in thermo-hydraulic cells that simulate the conditions of the buffer material in a radioactive waste repository are very useful to identify and quantify processes taking place in the engineered barrier. This kind of tests have evolved in the last decades from simple designs in which just temperatures inside the material were measured, to the current designs that involve the measurement of temperature and relative humidity, total pressure and water intake (Villar et al. 2012). These tests keep running for different periods of time (up to several years) and the analysis of the material upon dismantling includes mineralogical, geochemical, microstructural, hydro-mechanical and chemical studies, which allows gaining insights into the time evolution of the properties of the barrier.

In the TH cells the sealing material can be subjected simultaneously to heating and hydration (Figure 3-18). They are cylindrical and designed to be hermetic and non-deformable. The heat generated by the radioactive decay of the wastes in the containers is simulated by an electric heater and the simulated groundwater is injected through a porous stone or a stainless steel sinter that ensures a uniform distribution of water over the sample surface.

Although in the last years the heater was set in most tests at 100°C, two tests were performed to simulate the Äspö field test TBT (Äkesson et al. 2020), in which highly compacted MX-80 bentonite was used and the heater temperature was set to 140°C. The laboratory cell tests lasted 1.4 and 5 years, and the postmortem analyses focused on the mineralogical, microstructural and geochemical changes (Gómez-Espina & Villar, 2010; 2015). Problems to correctly measure the water intake and vapour leakages through the sensors' openings and the bottom of the cell were identified. These technological problems were solved and, in the framework of the PEBS project and to support the HE-E in situ test (section 3.2.3), two tests in which the heater was set to 140°C were launched in 2012 (Figure 3-18). Two sealing materials were tested: a granulate of MX-80 bentonite pellets (cell HEE-B) and a 65/35 sand/MX-80 bentonite mixture (cell HEE-S/B). The two materials have very different gas and liquid permeabilities, as well as water retention capacity, and this conditioned the water redistribution in the vapour phase triggered by heating as well as the liquid water intake, which were both much more restricted in the bentonite pellets. The HEE-S/B cell was dismantled after 2.8 years and evidence of soluble species transport and their precipitation close to the heater was found (Villar et al. 2016b).

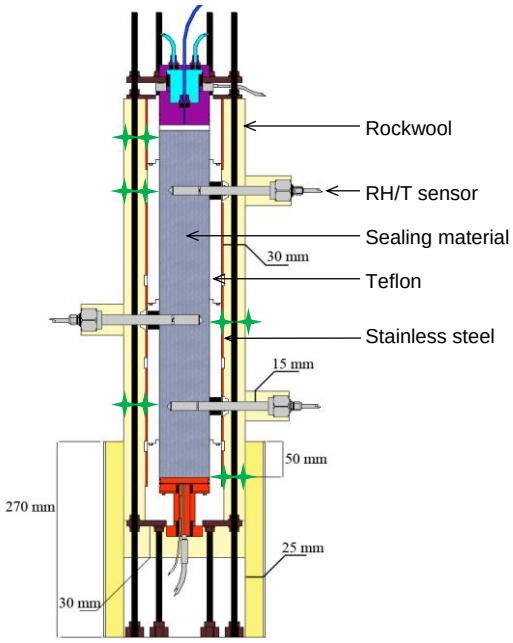

Figure 3-18. Schematic design of cell HEE-B and sensors with the external insulation (green crosses are temperature external sensor positions) (Villar et al. 2016b)

CEA performed two THM mock up tests in the laboratory on compacted MX-80 bentonite using two different initial water contents (Gatabin & Billaud, 2005). Each test consisted of two phases. In Phase 1 heat was applied to one end of the column while the temperature at the other end was kept at 20°C. A maximum temperature of 150°C was applied. Phase 2 started after thermal equilibrium had been achieved and involved the gradual hydration of the sample. A constant water pressure was applied to the end opposite to the one where the temperature variation was prescribed. Constant volume conditions were ensured in the two phases of the test. During the tests temperatures, relative humidity, pore pressure, total axial stress and total radial stress were measured. The samples had a diameter and a height of both 203 mm. The tests provided interesting information about temperature distribution, water movement and pressure development that were modelled as part of the SKB Task Force on Engineered Barrier Systems (Gens, 2019). The possible influence of the initial water content and sample length (scale effect) on the water transfer process was pointed out. In addition, conclusions concerning the instrumentation performance and gas tightness of the cell were reached.

In the framework of the Safe Barriers project, experimental work by Cardiff University explored THM-C evolution under non-isothermal conditions (Tripathy et al. 2017). Column cells were configured using compacted bentonite cylinders with heater elements at one end to achieve temperatures of 85 and 150°C, whereas the other end was maintained at 25°C. Monitoring of relative humidity, temperature and axial stress was undertaken. In parallel, hydraulic tests were conducted using the same configuration, where water was injected into the cool end of the sample. For the former, non-hydraulic tests, data highlighted moisture re-distribution occurred as a function of temperature, with greater relative humidity measured further from the heater. Increased drying near the heater over time was also observed. There was an increase in water content at the inlet end of the cell. However, difference in temperature between 85°C and 150°C and water injection pressures (5 and 600 kPa) appeared to have little impact upon axial stress over the experimental period.

More recently, a bench-scale (17 cm diameter, 46 cm length) experiment was conducted in an MX-80 bentonite compacted column (ρ_d=1.2 g/cm^3) experiencing heating up to 200°C in the axis and hydration from a sand-clay boundary surrounding the column, where the temperature was 95°C

(Chang et al. 2023). During the experiment, running for 1.5 years, frequent X-ray computed tomography (CT) scanning of bentonite provided insights into the spatiotemporal evolution of (1) hydration/dehydration, (2) clay swelling/shrinkage, and (3) displacement. The bentonite hydration was axi-symmetrical despite the initial heterogeneity due to packing, confirming the ability of bentonite to seal fast flow/transport paths. Compared to a non-heated control experiment, the heated column showed greater CT density variations along the radial distance, indicating that homogenization of bentonite might be more difficult if a temperature gradient is maintained in the repository. Precipitation of an anhydrite layer occurred in the inner hot zone.

Cell HEE-B, mentioned above, was dismantled during HITEC after 10 years of operation (Villar et al. 2022). The initial heating phase, lasting 7 months, showed that the thermal conductivity of the dry materials is low, which caused a high difference in temperature between the heater surface and the sensor located at 10 cm, generating a high thermal gradient near the heater, and low temperatures in the rest of the column. The movement of water in the vapour phase as a result of the thermal gradient was evinced by the increase in relative humidity recorded by the sensor closest to the heater –followed by a continuous decrease– and the slower increase recorded by the two other sensors (see Figure 3-18 for location of sensors). The temperatures were not affected by hydration and remained approximately constant until the end of the test. The evolution of relative humidity inside the bentonite highlighted the low permeability of the pellets. The water content and dry density distribution measured after dismantling of the column showed uniform degrees of saturation between 92 and 99% in the upper half of the column and a sharp decrease towards the heater in the bottom half of the column, with values close to 0% in the 5 cm closest to the heater. Vapour leaking through the sensor located at 10 cm from the heater could have contributed to the extremely low water contents measured in this area.

Also in the context of HITEC two tests were carried out in cylindrical stainless steel cells of dimensions 10x10 cm. The initial conditions of the Bara-Kade bentonite were the same for the two tests (ρ_d=1.55 g/cm^3, *w*=17%), and the heating phase was similar in the two tests: the heater temperature was increased from room to 150°C in 9 days, and it remained in this value for 3 months. Thermal equilibrium was quickly reached. The water vapour moved away from the heater, towards the upper part of the cell, and the bottom of the samples started to dry out. After quasi-steady hydraulic conditions were reached, hydration started with glacial water for cell HT1 and with saline water for cell HT2. The radial pressure sensors in the upper and middle parts of the cells recorded increasing trends since the beginning of hydration (quicker in the upper sensors). The pressure values at the same location were higher for cell HT1, hydrated with glacial water, which is consistent with the salinity-induced reduction of swelling capacity. Radial pressures between 5 and 7 MPa were measured in cell HT1 after 2.5 years of hydration, attesting the bentonite swelling capacity even under high temperature (Villar et al. 2023a).

3.3.4 Summary and conclusions

Different research groups determined properties and characteristics of bentonite dried at 150°C in dry and wet conditions after different periods of time up to 2 years. While no drastic changes were found in any case and for any bentonite, with remarkable preservation of the clay mineralogy, it seems clear that the slight changes observed were different depending on the drying conditions: if evaporation was allowed (dry conditions) the changes were more important, generally consisting in decreases in cation exchange capacity, specific surface area and sorption coefficients. However, heating under wet conditions had the opposite effect on these properties. Some evidence was found of changes in the cation exchange complex resulting from heating under wet conditions, with increases in the exchangeable calcium amount observed both in Bara-Kade and BCV bentonites. In any case, given that the deterioration of properties was only noticeable in the samples treated under dry conditions, it can

be presumed thus that this was caused not by the temperature itself, but probably by the loss of the water content induced by the elevated temperature. This is consistent with the changes observed in physico-chemistry, geochemistry and mineralogy of bentonite heated under thermal gradient for 10 years in the areas where evaporation was allowed (test HEE-B).

As for the HM properties of pre-heated material, the volumetric compression properties of Wyoming-type bentonite heated under dry conditions were not modified, and the swelling pressure and hydraulic conductivity deteriorated only in samples heated under dry conditions and compacted at high dry density. Also the water retention capacity was lower in samples that had been previously dry heated than wet heated, but this was to be expected given the hysteretic character of water retention.

Concerning the bentonite subjected to hydration under thermal gradient (TH tests in cells), no postmortem structural modifications of the bentonite were observed, but dissolution and precipitation of species occurred and were conditioned by the kind of bentonite and hydration water. These processes were accompanied by modification of the exchangeable cation complexes. The hydro-mechanical properties were not negatively affected if the bentonite reached a high degree of saturation during treatment, but hydraulic conductivity could slightly increase if the bentonite was heated in dry conditions (allowing evaporation). The use of pellets instead of compacted blocks does not seem to have been an additional source of uncertainty.

The material coming from the ABM5, which was also hydrated under high thermal gradient for ~5 years, did not present any noticeable specific high temperature reaction. Moreover, the modifications observed in the materials, e.g. Mg enrichment, corrosion, increase of trioctahedral character of smectite, were less pronounced compared to other tests conducted at lower temperature but for longer times with higher water contents.

The study of expansive clay materials at elevated temperatures, though started decades ago, still requires the development and improvement of testing equipment and methodologies, particularly for the application of experimental methods used for temperatures lower than 100°C to higher temperature. Special materials, such as invar, have been used in the developments made during HITEC. Vapour leakage through various rig elements (i.e. sensors' inlets) and gas tightness are among the most frequent issues. Calibration of the apparatus deformation is essential in HM tests, and failure to apply the right correction of deformation and pressures may lead to contradictory conclusions about the effect of temperature on the hydro-mechanical behaviour of clay. Other aspects, such as the accurate consideration of the dry density of the samples during testing (instead of after testing) can also significantly affect conclusions. Venting of testing cells to assist hydration may trigger sample drying at high temperatures. Precise measurement of water inflow/outflow, essential to rightly compute permeability, is also difficult, as well as the selection of the right water pressures.

The determination of properties at high temperatures is technologically challenging and it has been shown that the procedures followed may greatly impact the results. In particular the tests performed in the framework of HITEC have shown that heating under isochoric conditions a material that had been previously saturated at room temperature entailed progressive and permanent decrease of the swelling pressure with respect to the one measured at the end of saturation. This has been observed for sodic and divalent bentonites, but unexpectedly was not accompanied by impacts on hydraulic conductivity. However, saturating the material under high temperature gave place to lower equilibrium, but stable, swelling pressures, which is something frequently reported in the literature. In contrast, tests performed in purified smectite showed a decrease of swelling pressure with temperature for the sodic-exchanged material and no effect of temperature on the calcium-exchanged one.

Nevertheless, the results consistently indicate that the effect of temperature is more significant for the higher dry densities. In any case, even at the highest temperatures the bentonite had the ability to fill voids and was able to develop large swelling pressures at high densities.

The determination of water retention curves in the low suction range at high temperature has not been achieved in HITEC, neither using the vapour transfer technique (because of condensation issues) nor measuring suction with thermocouple psychrometers. Nevertheless, as expected, the water retention capacity has been shown to decrease with temperature in tests performed using different methodologies and materials, and this decrease was more significant for the predominantly sodic materials. Temperature increase from 25°C to 80°C had a very negligible effect on the interlayer water retention capacity, and hence the basal spacing at 80°C was only slightly lower than at 25°C.

Among the state-of-the-art developments in HITEC are the use of X-ray tomography to monitor wetting and swelling of bentonite samples during temperature-controlled hydration, which allowed to follow bentonite deformation and the spatial distribution of density and water content. The temporal evolution of the profiles of the degree of saturation suggested that diffusion may have a role in the transport process in addition to advection. Hydration and swelling pressure development were quicker as the temperature was higher.

3.4 State of THM models' development

One of the objectives of HITEC was the development and validation of suitable THM models for clay buffer at temperatures higher than 100°C and the incorporation in them, if necessary, of the processes identified during the WP activities, mostly those in subtask 3.3 "Small-scale experiments". A conclusion from the PEBS project (Johnson et al. 2014) was that the THM formulations developed and validated for temperatures below 100°C can be extended without modifications to temperatures above that value. Variations of retention curve, water permeability and surface tension with temperature can be taken into account without any modification of the basic formulation.

In the SKB Task force of Engineered Barrier System reported in Gens (2019), several teams modelled laboratory small-scale THM tests (some of them introduced in section 3.3.2). Some of the conclusions related to the thermal problem were:

- The main difference between the general formulations was their capacity to incorporate or not the air balance equation. Without the gas equation, the usual assumption is that gas pressure is constant. This may lead to non-physical situations if the vapour pressure exceeds 1 atmosphere when temperatures rise above 100°C.
- The only thermal effect considered on mechanical behaviour was the thermal expansion derived from a constant coefficient of thermal dilation.
- The dominant heat transfer mechanism identified was conduction. Hence, a good modelling of the thermal problem requires the consideration of the changes of thermal conductivity with degree of saturation.
- The differences between computed and observed hydraulic results were more apparent in the non-isothermal tests. The reason might be though, the existence of unnoticed vapour leaks from the testing cells not accounted for in the models.

Prior to HITEC, Thatcher (2017) performed a coupled THM modelling for the FEBEX experiment that built upon a HM model, called the Internal Limit Model (ILM), which was used for an MX-80 bentonite and sand mixture. Thatcher (2017) documents the first application of this model to an alternative bentonite, with the addition of thermal coupling, and tests its transferability to a large scale emplacement experiment. It was concluded that it is possible, after minimal calibration, that the model was effective at describing the THM evolution of the experiment, despite the new addition of thermal

parameters and the different materials modelled. It also concludes that under high strains, the bentonite behaviour is more akin to a fluid than an elastic material.

Also Ghiadistri (2019) developed a new constitutive framework for compacted highly expansive clays, which was implemented into the Imperial College Finite Element Program (ICFEP, Potts & Zdravkovic, 1999). The model built upon a single structure model previously developed at Imperial College (Georgiadis et al. 2005, Tsiampousi et al. 2013) by extending the formulation to capture the double porosity structure characteristic of highly expansive clays. The model was validated using available experimental data, demonstrating substantial improvements in the numerical predictions of the hydro-mechanically coupled processes in compacted bentonite, compared to those of the single-structure model. In conjunction with the THM formulation of the governing finite element equations in ICFEP, the model successfully reproduced the behaviour of compacted bentonite clays both at the laboratory scale, in the simulations of a series of swelling pressure tests, and at the field scale, in the simulation of the FEBEX large-scale experiment. A key outstanding knowledge gap identified by this research was a lack of experimental data to enable the quantification of the microstructure of compacted bentonites, which influences the calibration of microstructural parameters of the new constitutive model.

During the HITEC project UPC developed and verified a double-structure constitutive model (BExM-T) that incorporates the effects of temperature and considers the hydro-mechanical coupling between the micro- and macro-pore levels and the definition of retention curves for each structural domain (Vasconcelos, 2021). In addition, the following features were formulated and verified: i) possibility of decoupling between the elastic response of micro and macro levels, ii) dependence of the Bishop parameter (mechanical behaviour of microstructure) on the effective saturation of the micropores, iii) evolution of water retention curves with the structural changes at micro and macro levels. This model was applied to simulate the column test described in section 3.3.1.2 with MX-80 pellets. The simulations performed incorporated a number of relevant processes observed in the laboratory test such as heat conduction, water phase changes, vapour diffusion, differential thermal expansion of the solid and the liquid phases and swelling behaviour induced by thermo-hydraulic actions. The model predicted satisfactorily the evolution of temperature, RH, water intake and axial stress during the whole duration of the test; larger discrepancies, however, were observed regarding the final state (dry density, degree of saturation) of the bentonite column. Improvement of the constitutive model to include features such as the dependence of the water retention curves on the evolution of the pore volume fractions in micro and macro media, may be necessary (Vasconcelos et al. 2023).

Mašín (2017) developed a coupled thermo-hydro-mechanical model based on hypoplasticity principles combined with the concept of double structure by a hierarchical enhancement of the earlier model by Mašín (2013), which did not consider the effects of temperature. To include the thermal component, additional thermal dependency was introduced for water retention curves, volumetric behaviour of the microstructure and normal compression behaviour of the macrostructure. The updated model was capable of predicting the dependency of water content on suction for temperatures up to 80°C (Mašín, 2017). The complex behaviour of volume strains resulting from heating of MX-80 bentonite up to 80°C at various values of suction and mean total stress (described by Tang et al. 2008b) were predicted as follows:

- At high suctions (110 MPa), the model predicts swelling, whose magnitude is controlled by α_s (the dependency of microstructural volume strains on temperature); heating-induced swelling at high suctions is primarily reversible.
- At lower suction (9 MPa for a total stress of 0.1 and 39 MPa for a total stress of 5 MPa), the model predicts heating-induced compaction (collapse), irreversible and controlled by the offset of normal compression lines at different temperatures; however, for a stress of 0.1 MPa at a suction of 39

MPa, the state is well within the state boundary surface and heating-induced swelling is predicted, in agreement with experimental data. In principle, the model could also be calibrated using negative α_s to predict the heating-induced contraction observed by some authors.

– The model predicts cooling-induced contraction, which depends on suction such that it is most pronounced at 110 MPa and least significant at 39 and 9 MPa; these predictions are governed by the dependency of the double-structure coupling factor f_m on macrostructural degree of saturation.

In the framework of HITEC this model was used to simulate two small-scale TH tests in which BCV bentonite was saturated under the temperature gradient imposed by a heater set at 150°C on one side of the columns (Villar et al. 2023a). Although the dry density of the bentonite in the two tests were 0.9 and 1.4 g/cm^3, the initial material parameters were set for dry density 1.5 g/cm^3, because of convergency problems of the hypoplastic bentonite model for low dry densities. There was a good agreement in calculated and measured temperatures and the evolution of the vertical pressure (corresponding to swelling pressure) followed the gradual saturation of the bentonite and subsequent increase of water pressure. The model had convergence issues in the phase of water pressure increasing.

At VTT, the Varied Multiplicative Processes (VMP) model was upgraded to include thermal phenomena and dependencies. The VMP model is a large deformation model with terminology and concepts that deviate from those used in the standard linear deformation theories (Pulkkanen, 2019). The bentonite is divided into the skeleton, which contains the solid material and the adsorbed water, and the free porosity, filled with free water or gas. Thermal phenomena were added to the VMP model thermodynamically consistently. The upgraded model consists of 1) the mass balance equation for adsorbed water transport, 2) the force balance equation for mechanical behaviour, and 3) the thermal balance equation including thermal terms (Vasconcelos et al. 2023).

Hence, the work of the different groups during HITEC showed that THM formulations for expansive materials developed and validated for temperatures below 100°C can be extended to temperatures above that value by including the thermal dependence of some parameters.

4 Clay host rock

This chapter is devoted to the host rock formations. HITEC aimed to develop improved understanding of clay host rocks exposed to temperatures above 90°C for extended durations and evaluate whether or not higher temperature limits would be safe for a variety of geological disposal concepts (described in 2).

Three clay formations considered to host radioactive waste repositories in Europe were analysed in the EURAD-HITEC Project: the Boom Clay, the Callovo-Oxfordian claystone and the Opalinus Clay. A summary of their main mineralogical, geochemical and hydro-mechanical characteristics, based on the participant's input, is given in the first part of this chapter. The focus is set on the hydro-mechanical properties both of the sound and of the fractured/damaged materials. Then, large-scale tests that have been used as modelling benchmarks during the Project are described.

Next, the experimental (subchapter 4.3) and modelling (subchapter 4.4) activities carried out in the framework of the Project are summarised. The first subchapter starts with background information about what was known about the effect of elevated temperature on the host rocks properties and performance prior to HITEC. In particular, the experimental activities carried out in Task 2 of the Project analysed two aspects: the impact of temperature on the short- and long-term behaviour of the clay host rock and the self-sealing processes. The description of the results obtained during the Project is

based on deliverables D7.3 (Grgic et al. 2023a) and D7.5 (Grgic et al. 2023b). Subchapter 4.4 starts with an overview of the tools and approaches used to model the THM behaviour of the three formations prior to HITEC. The description of the modelling work done during the Project is finally presented, based on deliverable D7.6 (de Lesquen et al. 2024).

4.1 Materials considered in HITEC: properties and temperature impact

The following subsections aim at summarising the relevant properties of the three claystone formations proposed to host radioactive waste and analysed during HITEC:

- **The Boom Clay Formation.** A marine deposit from the Oligocene (Rupelian stage), between 33.9 and 28.4 Ma. The formation is composed of rhythmically alternating clay-rich and silt-rich materials resulting in a grey-tone banding (Vandenberghe et al. 2014). The Boom Clay is a poorly indurated clay with a well-developed particle alignment according to the bedding plane and high porosity.
- **The Callovo-Oxfordian (COx) claystone**. Deposited 160 Ma ago (Middle-Upper Jurassic) over a period of approximately five million years, in an open and calm marine environment. It consists of three major geological units, the relevant one being the argillaceous unit (UA) at the base, the most homogeneous and the richest in argillaceous minerals (more than 40% on average) of the three.
- **Opalinus Clay**. It occurs extensively in northern Switzerland and neighbouring countries. It is a moderately over-consolidated claystone originated from shallow marine sedimentation in the Middle Jurassic period (Aleanian), ~173 million years ago, with a complex burial and compaction history. It shows a low variability in facies and lithology, with a clay mineral content >40 wt.%.

Hence, all of them were deposited in a marine environment. As a consequence of their geologic histories (burial, subsidence, uplift, erosion) and particular mineralogy and grain size, the resulting porosity and mechanical characteristics are considerably different. Thus, the Boom Clay, which is the youngest and subjected to less burial, has a porosity of 35-40%, consequently with higher hydraulic conductivity and lower thermal conductivity than the other clays. It can be considered as a poorly indurated clay (OCR = 2.4 at the level of the URL). In contrast, the COx claystone has a porosity of 14-20% and the Opalinus clay of 10-16%, having been subjected to large extent of diagenesis and tectonic activity (in the case of Opalinus). The two are much stiffer than the Boom Clay, they can be considered as moderately over-consolidated claystones and are brittle materials at low confining pressure and more ductile at high confining pressure.

To make easier the comparison of the three clays properties, the following Tables summarise some of them.

Table 4-1. Mineralogical composition of the clay host rocks

Mineral (%)	Boom Clay[a]	Cox[b] (UA2)	Opalinus[c]
Clay minerals		24 – 52 (52)	>40
Illite	5 – 11	8 – 20 (17)	23
Smectite + Interstratified illite/smectite	7+7 – 17+25	15 – 30 (28)	12
Kaolinite	1 – 6	0 – 4 (4)	18
Chlorite	1 – 3	1 – 3 (3)	8
Interstratified chlorite/smectite	0 – 5		0
Interstratified kaolinite/smectite	1 -- 6		
Quartz	20 – 52	15 – 26 (17)	20
K-Feldspars	3 – 9	1 (1)	2
Plagioclase	1 – 5	1 (1)	1

Mineral (%)	Boom Clay[a]	Cox[b] (UA2)	Opalinus[c]
Carbonates		24 – 46 (26)	
Calcite	0 – 6	20 – 40 (22)	14
Siderite	0 -- 4	Present	3
Dolomite	0 -- 1	3 – 8 (4)	<1
Ankerite			
Muscovite	5 -- 9		
Pyrite	0 -- 4	1 – 3 (1)	<1
Organic Carbon	0 – 5	0.5 – 1	1
Others			
Gypsum	0 -- 1	Present	
Glauconite, apatite, rutile, anatase, ilmenite	Present	Present	
Zircon, monazite, xenotime			

[a] Frederickx (2019), [b] Rebours et al. 2005: [c] NAGRA 2014c

Table 4-2. Pore water composition of the clay host rocks

Element (mmol/L)	Boom Clay[a]	COx[b]	Opalinus[c]
pH	8.2	7.1	7.2
Ionic strength (mol/L)		0.1	0.23
Na	13.4	47	164
K	0.2	0.5	2.6
Ca	0.06	5	12.5
Mg	0.07	4.3	9.6
Fe	0.005	0.02	0.05
Si	0.19	0.2	0.18
Al	$1.8 \cdot 10^{-5}$		-
Sr	$6.8 \cdot 10^{-4}$	0.2	0.2
HCO_3^-	14.4		2.04
TIC	12.2	2.5	1.5 – 4.0
Cl	0.57	37	160
Total S	0.02		25
SO_4^{2-}	0.02	12.9	75

[a] De Craen et al. 2004, Honty et al. 2022 [b] Gaucher et al. 2006, [c] NAGRA 2014c, Courdouan Merz 2008, Mäder 2009

Table 4-3. Hydraulic properties of the clay host rocks

	Boom Clay	Cox	Opalinus[a]
Hydraulic conductivity, k (m/s)	$1.5 - 4 \cdot 10^{-12}$	$\sim 10^{-13}$	$10^{-13} - 10^{-15}$
Vertical hydraulic conductivity, k_V (m/s)	$2 - 3.5 \cdot 10^{-12}$	$1 - 2 \cdot 10^{-13}$	$1.4 - 9.4 \cdot 10^{-14}$
Horizontal hydraulic conductivity, k_H (m/s)	$4 - 5.5 \cdot 10^{-12}$	$3 - 6 \cdot 10^{-13}$	$2.9 \cdot 10^{-14} - 1.1 \cdot 10^{-15}$

[a] Horseman & Harrington 2002

Table 4-4. Thermal conductivity of the clay host rocks (on site)

	Boom Clay	COx	Opalinus
λ_h	1.25 - 1.35	2.0±0.1	2.4
λ_v	1.61 - 1.70	1.30±0.05	1.3

Table 4-5. Mechanical properties of the clay host rocks

Property		Boom	Cox	Opalinus
Solid phase density (kg/m^3)	ρ_s	2639	2690	2340
Bulk density (kg/m^3)	ρ'	2000	2386	2030
Porosity	n	0.39	0.18	0.13
Isotropic intrinsic permeability (m^2)	k	$2.8{\cdot}10^{-19}$	$2.3{\cdot}10^{-20}$	$3{\cdot}10^{-20}$
Vertical intrinsic permeability (m^2)	k_v	$2{\cdot}10^{-19}$	$1.3{\cdot}10^{-20}$	$1{\cdot}10^{-20}$
Horizontal intrinsic permeability (m^2)	k_h	$4{\cdot}10^{-19}$	$3.9{\cdot}10^{-20}$	$5{\cdot}10^{-20}$
Isotropic Young's modulus (MPa)	ρ_s	300	7000	6000
Young's modulus parallel to bedding (MPa)	$E_{//}$	400	10000	8000
Young's modulus perpendicular to bedding (MPa)	$E_\perp$	200	6200	4000
Poisson's ratio (-)	ρ'	0.125	0.3	0.3
Poisson's ratio parallel to bedding (-)	$\nu_{//\,//}$	0.25	0.21	0.35
Poisson's ratio perpendicular to bedding (-)	$\nu_{\perp//}$	0.125	0.35	0.25
Linear thermal expansion coefficient (°C^{-1})	α_s	$1{\cdot}10^{-5}$	$1.25{\cdot}10^{-5}$	$1.7{\cdot}10^{-5}$
Solid phase specific heat (J/kg/K)	c_p	769	790	995

The following sections summarise for the three selected host clays (Boom Clay, Opalinus and Callovo-Oxfordian claystone) aspects of the geology of the formation, general parameters and, in different subsections, the hydro-mechanical and THM properties derived from laboratory tests and the impact of temperature on some of them. In particular, the following temperature-dependent material properties are considered to be important (Li et al. 2007): hydraulic conductivity, thermal conductivity, stiffness and strength, creep rates and the thermal sensibility on anisotropy.

Besides, drilling underground galleries or boreholes leads to stress redistribution around the hole and some damage in the near-field. Fractures are likely to form around the repository as it is constructed. The stress that was supported by the material removed during construction must be taken up by the remaining rock, leading to stress concentrations. Depending on the strength of the host-rock, this stress concentration is likely to result in fracturing and the formation of an Excavation Damaged Zone (EDZ). This EDZ has different mechanical, hydraulic and thermal properties to the sound host rock, and some information on them is also given below.

Most of the information gathered comes from research projects (including thesis) financed by or with participation of the WMOs.

4.1.1 Boom Clay

The Boom Clay Formation (Tertiary clay formation) is one of the potential clay formations studied in relation with the feasibility of a geological disposal of radioactive waste in Belgium. The Boom Clay

dips gently towards the northeast, is located in the north part of Belgium and covers a surface of almost 5000 km² (Figure 4-1). The thickness of the formation increases from a few decametres at outcrop to more than 150 m in the deeper part of the basin. At the level of the URL in Mol (Belgium), the Boom Clay has a thickness of about 100 m and is located at depths between 185 and 287 m, the underground laboratory is at a depth of 223 m (Mertens et al. 2004). The total vertical stress and pore water pressure at the level of the URL in Mol are respectively 4.5 MPa and 2.2 MPa. The K_0 value ranges from 0.7 to 0.8 (ONDRAF/NIRAS 2013).

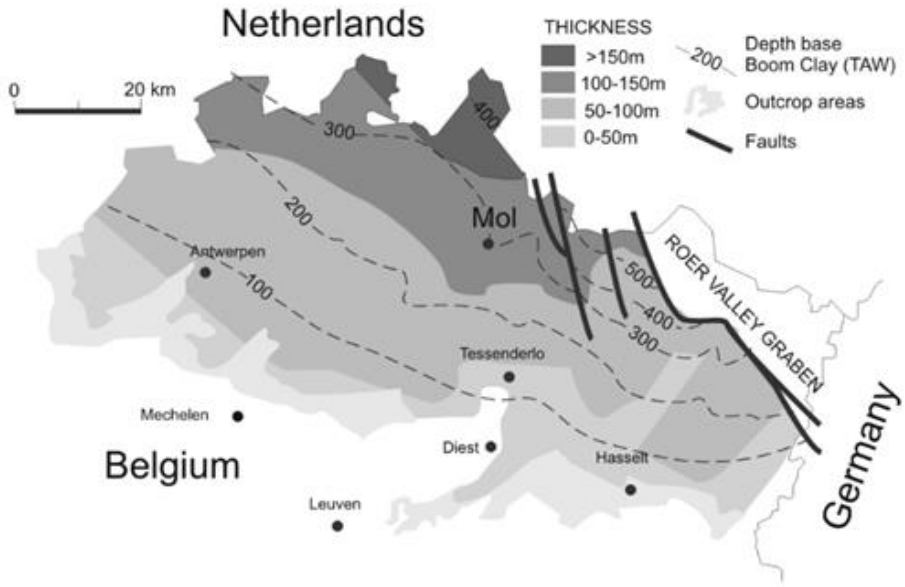

Figure 4-1. Extension of the Boom Clay Formation in the north part of Belgium. The formation dips towards the northeast. The underground research facility is located at Mol (from ONDRAF/NIRAS 2001)

The granulometry of the clay is composed of more than 60% of very fine particles (clay size) for the more clayey beds while there are 40% of clay particles for the more silty beds. The majority of the pores have a radius in the order of 0.01 µm with a unimodal distribution (Lima 2011). Based on the differences in granulometry and mineralogical content, the Boom Clay Formation is subdivided in three members: the Belsele-Waas Member, the Terhagen Member and the Putte Member.

The vertical and horizontal hydraulic conductivity values are different with a ratio (k_H/k_V) of ~2 (Table 4-3). The different values of the hydraulic conductivity are related with the granulometry, for instance, the values in the Belsele-Waas member are higher than those of the other members of the formation because of its higher sand content.

A critical review of the laboratory and in situ measurements can be found in Yu et al. (2013).

4.1.1.1 Hydro-mechanical behaviour

Since the operational start of HADES URL early in the 80s, many laboratory tests and in situ testing have been performed to understand the Boom Clay THM behaviour, among which triaxial and oedometer tests. Triaxial tests permit to determine deviatoric behaviour and then the strength parameters, while oedometer tests are more focused on the volume change behaviour. Clay samples have been studied in conditions as close as possible to their natural state around the HADES URL. As re-saturating Boom Clay samples at low confining pressure induces an important swelling that affects the microstructure and thus modifies clay properties (Coll 2005, Sultan 1997), Le (2008) suggested

saturating Boom Clay at a confining pressure close to the in situ state of stress to minimise this swelling and disturbance of the clay.

The Boom Clay behaviour is characterised by a non-linear stress–strain response. Laboratory tests showed a trend of stiffness variation with strain level: its tangent stiffness at 0.01% deformation may be one order of magnitude larger than that at 1% deformation (Bernier et al. 2007a).

The elastic properties which govern the clay behaviour in the reversible domain of deformation have been determined with triaxial tests. According to Bernier et al. (2007a) the isotropic elastic modulus of the Boom Clay is about 300 MPa. This value was deduced by back-analysis of the in-situ measurements during the excavation of the Test-drift obtained by Mair et al. (1992) and gives satisfactory results to model most of the triaxial tests on Boom Clay (Charlier et al. 2010). The value of the Poisson's ratio ranges from 0.125 (Bernier et al. 2007) to 0.15 (Horseman et al. 1987). In isotropic condition, a value of 0.125 is commonly admitted.

The uniaxial compressive strength (UCS) of the Boom Clay is not well documented. According to Coll (2005), who determined the UCS on Boom Clay samples from a depth of 223 m, it should be around 2.5 MPa. Bernier et al. (2007a) reported a value of 2 MPa.

Triaxial tests to determine the shear strength parameters of the Boom Clay have been performed for several decades starting from De Beer et al. (1977). These results were mostly obtained through undrained tests because of the very low permeability of the clay. The monitoring of the pore water pressure permits to calculate the mean effective stress and to interpret the tests in terms of effective parameters. As an example, Figure 4-2 presents classical results of an undrained test performed at very low confining pressure (high OCR) (Lima 2011). The results show that the deviatoric behaviour presents a peak before a decrease (strain softening) till a residual strength (Figure 4-2, left). Figure 4-2 (right) presents the stress path in the plane of the mean effective and deviatoric stresses during undrained tests for overconsolidated clay samples. The very low compressibility of the clay-water mixture implies that the volumetric deformation of the sample can be assumed theoretically as null. The representative stress path for such kind of tests is almost a straight line.

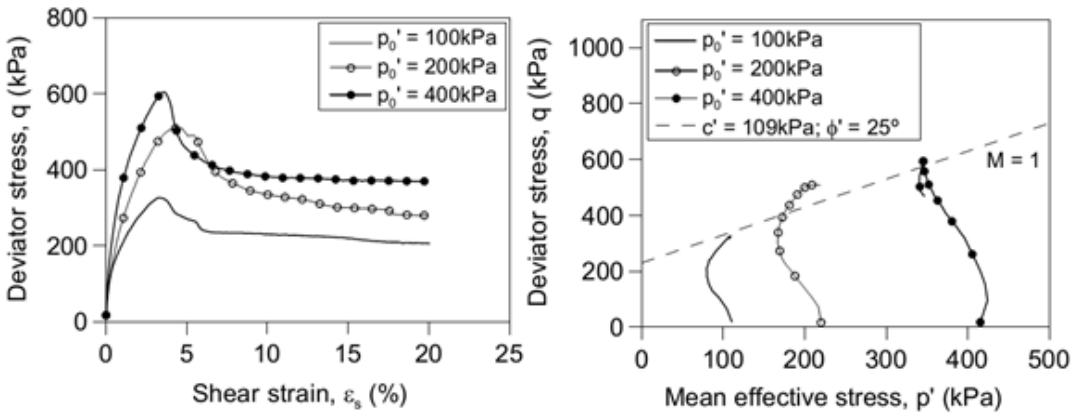

Figure 4-2. Typical response of the Boom Clay during an undrained triaxial tests and determination of the drained parameters (Lima 2011)

The values of the drained cohesion and the drained friction angle of the Boom Clay can be deduced from all the previous studies. According to Bernier et al. (2007a), who interpreted the tests of Baldi et al. (1987, 1991) and Mair et al. (1992) with a Mohr-Coulomb criterion, the drained cohesion is equal to 300 kPa and the friction angle to 18°. Figure 4-3 presents the comparison between the Drucker-Prager criterion with the chosen shear strength parameters and the peak strength values from the

triaxial tests on Boom Clay. With this set of parameters a relatively good agreement can be found for high values of the confining pressure, while for very low values, more discrepancies can be seen.

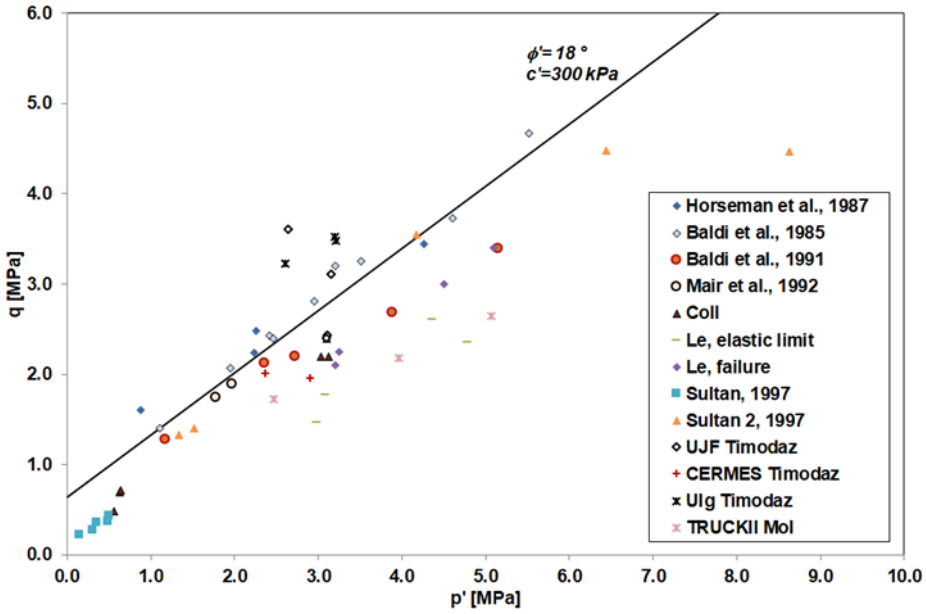

Figure 4-3. Drucker-Prager criterion with the chosen set of shear strength parameters for Boom Clay plotted with the peak strength values (Dizier et al. 2018)

The commonly admitted elastoplastic parameters for Boom Clay are summarised inTable 4-6.

Table 4-6. Elastoplastic parameters for the Boom Clay

Drained Young modulus (MPa)	300
Drained Poisson's ratio (-)	0.125
Drained cohesion (MPa)	0.3
Drained friction angle (°)	18

Concerning the volume change behaviour, Awarkeh (2023) summarised the results of oedometer tests performed on Boom Clay samples from Horseman et al. (1987) to Nguyen (2013) and gave a a range of variation of the swelling index (C_s) between 0.05 and 0.15, of the plastic slope (C_c) between 0.25 and 0.40, and of the preconsolidation pressure between 5 and 6 MPa. The parameters present a large variation that can be explained by the natural variability of the clay and by the evolution of the test protocols, which are constantly evolving from the early tests.

With a view on the long-term volume change behaviour, Deng et al. (2012) performed oedometer tests with the purpose of studying the secondary consolidation behaviour of Boom Clay samples taken from two different locations. They found that the secondary consolidation coefficient (C_α) was positive during the loading paths and negative during unloading, with an average value of about 0.024, which agrees with the general classification criterion for clay soils of Terzaghi et al. (1996), where a range from 0.02 to 0.05 is given for shales and mudrocks. Similar results were obtained by Awarkeh (2023).

A set of laboratory tests was performed under different conditions to investigate the elasto-visco-plastic behaviour of Boom Clay under long-term deviatoric conditions (creep). Triaxial creep tests performed by Coll et al. (2008) and Chen et al. (2017) at ambient temperature evidenced the creep behaviour: the steady strain rate increased with the deviatoric stress level as observed for most other

clay materials. Similar results were obtained more recently with the work of Awarkeh (2023). It was shown that the creep strain under a deviatoric loading starts at a certain value of the deviatoric stress, which means that there is a threshold under which no creep can be observed.

The coupling between mechanical and hydraulic properties was studied by Horseman et al. (1987) and Coll (2005), who performed series of hydraulic tests on Boom Clay samples at different confining pressures and determined a trend in the evolution of the hydraulic properties with the mean effective stress. As expected, an increase of the applied load induced a decrease of the hydraulic conductivity. Coll (2005) also studied the effect of the deviatoric stress on hydraulic conductivity. Even if a discontinuity was initiated in the sample, no clear modification of the hydraulic conductivity was observed. Indeed, even if the permeability was modified locally around the cracks, this was not measurable at the scale of the sample. After shearing, the cracks were characterised by a very thin size which made difficult the description of the porosity along the localised shear band. Few years later, Monfared (2011) performed permeability tests before and after shearing and observed again that the shear band had no significant effect on the permeability of the sample, although –consistently with the results of Coll (2005)– very small variations of the permeability could be noticed. The interpretations given to these results differed in both studies though. Coll (2005) assumed that the shear band had a very local and insignificant effect on the global permeability of the sample, while Monfared (2001) made the hypothesis that the absence of permeability variation was the result of the self-sealing behaviour of the clay.

The laboratory test programme summarised above mainly investigated the THM behaviour of the Boom Clay as isotropic, so far the anisotropic behaviour of Boom Clay has not been much studied. Baldi et al. (1987) compared the calculated and measured volumetric strain during a triaxial test. Later, Labiouse et al. (2014) and François et al. (2014) performed hollow cylinder tests and presented their interpretations with anisotropic numerical models. Different phases of loading and unloading were applied to the samples. Before and after unloading, the sample was submitted to microcomputerized tomography (µCT) and particle tracking to determine the displacement of some specific points. The hole clearly converged after unloading, but the convergence was not homogenous and varied with the direction of the bedding plane, which resulted in anisotropic behaviour and a final eye-shape of the hole (Labiouse et al. 2014). The radial displacements in hollow cylinder tests according to different directions was analysed by François et al. (2014), who found that they were not uniform, highlighting the anisotropic response of the clay. The higher displacement was parallel to the bedding plane, while the lowest one was perpendicular to the bedding. These results were confirmed more recently by Péguiron (2021). Also the back-analysis of the observed pore-water pressure variations in the far field of the HADES URF galleries during excavations and around the in-situ heater tests ATLAS and PRACLAY (see section 4.2.1) support the idea that the THM behaviour of the Boom Clay is anisotropic. These last analyses reveal notably that perturbations in the far field –where deformations are small– can be much better represented by models when using different Young's moduli along the vertical and horizontal directions, with values generally larger than those summarised in Table 4-5.

4.1.1.2 Hydro-mechanical behaviour of the fractured/damaged claystone

During the SELFRAC project, tests were performed to study the self-sealing capacity of the Boom Clay (Bernier et al. 2007b), using different pore water chemistries to saturate the samples after the initiation of a fracture. The Boom Clay showed very good capacity of self-sealing. Figure 4-4 presents the evolution of a fractured Boom Clay sample before and after re-saturation, when the fracture was no more visible. Van Geet et al. (2008) performed permeameter tests on a fractured Boom Clay sample and monitored the evolution of the hydraulic conductivity with time to highlight the sealing process (Figure 4-5). The hydraulic conductivity decreased with time, indicating the sealing process from a hydraulic point of view. Chen et al. (2014) showed that there is no positive or negative impact of the

temperature on the sealing properties of Boom Clay by exposing samples (damaged and intact) to a heating cycle from 20°C to 80°C under constant volume conditions in a permeameter cell.

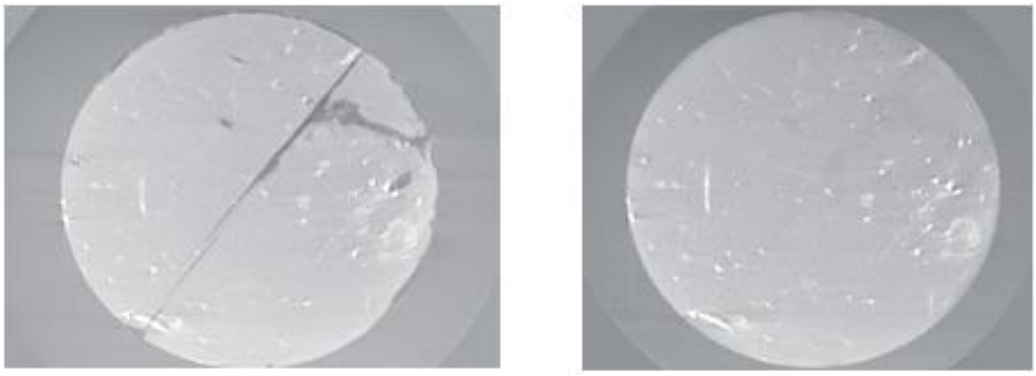

Figure 4-4. Visualisation by µCT technique of the sealing process of a fracture in a Boom Clay sample after saturation (Bernier et al. 2007b)

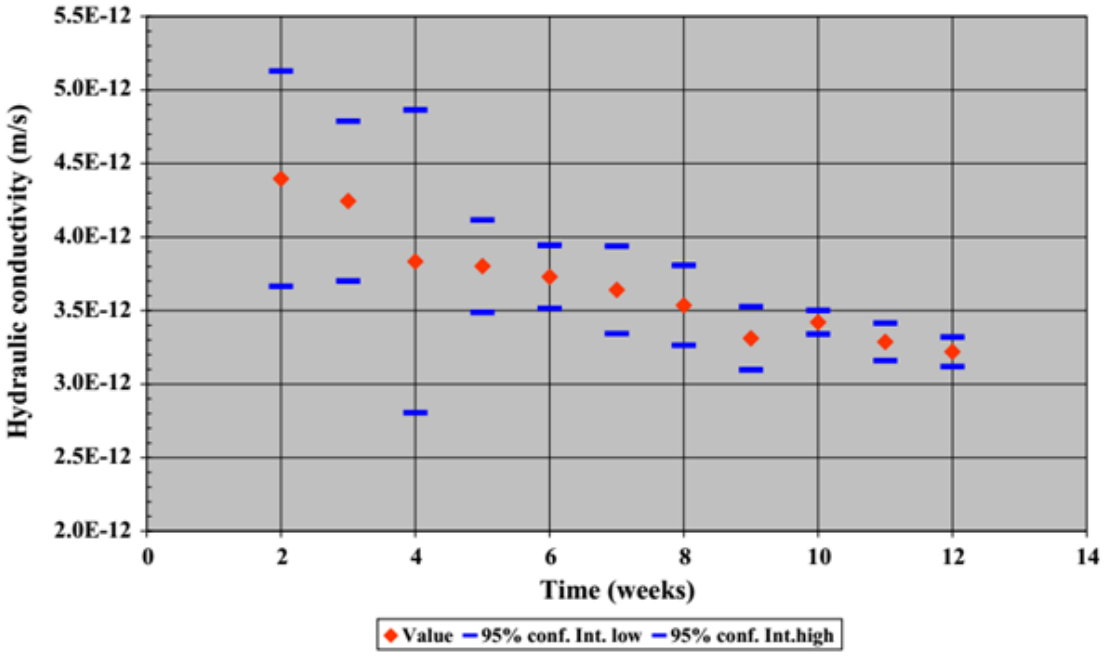

Figure 4-5. Weekly evolution of the hydraulic conductivity in a fractured Boom Clay sample. Permeameter test with synthetic Boom Clay water as pore water solution (Van Geet et al. 2008)

4.1.2 Callovo-Oxfordian claystone

The Callovo-Oxfordian (COx) claystone consists of three major geological units, among which the argillaceous unit (UA) at the base is the thickest (from 100 to 120 m in the zone of interest). It is subdivided into three subunits (UA1, UA2 and UA3) with small and progressive variations. Subunit UA2 corresponds to the stratigraphic level where the clay content is higher and where the Underground Research Laboratory experiments are carried out. The formation dips gently (average 1°) towards the northwest, the bedding plane can therefore be considered horizontal. The main level of the URL is located at a depth of 490 m.

The average porosity in the UA is 18%. The network of pores mainly comprises meso- and micropores with a predominant pore size of approximately 10 to 30 nm, and an extremely low connectivity for pores larger than 40 nm. The texture is finely divided and is an assembly of tectosilicate and carbonate grains, connected by a fine matrix formed of clay minerals and calcite microcrystals. Both the tectosilicate and the carbonate grains show a preferential orientation of their long axis parallel to the sedimentation plane.

The water permeability is very low and ranges from 10^{-21} m^2 to 10^{-19} m^2, with a relatively low anisotropy (2 to 3 ratio). The stress regime in the area is anisotropic, with the major principal stress being horizontal and the ratio between the maximum and minimum horizontal stresses being at ~1.3. For the calculations, at the URL level, the major horizontal stress σ_H is set at 16.1 MPa, σ_v=12.7 MPa, σ_h=12.4 MPa, and the pore pressure is 4.7 MPa. A geothermal gradient of 0.025°C/m is estimated in the area, with a temperature of 22°C at 490 m.

4.1.2.1 Hydro-mechanical behaviour

The COx claystone has a linear non-reversible (pseudo-elastic) behaviour at low levels of deviator stress (below 40-50% of failure) and a non-linear behaviour beyond a level, with significant irreversible strains and slightly lower moduli. Brittle failure is observed at low confining pressures and a more ductile behaviour is seen at high confining pressure (over 21 MPa in the UA). Beyond a certain level of cumulative total strain, some residual strength is shown.

The water saturation has a significant effect on the mechanical behaviour of the Cox claystone. It was shown that limited desaturation of the Callovo-Oxfordian leads to an increase in the elastic mechanical properties and in the strength of the material, despite some microcracking of the sample due to desaturation (Wang et al. 2013; Agboli et al. 2023).

Under tensile loading, the COx claystone shows a brittle behaviour. The measured tensile strength shows non-negligible dispersion, increasing with the carbonate content and with a mean value in the UA of 1.4 MPa.

Triaxial tests performed on samples with various orientations with regard to the bedding showed anisotropy, the $E_{//}/E_{\perp}$ ratio varying between 1.05 and 1.4. Similar numbers were obtained when calculating dynamic moduli from the compressive and shear wave velocities measured in both directions in parallelepipedic samples. The average values and standard deviations for the perpendicular and parallel moduli from UCS tests (calculated using the tangent method) in the UA unit were 5.7±2.5 GPa and 11.0±4.6 GPa, respectively. The average values show a ratio of almost 2, however these values are not directly comparable because many more samples were tested in the perpendicular direction (259 vs. 52). In addition, the standard deviation for the tests performed on samples parallel to the bedding (≈4 GPa) is related not only to the mineralogical variations, but also to the damage due to the difficulty to cut some plugs parallel to the lamination.

The Poisson's ratio (ν) calculated from all the results available at room temperature is on average 0.3 for all lithological levels.

The unconfined compressive strength in the different units of the COx formation ranges from 18 to 34 MPa. For the most argillaceous part of the UA (UA2=IMA subunit), the values are 23.3±5.1 MPa.

The experimental results of uniaxial compression tests were interpreted with the Hoek & Brown (1980) failure criterion, and the values in Table 4-7 were found, where *m* and *S* are fitting parameters and σ_c is the uniaxial compressive strength of the intact rock. For the COx claystone, this parameter is different from the UCS and is considered as a fitting parameter, not a rock property. In order to manage the uncertainties due to various effects (scale, time effect on the long-term strength, sample preservation, etc.) two criteria were defined: 1) an average criterion that goes through the cloud of

test results over a range of confining pressure $0<\sigma_3<25$ MPa, and 2) a low criterion that goes through the lower limit of test results over the same range of confining pressures. From these parameters the equivalent Mohr-Coulomb parameters shown in Table 4-8 were derived.

Table 4-7. Hoek & Brown fitting parameters for the unit UA of the COx claystone (ANDRA 2009)

	S	***m***	**σ_c (MPa)**	**Back-calculated UCS (MPa)**
Low criterion	0.128	2.0	33.5	12.0
Average criterion	0.430	2.5	33.5	22.0

Table 4-8. Mohr-Coulomb failure criterion parameters for the COx claystone for 0, 5 and 12 MPa minor stress

	σ_3 (MPa)	***c* (MPa)**	**ϕ (°)**
Average criterion	0	6.4	29
	5	7.4	24
	12	8.8	21
Low criterion	0	3.1	36
	5	4.5	26
	12	6.1	21

Because of the variability of their microstructure and of their mineralogy, the COx claystone has an anisotropic behaviour that results in:

- an anisotropy between 1 and 2 on the elastic moduli depending on the methods used for determination (dynamic and quasi-static modulus)
- compressive strengths measured on samples perpendicular to the stratification are similar to or slightly lower than those measured on samples parallel to the stratification. A decrease in strength was observed for test specimens at 45° but the natural variability of samples can give an opposite result. Figure 4-6 shows the effect of the orientation to bedding on the peak strength in recent samples from well-preserved cores with high water saturations.

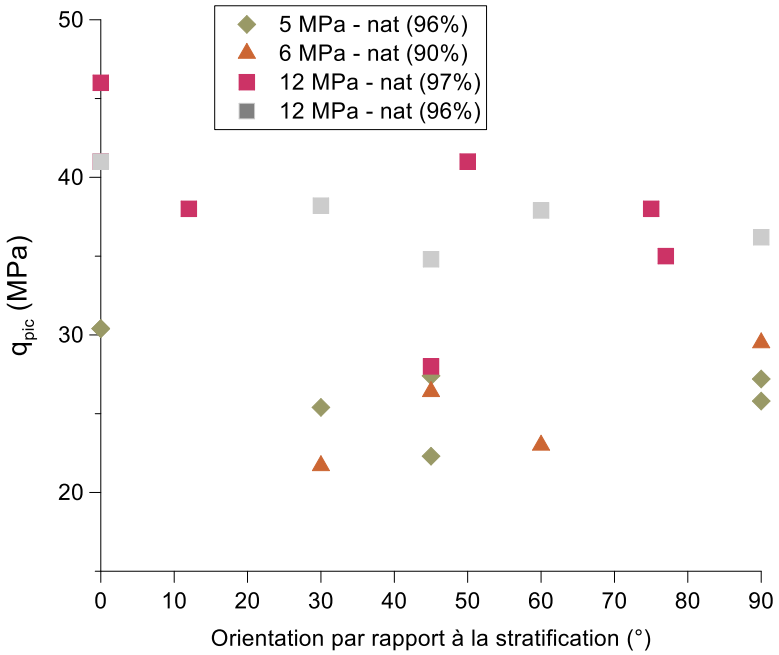

Figure 4-6. Peak strength of COx claystone as a function of the orientation to bedding

An investigation performed by Zhang et al. (2015) with cores drilled at different inclinations with respect to bedding, confirmed that the strength depends both on the loading path and on the direction of loading compared to the bedding plane. For a given loading orientation, the peak strengths developed during TCD (triaxial compression by axial deformation at constant radial stress) and TCS (triaxial compression by axial loading at constant radial stress) were higher than those reached during TES (triaxial extension by increasing radial stress at a constant axial stress) and TEM (triaxial extension by keeping the mean stress constant while simultaneously increasing the radial stress and decreasing the axial stress) and the lowest strength was achieved in triaxial extension with constant mean stress. For all loading paths, the maximum strengths were reached with an axial stress parallel and perpendicular to bedding, and the lowest strength was obtained at 45° in compression and 30° in extension.

The very low permeability and porosity of the COx claystone make it difficult to directly measure the pore pressure within a plug and to quantify its coupling with the mechanical behaviour. However, the hydro-mechanical coupling was revealed in situ through changes in pore pressure levels around the structures after excavation and through thermal experiments. It is currently described through the concept of effective stress using Biot's theory. The most recent experiments to define Biot's coefficient (Braun, 2019, Belmokhtar et al. 2017, Yuan et al. 2017) reduced the uncertainty on its value and gave higher values than previously, between 0.8 and 1 (Figure 4-7). A value of 0.85 may be retained for the COx claystone. However, it should be noted that these results strongly depend on the saturation and the mechanical state of the samples. The core processing, the sample preparation and the (re)saturation of the samples may create some damages prior to testing, which may partially explain the dispersion of experimental values obtained over all the studies. Furthermore, all the tests show that the Biot's coefficient seems to decrease with the confining pressure, while the drained bulk modulus increases. This could be explained by the closure of microfractures induced when cutting the core and/or preparing the samples. In addition, the very small pore size of the COx claystone, the presence of both clay-bound and free water, and the possible induced desaturation when acquiring or preparing the samples hinder the characterization of the poro-elastic parameters and the application of a simple behaviour model.

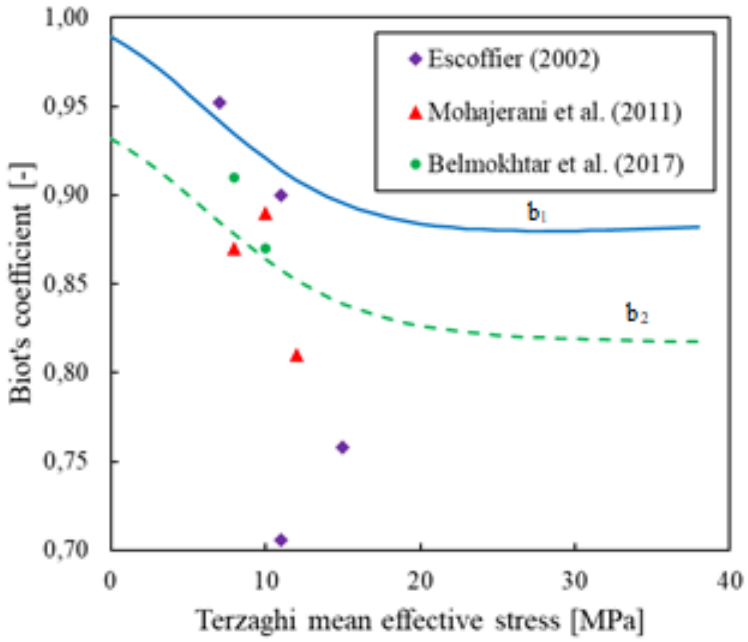

Figure 4-7. Biot coefficient of COx claystone calculated perpendicular to bedding (b_1) and parallel to bedding (b_2) *vs.* Terzaghi's effective stress (Braun 2019)

Creep tests were performed on dedicated rigs, with controlled temperature for periods of time of up to 3 years to characterise the long-term mechanical behaviour of the rock (Zhang et al. 2012). These tests faced important challenges related to the initial state of the samples, the duration of the experiments, the control of temperature and humidity and the precision of the measurements. The measured changes were indeed very low, sometimes of the same order of magnitude as the accuracy of the sensors. However, some general trends were observed:

- In most cases, the creeping rate diminished with time, although in some cases it appeared to reach an asymptote. The evolution of the creeping rate was very slow and because of the precision of the measurements, it is difficult to say whether a steady state was reached or not.
- The creeping rate appeared to increase with the deviator stress.
- The average stress seemed to have very little influence on the delayed deformations.
- The calcite content had a direct effect on the instantaneous behaviour but no clear trend was observed on the delayed mechanical behaviour; however, when checking the results per study, a slight decrease of the creeping rate with the carbonate content may be seen.

4.1.2.2 Hydro-mechanical behaviour of the fractured/damaged claystone

The EDZ can be split in a connected fractured zone (ZFC), where both tensile fractures and shear fractures coexist, and a discrete fractured zone (ZFD), where only the ends of some shear fractures are found. For HLW cells drilled in the direction of the maximum horizontal stress, the EDZ develops mainly on the right and left sides of the borehole. Its maximum extent is approximately one diameter wide on each side (0.8 radius for the ZFC and 2 radii for the ZFD), and there is no "scale effect" between large galleries or thin boreholes. The hydraulic conductivity in the ZFC is significant and related to open fractures. Because of this, the pore pressure drops rapidly to atmospheric pressure in the near field (ZFC), but an increase in pore pressure is observed further away from the hole with some delay.

The apparent stiffness of the ZFC has been evaluated in the CDZ experiment (de la Vaissière, 2015): it appears to increase rapidly, reaching already 3 GPa one metre away from the borehole wall.

Several observations in the UA showed that the EDZ has a hydraulic self-healing capacity due to the presence of swelling clay minerals such as smectite. Both laboratory and in-situ experiments showed that the hydraulic conductivity of the ZFC reduces rapidly when exposed to water and progressively reaches that of the intact claystone. De La Vaissière et al. (2015) showed the partial restoration of the COx claystone permeability during in situ resaturation experiments. Over a one-year resaturation period, the hydraulic conductivity measured in the boreholes decreased by up to four orders of magnitude, approaching, but not reaching, the value of the healthy claystone. This result illustrates the ability of the claystone to self-seal. However, water injection does not improve the stiffness of the EDZ that remains a mechanically weak zone.

A study on COx claystone looked at its flow properties (Cuss et al. 2017) and described the stress dependency fracture flow by a power-law or cubic relationship, which is likely to be dependent on the fracture roughness, thickness of gouge material, saturation state, permeability of the host material, and clay mineralogy (i.e. swelling potential). The stress-dependency of flow was also seen to be dependent on orientation with respect to bedding, in relation to the anisotropic swelling characteristics of COx. Fractures perpendicular to bedding accommodated greater compression and resulted in a lower transmissivity.

4.1.3 Opalinus clay

The Opalinus clay is slightly tilted and the surface of the formation lies between 0 to beyond 1000 m below ground surface. At Mont Terri, the Opalinus Clay reaches a maximum depth of about 1000 m and the present burial depth is about 200-300 m.

On a regional scale, the mineralogical composition of the Opalinus Clay exhibits moderate lateral variability and a slight increase in clay content with depth. At the Mont Terri URL a clay-rich and a sandy facies can be identified. The variability of the facies is expected to be low and the same structures can be found in southern Germany as well (Jahn et al. 2016).

The anisotropy due to bedding is largely a result of microscopic heterogeneity. Porosity depends on clay content and burial depth. The pore space of the rock is formed by a network of micro/meso and macropores, but the majority of pores can be classified as mesopores (1-25 nm) (NAGRA 2002).

Field investigations suggest a hydraulic conductivity of the Opalinus Clay in the order of 10^{-13} to 10^{-14} m/s. No significant variations in hydraulic conductivity are seen among the different facies. A reference value of $5 \cdot 10^{-13}$ m/s has been reported for the Opalinus Clay at Mont Terri (Bossart & Thury 2008). The water/air permeability experiments on the Opalinus Clay (NAGRA 2002a, Marschall et al. 2005, Poller et al. 2007, Croisé et al. 2006, Romero & Gomez 2013) show clear evidence for the dependency of water permeability on void ratio and thus on constitutive stress. A marked dependency of gas dissipation was observed on the direction of gas flow with respect to bedding orientation.

Figure 4-8 depicts a compilation of water retention curves (WRC) of Opalinus Clay samples from Mont Terri, determined by GRS, UPC and EPFL. Characteristic features of the Opalinus Clay are the high capillary pressures in the order of 10 MPa even at high water saturation >90% and the marked hysteresis between wetting and drying path. Information about the WRC of deep Opalinus core samples (880 m depth) can be found in Ferrari et al. (2013) and Romero & Gomez (2013).

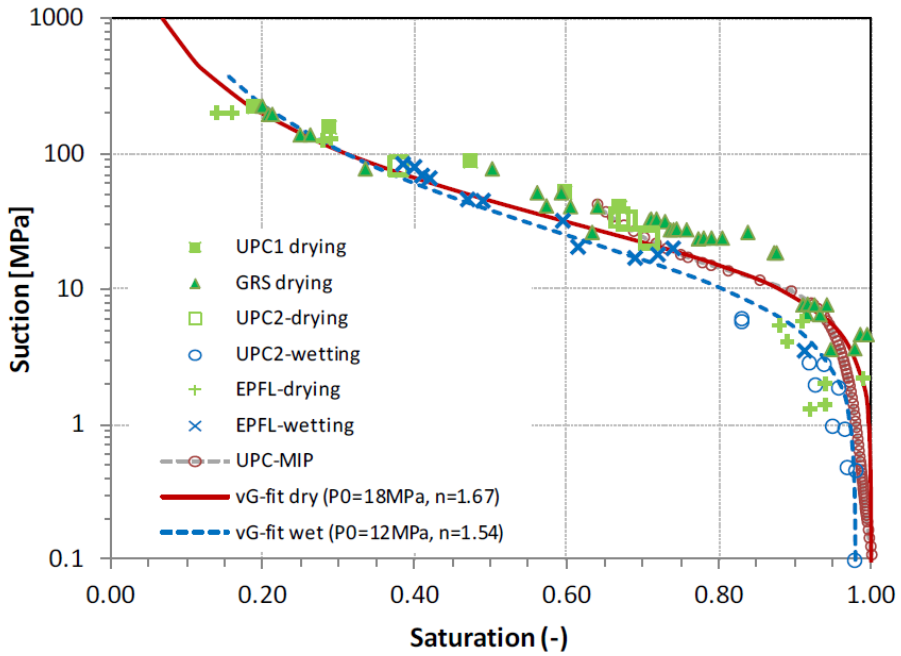

Figure 4-8. Capillary pressure measurements (water retention curves) by stepwise desaturation and re-saturation in a desiccator. The experiments were conducted by GRS (Zhang & Rothfuchs 2007), UPC (Muñoz et al. 2003, Romero & Gomez 2013) and EPFL (Ferrari & Laloui 2012)

4.1.3.1 Hydro-mechanical behaviour

Geotechnical characteristics of the Opalinus Clay have been determined as part of comprehensive laboratory programmes, revealing moderate stiffness (Young's modulus in the range 5–15 GPa), moderate strength (UCS values of the intact rock matrix between 10 and 35 MPa), distinct swelling pressures (0.5–2 MPa) and OCR of between 1.5 and 2.5 (NAGRA 2002b).

Parameters of the Opalinus Clay as defined for the FE Experiment in Alcolea et al. (2019) are shown in Table 4-9.

Table 4-9. Parameters of the Opalinus Clay used for the scoping calculations of the FE Experiment

Group	Parameter	Symbol	Units	Value
Elasticity	Young modulus parallel to bedding	$E_{\parallel}$	MPa	8000
	Young modulus perpendicular to bedding	$E_{\perp}$	MPa	4000
	Poisson ratio parallel to bedding	$n_{\parallel}$	-	0.35
	Poisson ratio perpendicular to bedding	$n_{\perp}$	-	0.25
	Thermal expansion	α_T	1/K	$1.7 \cdot 10^{-5}$
Retention curve	Type of curve	Van Genuchten		
	Entry pressure	p_0	MPa	20
	Shape parameter	n	-	1.67
	Res. liqu. sat.	$S_{r,l}$	-	0.3
Darcy	Intrinsic permeability parallel to bedding	$k_{\parallel}$	m^2	$5.0 \cdot 10^{-20}$

Group	Parameter	Symbol	Units	Value
	Intrinsic permeability perp. to bedding	$k_{\perp}$	m^2	$1.0 \cdot 10^{-20}$
	Shape factor (rel-perm)	ε, γ	-	0.5, 0.33
Fick	Tortuosity for vapour	τ	-	0.8
Fourier	Sat. thermal conductivity parallel to bedding	$l_{sat,\parallel}$	W/mK	2.4
	Saturated thermal conductivity perp. to bedding	$l_{sat,\perp}$	W/mK	1.3
General	Solid density	ρ_s	kg/m^3	2340
	Solid specific heat	c_s	J/kgK	995
	Initial porosity	ϕ	-	0.13
	Initial degree of saturation	S_l	-	1

4.1.3.2 Hydro-mechanical behaviour of the fractured/damaged claystone

Experiments at BGS looked at fracture transmissivity in Opalinus Clay along an idealised fracture (Cuss et al. 2009; 2011). A follow-on study investigated hydraulic flow along a realistic fracture (Cuss et al. 2012). This work showed that hydration alone reduced fracture transmissivity by one order of magnitude, while shear displacement reduced it by a second order of magnitude. Continued shear then resulted in increased flow, eventually increasing by five orders of magnitude, three orders of magnitude greater than the starting transmissivity. The injection of fluorescein showed that only around 25% of the fracture surface was conductive.

The values for the scoping calculations of the FE experiments used in Senger (2015) for the EDZ of the Opalinus clay are given in Table 4-10.

Table 4-10. Parameters of the Excavation Damage Zone as defined for the FE Experiment in Alcolea et al. (2019)

Group	Parameter	Symbol	Units	Value
Elasticity	Young modulus	E	MPa	6000
	Poisson ratio	n	-	0.3
	Thermal expansion	α_T	1/K	$1.7 \cdot 10^{-5}$
Retention curve	Type of curve	Van Genuchten		
	Entry pressure	p_0	MPa	9
	Shape parameter	n	-	1.67
	Res. liqu. sat.	$S_{r,l}$	-	0.3
Darcy	Intrinsic permeability parallel to bedding	$k_{\parallel}$	m^2	$5.0 \cdot 10^{-20}$
	Intrinsic permeability perp. to bedding	$k_{\perp}$	m^2	$1.0 \cdot 10^{-20}$
	Shape factor (rel-perm)	ε, γ	-	0.5, 0.33
Fick	Tortuosity for vapour	τ	-	0.8
Fourier	Sat. thermal conductivity parallel to bedding	$l_{sat,\parallel}$	W/mK	2.4
	Saturated thermal conductivity perp. to bedding	$l_{sat,\perp}$	W/mK	1.3
General	Solid density	ρ_s	kg/m^3	2340

Group	Parameter	Symbol	Units	Value
	Solid specific heat	c_s	J/kgK	1086
	Initial porosity	ϕ	-	0.13
	Initial degree of saturation	S_l	-	1

4.2 Relevant large-scale tests

Several heating tests have been performed in underground research laboratories excavated in clay host rocks. In the HADES facility excavated in Boom Clay, the small-scale ATLAS heater test was set up in 1992 with a very simple geometry (De Bruyn & Labat 2002), and has undergone several phases, providing information on the temperature and pore water pressure evolution over the years, particularly in the far field (Chen et al. 2011). At the CMHM URL, several in-situ heating tests on the COx claystone have been performed since 2006, among which the TER, TED, TFW, ALC 1604 and CRQ. At the Mont Terri URL, the heating tests HE-E and FE, excavated in Opalinus Clay and described above in sections 3.2.3 and 3.2.4, are currently running.

The following sections describe in some detail the tests selected as modelling benchmarks in HITEC: the PRACLAY in Boom Clay and the ALC 1605 in COx clay.

4.2.1 Large-scale in situ PRACLAY heater test

The PRACLAY gallery was excavated in 2007 at the HADES URL and has a length of 45 m. The heated part of the gallery is 34 m long and is separated from non-heated part by a hydraulic seal. The heated section of the gallery was backfilled with sand, saturated and pressurised with water after the installation of the seal in 2010. The main role of the seal is to hydraulically cut off the heated part from the non-heated part (Figure 4-9). Bentonite clay, which has a high swelling potential under hydration, was chosen to achieve this goal. In this way, the interface between the Boom Clay and the bentonite is sealed and permeability in the contact zone surrounding the seal is reduced. The high pressure inside the PRACLAY gallery is thus maintained.

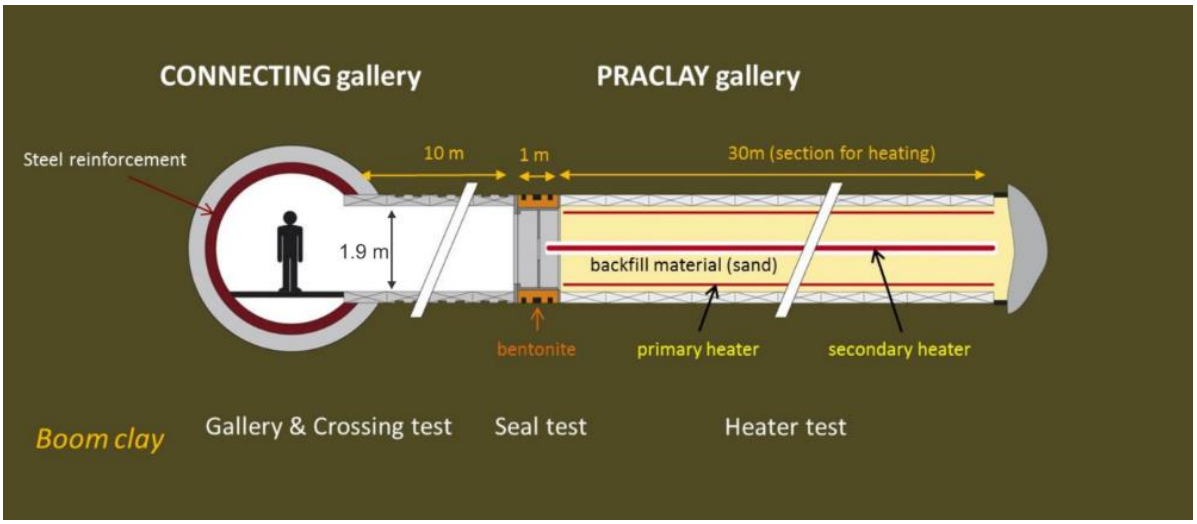

Figure 4-9. Overview of the PRACLAY In-Situ Experiment, including the component of heater test. The PRACLAY gallery has an inner radius of 0.95 m and the thickness of the lining is 30 cm (©EURIDICE)

The heating system consists of a primary heater, attached to the gallery lining, and a secondary heater, which is placed in a central tube that rests on a support structure. A control system regulating the heating power as a function of measured and target temperatures is also part of the heating system. During the start-up phase, the power was increased in a controlled manner to limit the thermal gradient over the gallery lining.

The heated part of the PRACLAY gallery is divided into three zones:

- Zone 1: front-end zone, 2.26 m long, close to the PRACLAY seal,

- Zone 2: middle zone, 28.48 m long, in the middle of the experimental part of the gallery,

- Zone 3: far-end zone, 3.29 m long, at the end of the gallery.

The power input can be controlled independently in each of the three zones. In this way, the end effects can be minimised and a temperature field that is as uniform as possible can be created along the heated section.

The sand that fills the gallery (Mol M34) was put in place by blowing it in a dry state into the gallery before September 2011. Subsequently, a total volume of about 43 m^3 of tap water was injected into this part of the gallery between January and May 2012. Saturation of the backfilled gallery was then naturally completed with the water flowing from the host Boom Clay into the gallery. The pore water pressure in the gallery gradually increased and after ~2.5 years it reached 1 MPa, and the backfilled PRACLAY gallery was estimated to be fully saturated. During the heating phase of the experiment, the pressure in the backfilled gallery evolves naturally without any human intervention (adding or subtracting an amount of water).

The PRACLAY In-Situ Experiment was intensively instrumented with about 1,100 sensors (piezometers, thermocouples, flat-jacks, strain gauges, etc.). Instrumented boreholes were drilled from both the Connecting gallery (CG) and the PRACLAY gallery (PG).

The heater was switched-on on the 3rd November 2014 with a constant power of 250 W/m for the three zones of the primary heating system. Two months later, the power was increased from 250 W/m to 350 W/m. Finally, the power was again increased to 450 W/m and maintained until the temperature at the extrados of the concrete lining reached 80°C, 8 months after the start of heating. This temperature was kept constant by gradually reducing the power in the three zones. After four years of heating, the zone in which temperature was affected by the test extended up to about 15–20 m and continued to grow smoothly and slowly. The evolution of the temperature was seen to be slightly different between the horizontal and the vertical directions, putting in evidence the anisotropy of the thermal conductivity. The pore water pressures in the experimental setup and in the clay also evolved smoothly, regularly and without any sudden or otherwise unexpected changes. The pore water pressure reached a value of 2.8 MPa in the backfilled part of the heated gallery and a maximum value of 3 MPa in the Boom Clay. In the far field, changes of pore water pressure were seen up to a distance of 22 m from the axis of the heated gallery, while the temperature had not increased at this location yet. At the end of 2023 the temperature at the interface between the Boom Clay and the extrados of the concrete lining was still maintained at 80°C.

More details about the large scale in-situ PRACLAY Heater test can be found in Dizier et al. (2021).

4.2.2 ALC 1605 HLW cell test

The ALC1605 full-scale heating experiment takes place in the Meuse/Haute-Marne Underground research laboratory (MHM URL) in north-eastern France. The 25-m long cell was drilled in the direction of the maximum horizontal stress from the GAN drift in November 2018. The characteristics of the cell correspond to the 2015 reference design of the Cigéo HLW cell, except for the length, which will be

either 80 m or 150 m long. Compared to the previous full-scale heating experiment (ALC1604, Bumbieler et al. 2020), the 30" casing is now centralised and the annulus between the casing and the formation is filled with an alkaline cement grout called MREA (Matériau de remplissage de l'Extrados des Alvéoles). The MREA is injected in the annulus to reduce the corrosion rate of the casing by: (i) neutralising the acidic drainage produced by pyrite oxidation, (ii) reducing the amount of oxygen coming from the drift.

The detailed objectives of the experiment are to:

- Study the impact of a thermal load on the TM behaviour of the casing when the annulus is filled with an MREA cement.
- Study the impact of a thermal load on the THM behaviour of the COx claystone in the near-field (but beyond the EDZ) and in the far-field (beyond a few cell diameters) with a filled annulus. The temperature and pressure evolution are monitored around the cell and at different offsets from the drift. A comparison with the measurements made during the ALC1604 experiment will help identify a potential impact of the filling material on the kinetics and the amplitude of the thermal pressuring in the near-field, and possibly the far-field.

The casing comprises thirteen interlocked elements, each measuring 2 m in length. Each casing element is equipped with temperature sensors on their inner surface, and five of them include convergence measurements to monitor casing ovalisation. Additionally, two casing elements are equipped with external fibre optics for strain and temperature measurements on the outer surface. In the formation, eight boreholes were drilled around the cell for pore pressure, temperature, and permeability measurements (Figure 4-10):

- 3 boreholes, diverging from the cell in a vertical plane with 5 measuring chambers and at least three of them in the heated zone;
- 4 boreholes in a horizontal plane on each side of the cell (2 of them diverging and 2 parallel to the cell) with 5 measuring chambers and at least three of them in the heated zone;
- 1 borehole parallel to the cell in a horizontal plane with 3 measuring chambers.

A last borehole called ALC1630, with five temperature sensors, was drilled parallel to the ALC1605 cell.

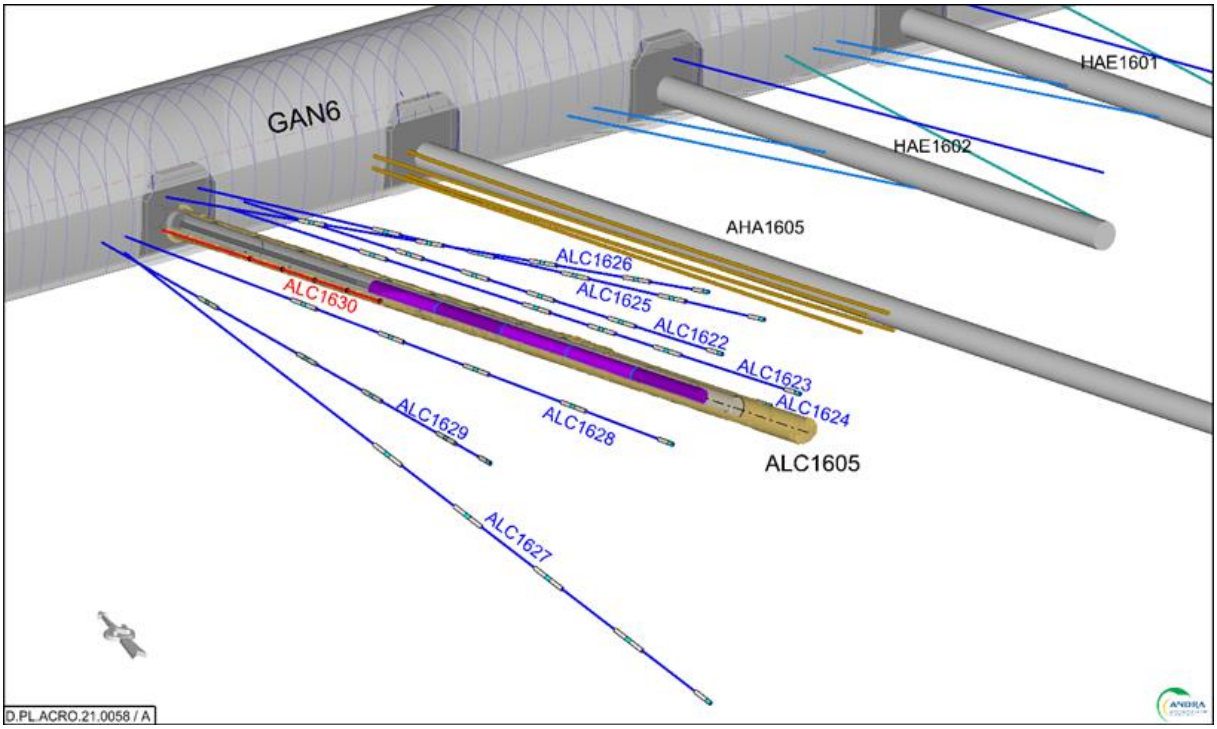

Figure 4-10. 3D schematic representation of the ALC1605 cell with peripheral boreholes

The cell is heated over 15 m by five heating elements, providing a power of 220 W/m. After a low power test in March 2020, the main heating phase started in June 2020. The heating power history from ALC1604 experiment was replicated to help comparing the two concepts (with and without filled annulus). After 3 years of heating in June 2023, the casing temperature was reaching 85°C in the upper side of the casing (Figure 4-11). The main heating phase is planned to last at least 5 years, until 2025.

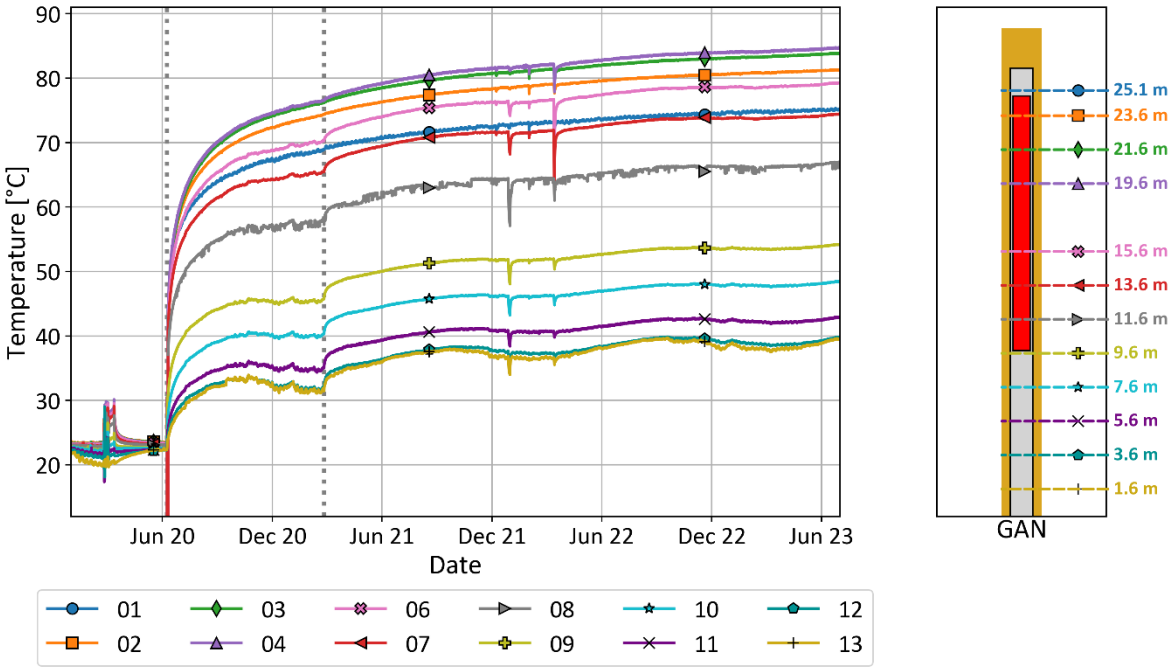

Figure 4-11. ALC1605 in-situ test - Temperature evolution in the casing

4.3 Effect of temperature on clay host rocks

4.3.1 Background

The thermal phase of a repository has consequences on 1) the clay behaviour around galleries, 2) the extent of the excavation damaged zone (EDZ), and 3) the clay properties within that EDZ. In turn, the THM behaviour of the clay is characterised by several coupled processes. As recalled in a synthesis by Li et al. (2023) on the THM behaviour of Boom Clay, the behaviour of clay submitted to heat is mainly governed by the coupling between the solid skeleton, the clay particles and the fluid phase.

The value of the thermal expansion coefficient of water is more than ten times greater than the value for the rock matrix. This large difference is the main cause of thermal pressurisation. The volumetric dilation of a solid is much lower than that of the fluid phase (water) filling the pore space. As a consequence, the fluid phase dilates more than the solid phase during heating and tends to occupy more space. Hence, the temperature rise in a low permeability porous medium, such as Callovo-Oxfordian and Opalinus claystones generates a pore pressure increase. This excess pressure reduces the effective stresses and may cause the failure of the sample. Among the usual constituents of the clay host rocks, the coefficients of the clay and quartz are similar, but those of calcite and feldspar are almost three times lower. This may also trigger some thermal damaging, especially at the interface between calcite and the clay matrix. Nevertheless, the competition between excess pore pressure due to thermal pressurisation and drainage due to pore pressure gradient increase is the key mechanism for the potential damage induced by the heat emitted from the waste.

High temperatures may also cause permanent damage to the EDZ, impacting the self-sealing capacity of the rock, and alterations in hydromechanical behaviour caused by prolonged heating. However, none of these processes has been observed so far. The ability of claystone to self-seal has been proven by several authors (see sections 4.1.1.2 and 4.1.2.2), and some processes involved (such as intraparticle swelling due to crack resaturation, inter-particle swelling due to osmotic effects, and plugging of fracture by particles aggregation) have been identified. Throughout the TIMODAZ experimental programme no evidence was found showing temperature-induced additional opening of fractures or a significant permeability increase of the EDZ. Instead, the thermal-induced plasticity, swelling and creep of clay are likely beneficial to the sealing of fractures and recovery of the permeability of the EDZ to the original state of the clay host rock (Yu et al. 2010).

Other findings of the TIMODAZ project were that in the absence of plastic deformation, elevated temperatures do not seem to adversely affect the pore structure of the clay, since the intrinsic permeability remains constant or even decreases with the increase of temperature. Temporary increases of hydraulic conductivity of clay could be explained entirely by the decrease of water viscosity and would be therefore reversible with temperature. Where thermo-plasticity was observed, thermoconsolidation was most likely to occur resulting in a void ratio and intrinsic permeability decrease.

4.3.1.1 Thermo-hydro-mechanical behaviour of Boom Clay

The thermal dissipation in a medium can be defined by two parameters, the thermal conductivity, which defines the dissipation of heat, and the volumetric heat capacity, a storage parameter. Djéran et al. (1994) performed laboratory experiments with a needle probe to determine the thermal conductivity (λ) and the volumetric heat capacity of the clay. Buyens & Put (1984) estimated the different thermal parameters by back calculation of an in-situ experiment in the quarry of Terhagen. Later, the in-situ heater test called ATLAS conducted at the HADES URL allowed the determination of the thermal conductivity in different directions. All these values are summarised in Table 4-11.

Table 4-11. Thermal properties of the Boom Clay

	Thermal conductivity (W/m°C)	Volumetric heat capacity (J/m^{3}K)
Buyens & Put (1984)	1.69	$2.83 \cdot 10^6$
Djéran et al. (1990)	1.44	$3.27 \cdot 10^6$
Charlier et al. 2010 (TIMODAZ project)	1.25 (vertical direction) 1.70 (horizontal direction)	$2.84 \cdot 10^6$
Chen et al. (2023)	1.20 (vertical direction) 1.90 (horizontal direction)	$2.84 \cdot 10^6$

These results show that depending on the test conditions (laboratory, in situ) different values of the thermal conductivity can be found. Djéran et al. (1994) explained these differences by the induced swelling due to the removal of the in-situ stress that can disturb the sample and modify the contact between the clay particles. As a consequence, a possible modification of the density may occur resulting in a change in the thermal conductivity. Dao (2015) measured the thermal conductivity in clay samples located at different distances from the wall of the connecting gallery. A decrease of the thermal conductivity in the first metres from the wall was observed. This decrease may be linked to a modification of the fundamental properties of the clay induced by excavation and so by the release of the confining pressure.

Hueckel et al. (2009) performed undrained triaxial tests on normally consolidated Boom Clay where one sample was heated at a given deviatoric stress. The excess pore water pressure induced in the heated sample followed a stress path towards the critical state line, leading to the failure of the sample. During the TIMODAZ project (Delage et al. 2010), Monfarred (2011) showed that undrained heating can be responsible for the reactivation of a pre-existing shear band during thermal pressurisation of a hollow cylinder in Boom Clay.

The mechanical behaviour of Boom Clay submitted to heating/cooling phases has been studied for a long time (Baldi et al. 1987, 1988, 1991; Sultan, 1997; Cui et al. 2000; Delage, 2000). The contractive/dilative behaviour was observed in drained heating tests at different confining pressures by Baldi et al. (1991) and Sultan (1997). For normally consolidated and slightly overconsolidated samples, the behaviour remained contractive during the heating phase, while for highly overconsolidated samples dilation was followed by contraction.

In addition to this dilative/contractive behaviour, clayey soils undergo variation of their elastic limit with temperature. In the case of fine grained soils, the preconsolidation pressure decreases with the increase in temperature. Indeed Le (2008) obtained in two oedometer tests a preconsolidation pressure of 5 MPa at ambient temperature and of 4 MPa at 80°C. Also, when a clay sample is submitted to temperature increase, an overconsolidation effect occurs. This was observed by Cui et al. (2000) during isotropic compression of Boom Clay samples when the clay was heated at a constant pressure and then reloaded at a higher temperature.

The hydraulic conductivity is also affected by temperature, and more specifically, the viscosity of water decreases with the increase of temperature. As a consequence, the hydraulic conductivity will normally increase with temperature (e.g. Delage et al. 2000, Lima 2011). This change in water viscosity with temperature only affects the hydraulic conductivity of the clay, but not its intrinsic permeability, as experimentally shown by Delage et al. (2000) and Lima (2011).

Djéran et al. (1994) performed tests to study the influence of temperature on creep and showed that at high temperature the rate of creep seems to increase: the clay became more ductile and viscous. The thermal effect on secondary compression was analysed by Cui et al. (2009). With the increase of

temperature, the strain rate increased more with time than at ambient temperature, i.e. the consolidation rate increased with temperature.

4.3.1.2 Thermo-hydro-mechanical behaviour of COx claystone

The thermal conductivity of the UA was both measured on samples taken in boreholes drilled for the TED experiment and determined by inverse analysis during this experiment (Tourchi et al. 2019). The results shown in Table 4-12 match very well, which shows that there is no scale effect and that laboratory measurements can be used to characterise the thermal behaviour of the COx claystone.

Table 4-12. Thermal conductivity of COx claystone (in $W \cdot m^{-1} \cdot K^{-1}$) measured in boreholes drilled for the TED experiment (a) and determined by inverse analysis (b)

	LAEGO (a)	DBETEC (a)	UPC-TED1 (b)	UPC-TED2 (b)	CEA (b)	DBETEC (b)
λ_h	1.89±0.05	1.96±0.07	1.95	1.93	2.07	2.07
λ_v	1.26±0.05	1.28±0.06	1.30	1.26	1.37	1.32
λ_0			1.69	1.67	1.80	1.78
λ_h/λ_v			1.50	1.53	1.51	1.57

The thermal and THM modelling of the TED experiment using the parameters in Table 4-12 matched well the evolution of temperature during the whole heating phase, showing that thermal conductivity does not vary with temperature. This point was also proven by laboratory measurements: for tests performed at temperatures between 20 and 150°C, the horizontal and vertical thermal conductivities were almost independent of temperature, whereas there was a clear increase of the conductivity with the water saturation (Jobmann et al. 2013).

Specific heat measurements performed on samples from four different boreholes show that it does not vary much with depth. In the UA, the average value at 20°C is 973 $J \cdot kg^{-1} \cdot K^{-1}$. Inverse analyses from the TED experiment gave 971 and 987 $J \cdot kg^{-1} \cdot K^{-1}$.

Although there is no direct measurement of the thermal properties of the EDZ, they have been estimated by inverse analysis of the temperatures measured during the ALC1604 HLW cell heating test (Tourchi et al. 2019). The 3D modelling of the experiment matched well the temperature measurements using the same conductivity in the EDZ as in the intact rock. A sensitivity study showed that the temperature field beyond the EDZ is very weakly influenced by the thermal properties of this zone. It appears therefore justified to use the same conductivity in the EDZ and in the intact COx claystone.

The undrained thermal expansion coefficients (α_u) parallel and perpendicular to bedding found in laboratory tests performed on samples as part of the TED in-situ experiment were $10.2 \pm 1.9 \cdot 10^{-6}$ $°C^{-1}$ and $18.2 \pm 4.9 \cdot 10^{-6}$ $°C^{-1}$, respectively. The drained linear thermal expansion coefficients (α_d) obtained by Braun (2019) parallel and perpendicular to bedding were $0.5 \cdot 10^{-5}$ $°C^{-1}$ and $0.2 \cdot 10^{-5}$ $°C^{-1}$, respectively. These values are lower than the ones obtained in undrained conditions and the one used by Tourchi et al. (2019) in their inverse analysis of the TED experiment ($1.3 \cdot 10^{-5} °C^{-1}$), but all remain much lower than the coefficient for water. Tourchi et al. (2019) showed that this parameter does not have much influence on the pressure variations.

The effect of temperature on various THM parameters was studied in the 25-80°C range. The elastic modulus showed a very slight tendency to decrease as the temperature increased, although this reduction could also be attributed to the mineralogical variability between samples (Zhang et al. 2012).

The stress at failure decreased slightly with the increase in temperature and this phenomenon was more pronounced for low confinement values (Zhang et al. 2012).

Several authors (Baldi et al. 1991, Delage et al. 2000) showed that normally consolidated clays subjected to constant mechanical load and slow temperature increase generally incur an irreversible contraction. Weakly overconsolidated clays experience first a thermal expansion, followed by a contraction. This phenomenon is interpreted by a variation in the elasticity limits with temperature called "thermal hardening". COx samples exhibited a thermo-elastic expansion up to a temperature around 45°C, followed by thermo-plastic contraction at higher temperature that could be enhanced by the appearance of microcracks resulting from some desaturation of the samples (Belmokhtar et al. 2017).

Braun (2019) performed a series of tests under thermal load in drained conditions. The contraction was essentially localised perpendicularly to bedding, whereas the strains parallel to bedding were reversible and linear. In this direction, the samples expanded when heated, and contracted when cooled down, showing that the response to thermal loading is thermo-elastic (Figure 4-12). Perpendicular to bedding, the rock expanded up to 40°C, then contracted for higher temperatures. While cooling, a linear contraction was observed. This phenomenon was not observed in small-scale in situ experiments such as TER or TED, where measurements were performed in the far field. However, the full-scale ALC1604 experiment showed in some cases a “relaxation” of the radial load applied by the rock on the steel casing, that could be a sign of thermal hardening in the EDZ.

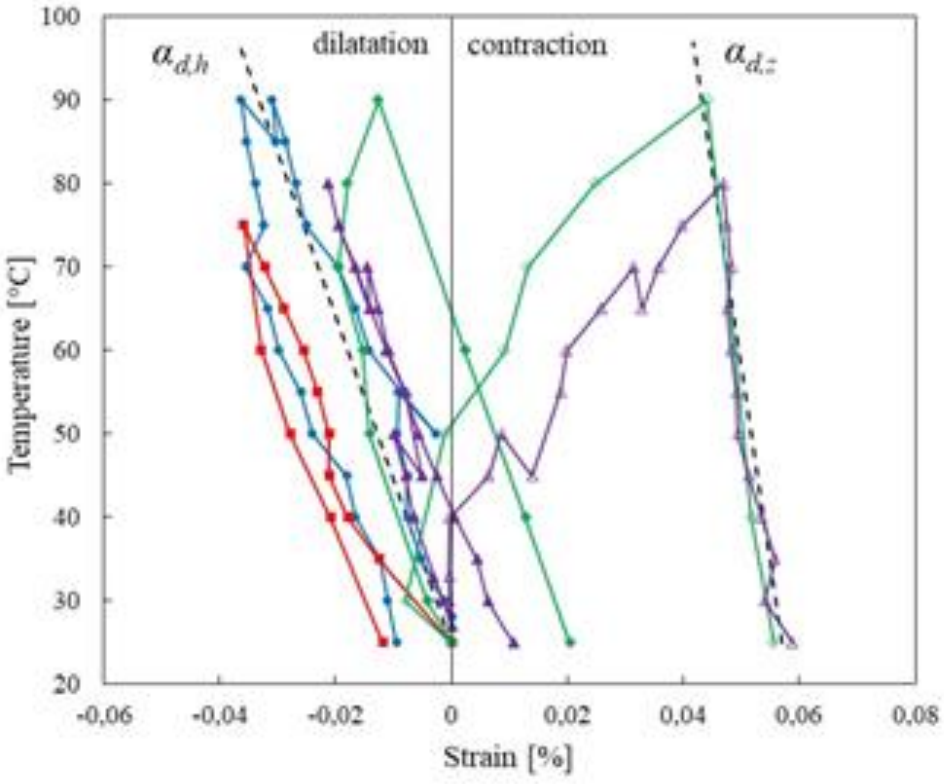

Figure 4-12. Strain measured on COx samples under drained conditions as a function of temperature – purple and green curves: vertical/perpendicular, blue and red curves: horizontal/parallel to bedding (Braun, 2019)

The change of pore pressure may be related to the applied temperature variations by the thermal pressurisation coefficient, Λ. This coefficient depends on the nature of the rock, the range of

temperature variation, the level of damage of the material, and the state of stress. A special isotropic cell was designed to conduct thermal pressurisation tests under stress conditions close to the in situ state (Tang et al. 2008b; Mohajerani et al. 2012). With the same device, Braun (2019) performed two heating tests in three phases with application of a thermal load. The resulting thermal pressurisation coefficients shown on Figure 4-13 are consistent with the theoretical values (dashed line), they increased from 0.12 MPa/°C at 25°C to 0.30 MPa/°C at 80°C, whereas values by Mohajerani et al. (2012) were almost constant. The stress conditions during the experiments explains this difference: Mohajerani et al. (2012) did not maintain constant effective stresses and their reduction led to a decrease in the Biot modulus and a practically constant thermal pressurisation coefficient.

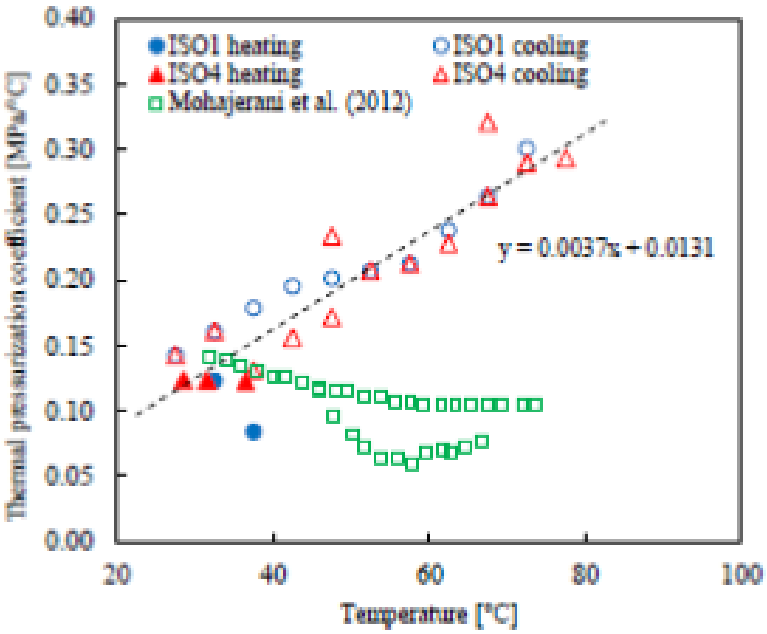

Figure 4-13. Measured/corrected thermal pressurisation coefficients of COx claystone at different temperatures (Braun, 2018b; Mohajerani et al. 2012)

Temperature may play a role in the long-term behaviour of the COx claystone. Pellet (2007) reviewed the studies performed on time-dependent deformation and found that, despite the large dispersion of data, the deviator stress had a clear influence on the creep rate, whereas the effect of temperature overall was not obvious. Zhang et al. (2010) performed uniaxial compression tests under two different confining pressures (0.74 and 13.8 MPa) and a series of triaxial tests with a constant axial stress (15 MPa) but different radial stresses, 3.1 and 5 MPa. During these tests, temperature was increased and decreased in steps. This led to a slight increase in deformation due to thermal expansion, followed by a resumption of the creep. The higher temperature caused in general an increase of the deformation rate (up to 5 times larger), which may be related to the fact that water viscosity decreases as temperature increases.

Auvray et al. (2015) performed self-sealing tests on the COx argillite in a PEEK triaxial cell under room temperature, but with only 2D X-ray scans. Giot et al. (2019) performed the same kind of tests with 3D X-ray scans but with a limited amount of data and basic voxel data analysis.

4.3.2 Progress made during HITEC

During the HITEC project two aspects were mainly analysed: the impact of temperature on the short- and long-term behaviour and the self-sealing processes. In the first case the focus was on the thermal pressurisation and the risk of damage if the effective vertical stress becomes tensile. In the near field, characterised by a fractured zone, thermal pressurisation could induce fracture opening or propagation in the EDZ, altering its permeability. In the far field, this could induce rock damage and reactivate fractures/faults (if they exist).

Furthermore, fractures subject to water circulation in clay rocks can fully or partially close, leading to self-sealing processes. The availability of water within the EDZ may change over the timeline of a repository and therefore self-sealing of fractures could occur at a time where the repository is producing elevated temperatures. The swelling phenomena of the material around the lips of the crack are sensitive to water re-saturation, they could also be sensitive to temperature: geometric characteristics (opening and volume) and permeability of fractures could evolve as a function of temperature.

4.3.2.1 Hydro-mechanical behaviour

The short-term effect of temperature on the mechanical behaviour of the Callovo-Oxfordian claystone was analysed by compression tests performed in a triaxial cell with strain measurements at different temperatures (20, 40, 60, 80, 100 and 150°C), confining pressures (0, 4 and 12 MPa) and sample orientations (parallel and perpendicular to the bedding plane) (Grgic et al. 2023b). The tested samples were initially a little unsaturated (degree of saturation between 90 and 97%) and the compression tests were performed under the so-called pseudo-drained condition, with the drainage circuit of pore fluid open and connected to the atmospheric pressure. Indeed, with respect to the small size of samples, the selected strain rate ($5 \cdot 10^{-6}$/s) is considered slow enough to avoid significant over-pressurisation of the pore fluid. The analysis of elastic coefficients from the short-term compression tests indicated that in all cases an anisotropic damage developed during the deviatoric loading due to the opening of axial microcracks. This result had already been observed in previous works and was confirmed here on the Cox claystone at high temperatures. In addition, the peak deformation and strength increased when confining pressures increased. The initial heating stage generated a transitory pore water overpressure due to thermal expansion (because of the rapid thermal loading rate), which created microcracks probably parallel to the bedding plane. Despite the scattering of results, an overall decrease of the peak strength with increasing temperature (until 100°C) was observed because of the THM damage induced by the initial heating (Figure 4-14). For the parallel samples under uniaxial conditions, this decrease was the most important and volumetric dilatancy developed during loading for the highest temperatures. For all other conditions, the decrease was more moderate and there was no dilatancy because the confining pressure reduced the creation of initially thermo-induced microcracks. Hence, a lower thermal loading rate would have induced a lower overpressure and probably a much lower damage. The microcracks were closed when the axial stress increased during the compression tests when the orientation was perpendicular. There was no noticeable impact of temperature up to 100°C on the evolutions of the elastic coefficients. The peak strength increased at the highest temperature (150°C) in all cases due to the water vaporisation and consequently strong desaturation of the samples, which induced the development of a very significant capillary suction.

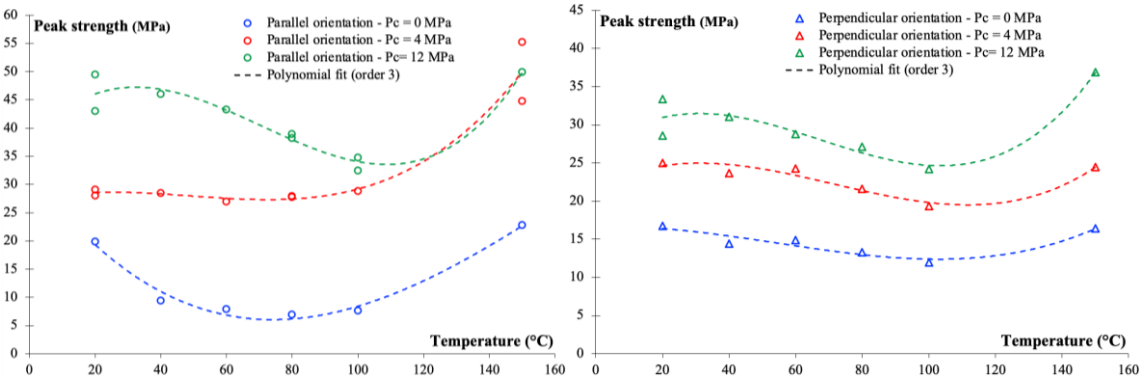

Figure 4-14. Evolution of the deviatoric stress at peak (peak strength) as a function of temperature for parallel (left) and perpendicular (right) orientations and for various confining pressures (Gbewade et al. 2023)

BGS undertook a series of oedometric (K_0) experiments measuring the spatial and temporal development of porewater pressure caused by thermal expansion and its subsequent impact on the evolution of intrinsic permeability (Grgic et al. 2023b). Samples of clay/mudrock were tested from ambient to 90°C for orientations both parallel and perpendicular to bedding. A bespoke apparatus was specifically designed (Figure 4-15). After rehydration with synthetic solutions permeability was measured. The temperature designated for a particular test was then applied in a single step, and the development of overpressure was monitored along with the thermal expansion of the sample. Permeability was measured during this phase and after final cooling. Backpressure was between 2 and 4.5 MPa, injection pressure between 2 and 6 MPa and the axial stresses between 4 and 14 MPa.

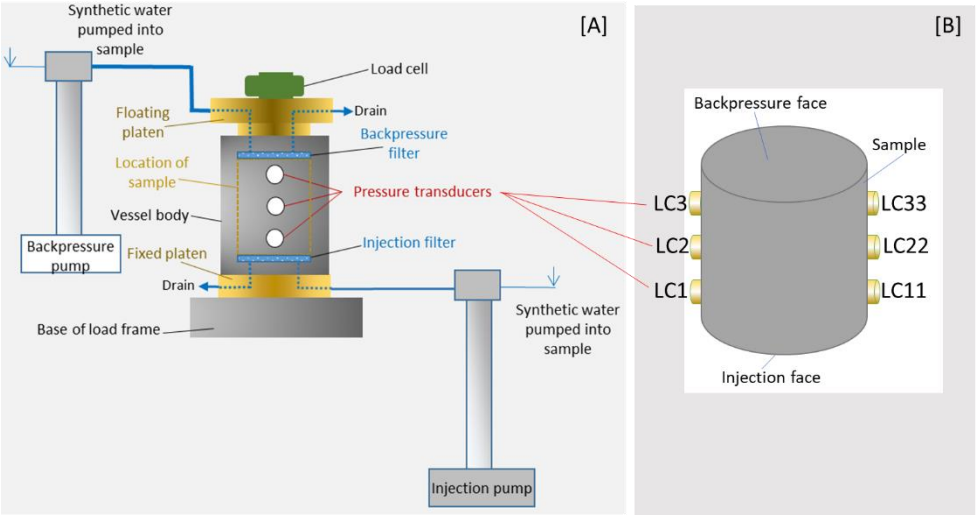

Figure 4-15. Schematic showing the layout of the BGS key apparatus components and the position of the pore pressure sensors around the periphery of the sample (Grgic et al. 2023b)

In all cases permeability decreased with the increase of effective stress and on heating, with the rate of change linked to the initial permeability of the sample (Figure 4-16). The observed drop in permeability with temperature could be explained by the thermal contraction of the OPA by a small amount. As expected, permeability was lower perpendicular to bedding, with anisotropy ratios ranging from around 2.1 to 3.3 at 25°C and 85°C respectively. Only one COx sample was tested and its permeability (7.10^{-21} m^2) was considerably lower than that of Opalinus (and in contrast to the numbers reported in Table 4-3 and Table 4-5 that take also into account the measurements acquired in in-situ

experiments), leading to higher peak porewater pressures and possible evidence of thermally induced mechanical failure. However, in all experiments, no evidence for the degradation of hydraulic properties was observed once temperatures had dissipated.

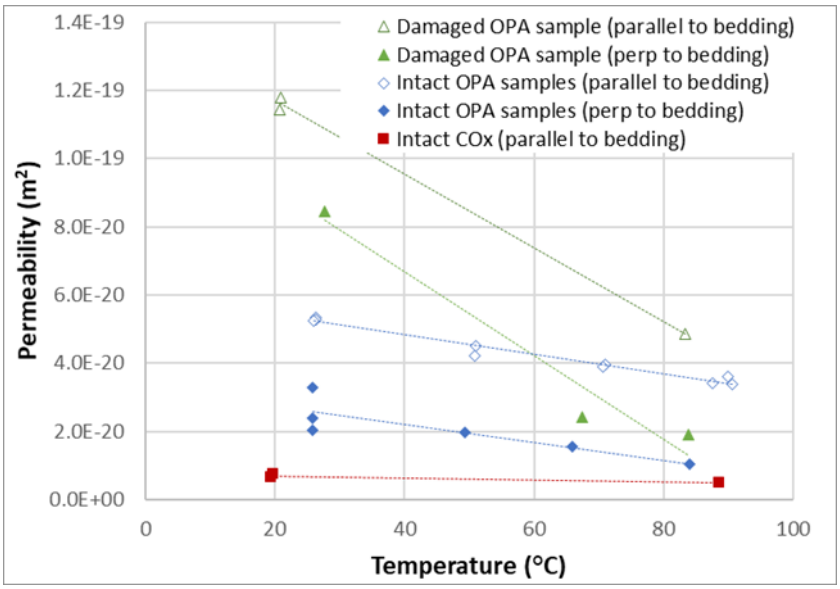

Figure 4-16. Permeability for OPA and COx against temperature obtained by BGS (Grgic et al. 2023b)

In all tests, the pulse in porewater pressures caused by heating of the sample was short-lived (<24 h), reflecting the stiffness of the materials and the small amounts of water moved due to thermal expansion/contraction. In Opalinus Clay, heating to temperatures of 70°C and upwards resulted in the development of local porewater pressures exceeding the axial stress, with peak pressure increasing with temperature. However, in the test performed at elevated axial stress, peak porewater pressures remained below axial stress. This suggests that while the development of internal porewater pressure is linked to the heat applied and the permeability of the material, the magnitude of the effective stress is also important in limiting the potential for localised thermally induced hydraulic damage. Porewater pressures exhibited local anisotropy (measurements of pore pressure on the same plane of a sample at locations 180° apart were different) and possible heterogeneity effects (variability in the response between individual samples prepared with the same bedding orientation, for example differences in the magnitude of the peak porewater pressures) at least on the length scale of the experiments.

To analyse the long-term behaviour a series of multi-step creep tests were performed on Opalinus and Boom Clay under constant elevated temperature by CEA (Grgic et al. 2023b). Samples taken from close positions along a core were first saturated under isochoric conditions and at room temperature with solutions representative of the clay pore water in triaxial cells. Then each sample was heated to a different temperature and the deviatoric stress was increased by steps, keeping constant the confining and pore pressures (confining pressure 4.7 MPa and pore pressure 2.2 MPa for Boom Clay, confining pressure 6 MPa and pore pressure 2 MPa for Opalinus Clay). The natural variability of the samples hindered a straightforward comparison of the effect of temperature, but for Opalinus clay, the magnitude of the strain for a given deviatoric stress was more important when the temperature was higher (Figure 4-17). Moreover, the kinetics of the strain development was faster for the higher temperature. During some steps under a great deviatoric stress failure occurred.

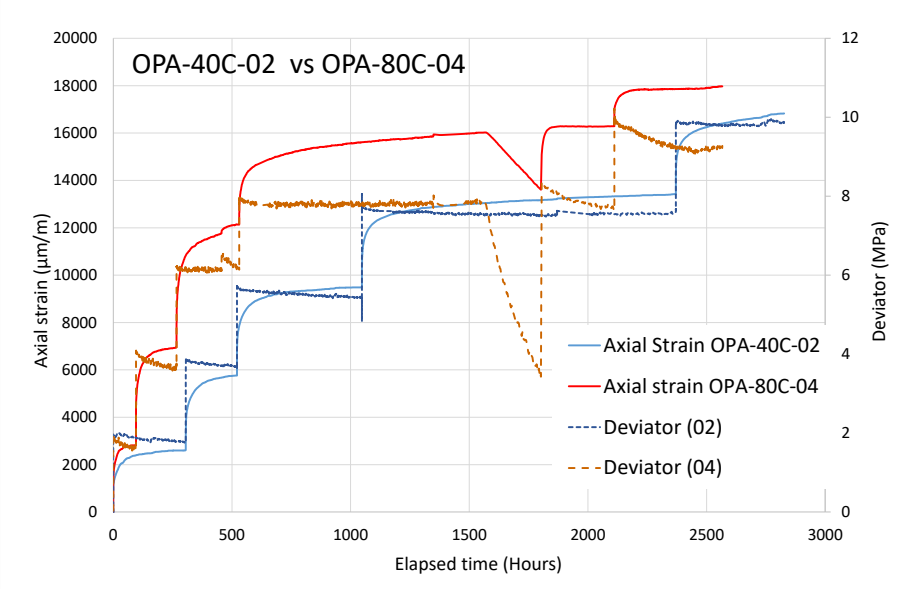

Figure 4-17. Creep tests for two samples of Opalinus Clay tested at 40°C and 80°C by CEA (Grgic et al. 2023b)

4.3.2.2 Self-sealing

During HITEC the self-sealing process in the Callovo-Oxfordian claystone was analysed by performing self-sealing tests with water injection on initially (artificially) fractured cylindrical samples under different temperatures, sample orientations (parallel and perpendicularly to the bedding plane), calcite contents and initial crack openings (Grgic et al. 2023a). Self-sealing tests were performed in a novel mini-triaxial compression cell made of PEEK CF30 transparent to X-rays which made it possible to follow the evolution of the crack volume in the sample at different times under a high-resolution X-ray computed tomography (CT) scanner. 3D scans were performed on all tested samples before, during and after the experiments. These self-sealing tests were performed under a confining pressure of 4 MPa. Water permeability was measured continuously during all tests.

Overall the self-sealing process was fast at the beginning of the tests and stabilised after one month (Figure 4-18). Thanks to the self-sealing process, the permeability of the COx claystone samples (Figure 4-18, right) was partially restored (~10^{-18}-10^{-19} m^2) compared to the initial permeability of the healthy (i.e. without fracture) claystone (~10^{-20}-10^{-21} m^2). The mineralogical composition of the COx claystone influenced the self-sealing process: the higher the calcium carbonate content (and therefore the lower the clay content), the less effective the self-sealing process, whatever the sample orientation. To have an effective sealing, a carbonate content lower than 40% was necessary (Figure 4-19). No significant influence of the sample orientation on the self-sealing kinetics was identified at this stage; the self-sealing process was equally efficient for both parallel and perpendicular orientations. In contrast, the opening of the initial artificial crack did influence the kinetics of the self-sealing process: it was faster for an initial crack opening of 0.4 mm than 0.8 mm. Finally, temperature may have a slight delaying effect on the self-sealing process, since the volume of the crack decreased more slowly at higher temperature (80°C). However, the permeability reduction did not seem to be impacted by temperature.

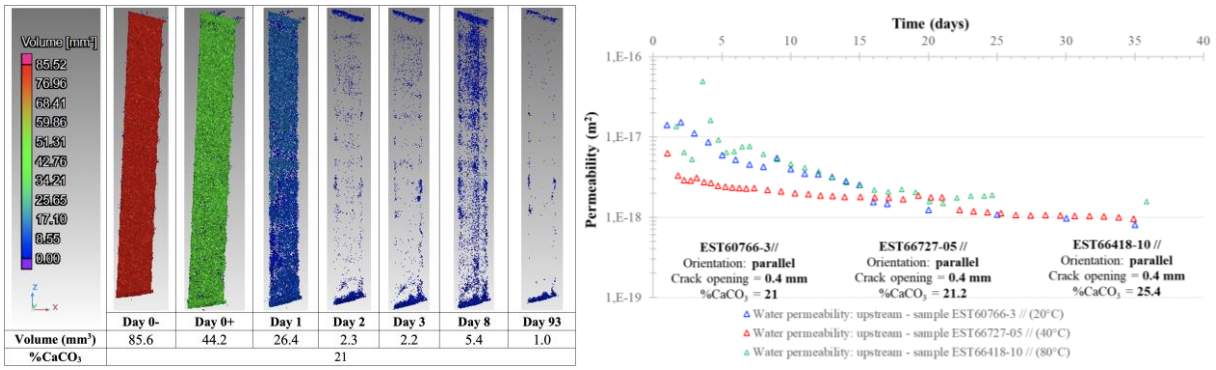

Figure 4-18. X-ray 3D tomography images of a parallel sample showing the evolution of the crack volume with time (initial crack opening = 0.4 mm) during self-sealing test at 20°C (Day 0-: after hydrostatic loading; Day 0+: after crack saturation) (left, Agboli et al. 2023); and evolution of water permeability during self-sealing tests on parallel samples at 80, 40 and 20°C (right, Grgic et al. 2023a)

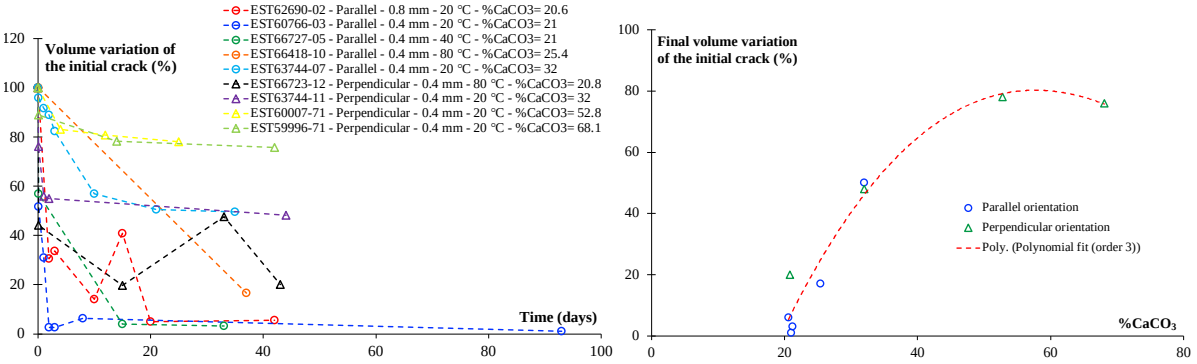

Figure 4-19. Volume variation percentage of the initial crack (normalized with the volume after hydrostatic loading) obtained from X-ray tomography 3D images during all self-sealing tests with water, for parallel and perpendicular orientations (left); and volume variation percentage of the initial crack at the end of the tests as a function of the calcite content for both orientations (right) (Grgic et al. 2023a)

The University of Grenoble developed a cell to be used with a laboratory X-ray tomograph, a D50 beamline from ILL for dual X-ray and neutron tomography and with a temperature control up to 90°C (Grgic et al. 2023a). Cylindrical specimens (centimetric size) were cut from in-situ collected cores and prepared with a synthetic crack in the middle axial plane. The crack was initially open and the specimen placed in oedometric conditions (no radial displacement of the outer boundary). Neutron and X-ray scans were done every 15 minutes during the flow of synthetic host pore water through the crack. Crack closure, local swelling around crack and water re-saturation (water content evolution) were quantified thanks to the neutron and X-ray scans and DIC analysis based on Stavropoulou et al. (2020). Tests were performed at three different temperatures on samples parallel and perpendicular to bedding. Although the tests conducted had a very short duration, it was possible to observe some features of behaviour. At 25°C, quasi-instantaneous closure of the crack was favoured by the formation of a dense network of micro-cracks sub-parallel to the bedding in the area close to the interface lips, creating a highly damaged material that filled the interface space. At 90°C, the mechanism was more diffuse and secondary cracks were scattered. Hence, the reclosure kinetics was more gradual and greater in intensity at 90°C, favoured by a diffuse swelling in the whole sample. In both cases, the interface with an initial opening of around 0.3 mm was completely filled within around 3 h, although the mechanisms were slightly different, showing a more ductile character at 90°C.

BGS performed a series of novel experiments using a highly instrumented bespoke direct shear apparatus, the Heated Shear Rig (described in e.g. Cuss et al. (2011)), using heating cartridges and band

heaters attached to the rig to increase temperature up to 90°C. The samples, prepared by machine lathing, were 60±0.01 mm in diameter and 53±1 mm in height. The intact samples were initially sheared, then hydraulic flow was imposed into the fracture, and finally active shearing took place under constant hydraulic flow. The results resported in Grgic et al. (2023a) showed that temperature has a considerable effect on the shear properties of Opalinus Clay and COx.

All tests with Opalinus Clay showed elastic-brittle behaviour, with peak shear stress increasing by 0.47 MPa per 10°C temperature. Residual strength also increased with temperature at a rate of 0.09 MPa per 10°C. Shear modulus showed considerable spread in the data, but also showed an increase with temperature. Repeat shear in Opalinus Clay also showed a clear increase in peak strength of 0.175 MPa per 10°C and residual strength of 0.178 MPa per 10°C. A small increase in shear modulus was seen but with considerable spread in the data. Therefore, in intact and re-sheared Opalinus Clay, strength and compliance increase with temperature. The increase was greater in intact OPA.

Considerable variation was seen in the flowrate into the fracture that could not be described by fracture surface characteristics. Therefore, two different self-sealing potential (SSP) coefficients were defined: a) as a result of hydraulic flow along the fracture (SSP_{H2O}); b) as a result of active shear along the fracture while hydraulic flow continued (SSP_{τ}). The SSP coefficient describes the proportional change in flow as opposed to the absolute change in flowrate. Self-sealing potential was seen to change with temperature in Opalinus Clay. A clear relationship was seen with SSP_{H2O}, with a reduction in self-sealing capacity with increasing temperature (Figure 4-20). At a temperature of 90°C, the self-sealing potential was negligible. A difference was seen between SSP_{H2O} for fractures that were formed at ambient temperature and those formed at temperature, although this may simply be explained by natural variation between samples. This result suggests that SSP_{H2O} is better in fractures that have formed at temperature. This may be related to differences in fracture topology. Considerable spread of results was seen for self-sealing potential because of active shear (SSP_{τ}). However, a reduction in SSP_{τ} was seen with increasing temperature. In conclusion, for Opalinus Clay, the effectiveness of self-sealing processes reduced at elevated temperatures.

All fracture surfaces were laser scanned following the initial and re-shear stages of the experiment. Little variation was seen in roughness characteristics for the initial shear samples, with a reduction in roughness seen during re-shear. Little variation was seen in fracture topology for shear fractures created at different temperatures in initially intact samples. The presence of water during the re-shear phase resulted in the reduction in fracture roughness. As self-sealing potential (SSP_{H2O}) is a function of temperature and fracture roughness alters with temperature, it is likely that fracture roughness played a role in the effectiveness of fractures to self-seal.

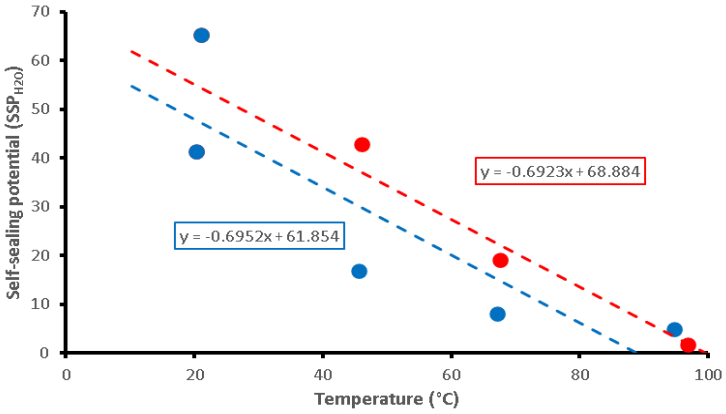

Figure 4-20. Influence of temperature on self-sealing potential of Opalinus Clay as a result of hydration (BGS results in Grgic et al. 2023a)

In the tests performed with Callovo-Oxfordian claystone by BGS the stress-strain response showed a similar form over the full range of temperatures, although as temperature increased the response was more brittle. Peak strength was seen to increase by 0.13 MPa per 10°C, with residual stress increasing by 0.01 MPa per 10°C. Shear modulus reduced with temperature, although this result may be influenced by a low modulus seen at the highest temperature. Callovo-Oxfordian claystone therefore increases in strength with temperature but has a reducing stiffness. Self-sealing processes in Callovo-Oxfordian claystone were seen to greatly change over the range of temperatures investigated. At ambient temperatures, SSP_{H2O} of COx was 132 and reduced to just 7 at 90°C. Therefore, a near two-order of magnitude reduction was seen in the effectiveness of self-sealing because of water flow. A reduction was also seen in the effectiveness of self-sealing because of active shear (SSP_{τ}), although the reduction was not as marked as for water and the data showed considerable spread. The preliminary data for Callovo-Oxfordian claystone suggest that the favourable self-sealing properties of the rock reduce with temperature and become almost negligible at 90°C, that is in contradiction with what ULorraine found (Figure 4-18).

4.3.2.3 Summary and conclusions about the THM behaviour of claystones

Working at high temperature with claystones poses experimental challenges, and in this sense experimental improvements were achieved during the HITEC project. Different testing cells (triaxial, oedometric and shear ring) and monitoring tools (X-ray and neutron tomography) were used by the different partners and adapted to work at high temperature, although most tests were performed below 90°C. The use of triaxial cells with heating collars, though not uncommon, has been particularly developed during the project and tests at temperatures as high as 150°C were performed by ULorraine, although with considerable evaporation of the samples. Adding heating to the direct shear rig of BGS was particularly complicated. X-ray CT and neutron tomographic images were used to follow the evolution of cracks, but a need to improve the quality of images and the testing protocols (recreate in situ stress conditions and measure the hydraulic conductivity of the interface during self-sealing) was identified.

The impact of the testing protocols on the results obtained is always a concern. For example, it cannot be ruled out that thermal loading rates applied, much higher than those to be expected in a repository, could damage the samples and consequently their subsequent behaviour. Furthermore, the particular stress conditions during the tests may affect the results. Thus, the formation of microcracks in COx claystone induced by the thermal expansion of the porewater under uniaxial conditions –leading to a significant decrease in the peak strength with temperature– may be reduced by application of confining pressure during heating. Also in relation to the stress conditions, while K_0 experiments allow the measurement of formation overpressures, they impose a slightly artificial boundary condition under which the sealing of indurated materials such as OPA and COx may be more difficult. This geometry may also limit some failure mechanisms.

Important hydro-mechanical couplings between peak porewater pressure, temperature, permeability and confining stress were identified. Temperature was seen to have a clear effect on the fracture shear properties of both COx and Opalinus claystones (increase in peak strength, residual strength and shear modulus). From the triaxial compression tests, temperature has a likely negative impact on the short-term strength to failure of the COx claystone. But if this THM damage were induced, it would probably be limited to the very near field of the EDZ, where the confining pressure is the lowest. At 100 and 150°C, in unsaturated samples, the peak strength and the stiffness of the COx claystone increased, irrespective of the sample orientation. The thermal pressurisation tests on Opalinus Clay and Callovo-Oxfordian claystone samples did not show any strong impact of heating on the clay permeability.

The results of these laboratory experiments are positive and confirm that the claystone keeps its good mechanical and self-sealing properties, even when heated at high temperature (up to 100°C).

Nonetheless, considering the heat output of the waste and the thermally induced porewater pressures, a repository should be located at a depth below which thermally induced porewater pressures could remain lower than the in-situ stress.

Many parameters could influence the efficiency of the self-sealing process: the calcium carbonate content, the sample orientation with respect to bedding, the opening of the initial artificial crack, and the temperature. The tests performed confirmed the self-sealing capacity of the COx claystone, even when heated at 80°C. Provided that the clay content of the samples was high enough, self-sealing was an efficient mechanism whatever the experimental conditions. Temperature may have a slight delaying effect on the self-sealing process though. However, the effectiveness of self-sealing processes as a result of hydration and shear was seen to reduce significantly at elevated temperatures. Indeed, fracture roughness, which plays likely a role in this process, is reduced by the presence of water during the re-shear phase and by temperature.

Overall, confidence was gained in the positive impact of the self-sealing process on the restoration of the initial sealing properties of the clay host rock. It is all the more promising that the duration of the laboratory experiments is much shorter than the repository time scale.

4.4 Modelling tools and approaches

4.4.1 Callovo-Oxfordian Clay

In order to validate the rheological models at the scale of a HLW cell and, and if possible, to improve the determination of the parameters used, ANDRA set up from 2003 an in situ experimental programme to progressively:

- Confirm the thermal design parameters for the disposal
- Provide a better quantification for the THM processes around the HLW cells
- Perform some experiments to validate the concepts for the HLW cells

The in-situ tests in the Bure URL made it possible, through inverse analysis, to estimate certain THM parameters on a metric scale and to compare them with the measurements on samples (Garitte et al. 2014). For example, the inverse analysis of the thermal parameters (thermal conductivity, heat capacity) confirmed the low variability between the values obtained in the laboratory experiments and those measured in the field.

The small-scale thermal tests (TER, TED) demonstrated that the numerical simulations conducted with a linear thermo-poro-elastic model could accurately reproduce the temperature and the pore pressure variations, while also taking into consideration the thermal, mechanical and hydraulic anisotropy. From these tests, the sensitivity analyses showed that the major parameters were the stiffness of the COx claystone, the permeability, and, to a lesser extent, the thermal conductivity and the Biot coefficient.

The first results from the full-scale HLW disposal cell demonstration test with the 2009 concept in the Bure underground laboratory (ALC1604), showed that the small-scale approach that was used, without considering the change in thermal parameters in the EDZ, enables a reasonable prediction of the temperature range. For the changes in the "far-field" pore pressure (several metres away from the heating cell), the influence of the modifications on the near-field hydro-mechanical properties caused by the cell excavation, remain low. However, in the near-field, the purely linear poro-elastic approach is not good enough to correctly reproduce the change in pore pressure or the deformations. A more complete modelling approach is therefore required to better represent the physical processes in the fractured zone caused by cell excavation (variations in permeability, mechanical behaviour of fractured zone, etc.).

The analysis of the temperature, pressure and stress variations around the HLW cells as a function of the thermal load and of the inter-cell spacing was done internally using two well-known numerical simulation programs: Code-Aster and Code_Bright. UPC also performed the modelling on Code_Bright of the ALC1604 heating experiment (Tourchi et al. 2021).

In addition, some benchmarking exercises were carried out, for example:

- **Constitutive model for the EDZ**. A benchmark exercise was organised in 2012 to model the induced fracture networks around a drift (Seyedi et al. 2017, Guayacan 2016). Several constitutive models were developed, divided into four main families: most were based on visco-elasto-plasticity, but damage-mechanics, rigid body spring and computational homogenised models were also tested. It was shown that accounting for material anisotropy and strain localisation treatment techniques could improve the results when elasto-visco-plastic models are used.
- **THM modelling of the TED in-situ heating test**. A benchmark exercise was organised as part of the DECOVALEX 2019 international program with the purpose to upscale the THM modelling from small-size experiments (some cubic metres) to real-scale cell experiments (tens of cubic metres) and finally to the scale of the waste repository (cubic kilometres). It was based on the TED small-scale heating experiment (Conil et al. 2020) and focused on the THM behaviour of the undisturbed claystone in the far-field (Seyedi et al. 2021). It was concluded that a good prediction of the evolution of temperature and pore pressure can be achieved if anisotropic poro-elastic behaviour is considered.

4.4.2 Boom Clay

The hydro-mechanical behaviour of Boom Clay is reproduced with models such as the Drucker-Prager criterion (Drucker & Prager 1952) or the Cam-Clay model. Many other constitutive mechanical laws have been developed to simulate the clay in various thermo-hydro-mechanical conditions. For example, the development of thermo-plastic strains by the increase of temperature was taken into account in models such as ACMEG-T (François 2008) and in other thermo-mechanical cap models (Cui et al. 2000, Dizier 2011). Dizier (2011) developed a thermo-mechanical model consisting in an extension of the cap model to thermo-plasticity. The model combines different plastic mechanisms, i.e. modified Cam-clay, friction angle criterion and a traction criterion. In addition to these three yield surfaces, a thermo-plastic mechanism is added based on the work done by Sultan (1997) and Cui et al. (2000). The thermo-plastic model is based on the model developed by Hueckel & Borsetto (1990) in which two plastic mechanisms were added to represent the thermo-mechanical behaviour of soils. These mechanisms make possible to reproduce the volume change induced by temperature and the decrease of the preconsolidation pressure with the increase of temperature. Figure 4-21 represents these mechanisms in the (p', T) plane. The thermal yield limit (TY) reproduces the generation of volumetric thermal strain depending on the stress state or OCR of the clay. This curve is close to the p' axis because the soil is assumed to be initially virgin of any temperature effects. The loading yield limit (LY) represents the decrease of the preconsolidation pressure with temperature.

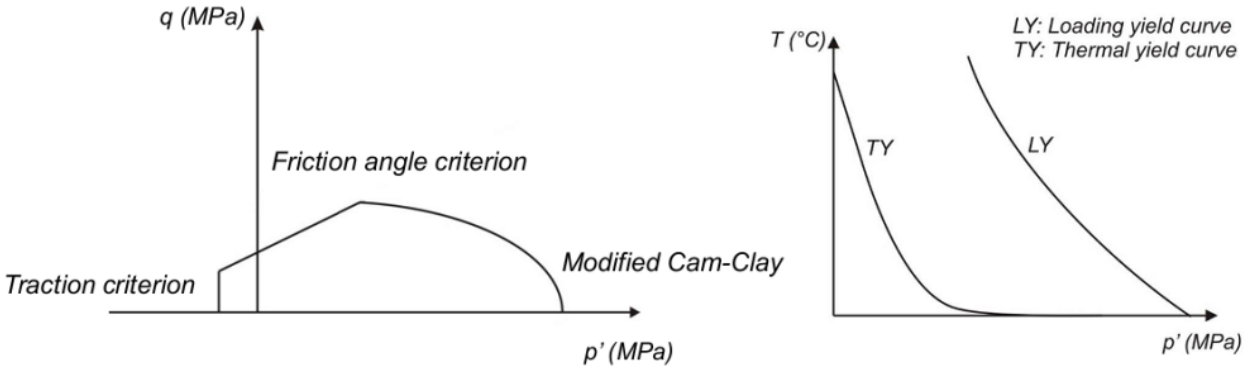

Figure 4-21. Thermal yield limit (TY) and loading yield limit (LY) in the *(p', T)* plane (Dizier 2011, Charlier et al. 2010)

Considering cross-anisotropic models with anisotropic properties of the clay helps to have a better understanding of the Boom Clay behaviour. The first integration of this elasto-plastic anisotropy was done during the TIMODAZ project (Charlier et al. 2010). Even if the simple approach proposed at that time already provided very promising results, anisotropic models for Boom Clay still need further investigations to completely describe its elasto-plastic response.

Some of the modelling exercises carried out using tests performed with Boom Clay (from triaxial tests to large-scale in-situ tests) and their main conclusions are summarised below. Some of these exercises were particularly useful for obtaining parameters.

- Within the framework of the EC project TIMODAZ, a backanalysis of several triaxial tests was performed (Dizier 2011, TIMODAZ 2010) to determine a set of mechanical parameters. The modelling results put in evidence that deviatoric behaviour is well represented when considering hardening or softening, but the volumetric behaviour is more difficult to capture. The main conclusion of these modelling activities is that a classical elasto-plastic model may be used to simulate qualitatively the deviatoric behaviour of the clay under drained and undrained conditions. The smooth transition between the elastic and plastic part may be captured thanks to well adapted hardening parameter values. In that way, the elastic domain is reduced and the plastic strains are generated earlier.
- A Drucker-Prager model, which takes into account the anisotropic nature of Boom Clay, was used to model a hollow cylinder test performed at EPFL during the TIMODAZ project (François et al. 2014). The anisotropy of the clay was considered by using a transverse elasticity and by an effective cohesion varying according to the angle between the stratification plane and the direction of the principal stress. This approach was implemented within the LAGAMINE finite element software (Collin 2003). The comparison between observations and numerical results in the three directions confirmed the importance of the cross-anisotropy properties of the Boom Clay.
- The large scale PRACLAY Heater test (section 4.2.1) was modelled considering a Drucker-Prager model with a cross-anisotropic elasticity and a hardening behaviour of the effective friction angle (Dizier et al. 2016, 2017). In this model, the temperature induces thermal elastic strains only and the thermo-plasticity was not considered. Distinct vertical and horizontal total stresses were imposed and a coefficient of earth pressure at rest (K_0) of 0.7 (based on Bernier et al. 2002, 2007a; Dehandschutter et al. 2004, Cornet 2009). The effective stresses were defined according to the Terzaghi's principle, the heat transfer using Fourier's law of conduction and the flow of water using the classic Darcy's law. The thermo-hydraulic properties selected were based on Bernier et al. (2007a), Bastiaens et al. (2006), Chen et al. (2011), Garitte et al. (2014), Horseman et al. (1987), Chen (2012), Chen et al. (2014). The mechanical properties of the excavation-damaged zone

decreased due to the excavation and remained the same for the heating phase as their potential restoration requires a longer time (self-healing). Although the modelling results were in a good agreement with the observations, the following limitations were identified:

1. Blind predictions of Dizier (2011) showed that at this scale the effect of thermo-plasticity should be very limited in comparison with thermo-elastic models. The temperature around PRACLAY heater tests should induce only reversible deformations. This conclusion needs to be reconsidered with the current knowledge of the PRACLAY Heater test, which started in 2014.
2. In the modelling of the PRACLAY Heater test, the influence of the EDZ is limited to an abrupt variation of parameters with time. This description of the EDZ requires further investigations to improve the modelling of hydro-mechanical disturbances induced by the excavation.
3. The viscous characteristics of Boom Clay were not taken into account while it is known that it exhibits a visco-elasto-plastic behaviour. This effect needs to be integrated in the constitutive models to simulate the long-term behaviour of the Boom Clay.

4.4.3 Opalinus Clay

The modelling of several large-scale heating experiments performed at the Mont Terri URL, such as the HE-D (Bossart et al. 2017), modelled by e.g. Gens et al. (2007) and Garitte et al. (2017b) and the HE-E (Gaus et al. 2014a and b) modelled by Garitte et al. (2017a), facilitated the hierarchical classification of cross-coupling between different THM processes in OPA:

- The strongest coupling was found from thermal to hydraulic and mechanical behaviour. Pore water pressure generation is mainly controlled by temperature increase, with thermal expansion being the primary contributor to strains and displacements.
- Significant but moderate effects result from the coupling of hydraulic to mechanical behavior. Dissipation of pore pressures induces additional displacements and strains, albeit smaller than thermally-induced deformations due to clay stiffness.
- Mechanical damage could theoretically impact hydraulic results, causing higher permeability, but the damaged zone's size seems limited, with minimal impact.
- No noticeable coupling was observed from hydraulic to thermal behavior. Heat transport is predominantly by conduction, and material saturation remains constant during heating.
- Coupling from mechanical to thermal behavior is negligible. Subtle porosity variations in the clay host rock do not affect thermal conductivity, and mechanical energy dissipation is insignificant in the non-isothermal case of the HE-D experiment.

In the context of the FE experiment, various modelling exercises (e.g. Ewing & Senger 2011, Senger 2015, Garitte et al. 2014, NAGRA 2018) estimate key parameters, including temperature evolution, degree of saturation, pore water pressure, and strain in the Opalinus Clay. Scoping calculations using the THM code Code_Bright (Olivella et al. 1994, 1996), as reported in NAGRA (2018), yielded key conclusions:

- Peak temperatures at the heater surface range from approximately 100°C to 195°C, depending on buffer properties.
- The maximum simulated temperature at the interface between buffer and rock in the direction of the bedding planes remains at 85°C, irrespective of buffer properties.
- Desaturation of the Opalinus Clay is limited.
- The combined effect of pore water flux and differential thermal expansion results in a maximum pore water pressure increase of around 3 MPa at a distance between 7 and 15 m from the tunnel axis.

4.4.4 Modelling work done during HITEC

The modelling of generic cases of a high-level waste repository was undertaken during HITEC to compare the output of the different codes and the behaviour of three clay host rocks (both in the near-field and in the far-field). The modelling of some of the laboratory experiments described in section 4.3.2 was also carried out, and the last step of the benchmark consisted in modelling two full-scale in-situ heating experiments (described in section 4.2). All this work is described in detail in deliverable D7.6 (de Lesquen et al. 2024).

A comparative 2D modelling exercise of the near- and far-field was carried out for three clay rocks considered to host radioactive waste repositories in Europe: the Boom Clay, the Callovo-Oxfordian claystone and the Opalinus Clay. The near-field generic case considered the problem of a single deposition drift during excavation, waiting and heating phases. Three subcases were considered: 1) isotropic elastic conditions, 2) anisotropic stress conditions with cross-anisotropic elasticity and thermo-elasticity and 3) anisotropic stress conditions with elasto-plasticity/damage. The goal of these subcases was to compare the numerical codes on fixed exercises (subcases 1 and 2) by prescribing the same boundary conditions and mechanical constitutive laws and properties, and to compare different approaches to reproduce the behaviour of the host rock and the development of the EDZ (subcase 3). Both unsupported and supported tunnels were considered. The far-field exercise considered the effect of heating further away from the disposal tunnels and over a much longer time period (1000 years).

A brief description of the approaches of the various modelling teams is given below:

- ANDRA ran the elastic cases on COMSOL Multiphysics and Code_Aster. In the framework of an ongoing scientific collaboration, Ineris developed a regularized anisotropic elastoplastic and damage model including both non-linear short- and long-term responses (Souley et al. 2023). This model was implemented in COMSOL Multiphysics and applied to subcase 3. The far-field model was also run on COMSOL Multiphysics.
- BGE worked with the numerical code FLACD3D and the open-source code OpenGeoSys. Within the latter, a material model for claystone, which incorporates its mechanical, thermal, and hydraulic behaviour, was developed and implemented (Mánica, 2018). The model falls within the frameworks of the elasto-viscoplasticity theory and the plasticity-creep partition approach (Chaboche, 2008), and it incorporates features relevant for the description of indurated clays behaviour: a non-linear yield criterion, strength and stiffness anisotropy, a non-associated flow rule, rate-dependency, strain hardening/softening, non-local regularisation, creep deformations, and permeability increase with damage. Concerning the thermal enhancement of the model, two main phenomena were considered for implementation (Tourchi et al. 2023): the continuous variation of mechanical properties (e.g. shear strength) with temperature, and the temperature-induced reversible expansive strains followed by, at some threshold temperature values, irreversible contractive strains.
- EDF used their in-house software Code_Aster and the LKR model based on Laigle (2004), Kleine (2007) and Raude (2015).
- EURIDICE/ SCK•CEN used the finite element code COMSOL Multiphysics.
- LEI worked on the development of a constitutive model using the COMSOL Multiphysics. Thermo-poroelasticity was considered for the modelling of near field effects in the isotropic and anisotropic stress conditions. For modelling of the excavation damaged zone elastoplasticity was considered.
- The constitutive model of ULiege for the near-field in the second subcase considered anisotropic elasticity, permeability, thermal conductivity, stress and Biot coefficient. They also developed a new THM second gradient model able to reproduce the strain localisation processes occurring within the EDZ (Song et al. 2023). The model to simulate the far field considered the anisotropy of the elasticity, the permeability, the thermal conductivity, the stresses and the Biot coefficient with two thermal loads (Rawat, 2023).

- UPC developed a fully coupled THM constitutive model for clay rocks for saturated and unsaturated states. The constitutive model is formulated within the framework of elastic-viscoplasticity, which considers non-linearity and softening after peak strength, anisotropy of stiffness and strength, as well as permeability variation due to damage. In addition, mechanical properties were coupled with thermal history (Song et al. 2024). The model was implemented in the finite element method software CODE_BRIGHT.

After fixing several discrepancies on the input parameters for the near-field generic cases, all teams obtained matching results for the isotropic elastic step (Figure 4-22). Some variations were however observed on the pressure and stress calculations in the anisotropic cases. Differences in the THM formulations and assumptions made in the different codes may be the main reason for these disparities. The precise location of the integration point depending on the mesh and on the averaging method may also explain some discrepancies, especially at or near the contour of the tunnel where the gradients are the largest (Simo et al. 2023). The analysis of LEI showed that the water drainage condition on the tunnel boundary had no effect on the thermal state around the tunnel, but it had a significant impact on the hydro-mechanical response (Narkūnienė et al. 2022). The heating applied to the low-permeability claystone / poorly indurated clay results in pore pressure build-up because of the difference in the thermal expansion coefficients of water and of the solid matrix. As expected, the resulting overpressure is relatively low in the softer Boom Clay, but the exercise showed that the same heat load produced a very different pressure and stress responses in the Callovo-Oxfordian claystone and Opalinus Clay that have similar properties. All these elastic models predict some tensile effective horizontal stress at the borehole wall for the three clay host rocks. In reality, the excavation induces some fracturing in this area, and more advanced models are needed to account for the presence of the damaged zone. The last step of the near-field benchmark (modelling of the EDZ) gave an opportunity to improve the existing models and study the impact of heating on the extension of the EDZ (Song, 2023). The results of ULiege showed that the gap distance between the drift wall and the liner plays a significant role on the evolution of the strain localisation process. ANDRA's Comsol model was improved implementing a regularised anisotropic elastoplastic and damage model including both non-linear short and long-term response. The influence of damage and fracturing on the transport and viscous properties was also considered (Souley et al. 2023). This model was further developed to be able to take into account the decrease of strength with temperature that was observed in laboratory experiments (section 4.3.2.1). Different approaches were used but similar results were obtained, matching the EDZ geometry observed in situ. Some variations appear on the size of the damaged zone, but the high plastic strains are always localised in the very near field and all the models predict that heating for ten years at constant power does not result in any EDZ expansion.

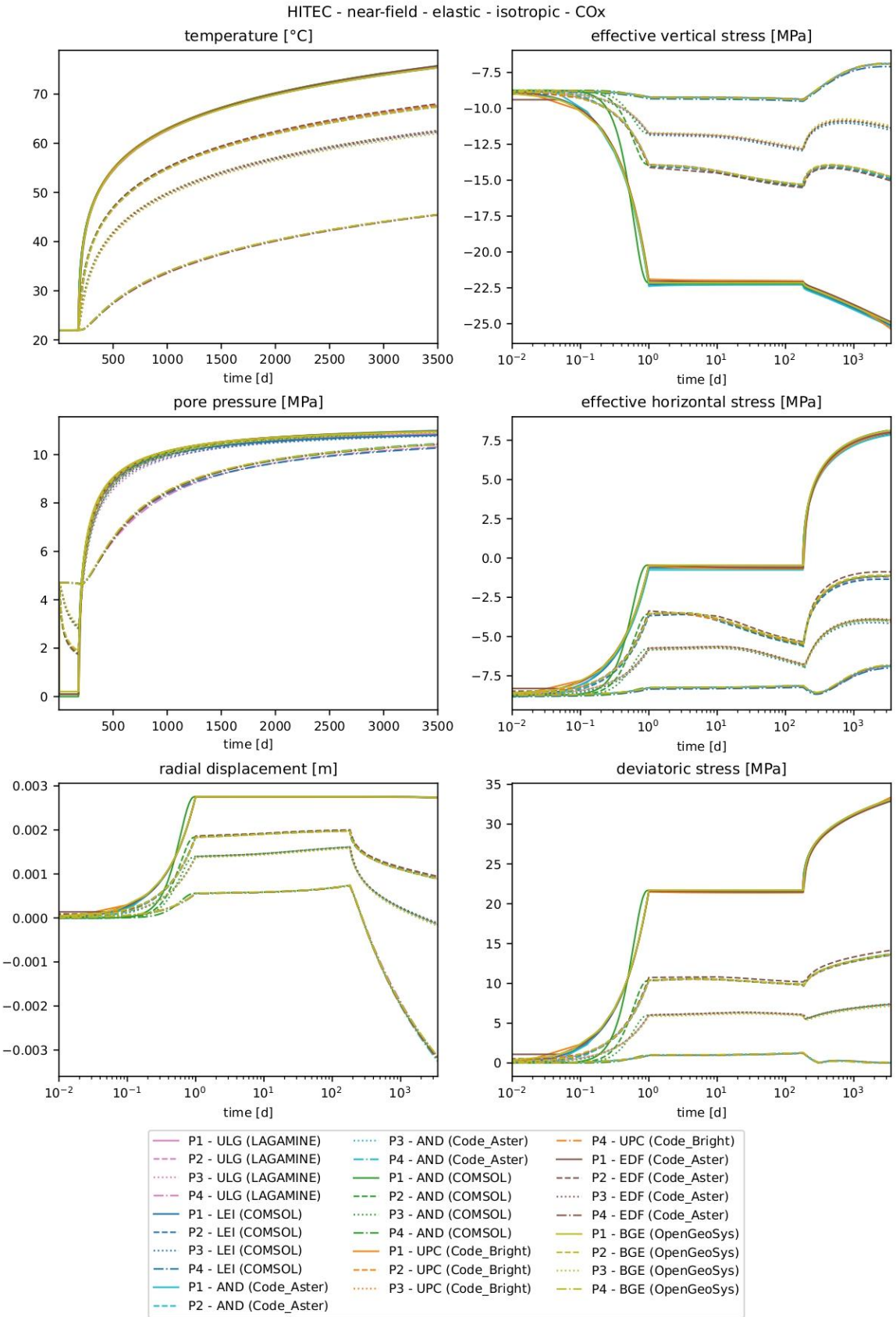

Figure 4-22. Evolution of temperature, pore pressure, radial displacement and stresses for the Callovo-Oxfordian clay - isotropic case

In the far-field benchmarking exercise, all teams considered an anisotropic poro-elastic behaviour – which is known to provide a good prediction of the evolution of both temperature and pore pressure (Seyedi et al. 2021)– and got matching results for the pressure and stress evolution at mid-distance between two parallel high-level waste cells (Figure 4-23). This outcome with six modelling teams and four different codes improves the confidence in these computations and the modelling approach used to dimension repositories. A sensitivity study performed by LaMcube on behalf of Andra with a phase-field model showed that when taking into account the presence of the EDZ, the extension of damage remains limited to the near-field (Shao et al. 2024) and it has no impact on the pore pressure evolution in the far field.

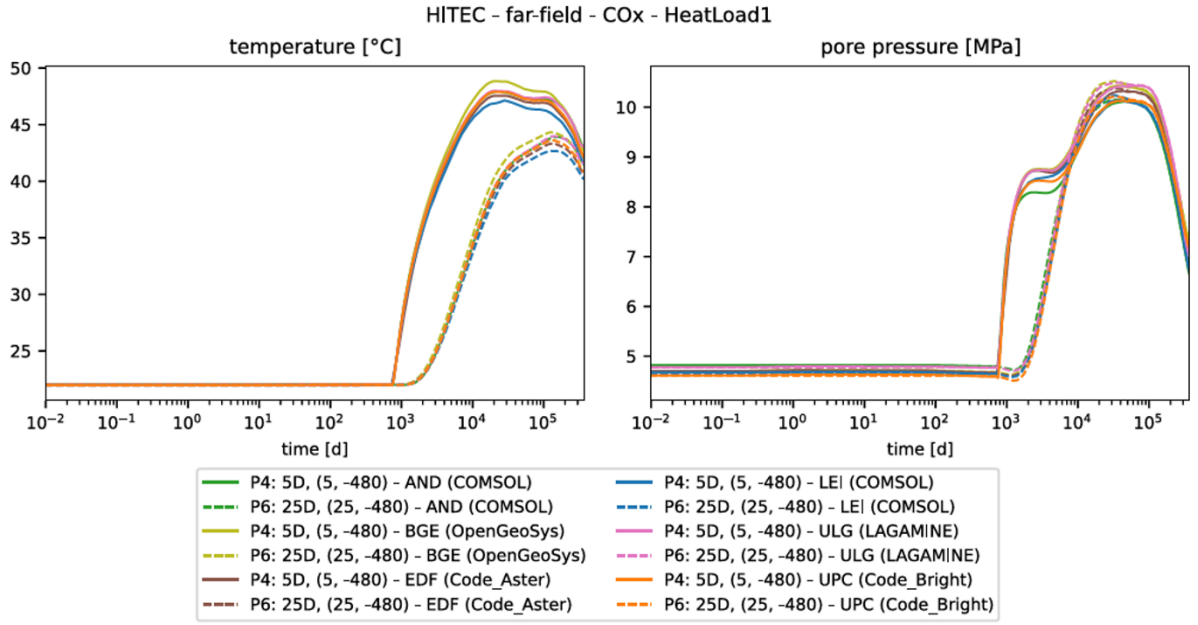

Figure 4-23. Evolution of temperature and pore pressure effective stresses for the Cox far-field case (de Lesquen et al. 2024)

The triaxial compression tests performed at different temperatures by ULorraine on heated COx samples (section 4.3.2.1) were modelled by five teams. The BGE model developed by Mánica (2018) and implemented in the OpenGeoSys open-source code was applied successfully to this case. A non-local formulation was also employed by UPC in the simulation of these tests to allow a proper simulation of localisation phenomena. The constitutive model was elasto-plastic and included softening and anisotropy of stiffness and strength and thermal effects. Realistic drainage boundary conditions were adopted (Figure 4-24). The family of yield surfaces were based on a hyperbolic approximation to the Mohr-Coulomb envelope. A parametric study was performed to check the influence of the rate of temperature rise and of the resting period. The agreement with experimental results was satisfactory (Song et al. 2024). This exercise showed that a good understanding of the boundary conditions is essential for a correct interpretation of the experiments and use of their results. The modelling of the heating phase under undrained conditions revealed the generation of overpressures when fast heating rates were applied, that may induce some damage in the samples. It may explain the strength reduction observed in the tests conducted at low confining pressures, implying that the heating phase was not conducted under fully drained conditions. Postmortem analysis of samples heated in the ALC1604 and CRQ in-situ heating experiments actually showed no changes in the mechanical properties. Some of the models were nevertheless developed to take into

account the observed strength reduction with temperature (Souley et al. 2024) and its impact on the near-field and far-field calculations will be evaluated.

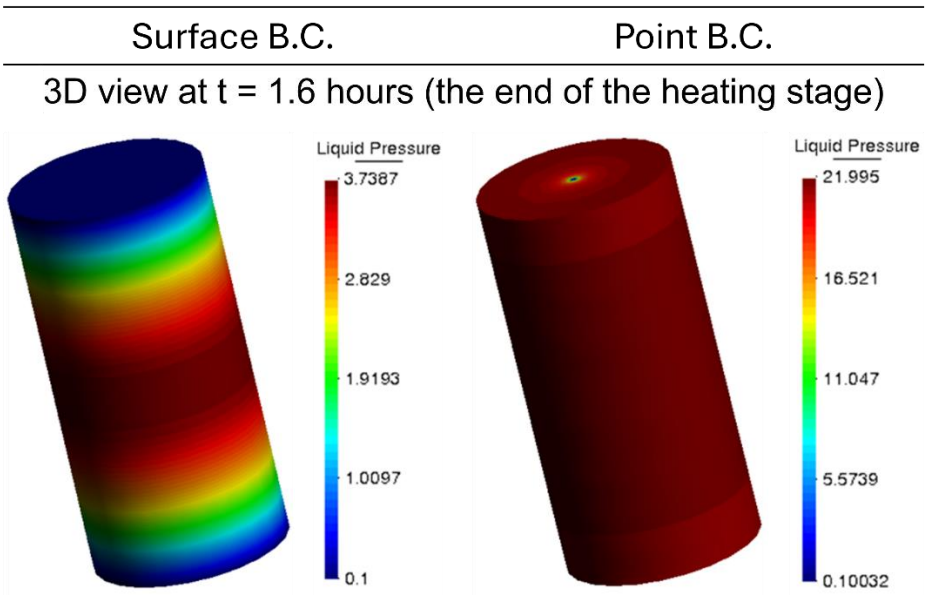

Figure 4-24. Pore pressure contours fo both surface boundary condition (left) and point boundary condition (right). Cell pressure is 12 MPa, temperature 100°C and anisotropy angle θ = 0° (UPC results in deliverable D7.6, de Lesquen et al. 2024)

Five teams modelled the ALC1605 in-situ heating experiment (section 4.2.2) in 2D (LEI and ULg) and in 3D (Andra, BGE and EDF). After the initial predictive modelling step, using the Callovo-Oxfordian parameters provided in the first benchmarking exercises, large differences were observed between the modelling and the measurements. Most teams underestimated the anisotropic impact of the cell excavation on the pore pressure. On the other hand, plane strain conditions do not allow longitudinal fluid flow and heat flux; as a result, the temperature and pore pressure evolution on heating was overestimated when 2D models were used. In the interpretative modelling step, the teams had access to the historical data and could adapt their models to match the results and improve the understanding of the behaviour of the Callovo-Oxfordian claystone. To this aim the models were modified by reducing the value of the applied heat flow, modifying the COx material properties, considering the heat loss, or introducing an EDZ. However, none of this resulted in a significant improvement of the match between predictions and measurements. More advanced models are needed to take into account the processes occurring around the tunnels (e.g. modification of hydraulic properties within the EDZ, creep).

Four teams modelled the large-scale in situ PRACLAY Heater test (section 4.2.1): BGE, ULiège, UPC and EURIDICE/ SCK CEN. The benchmark exercise started by an academic case, using an elastic model with parameters appropriate for Boom Clay, and then increased in complexity. The results of the first step showed a good agreement between the involved teams when modelling the experiment with elastic and elasto-plastic constitutive laws. In all cases, the anisotropy of the clay was taken into account, with anisotropic intrinsic permeability and thermal conductivity, and the elastic behaviour was modelled with cross-elasticity. For the second phase, ULiege used an isotropic strain hardening Drucker-Prager elastoplastic model. An EDZ with a higher permeability was introduced and the parameters of the sound layer were optimised in order to get a good agreement with the in-situ measurements. They also introduced a strain-dependent isotropic evolution of the hydraulic permeability tensor and the shear strain reproducing the stiffness degradation curve (Figure 4-25). To model the PRACLAY experiment UPC used the advanced Hyperbolic Mohr-Coulomb (HMC) model with hardening-softening

and nonlocal formulation, with the air gap approach to represent the contact between the host clay and the concrete lining. A satisfactory agreement with field observations was achieved by both teams, and the analyses showed that pore pressures depend strongly on stiffness parameters and that thermal pressurization is larger when the drained bulk modulus increases. This modelling work also showed that intrinsic permeability plays a significant role in the liquid dissipation and, therefore, changing the intrinsic permeability can significantly modify the pore pressure evolution.

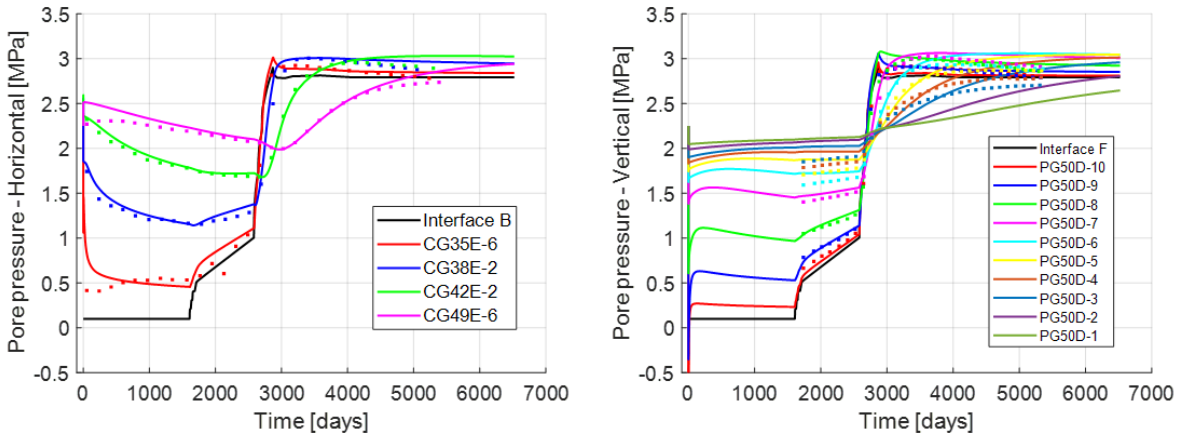

Figure 4-25. Pore pressure evolution around the Praclay gallery in the horizontal and vertical directions depending on the permeability and stiffness modification (ULiège results in deliverable D7.6, de Lesquen et al. 2024)

An overall conclusion of these modelling exercises is that very consistent results can be obtained with different codes using a poro-elastic approach when the parameters and boundary conditions are correctly set. As this type of model is known to predict correctly the temperature and pressure evolutions in the far field, this benchmark increases the confidence and shows the robustness of the modelling approach used to design the repositories. More advanced models are however needed to account for the processes occurring around the tunnels (e.g. modification and strain dependency of hydraulic and mechanical properties within the EDZ, creep). The modelling of laboratory experiments showed the importance of a good understanding of the test setups and of the boundary conditions and helped explain some of the results.

5 Conclusions

The primary aim of the EURAD-HITEC Project was to ascertain if temperatures higher than the limits currently established in most repository concepts (a maximum of 100°C for the buffer and 90°C for the clay host rock) would compromise the safety functions of the engineered and geological barriers. Significant advantages would result if a design able to tolerate greater temperatures could be achieved, most notably a reduced repository footprint, but also higher confidence on the current design and predictions for lower temperatures. This report summarises results obtained in Tasks 2 (clay host rock) and 3 (bentonite buffer) of the Project, along with others from the literature, concerning the impact of high temperature on the behaviour of clay materials. Bentonites under assessment included Wyoming-type (MX-80, Barakade), BCV and FEBEX, and the clay formations studied were Boom Clay, Opalinus Clay and Callovo-Oxfordian claystone.

The study of the effect of temperature on bentonite properties has been approached in HITEC by analysing the change of properties of preheated material and by determining the properties of the bentonite at high temperatures.

The material submitted to high temperatures over long periods experiences desiccation and other changes that may affect its long-term performance if they were irreversible. This concern has been tackled in HITEC by subjecting bentonite to high temperatures under different conditions and time periods and determining their characteristics and properties afterwards. The most representative condition would be that experienced by the material in field tests, such as the ABM5, which are also in operation for several years, and in laboratory thermo-hydraulic tests in cells that reproduce the in situ conditions in a controlled way. An additional approach is the drying of powder material in the oven, which simulates the transient situation of the buffer closest to the canisters. The clay crystallo-chemistry was preserved in all cases and changes, such as the Mg enrichment or slight increase of trioctahedral character of smectite, could not be specifically linked to the high temperature, because they had also been observed under lower temperatures. If evaporation during drying was allowed, the changes were more important, generally consisting in decreases in cation exchange capacity, specific surface area, water adsorption capacity and sorption coefficients. However, heating under wet conditions had the opposite effect on these properties. It is presumed that these changes were caused not by the temperature itself, but by the loss of the water induced by the elevated temperature. Additionally, some of these changes, such as the decrease in water adsorption capacity, are reversible when the material is rehydrated. The hydro-mechanical properties of preheated material were only affected in samples heated under dry conditions and compacted at high dry density, in which a slight increase in hydraulic conductivity was observed.

The field and laboratory tests imply hydration under thermal gradient, and consequently water movement and associated geochemical processes. As it had been observed under lower temperatures or thermal gradients, dissolution and precipitation of species occurred in those tests, along with modification of the exchangeable cation complex of the smectite. These processes were conditioned by the kind of bentonite and hydration water. Some of the modifications observed, e.g. corrosion, were less pronounced compared to other tests conducted at lower temperature but with higher water contents.

The hydro-mechanical properties of the compacted bentonite have been determined in HITEC across a range of temperatures (predominantly 80-200°C). The determination of properties at high temperatures is technologically challenging and the procedures followed, despite the significant advances in methodology and equipment made during the project, may greatly impact the results. Hydration and swelling pressure development were quicker as the temperature was higher. Once saturated, higher temperatures resulted in lower swelling pressures for all bentonites (but not for calcium-exchanged purified smectite). However, under some particular conditions (heating under isochoric conditions a material previously saturated at room temperature) progressive and permanent decrease of the swelling pressure with respect to the one measured at the end of saturation was observed (thermally-induced creep). The underlying mechanisms that could explain this behaviour are unknown. This decrease in swelling pressure was not accompanied by impacts on hydraulic conductivity, which was not detrimentally affected by thermal loading up to temperatures of 200°C. The water retention capacity decreases with temperature, more significantly for the predominantly sodic materials. The results consistently indicate that the effect of temperature is small below 80°C and, for higher temperatures, is more significant for the higher dry densities. In any case, even at the highest temperatures, the bentonite had the ability to fill voids and was able to develop large swelling pressures at high densities. Given the impact that experimental boundary conditions may have on the results obtained, assessment of measurements in field tests would be very helpful to confirm the long-term evolution of swelling.

It is considered that THM formulations for expansive materials developed and validated for temperatures below 100°C can be extended to temperatures above that value by including the thermal dependence of some parameters, such as the water retention curve, permeability, thermal

conductivity, surface tension, volumetric behaviour of the microstructure and normal compression behaviour of the macrostructure. The modification during HITEC of previous models also included the incorporation of the hydro-mechanical coupling between the micro- and macropore levels and the definition of retention curves for each structural domain. To further improve the models, inclusion of the dependence of the water retention curves on the evolution of the micro and macropore volume fractions may be necessary. A lack of experimental data to enable the quantification of the microstructure of compacted bentonites, which influences the calibration of microstructural parameters, has been identified.

As it happens for the buffer, working at high temperature with claystones is challenging, and the impact of the testing protocols (thermal loading rates, stress conditions) on the results obtained is also a concern. For example, modelling of the triaxial tests showed that, if fast heating rates (not representative of the actual case) are applied under undrained conditions, overpressures may build up and the samples may be damaged.

Important hydro-mechanical couplings between peak pore water pressure, temperature, permeability and confining stress were identified. The results of the laboratory experiments confirmed that the claystone keeps its good mechanical and retention properties, even when heated at up to 100°C. Nonetheless, considering the heat output of the waste and the thermally induced pore water pressures, a repository should be located at a depth below which thermally induced pore water pressures could remain lower than the in-situ stress.

Although many parameters can influence the efficiency of the self-sealing process (calcite and clay content, sample orientation with respect to bedding, temperature), confidence was gained in the positive impact of the self-sealing process on the restoration of the initial sealing properties of the clay host rock, which always occurs rapidly (relative to repository life), whatever the temperature conditions. Temperature may have a slight delaying effect on the self-sealing process though.

The modelling activities undertaken during HITEC intended to compare the output of the different codes used by the participants and the behaviour of the three clay host rocks. One of the benchmarks consisted in the modelling of a near-field generic case, which showed the pore pressure build-up resulting from the heating applied to the clay host rock, and, as expected, a relatively lower overpressure in the softer Boom Clay than in the Opalinus clay and the Cox claystone. All the models predicted that the high plastic strains (associated to the EDZ development) are always localised in the very near field. The consistency among the simulation results of different groups for the far-field improves confidence in the modelling approach used to dimension repositories.

Very consistent results can be obtained with different codes using a poro-elastic approach when the parameters and boundary conditions are correctly set. For example, the evolutions of temperature and pore pressure in field tests were well modelled in the far field with an anisotropic poro-elastic approach, but more advanced models are needed to account for the processes occurring around the tunnels (e.g. modification of hydraulic and mechanical properties within the EDZ, creep). Accurate knowledge of the stiffness and permeability of both the sound and the damaged clay rock are necessary for a good reproduction of field results.

6 References

Aertsens, M., Wemaere, I., Wouters, L. 2004. Spatial variability of transport parameters in the Boom Clay. Applied Clay Science 26: 37-45.

Agboli, M., Grgic, D., Moumni, M., Giraud, A. 2023. Study under X-ray tomography of the impact of self-sealing process on the permeability of the Callovo-Oxfordian claystone. Rock Mechanics and Rock Engineering.

Agboli, M., Grgic, D., Giraud, A., 2023. Self-sealing experiments with water and gas injection on Callovo-Oxfordian claystone under X-ray tomography. 15th International Congress on Rock Mechanics ISRM 2023, Salzburg (Austria), 9-14 October 2023.

Åkesson, M., Kristensson, O., Börgesson, L., Dueck, A., Hernelind, J. 2010. THM modelling of buffer, backfill and other system components – Critical processes and scenarios. SKB TR-10-11. Svensk Kärnbränslehantering AB.

Åkesson, M., Olsson, S., Dueck, A., Nilsson, U., Karnland, O., Kiviranta, L., Kumpulainen, S., Lindén, J. 2012. Temperature buffer test. Hydro-mechanical and chemical/mineralogical characterizations. SKB Report P-12-06. Svensk Kärnbränslehantering AB.

Akinwunmi, B., Sun, L., Hirvi, J. T., Kasa, S., Pakkanen, T. A. 2019. Influence of temperature on the swelling pressure of bentonite clay. *Chemical Physics*, *516*, 177-181

Alcolea, A., Marschall, P., FE Team. 2019. FE-Modelling Task Force / Task 1: Validation of thermally induced THM effects in the rock around the FE-tunnel. NAGRA Arbeitsbericht NAB 19-040.

Alonso, E.E., Vaunat, J., Gens, A. 1999. Modeling the mechanical behaviour of expansive clays. Eng. Geol. 54: 173–183.

Alonso, J., García-Siñeriz, J.L., Bárcena, I., Alonso, M.C., Fernández Luco, L., García, J.L., Fries, T., Pettersson, S., Bodén, A., Salo, J.-P. 2008. ESDRED. Deliverable 9 of Module 4, WP4. Module 4 (Temporary Sealing Technology). Final Technical Report. 84 pp.

Amec 2016. Project Ankhiale: Disposability and full life cycle implications of high-heat-generating UK Wastes. Thermal analysis of disposal concepts for high-heat-generating wastes. Amec Report to RWM 103726-0011-UA00-TLN-0001. Issue 2, February 2016.

Amec 2018a. Vaults for High-heat-generating Waste – Integrated Report for Radioactive Waste Management, January 2018.

Amec 2018b. Mined Borehole Matrices for High-heat-generating Waste – Integrated Report for Radioactive Waste Management, January 2018.

ANDRA 2005. Dossier 2005 Argile - Synthesis - Evaluation of the feasibility of a geological repository in an argillaceous formation. Meuse/Haute-Marne site. https://international.andra.fr/sites/international/files/2019-03/3-%20Dossier%202005%20Argile%20Synthesis%20-%20Evaluation%20of%20the%20feasibility%20of%20a%20geological%20repository%20in%20an%20argillaceous%20formation_0.pdf

ANDRA 2009. Référentiel de site Meuse/Haute-Marne – Dossier 2009. Tome 2 : Caractérisation comportementale du milieu géologique sous perturbation - N° Andra : C.RP.ADS.09.0007.

ANDRA 2016. Safety Options Report - Post-Closure Part. Andra Technical Report CG-TE-D-NTE-AMOA-SR2-0000-r5-0062. https://international.andra.fr/sites/international/files/2019-03/Safety%20Options%20Report%20-%20Operations_2.pdf

ANDRA 2018. Le socle des connaissances scientifiques et techniques de CIGÉO. Les référentiels de connaissances du site de Meuse/Haute-Marne. Tome 4. Le comportement THM des formations géologiques sur le site de Meuse/Haute-Marne. CG.RP.AMFS.1 7.0031.

Arcos, D., Grandia, F., Domènech, C. 2006. Geochemical evolution of the near field of a KBS-3 repository. SKB TR-06-16. Svensk Kärnbränslehantering AB.

Armand, G., Bumbieler, F., Conil N., de la Vaissière, R., Bosgiraud, J.M., Vu, M.-N. 2017. Main outcomes from in situ thermo-hydro-mechanical experiments programme to demonstrate feasibility of radioactive high-level waste disposal in the Callovo-Oxfordian claystone. Journal of Rock Mechanics and Geotechnical Engineering 9(3): 415-427.

Autio, J., Hassan, Md.M., Karttunen, P., Keto, P. 2013. Backfill design 2012. Report POSIVA 2012-14, Posiva Oy, ISBN 978-951-652-196-4.

Auvray, C., Grgic, D., Morlot, C., Fourreau, E., Talandier, J. 2015) X-Ray Tomography Applied to Self-Healing Experiments on Argillites. 13th ISRM International Congress of Rock Mechanics, Montréal, (Québec, Canada).

Awarkeh M. 2023. Investigation of the long-term behaviour of Boom Clay. PhD thesis, École Nationale des Ponts et Chaussées, France.

Baldi, G., Borsetto, M., Hueckel, T. 1987. Calibration of mathematical models for simulation of thermal, seepage and mechanical behaviour of Boom Clay. Commission of the European Communities. Nuclear science and Technology EUR 10924.

Baldi, G., Hueckel, T., Peano, A., Pellegrini, R., 1991. Developments in modelling of thermo-hydro-mechanical behaviour of Boom Clay and clay-based buffer (vol.2). Commission of the European Communities. Nuclear science and Technology EUR 13365/2.

Baldi, G., Hueckel, T., Pellegrini, R. 1988. Thermal volume changes of the mineral-water system in low-porosity clay soils. Canadian Geotechnical Journal 25(4): 807-825.

Bamforth, P., Chisholm, D., Gibbs, J., Harrison, T. 2008. Properties of Concrete for Use in Eurocode 2.

Bárcena, I., García-Siñeriz, J.L., Huertas, F., 2006. FEBEX Project Final Report. Addendum sensors data report. In situ experiment. Publicación Técnica ENRESA 05-5/2006. Madrid, 157 pp.

Barnichon, J.D. 1998. Finite Element Modelling in Structural and Petroleum Geology. PhD thesis. University of Liege.

Bass, J.D. 1995. Elasticity of Minerals, Glasses, and Melts. In: Thomas J.A. (eds). Mineral Physics and Crystallography: A Handbook of Physical Constants, American Geophysical Union Online Reference Shelf 2: 45-63.

Bastiaens, W., Bernier, F., Li, X.L. 2006. An overview of long-term HM measurements around HADES URF. In: EUROCK 2006 Multiphysics coupling and long term behaviour in rock mechanics, 15–26.

Basu, S., Jones A., Mahzari P., 2020. Best Practices for Shale Core Handling: Transportation, Sampling and Storage for Conduction of Analyses. Journal of Marine Science and Engineering 8(2): 136. https://doi.org/10.3390/jmse8020136

Baxter, S., Holton, D., Williams, S., Thompson, S. 2018. Predictions of the wetting of bentonite emplaced in a crystalline rock based on generic site characterization data. Geological Society Special Publications 482: 285-300, London.

Beauheim, R.L. 2013. Hydraulic conductivity and head distributions in the host rock formations of the proposed siting regions. NAGRA Arbeitsbericht NAB 13-013.

Belmokhtar, M., Delage, P., Ghabezloo, S., Conil, N. 2017. Thermal volume changes and creep in the Callovo-Oxfordian claystone. Rock Mechanics and Rock Engineering, Springer Verlag, 50(9): 2297-2309.

Bernier, F., Li, X.L., Bastiaens, W. 2007a. Twenty-five years' geotechnical observation and testing in the Tertiary Boom clay formation. Géotechnique 57(2): 229-237.

Bernier, F., Li, X.L., Bastiaens, W., Ortiz, L. 2007b. SELFRAC: Fractures and self-healing within the excavation disturbed zone in clays. Final report. Euridice report, December 2007.

Bésuelle, P., Viggiani, G., Desrues, J., Coll, C., Charrier, P. 2014. A laboratory experimental study of the hydromechanical behaviour of Boom Clay. Rock Mechanics and Rock Engineering 47(1): 143-155.

BGE 2020a. Zwischenbericht Teilgebiete gemäß § 13 StandAG, Stand 28.09.2020, Bundesgesellschaft für Endlagerung mbH (BGE) Peine.

BGE 2020b. Endlagerkonzepte Überblick über grundsätzliche Rahmenbedingungen in der ersten Phase des Standortauswahlverfahrens, Stand 28.09.2020, Report Number SG02302/3-1/1-2020#1 – Objekt-ID: 826885 – Revision: 000, Bundesgesellschaft für Endlagerung mbH (BGE), Peine.

Birgersson, M., Karnland, O. 2009. Ion equilibrium between montmorillonite interlayer space and an external solution – Consequences for diffusional transport. Geochimica et Cosmochimica Acta 73: 1908–1923.

Börgesson, L., Hökmark, H., Karnland, O. 1988. Rheological properties of sodium smectite clay. SKB TR-88-30. Svensk Kärnbränslehantering AB, 65 pp.

Bossart, P., Thury, M. 2008. Mont Terri Rock Laboratory. Project, Programme 1996 to 2007 and Results. Rep. Swiss Geol. Surv. 3, swisstopo, 3084 Wabern, Switzerland.

Braun, P. 2019. Thermo-hydro-mechanical behaviour of the Callovo-Oxfordian claystone Effects of stress paths and temperature changes. PhD Thesis. Université Paris-Est.

Braun, P., Ghabezloo, S., Delage, P., Sulem, J., Conil, N. 2018. Determination of multiple thermo-hydro-mechanical rock properties in a single transient experiment: application to shales. Rock Mechanics and Rock Engineering 52: 2023-2038.

Brooks, R., Corey, A. 1964. Hydraulic properties of porous media. Hydrology paper 3. Colorado State University.

Burland, J. 1990. On the compressibility and shear strength of natural clays. Rankine Lecture, Géotechnique 40(3): 329-378.

Buyens, M., Put, M. 1984. Heat transfer experiment in Boom Clay. 9th European Conference on Thermophysical properties. 17-21 September, Manchester, UK.

Červinka, R., Vašíček, R., Večerník, P., Kašpar, V. 2018. Kompletní charakterizace bentonitu. BCV 2017, SÚRAO TZ 419/2019.

Chaaya, R. 2023. Couplage entre processus mécaniques et chimiques lors de l'hydratation d'une bentonite en temperature. Université d'Orléans. Ph.D. thesis. 169 pp.

Chaaya, R., Gaboreau, S., Milet, F., Maubec, N., Tremosa, J., Raimbourg, H., Ferrage, E. 2023. In-operando X-ray scattering characterization of smectite swelling experiments. Applied Clay Science 245: 107124, https://doi.org/10.1016/j.clay.2023.107124.

Chaboche, J.L. 2008. A review of some plasticity and viscoplasticity constitutive theories. International Journal of Plasticity 24(10): 1642-1693, https://doi.org/10.1016/j.ijplas.2008.03.009

Chang, C., Borglin, S., Chou, C., Zheng, L., Wu, Y., Kneafsey, T.J., Nakagawa, S., Voltolini, M., Birkholzer, J.T. 2023. Hydro-mechanical behavior of heated bentonite buffer for geologic disposal of high-level radioactive waste: A bench-scale X-ray computed tomography investigation. Applied Clay Science 232: 106792. https://doi.org/10.1016/j.clay.2022.106792

Charlier, R., Chalandar, S., Collin F., Dizier, A. 2010. Delivrable D13 – Annex 4. In situ heating test ATLAS in Mol. TIMODAZ project, F16W-CT-2007-036449.

Chen, G.J. 2012. Modeling of PRACLAY tests: improved HM parameters of Boom Clay based on in-situ measured PWP around PG, SAC 41 meeting. Internal presentation.

Chen, G.J., Sillen, X., Verstricht, J., Li, X.L. 2011. ATLAS III in situ heating test in boom clay: Field data, observation and interpretation. Computers and Geotechnics 38(5): 683-696.

Chen, G.J., Maes, T., Vandervoort, F., Sillen, X. 2014. Thermal Impact on Damaged Boom Clay and Opalinus Clay: Permeameter and Isostatic Tests with µCT Scanning. Rocks mechanics and Rock Engineering 47(1): 87-99.

Chen, W.Z., Gong, Z., Ma, Y.S., Yu, H.D., Li, X.L. 2017. Temperature effect on the drained creep behavior of Boom Clay. Clay Conference, Davos, 2017.

Chen, G., Li, X., Dizier, A., Verstricht, J., Sillen, X., Levasseur, S. 2023. Characterization of Boom Clay anisotropic THM behaviour based on two heating tests at different scales in the HADES URL. Geological Society, London, Special Publications 536(1). SP536-2022.

Coll, C., Collin, F., Radu, J.P., Illing, P., Schroeder, C.H., Charlier, R. 2008. The report of long term behaviour of Boom clay – influence of clay viscosity on the far field pore pressure distribution. EURIDICE 2006: 154.

Coll, C. 2005. Endommagement des roches argileuses et perméabilité induite au voisinage d'ouvrages souterrains. Thèse de doctorat. Université Joseph Fourier, Grenoble 1.

Collin, F. 2003. Couplages thermo-hydro-mécaniques dans les sols et les roches tendres partiellement saturés. Thèse de doctorat. Université de Liège, Faculté des Sciences Appliquées.

Conil, N. 2012b. Essai de chauffe à surface libre – Rapport d'installation – Centre de Meuse / Haute-Marne, rapport Andra D.RP.AMFS.11. 0064.

Conil, N., Tallandier, J. 2019. Good practice guide for the use of claystone samples in hydromechanical tests. Rapport Andra D.NT.AMFS.19.0025.

Conil, N., Armand, G., Garitte, B., Jobmann, M., Jellouli, M., Fillipi, M., De La Vaissière, R., Morel, J. 2012a. In-situ heating test in the Callovo Oxfordian clay: measurement and interpretation. In: Clays in natural and engineered barriers for radioactive waste confinement. Proceedings of the 5th international meeting, Montpellier, France.

Conil N., Talandier J., Djizanne H., de La Vaissière R., Righini-Waz C., Auvray C., Morlot C., Armand G. 2018. How rock samples can be representative of in situ condition: a case study of Callovo-Oxfordian claystones. Journal of Rock Mechanics and Geotechnical Engineering 10(4): 613-623. https://doi.org/10.1016/j.jrmge.2018.02.004

Conil, N., Vitel, M., Plua, C. et al. 2020 In Situ Investigation of the THM Behavior of the Callovo-Oxfordian Claystone. Rock Mech Rock Eng 53, 2747–2769. https://doi.org/10.1007/s00603-020-02073-8

Cornet F.H., 2009. In situ stress measurement campaign at SCK•CEN Underground Laboratory. École et Observatoire des Sciences de la Terre, Université de Strasbourg, Internal report.

Courdouan Merz, A. 2008. Nature and reactivity of dissolved organic matter in clay formations evaluated for the storage of radioactive waste. PhD thesis. ETH Zürich. Diss. ETH 17723, 111 pp.

Croisé, J., Mayer, G., Marschall, P., Matray, J.M., Tanaka, T., Vogel, P. 2006. Gas threshold pressure test performed at the Mont Terri Rock Laboratory (Switzerland): Experimental data and data analysis. Oil & Gas Science and Technology 61(5): 631-645.

Cuadros, J., Linares, J. 1996. Experimental kinetic study of the smectite-to-illite transformation. Geochim. Cosmochim. Acta 60: 439-453.

Cui, Y.J., Le, T.T., Tang, A.M., Delage, P., Li, X.L. 2009. Investigation the time dependent behavior of Boom Clay under thermo-mechanical loading. Géotechnique 59(4): 319-329.

Cui, Y.J., Sultan, N., Delage, P. 2000. A thermomechanical model for saturated clays. Canadian Geotechnical Journal 37: 607-620.

Cuss, R.J., Milodowski, A.E., Harrington, J.F., Noy, D.J. 2009. Fracture transmissivity test of an idealised fracture in Opalinus Clay. British Geological Survey Commissioned Report, CR/09/163. Nottingham, 74pp.

Cuss, R.J., Milodowski, A., Harrington, J.F. 2011. Fracture transmissivity as a function of normal and shear stress: first results in Opalinus clay. Physics and Chemistry of the Earth 36: 1960-1971. DOI: 10.1016/j.pce.2011.07.080

Cuss, R.J., Sathar, S., Harrington, J.F. 2012. Fracture transmissivity test in Opalinus Clay; test conducted on a realistic fracture. British Geological Survey Commissioned Report, CR/12/132. Nottingham, 63 pp.

Cuss, R.J., Harrington, J.F., Sathar, S., Norris, S., Talandier, J. 2017. The role of the stress-path and importance of stress history on the flow of water along faults; an experimental study. Applied Clay Science 150: 282-292, https://dx.doi.org/10.1016/j.clay.2017.09.029

Daniels, K.A., Harrington, J.F., Zihms, S.J., Wiseall, A.C. 2017a. Bentonite Permeability at Elevated Temperature. Geosciences 7(3): 1 – 24.

Daniels, K.A., Harrington, J.F., Zihms, S.J., Wiseall, A.C. 2017b. Bentonite permeability: the effect of elevated temperature. Abstract from Clay Conference, Davos, 2017.

Dao, L.Q. 2015. Etude du comportement anisotrope de l'Argile de Boom. PhD thesis, CERMES, Ecole Nationale des Ponts et Chaussées, Paris.

Davies, C.W., Davie, C.T., Edward, C.A., White, M.L. 2017. Physiochemical and Geotechnical Alterations to MX80 Bentonite at the Waste Canister Interface in an Engineered Barrier System. Geosciences 7(3): 69.

De Beer, A., Carpentier, R., Manfroy, P., Heremans, R. 1977. Preliminary studies of an underground facility for nuclear waste burial in a tertiary clay formation. Rockstore Conference 3: 771-780, Stockholm. 112 pp.

De Book, C., Bosgiraud, J.M., Breen, B., Johnson, M., Rothfuchs, T., Weber, H.P., van Marcke, P. 2009. ESDRED Deliverable 6 Module 1 WP6. Module 1 Final Report.

De Bruyn, D., Labat, S. 2002. The second phase of ATLAS: the continuation of a running THM test in the HADES underground research facility at Mol. Engineering Geology 64: 309–316. ISSN 0013-7952.

De Craen, M., Wang, L., Van Geet, M., Moors, H. 2004. Geochemistry of Boom Clay pore water at the Mol site. Scientific report, SCK•CEN-BLG-990.

Dehandschutter, B., Vandycke, S., Sintubin, M., Vandenberghe, N., Gaviglio, P., Sizun, J.P., Wouters, L. 2004. Microfabric of fractured Boom Clay at depth: a case study of brittle-ductile transitional clay behaviour. Applied Clay Science 26: 389-401.

Dehandschutter, B., Vandycke, S., Sintubin, M., Vandenberghe, N., Wouters, L. 2005. Brittle fractures and ductile shear bands inargillaceous sediments: inferences from Oligocene Boom Clay (Belgium). Journal of Structural Geology 27: 1095-1112.

Delage, P., Sultan, N., Cui, Y.J. 2000. On the thermal consolidation of Boom Clay. Canadian Geotechnical Journal 37: 343-354.

De La Vaissière, R., Armand, G., Talandier, J. 2015. Gas and water flow in an excavation-induced fracture network around an underground drift: a case study for a radioactive waste repository in clay rock. Journal of Hydrology 521: 141–156.

De Lesquen, C., Vu, M.N., Plua, C., Simo, E., Tatomir, A., León, P., Bésuelle, P., dal Pont, S., di Donna, A., Zalamea, N., Raude, S., El Tabbal, G., Dizier, A., Seetharam, S., Narkuniene, A., Poskas, G., Poskas, P., Collin, F., Song, H., Rawat, A., Gens, A. Song, F. 2024. Modelling report on the effect of temperature on clay host rocks behaviour. Final version as of 06/06/2024 of deliverable 7.6 of the HORIZON 2020 project EURAD. EC Grant agreement N˚ 847593. 288 pp.

Deng, Y.F., Cui, Y.J., Tang, A.M., Li, X.L., Sillen, X. 2012. An experimental study on the secondary deformation of Boom Clay. Applied Clay Science 59(60): 19-25.

Desai, C.S., Siriwaradane, H.J. 1984. Constitutive laws for engineering materials with emphasis on geological materials, Prentice-Hall.

Dixon, D. A., Birch, K., Stone, J., Kim, C. S., Barone, F. 2023. Measured swelling, hydraulic and thermal properties of MX-80 bentonite: Distinguishing between material variability and measurement limitations. Applied Clay Science 241 : 106998.

Dizier, A., 2011. Caractérisation des effets de température dans la zone endommagée autour des tunnels de stockage de déchets nucléaires dans des roches argileuses. PhD thesis. Université de Liège.

Dizier, A. 2018. Thermal analysis of C-Waste geological disposal facility in clay formations. ESV Euridice - European Underground Research Infrastructure for Disposal of nuclear waste in Clay Environment (Internal report).

Dizier, A., Chen, G.J., Li, X.L., Leysen, J., Verstricht, J., Troullinos, I., Rypens, J. 2016. The Start-up Phase of the PRACLAY Heater Test. EUR_PH_16_025. Mol, Belgium.

Dizier, A., Chen, G.J., Li, X.L., Rypens, J. 2017. The PRACLAY Heater test after two years of the stationary phase. EUR_PH_17_043. Mol, Belgium.

Dizier, A., Chen, G., Li, X.L., Levasseur, S. 2020. Thermo-hydro-mechanical modelling of a C-Waste geological geological disposal. ESV Euridice - European Underground Research Infrastructure for Disposal of nuclear waste in Clay Environment (Internal report).

Dizier, A., Chen, G. J., Verstricht, J., Li, X. L., Sillen, X., Levasseur, S. 2021. The large-scale in situ PRACLAY heater test: first observations on the in situ thermo-hydro-mechanical behaviour of Boom Clay. International Journal of Rock Mechanics and Mining Sciences 137: 104558.

Djéran, I., Bazargan, B., Giraud, A., Rousset, G. 1994. Etude expérimentale du comportement thermo-hydro-mécanique de l'Argile de Boom. Rapport G3S (Groupement pour l'étude des Structures Souterraines et de Stockage). (Internal report).

Dohrmann, R., Kaufhold, S., Gröger-Trampe, J. (in prep.) Characterization of the third package of the alternative buffer material (ABM-5) experiment operated at up to 250 °C. Clays and Clay Minerals

Drucker, D.C., Prager, W. 1952. Soil mechanics and plasticity analysis or limit design. Quarterly Applied Mathematics 10(2): 157-165.

Dueck, A. 2014. Laboratory studies on stress-strain behavior. PEBS Deliverable D2.2-12.

Dueck, A., Johannesson, L.E., Kristensson, O., Olsson, S. 2011. Report on hydro-mechanical and chemical-mineralogical analyses of the bentonite buffer in Canister Retrieval Test. SKB Technical Report TR-11-07. Svenska Kärnbränslehanterin AB.

Eberl, D., Whitney, G., Khoury, H. 1978. Hydrothermal reactivity of smectite. American Mineralogist 63: 401–409.

Eberl, D.D., Velde, B., McCormick, T.D. 1993. Synthesis of illite-smectite from smectite at earth surface temperatures and high pH. Clays and Clay Minerals 28: 49-60.

Eng, A., Nilsson, U., Svensson, D. 2007. Äspö Hard Rock Laboratory. Alternative buffer material installation report. SKB report IPR-07-15.

ENRESA 2006. FEBEX Full-scale Engineered Barriers Experiment. Updated Final Report 1994-2004. Publicación Técnica ENRESA 05-0/2006, Madrid, 590 pp.

Ewing, J., Senger R. 2012. Evolution of Temperature, Pressure and Saturation in the Bentonite Buffer: Scoping Calculations in Support of the Design of the Full-Scale Emplacement Experiment at the Mont Terri URL. Unpubl. NAGRA Interner Bericht NIB 10-040.

Ewy, R.T. 2015. Shale/Claystone Response to Air and Liquid Exposure, and Implications for Handling, Sampling and Testing. International Journal of Rock Mechanics and Mining Sciences 80: 388–401. https://doi.org/10.1016/j.ijrmms.2015.10.009

Fei, Y. 1995. Thermal expansion. In: Thomas J.A. (ed.) Mineral physics and crystallography: a handbook of physical constants. American Geophysical Union Online References Shelf 2: 29 – 44.

Fernández, A.M. 2004. Caracterización y modelización del agua intersticial en materiales arcillosos: Estudio de la bentonita de Cortijo de Archidona. PhD thesis. CIEMAT, Madrid, 505 pp.

Fernández, A.M., Villar, M.V. 2010. Geochemical behaviour of a bentonite barrier in the laboratory after up to 8 years of heating and hydration. Applied Geochemistry 25: 809-824. DOI:10.1016/j.apgeochem.2010.03.001

Ferrari, A., Laloui, L. 2012. Advances in testing the hydro-mechanical behaviour of shales. In L. Laloui and A. Ferrari editors. Multiphysical Testing of Soils and Shales, Springer, 57-68.

Ferrari, A., Favero, V., Manca, D., Laloui, L. 2013. Geotechnical characterization of core samples from the geothermal well Schlattingen SLA-1. NAGRA Arbeitsbericht NAB, NAGRA, Wettingen, Schweiz, 12-50.

Franče, J. 1992. Bentonity ve východní části Doupovských hor. Sborník geologických věd 30: 43-90.

Francois, B., Laloui, L., 2009. ACMEG-T: Soil Thermoplasticity Model. Journal of Engineering Mechanics 135(9).

François, B. 2008. Thermo-plasticity of soils at various saturation state: application to nuclear waste disposal. PhD thesis. École Polytechnique Fédérale de Lausanne.

François, B., Labiouse, V., Dizier, A., Marinelli, F., Charlier, R. 2014. Hollow Cylinder Tests on Boom Clay: Modelling of Strain Localization in the Anisotropic Excavation Damaged Zone. Rock Mechanics and Rock Engineering 47(1): 71-86.

François, B., Laloui, L., Laurent, C. 2009. Thermo-hydro-mechanical simulation of ATLAS in situ large scale test in Boom Clay. Computers and Geotechnics 36: 626-640. ISSN 0266-352X.

Frederickx, L. 2019. An advanced mineralogical study of the clay mineral fractions in the Boom Clay. PhD thesis. KU Leuven.

Fritz, B., Kam, M., Tardy, Y. 1984. Geochemical simulation of the evolution of granitic rocks and clay minerals submitted to a temperature increase in the vicinity of a repository for spent nuclear fuel. KBS TR 84-10. Svensk Kärnbränslehantering AB.

Garitte, B., Vaunat, J. 2008. Thermo-Hydro-mechanical Design calculation for the TED experiment. Laboratoire de recherche souterrain de Meuse/Haute-Marne, Rapport n°D.RP.0UPC.080001.

Garitte, B., Gens, A., Vaunat, J., Armand, G. 2014. Thermal conductivity of argillaceous rocks: Determination methodology using in situ heating tests. Rock Mechanics and Rock Engineering 47(1): 111–129.

Gatabin, C., Billaud, P. 2005. Bentonite THM mock up experiments. Sensors data report. CEA, Report NT-DPC/SCCME 05-300-A.

Gaucher, E.C., Blanc, P., Bardot, F., Braibant, G., Buschaert, S., Crouzet, C., Gautier, A., Girard, J. P., Jacquot, E., Lassin, A., Negrel, G., Tournassat, C., Vinsot, A., Altmann S. 2006. Modelling the porewater chemistry of the Callovian-Oxfordian formation at a regional scale. Comptes Rendus Geoscience 338: 917-930.

Gaus, I. (Ed.) 2011. Long term Performance of Engineered Barrier Systems (PEBS): Mont Terri HE-E experiment: detailed design. NAGRA-Arbeitsbericht NAB 11-01. NAGRA, Wettingen, Switzerland.

Gaus, I., Garitte, B., Senger, R., Gens, A., Vasconcelos, R., Garcia-Sineriz, J.L., Trick, T., Wieczorek, K., Czaikowski, O., Schuster, K., Mayor, J.C., Velasco, M., Kuhlmann, U., Villar, M.V. 2014. The HE-E Experiment: Lay-out, Interpretation and THM Modelling Combining D2.2-11. Final Report on the HE-E Experiment and D3.2-2: Modelling and Interpretation of the HE-E Experiment of the PEBS Project. NAGRA Working Report NAB 14-53, Wettingen, Switzerland and EU PEBS Project report downloadable from http://www.pebs-eu.de/

Gautschi 2017. Safety-relevant hydrogeological properties of the claystone barrier of a Swiss radioactive waste repository: An evaluation using multiple lines of evidence. (Grundwasser – Zeitschrift der Fachsektion Hydrogeologie).

Gbewade, C.A.F., Grgic, D., Giraud, A., Schoumacker, L. 2023. Experimental study of the effect of temperature on the mechanical properties of the Callovo-Oxfordian Claystone. Rock Mechanics and Rock Engineering.

Gens, A. 2019. Task Force on Engineered Barrier System (EBS). Task 1 Laboratory tests. SKB Technical Report TR-14-24. Stockholm, 141 pp.

Gens, A., Alonso, E.E. 1992. A framework for the behaviour of unsaturated expansive clays. Can. Geotech. J. 29: 1013–1032.

Gens, A., Valleján, B., Zandarín, M.T., Sánchez, M. 2013. Homogenization in clay barriers and seals: Two case studies. Journal of Rock Mechanics and Geotechnical Engineering 5(3): 191-199.

Gens, A., Vaunat, J., Garitte, B., Wileveau, Y. 2007. In-situ behaviour of a stiff layered clay subject to thermal loading. Observations and interpretation. Géotechnique 57(2): 207-228.

Georgiadis, K., Potts, D.M., Zdravkovic, L. 2005. Three-dimensional constitutive model for partially and fully saturated soils. International Journal of Geomechanics 5(3): 244-255.

Ghabesloo, S., Sulem, J. 2007. Pressurisation thermique d'une roche saturée. 18ème Congrès Français de Mécanique. http://hdl.handle.net/2042/16547

Ghiadistri 2019. Constitutive modelling of compacted clays for applications in nuclear waste disposal. PhD Thesis. Imperial College London, April 2019.

Giot, R., Auvray, C., & Talandier, J. (2019). Self-sealing of claystone under X-ray nanotomography. Geological Society, London, Special Publications 482(1): 213-223. https://doi.org/10.1144/SP482.4.

Göbel, I., Alheid, H.J., Alonso, E., Ammon, C.H., Bossart, P., Bühler, C.H., Emmerich, K., Fernandez, A.M., García-Siñeriz, J.L., Graf, A., Jockwer, N., Kaufhold, St. Kech, M., Klubertanz, G., Lloret, A., Mayor, J.C., Meyer, T., Miehe, R., Muñoz, J.J., Naumann, M., Nussbaum, C.H., Pletsch, T., Plischke, I., Ploetze, M., Rey, M., Schnier, H., Schuster, K., Sprado, K., Trick, Th., Weber, H., Wieczorek, K., Zingg, A. 2007. Heater Experiment: Rock and bentonite thermohydro-mechanical (THM) processes in the near field of a thermal source for development of deep underground high level radioactive waste repositories. In: Bossart, P., Nussbaum, P. (eds.). Mont Terri Project - Heater experiment, engineered barrier emplacement and ventilation experiment. Reports of the Swiss Geological Survey 1, Swisstopo, Wabern, 7-114.

Gómez-Espina, R., Villar, M.V. 2010. Geochemical and mineralogical changes in compacted MX-80 bentonite submitted to heat and water gradients. Applied Clay Science 47: 400–408.

Gómez-Espina, R., Villar, M.V. 2015. Effects of heat and humidity gradients on MX-80 bentonite geochemistry and mineralogy. Applied Clay Science 109-110: 39–48.

Gómez-Espina, R., Villar, M.V. 2016. Time evolution of MX-80 bentonite geochemistry under thermo-hydraulic gradients. Clay Minerals 51: 145-160.

Graham C.C., Daniels K., Harrington J. F., Chaaya R., Gaboreau S., Tremosa J., Villar M.V., Gutiérrez-Álvarez C., García-Herrera, G., Iglesias, R. J., Gimeno, N., Svoboda J., Černochová K., Najser J., Mašín D., Yliharju J., Sayenko S., Pulkkanen V., Rauhala O., Vettese G., Pakkanen N., Siitari-Kauppi M. 2023. HITEC technical report on Material characterisation. Final version as of 09.11.2023 of deliverable D7.8 of the HORIZON 2020 project EURAD. EC Grant agreement no: 847593.

Grgic, D., Bésuelle, P., Cuss, R., 2023a. Technical report on thermal effects on near field properties. Final version as of 01.11.2023 of deliverable D7.3 of the HORIZON 2020 project EURAD. EC Grant agreement no: 847593. 85 pp.

Grgic, D., Imbert, C., Harrington, J. & Tamayo-Mas, E., 2023b. Technical report on thermal effects on far field properties. Final version as of 01.11.2023 of deliverable D7.5 of the HORIZON 2020 project EURAD. EC Grant agreement no: 847593. 112 pp.

Guayacan Carrillo, L.M. 2016. Analysis of long-term closure in drifts excavated in Callovo-Oxfordian claystone: roles of anisotropy and hydromechanical couplings. PhD thesis. Université Paris-Est.

Gudehus, G. 1996. A comprehensive constitutive equation for granular materials. Soils and Foundations 36 (1): 1–12.

Hanusová., I., Šťástka, J. 2017. Mock-Up Josef experiment – mineralogical study. Abstract for the 7th International Conference on Clays in Natural and Engineered Barriers for Radioactive Waste Confinement, Davos.

Harjupatana, T., Alaraudanjoki, J., Kataja, M. 2015. X-ray tomographic method for measuring three-dimensional deformation and water content distribution in swelling clays. Applied Clay Science 114: 386-394. https://doi.org/10.1016/j.clay.2015.06.016

Hausmannová, L., Hanusová, I., a Dohnálková, M. 2018. Summary of the research of Czech bentonites for use in the deep geological repository – up to 2018, SÚRAO 309/2018/ENG.

Heuser, M., Weber, C., Stanjek, H., Chen, Hong., Jordan, G., Schmahl, W.W., Natzeck, C. 2014. The Interaction Between Bentonite and Water Vapor. I: Examination of Physical and Chemical Properties. Clays and Clay Minerals 62: 188–202. https://doi.org/10.1346/CCMN.2014.0620303

Hill, R. 1952. The elastic behavior of crystalline aggregate. Proc. Physical Soc. A 65: 349–354, London.

Hinson, S. 2019. New Nuclear Power, Briefing Paper. House of Commons Library. Number CBP 8176, September 2019.

HökmarkK, H., Karnland, O., Pusch, R. 1997. A technique for modeling transport/conversion processes applied to smectite-to-illite conversion in HLW buffers. Engineering Geology 47: 367–378.

Honty M., Frederickx L., Wang L., De Craen M., Thomas P., Moors H., Jacops E., 2022. Boom Clay pore water geochemistry at the Mol site: Experimental data as determined by in situ sampling of the piezometers. Applied Geochemistry 136: 105156. https://doi.org/10.1016/j.apgeochem.2021.105156

Horseman, S.T., Winter, M.G., Entwistle, D.C. 1987. Geotechnical characterisation of Boom clay in relation to disposal of radioactive waste. Publications of the European Communities, EUR 1087 EN, Luxembourg.

Horseman, S.T., Winter, M.G., Entwistle, D.C. 1993. Triaxial experiments on Boom clay. In: Cripps, J.C., Coulthard, J.M., Culshaw, M.G., Forster, A., Hencher, S.R., Moon, C.F. (eds). The engineering geology of weak rock. Rotterdam: Balkema, 36–43.

Horseman, S.T., Harrington, J.F. 2002. Laboratory experiments on gas migration in Opalinus Clay samples from the Benken borehole, Switzerland. Unpublublished NAGRA Interner Bericht.

Hoth, P., Wirth, H., Reinhold, K., Bräuer, V., Krull, P., Feldrappe, H. 2007. Endlagerung radioaktiver Abfälle in tiefen geologischen Formationen Deutschlands – Untersuchung und Bewertung von Tongesteinsformationen. Bundesanstalt für Geowissenschaften und Rohstoffe: 118 S. Berlin/Hannover.

Huang, W.L., Longo, J.M., Pevear, D.R. 1993. An experimentally derived kinetic model for smectite-to-illite conversion and its use as a geothermometer. Clays and Clay Minerals 41: 162–177.

Hueckel, T., François, B., Laloui, L. 2009. Explaining thermal failure in saturated clays. Géotechnique 53(3): 197-212.

Hueckel, T., Borsetto, M. 1990. Thermoplasticity of saturated clays: Experimental constitutive study. Journal of Geotechnical Engineering 116(12): 1765-1777, ASCE.

Ikonen, K., Kuutti, J., Raiko, H., 2018. Thermal dimensioning for the Olkiluoto Repository - 2018 update. Workreport 2018-26, Posiva Oy.

Inoue, A. 1983. Potassium fixation by clay minerals during hydrothermal treatment. Clays and Clay Minerals 31: 81-91.

Inoue, A. 1995. Formation of clay minerals in hydrothermal environments. In: Velde, B. (ed.). Origin and Mineralogy of Clays. Springer, 268-329.

Jacinto, A.C., Villar, M.V., Gómez-Espina, R., Ledesma, A. 2009. Adaptation of the van Genuchten expression to the effects of temperature and density for compacted bentonites. Applied Clay Science 42: 575–582.

Jadda, K., Bag, R. 2020. Effect of initial compaction pressure and elevated temperature on swelling pressure of two Indian bentonites. Environmental Earth Sciences 79: 1-15.

Jahn, S., Mrugalla, S., Stark. L. 2016. Endlagerstandortmodell SÜD - Teil II: Zusammenstellung von Gesteinseigenschaften für den Langzeitsicherheitsnachweis, Bundesanstalt für Geowis-senschaften und Rohstoffe (BGR), Hannover.

Jobmann, M., Amelung, P., Billaux, D., Polster, M., Schmidt, H., Uhlig L. 2007. Untersuchungen zur sicherheitstechnischen Auslegung eines generischen Endlagers im Tonstein in Deutschland - GENESIS – Abschlussbericht. DBE TECHNOLOGY GmbH, Peine.

Jobmann, M., Breustedt, M., Li, S., Polster, M., Schirmer, S. 2013. Investigations on THM effects in buffer, EDZ and argillaceous host rock. Final Report. TEC-09-2012-AB, DBE TECHNOLOGY, Peine.

Jobmann, M., Bebiolka, A., Jahn, S., Lommerzheim, A., Maßmann, J., Meleshyn, A., Mrugalla, S., Reinhold, K., Rübel, A., Stark, L. Ziefle, G. 2017. Projekt ANSICHT - Sicherheits- und Nachweismethodik für ein Endlager im Tongestein in Deutschland. Synthesebericht. Förderkennzeichen 02E11061A/B, DBE TECHNOLOGY GmbH, TEC-19-2016-AB, Peine.

Jockwer, N., Wieczorek, K., Miehe, R., Fernández Diaz, A.M. 2006. Heater Test in the Opalinus Clay of the Mont Terri URL. Gas Release and Water Redistribution Contribution to Heater Experiment (HE). Rock and bentonite thermohydro- mechanical (THM) processes in the nearfield. GRS Report 223 ISBN 3-931995-93-3. http://www.grs.de/sites/ default/files/pdf/GRS-223.pdf

Johnson, L.H., Niemeyer, M., Klubertanz, G., Siegel, P., Gribi, P. 2002. Calculations of the Temperature Evolution of a Repository for Spent Fuel, Vitrified High-Level Waste and Intermediate Level Waste in Opalinus Clay. NAGRA TR 01-04.

Johnson, L., Gaus, I., Wieczorek, K., Mayor, J.C., Sellin, P., Villar, M.V., Samper, J., Cuevas, J., Gens, A., Velasco, M., Turrero, M.J., Montenegro, L., Martín, P.L., Armand, G. 2014. Integration of the short-term evolution of the engineered barrier system (EBS) with the long-term safety perspective (Deliverable D4.1 of the PEBS project). NAGRA Arbeitsbericht NAB 14-079.

Juvankoski, M. 2013. Buffer design 2012. Report POSIVA 2012-14, Posiva Oy. ISBN 978-951-652-195-7.

Kamei, G., Mitsui, M.S., Futakuchi, K., Hashimoto, S., Sakuramoto, Y. 2005. Kinetics of long-term illitization of montmorillonite—a natural analogue of thermal alteration of bentonite in the radioactive waste disposal system. Journal of Physics and Chemistry of Solids 66 (2-4): 612-614.

Karnland, O., Birgersson, M. 2006. Montmorillonite stability. With special respect to KBS-3 conditions. SKB TR-06-11, Svensk Kärnbränslehantering AB.

Karnland, O., Sandén, T., Johannesson, L.E., Eriksen T.E., Jansson, M., Wold, S., Pedersen, K., Motamedi, M., Rosborg B. 2000. Long-term test of buffer material. Final report on the pilot parcels. SKB report TR-00-22, Svensk Kärnbränslehantering AB. Stockholm, 131 pp.

Karnland, O., Nilsson, U., Weber, H.P., Wersin, P. 2008. Sealing ability of Wyoming bentonite pellets foreseen as buffer material – Laboratory results. Physics and Chemistry of the Earth Parts A/B/C 33(1): S472-S475.

Karnland, O., Olsson, S., Dueck, A., Birgersson, M., Nilsson, U., Hernan-Hakansson, T., Pedersen, K., Nilsson, S., Eriksen, T.E., Rosborg, B. 2009a. Long-term test of buffer material at the Äspö Hard Rock Laboratory, LOT project. Final report on the A2 test parcel. SKB report TR-09-29, Svensk Kärnbränslehantering AB. Stockholm, 295 pp.

Karnland, O., Olsson, S., Sandén, T., Fälth, B., Jansson, M., Eriksen, T.-E., Svärdström, K., Rosborg B., Muurinen, A. 2009a. Long-term test of buffer material at the Äspö Hard Rock Laboratory, LOT project. Final report on the A0 test parcel. SKB report TR-09-31, Svensk Kärnbränslehantering AB. Stockholm, 123 pp.

Karnland, O., Birgersson, M., & Hedström, M. 2011. Selectivity coefficient for Ca/Na ion exchange in highly compacted bentonite. Physics and Chemistry of the Earth, Parts A/B/C, 36(17-18), 1554-1558.

Kašpar, V., Šachlová, Š., Hofmanová, E., Komárková, B., Havlová, V., Aparicio, C., Černá, K., Bartak, D., Hlaváčková, V. 2021. Geochemical, Geotechnical, and Mineralogical Changes in Mg/Ca bentonite after Thermal Loading at 150 °C. Minerals 11(9): 965. DOI 10.3390/min11090965.

Kaufhold, S., Dohrmann, R., Ufer, K., Svensson, D., Sellin, P. 2021. Mineralogical Analysis of Bentonite from the ABM5 Heater Experiment at Äspö Hard Rock Laboratory, Sweden. Minerals 11(7): 669. https://doi.org/10.3390/min11070669.

Kirkham, A., Tsiampousi, A., Potts, D. 2020. Development of a new temperature-controlled oedometer. ICEGT 2020. E3S Web of Conferences 205: 04015. https://doi.org/10.1051/e3sconf/202020504015

Kiviranta, L., Kumpulainen, S. 2011. Quality Control and Characterization of Bentonite Materials, Workreport 2011-84, Posiva Oy.

Kiviranta, L., Kumpulainen, S., Pintado, X., Karttunen, P., Schatz, T. 2018. Characterization of Bentonite and Clay Materials 2012-2015. Workreport 2016-5, Posiva Oy.

Kleine, A. 2007. Modélisation Numérique du Comportement des Ouvrages Souterrains par une Approche Viscoplastique. PhD thesis.

Kober, F., García-Siñeriz, J.L., Villar, M.V., Lanyon, G.W., Cloet, V., Mäder, U., Wersin, P., Leupin, O., Sellin, P., Gens, A., Schneeberger R. 2021. FEBEX-DP Synthesis Summary of the Full-Scale Engineered Barriers Experiment – Dismantling Project. NAGRA Technical Report 17-01. Wettingen, 204 pp.

Kotnour, P. 2017. Výzkum a vývoj ukládacího obalového souboru pro hlubinné ukládání vyhořelého jaderného paliva do stádia realizace vzorku 3. etapa, TZ SÚRAO, 2017.

Labiouse, V., Sauthier, C., You, S., 2014. Hollow cylinder experiments of galleries in Boom Clay Formation. Rock Mechanics and Rock Engineering 47(1): 43-55.

Laigle, F. 2004. Modèle Conceptuel pour le Développement de Lois de Comportement adaptées à la Conception des Ouvrages Souterrains. PhD thesis.

Laine, H., Karttunen, P. 2010. Long-Term Stability of Bentonite A Literature Review. POSIVA Working Report 2010-53: 128 pp.

Lanyon, G.W. 2019a. Update of synopsis regarding EDZ development and evolution at the Mont Terri Rock Laboratory. NAGRA Arbeitsbericht NAB 18-045.

Lanyon, G.W. 2019b. Update of synopsis regarding EDZ development and evolution at the Mont Terri Rock Laboratory. NAGRA Arbeitsbericht NAB 18-045.

Le, T.-T. 2008. Comportement thermo-hydro-mécanique de l'argile de Boom. PhD thesis. CERMES, Ecole Nationale des Ponts et Chaussées, Paris.

Leal-Olloqui, M. 2019. A study of alteration processes in bentonite. PhD thesis. University of Bristol. 328 pp.

Lenoir, N., Bornert, M., Desrues, J., Bésuelle, P., Viggiani, G. 2007. Volumetric digital image correlation applied to X-Ray microtomography images from triaxial compression tests on argillaceous rocks. Strain 43: 193-205.

Leonard, D. 2017. Design and construction of the supercontainer for category C waste. Technical report. NIROND-TR 2017-11 E V2 (Internal report ONDRAF/NIRAS).

Leupin, O., Johnson, L. 2014. Requirements for buffer for a repository for SF/HLW in Opalinus Clay. NAGRA Working Report NAB 13-46. NAGRA, Wettingen.

Leupin, O.X. (Ed.), Birgersson, M., Karnland, O., Korkeakoski, P., Sellin, P., Mäder, U., Wersin, P. 2014. Montmorillonite stability under near-field conditions. NAGRA TR14-12. Wettingen, 104 pp.

Leupin, O.X., Smith, P., Marschall, P., Johnson, L., Savage, D., Cloet, V., Schneider, J., Senger, R.K. 2016. High-level waste repository-induced effects. NAGRA Technical Report NTB 14-13.

Li, X., Bernier, F., Vietor, T., Lebon, P. 2007. TIMODAZ. Deliverable 2. EC Contract: FI6W-CT-036449, 104 pp.

Li, X.L., Dizier, A., Chen, G., Verstricht, J., Levasseur, S. 2023. Forty years of investigation into the thermo-hydromechanical behaviour of Boom Clay in the HADES URL. Geological Society, London, Special Publication 536.

Lima, A. 2011. Thermo-hydro-mechanical behaviour of two deep Belgium clay formations: Boom Clay and Ypresian clays. PhD Thesis. Universitat Politècnica de Catalunya, Spain.

Lima, A., Romero, E., Piña, Y. 2011. Water retention properties of two deep Tertiary clay formations within the context of radioactive waste disposal. A: Simpósio Brasileiro de Solos Nao Saturados. VII Brazilian Symposium on Unsaturated Soil. Pirenópolis, Goiania, 315-321.

Mäder, U.K. 2009. Reference pore waters for the Opalinus Clay and "Brown Dogger" for the provisional safety-analysis in the framework of sectoral plan - interim results (SGT-ZE). NAGRA Arbeitsbericht NAB 09-014.

Madsen, F.T. 1998. Clay mineralogical investigations related to nuclear waste disposal. Clay minerals 33(1): 109-129.

Mair, R., Taylor, R., Clarcke, B. 1992. Repository tunnel construction in deep clay formations. Commission of the European Communities. Nuclear science and Technology EUR 13964.

Mánica, M.A. 2018. Analysis of underground excavations in argillaceous hard soils - weak rocks. PhD thesis. Technical University of Catalonia. Barcelona, 196 pp. http://hdl.handle.net/10803/663452

Marschall, P., Horseman, S., Gimmi, T. 2005. Characterization of gas transport properties of the Opalinus Clay, a potential host rock formation for radioactive waste disposal. Oil & Gas Science and Technology 60(1): 121-139.

Martínez, V., Abós, H., García-Siñeriz, J.L. 2016. FEBEXe: Final Sensor Data Report (FEBEX 'In situ' Experiment). NAGRA Arbeitsbereicht NAB 16-019. Wettingen, 230 pp.

Mašín, D. 2005. A hypoplastic constitutive model for clays. International Journal for Numerical and Analytical Methods in Geomechanics 29(4): 311-336.

Mašín, D. 2010. Predicting the dependency of a degree of saturation on void ratio and suction using effective stress principle for unsaturated soils. International Journal for Numerical and Analytical Methods in Geomechanics 34 (1): 73-90.

Mašín, D. 2012. Hypoplastic Cam-clay model. Géotechnique 62(6): 549-553.

Mašín, D. 2013. Double structure hydromechanical coupling formalism and a model for unsatu-rated expansive clays. Engineering Geology 165: 73-88.

Mašín, D. 2014. Clay hypoplasticity model including stiffness anisotropy. Géotechnique 64(3): 232-238.

Mašín, D. 2017. Coupled thermohydromechanical double structure model for expansive soils. ASCE Journal of Engineering Mechanics 143(9).

Mašín, D., Khalili, N. 2008. A hypoplastic model for mechanical response of unsaturated soils. International Journal for Numerical and Analytical Methods in Geomechanics 32(15): 1903-1926.

Mašín, D., Khalili, N. 2016. Swelling phenomena and effective stress in compacted expansive clays. Canadian Geotechnical Journal 53(1): 134-147.

Mayor, J.C., García-Siñeriz, J.L., Alonso, E. Alheid, H.J., Blümling P. 2005. Engineered barrier emplacement experiment in Opalinus Clay for the disposal of radioactive waste in underground repositories. Report EUR 21920.

Mazurek, M., Pearson, F.J., Volckaert, G., Bock, H. 2003. Features, Events and Processes Evaluation Catalogue for Argillaceous Media. Radioactive Waste Management. OECD Nuclear Energy Agency (NEA), France, 380 pp. ISBN 92-64-02148-5.

McTigue, D.F. 1986. Thermoelastic response of fluid-saturated porous rock. Journal of Geophysical Research 91(B9): 9533—9542.

Mertens, J., Wouters, L. 2003. 3D Model of the Boom Clay around the HADES-URF, Construction of an AUTOCAD 3D-model of the URF, together with the internal clay layering. NIROND 2003-02, 31 pp.

Mertens, J., Vandenberghe, N., Wouters, L., Sintubin, M. 2003. The origin and development of joints in the Boom Clay Formation (Rupelian) in Belgium. In: Van Rensbergen, P., Hillis, R.R., Maltman, A.J., Morley, C.K. (eds). Subsurface Sediment Mobilization. Geological Society Special Publication 217: 311-323, London.

Mertens, J., Bastiaens, W., Dehandschutter, B. 2004. Characterisation of induced discontinuities in the Boom Clay around the underground excavations (URF, Mol, Belgium). Applied Clay Science 26: 413-428.

Mohajerani, M., Delage, P., Sulem, J., Monfared, M., Tang, A.M., Gatmiri, B. 2012. "A laboratory investigation of thermally induced pore pressures in the Callovo-Oxfordian claystone". International Journal of Rock Mechanics and Mining Sciences 52: 112–121.

Monfared, M. 2011. Couplages température-endommagement-perméabilité dans les sols et les roches argileuses. PhD thesis. École Nationale des Ponts et Chaussées.

Morodome, S., Kawamura, K. 2009. Swelling behaviour of Na- and Ca- montmorillonite up to 150◦C by in situ X-ray diffraction experiments. Clays and Clay Minerals 57(2): 150–160.

Müller, H.R., Garitte, B., Köhler, S., Vogt, T., Sakaki, T., Weber, H., Vietor, T. 2015. LUCOEX (EURATOM Grant Agreement 269905). Deliverable D2.6 Final Report of WP2. 56 pp.

Müller-Vonmoos, M., Kahr, G. 1983. Mineralogische Untersuchungen von Wyoming bentonit MX-80 und Montigel. NAGRA. Technischer Bericht 83-12.

Muñoz, J.J., Lloret, A., Alonso, E. 2003. "VE" Experiment - Laboratory Report: Characterization of hydraulic properties under saturated and non-saturated conditions Project Deliverable 4, EC contract FIKW-CT2001-00126.

Muurinen, A., Karnland, O., Lehikoinen, J. 2004. Ion concentration caused by an external solution into the porewater of compacted bentonite. Physics and Chemistry of the Earth 29: 119–127.

Muurinen, A. 2011. Measurements on Cation Exchange Capacity of Bentonite in the Long-Term Test of Buffer Material (LOT) Posiva Working Report 10 : 26 pp, January 2011.

NAGRA 2002a. Project Opalinus Clay: Safety report: Demonstration of disposal feasibility for spent fuel, vitrified high-level waste and long-lived intermediate-level waste (Entsorgungsnachweis). NAGRA Technical Report NTB 02-05.

NAGRA 2002b. Projekt Opalinuston: Synthese der geowissenschaftlichen Untersuchungsergibnisse - Entsorgunsnachweis für abgebrannte Brennelemente, verglaste hochaktive sowie langlebige mittelaktive Abfälle. NAGRA Technischer Bericht NTB 02-03.

NAGRA 2008. Vorschlag geologischer Standortgebiete für ein SMA- und ein HAA-Lager: Begründung der Abfallzuteilung, der Barrierensysteme und der Anforderungen an die Geologie (Bericht zur Sicherheit und Machbarkeit). NAGRA Technischer Bericht NTB 08-05.

NAGRA 2014a. An Assessment of the Impact of the Long Term Evolution of Engineered Structures on the safety-Relevant Functions of the Bentonite Buffer in a HLW Repository. NAGRA Technical Report. NTB 13-02.

NAGRA 2014b. Montmorillonite stability under near-field conditions. NAGRA Technical Report. NTB 14-12.

NAGRA 2014c. SGT Etappe 2: Vorschlag weiter zu untersuchender geologischer Standortgebiete mit zugehörigen Standortarealen für die Oberflächenanlage: Geologische Grundlagen Dossier VI Barriereneigenschaften der Wirt- und Rahmengesteine. Nagra Technischer Bericht. NTB 14-02 Dossier VI.

NAGRA 2015. Thermo-hydro-mechanical characterization and modelling of Wyoming granular bentonite. NAGRA Technical Report NTB 15-05. NAGRA, Wettingen, Switzerland.

NAGRA 2016. High-level waste repository-induced effects. NAGRA Technical report. NTB 14-13.

NAGRA 2018. Implementation of the Full-scale Emplacement Experiment in Mont Terri: Design, Construction and Preliminary Results. Nagra Technical Report NTB 15-02.

NAGRA 2019. Implementation of the Full-scale Emplacement Experiment at Mont Terri: Design, Construction and Preliminary Results. NAGRA Technical Report. NTB 15-02. Wettingen, 147 pp.

NAGRA 2022. Module der Lagerarchitektur. Nagra Working Report NAB 22-35.

Narkūnienė, A., Poskas, G., Justinavicius, D., Kilda, R. 2022. THM Response in the Near Field of an HLW Disposal Tunnel in the Callovo-Oxfordian Clay Host Rock Caused by the Imposed Heat Flux at Different Water Drainage Conditions. Minerals 12: 1187, https://doi.org/10.3390/min12101187

Nguyen, X.P., Cui, Y.J, Tang, A.M., Deng, Y.F., Li, X.L., Wouters, L. 2013. Effects of pore water chemical composition on the hydro-mechanical behavior of natural stiff clays. Engineering Geology 166: 52-64.

Ni, H., Liu, J., Zhang, Q., Ma, L., Guo, J., Mao, X. 2022. Water retention behavior and double porosity model study of GMZ bentonite considering temperature effects. Engineering Geology 304: 106695.

Olivella, S., Gens, A., Carrera, J., Alonso, E.E. 1994. Nonisothermal multiphase flow of brine and gas through saline media. Transport in Porous Media 15, 271–293.

Olivella, S., Gens, A., Carrera, J., Alonso, E.E. 1996. Numerical formulation for a simulator (CODE_BRIGHT) for the coupled analysis of saline media. Engineering Computations 13(7): 87-112.

Olsson, S., Jensen, V., Johannesson, L.E., Hansen, E., Karnland, O., Kumpulainen, S., Kiviranta, L., Svensson, D., Hansen, S., Lindén, J. 2013. Prototype Repository. Hydro-mechanical, chemical and mineralogical characterization of the buffer and tunnel backfill material from the outer section of the Prototype Repository. SKB report TR-13-21.

ONDRAF/NIRAS 2013. Research, Development and Demonstration (RD&D) plan for the geological disposal of high level and / or long-lived radioactive waste including irradiated fuel if considered as

waste. State-of-the-art report as of December 2012. Belgian Agency for Radioactive Waste for Enriched Fissile Materials. NIROND-TR 2013-12 E.

ONDRAF/NIRAS 2020. Design and Construction of the Geological Disposal Facility for Category B and Category C Wastes (V3). Technical Report NIROND-TR 2017-12 E V3. Category B&C. Brussels, Belgium.

Ouvry, J.F. 1983. Caractéristiques géotechniques de l'argile de Boom (Belgique) à partir des essais de laboratoires communiqués par le CEN/SCK. Service géologique régional du Nord-Pas-de-Calais, Lille, France.

Péguiron F. 2021. Modélisations physique et numérique de la zone endommagée autour de galeries creusées dans l'argile de Boom. PhD thesis University of Lorraine.

Pellet, F. 2007. Expertise sur le comportement différé des argilites. Rapport interne ANDRA N° CRP0FLO070024.

Petley, D.N. 1999. Failure envelopes of mudrocks at high effective stresses. In: Aplin, A.C., Fleet, A.J., Macquaker, J.H.S. (eds). Physical Properties of Muds and Mudstones. Special Publication of the Geological Society of London 158: 61-71.

Pintado, X., Ledesma, A., Lloret, A. 2002. Backanalysis of thermohydraulic bentonite properties from laboratory tests. Engineering Geology 64(2): 91–115

Pintado, X., Mamunul, H.M., Martikainen, J. 2013. Thermo-Hydro-Mechanical Tests of Buffer Material. POSIVA 2012-49. Olkiluoto, 152 pp. ISBN 978-951-652-231-2.

Pöhler, M., Amelung, P., Bollingerfehr, W., Engelhardt, H.J., Filbert, W., Tholen, M. 2010. Referenzkonzept für ein Endlager für radioaktive Abfälle im Tongestein. ERATO. Abschlussbericht. Förderkennzeichen 02E 10288, DBE TECHNOLOGY GmbH, TEC-28-2008-AB, Peine.

Poller, A., Mayer, G., Croisé, J. 2007. Two-phase Flow Analysis of Gas Tests in Opalinus Clay Core Specimen: Complementary Analysis. Mont Terri TN 2007-01.

POSIVA, 2013. Safety Case for the Disposal of Spent Nuclear Fuel at Olkiluoto – Performance Assessment 2012. Posiva report 2012-04, ISBN 978-951-652-185-8.

Potts, D.M., Zdravkovic, L. 1999. Finite element analysis in geotechnical engineering: Theory. Thomas Telford, London.

Pulkkanen, V.M., 2019. A large deformation model for chemoelastic porous media - Bentonite clay in spent nuclear fuel disposal. D.S. (Tech.) Thesis. Aalto University, Finland.

Pusch, R. 2001. The buffer and backfill handbook. Part 2: Materials and techniques: Swedish Nuclear Fuel and Waste Management Co. SKB TR-02-12. 197 pp.

Pusch, R., Kasbohm, J., Thao, H.M. 2010. Chemical stability of montmorillonite buffer clay under repository-like conditions - A synthesis of relevant experimental data. Applied Clay Science 47(1–2): 113–119.

Raude, S. 2015. Prise en compte des solicitations thermiques sur les comportements instantané et différé des géomatériaux. PhD thesis, Université de Lorraine Géoressources.

Rawat, A. 2023. EURAD HITEC Technical Report Task 2.3: Influence of temperature on clay-based material behaviour-far field generic case.

Raymaeckers, D., D'Orazio, D., Leonard, D. 2019. Les déchets de forte activite et/ de longue durée de vie. Le design et l'architecture du stockage géologique. Journée d'étude du SBGIMR – Le stockage des déchets nucléaires, Liège 21 Février 2009 (Presentation).

Rebours, H., Andre, G., Cruchaudet, M., Dewonck, S., Distinguin, M., Drouiller, Y., Morel, J., Wileveau, Y., Vinsot, A., 2005. Callovo-Oxfordien - Rapport de synthèse. D.RP.ADPE.04.1110, Andra, Paris, France.

Reinhold, K., Sönnke, J. 2012. Geologische Referenzprofile in Süd- und Norddeutschland. Projekt ANSICHT: Methodik und Anwendungsbezug eines Sicherheits- und Nachweiskonzeptes für ein HAW-Endlager im Tonstein, Bundesanstalt für Geowissenschaften und Rohstoffe (BGR), Berlin und Hannover.

Reinhold, K., Stark, L., Kühnlenz, T., Ptock, L. 2016. Endlagerstandortmodell SÜD – Teil I: Be-schreibung des geologischen Endlagerstandortmodells. Projekt ANSICHT: Methodik und Anwendungsbezug eines Sicherheits- und Nachweiskonzeptes für ein HAW-Endlager im Ton-stein, Bundesanstalt für Geowissenschaften und Rohstoffe (BGR), Berlin und Hannover.

Roaldset, E., Wei, H., Grimstad, S. 1998. Smectite to illite conversion by hydrous pyrolysis. Clays and Clay Minerals 33: 147-158.

Robinet, J.C., Sardini, P., Coelho, D., Parneix, J.-C., Prêt, D., Sammartino, S., Boller, E., Altmann S. 2012. Effects of mineral distribution at mesoscopic scale on solute diffusion in a clay-rich rock. Example of the Callovo-Oxfordian mudstone of Bure (France), Water Ressources Research (48), W05554.

Romero, E., Gens, A., Lloret, A. 2001. Temperature effects on the hydraulic behaviour of an unsaturated clay. Geotechnical and Geological Engineering 19: 311–332.

Romero, E. Gens, A. Lloret, A. 2003. Suction effects on a compacted clay under non-isothermal conditions. Geotechnique 53(1): 65–81.

Romero, E., Gómez, R. 2013. Water and air permeability tests on deep core samples from Schlattingen SLA-1 borehole. NAGRA Arb. Ber. NAB 13-51. NAGRA, Wettingen, Switzerland.

Ruan, K., Wang, H., Komine, H., Ito, D. 2022. Experimental study for temperature effect on swelling pressures during saturation of bentonites. Soils and Foundations 62: 101245. https://doi.org/10.1016/j.sandf.2022.101245

RWM 2016. Geological Disposal Part B: Technical Specification Generic Disposal System Specification. NDA Report no. DSSC/402/01.

RWM 2017. Geological Disposal GEOWASTE Project: Summary of Output from a Joint EPSRC NDA RWMD Co-funded Project. January 2017. NDA Report no. NDA/RWM/152.

Salager, S., Rizzi, M., Laloui L. 2011. An innovative device for determining the soil water retention curve under high suction at different temperatures. Acta Geotechnica 6(3): 135-142.

Sandén, T., Nilsson, U., Andersson, L., Svensson, D., 2018. ABM45 experiment at Äspö Hard Rock Laboratory. Installation report. SKB Report P-18-20.

Sarikaya, Y., Onal, M., Baran, B., Alemdaroglu, T. 2000. The effect of thermal treatment on some of the physicochemical properties of a bentonite. Clays and Clay Minerals 48(5): 557–562.

Sena, C., Salas, J., Arcos, D. 2010. Thermo-hydro-geochemical modelling of the bentonite buffer. The LOT-A2 experiment. SKB TR-10-65. Svensk Kärnbränslehantering AB.

Seiphoori, A., Ferrari, A., Laloui, L. 2014. Water retention behaviour and microstructural evolution of MX-80 bentonite during wetting and drying cycles. Géotechnique 64(9): 721-734.

Sellin, P., Leupin, O. 2013. The Use of Clay as an Engineered Barrier in Radioactive-Waste Management – A Review. Clays and Clay Minerals 61: 477-498.

Senger, R. 2015. Scoping Calculations in Support of the Design of the Full-Scale Emplacement Experiment at the Mont Terri URL, Evaluation of the Effects and Gas Transport Phenomena. Nagra Work Report NAB 13-98, Wettingen, Switzerland.

Senger, R.K., Papafotiou, A., Marschall, P. 2014. Thermo-hydraulic simulations of the near-field of a SF/HLW repository during early- and late-time post-closure period. NAGRA Arbeitsbericht NAB 14-011.

Seyedi, D.M., Armand, G., Noiret, A. 2017. "Transverse Action" – A model benchmark exercise for numerical analysis of the Callovo-Oxfordian claystone hydromechanical response to excavation operations. Computers and Geotechnics 85: 287-305.

Seyedi, D.M., Plúa, C., Vitel, M., Armand, G., Rutqvist, J., Birkholzer, J., Xu, H., Guo, R., Thatcher, K.E., Bond, A.E., Wang, W., Nagel, T., Shao, H., Kolditz, O., 2021. Upscaling THM modeling from small-scale to full-scale in-situ experiments in the Callovo-Oxfordian claystone, International Journal of Rock Mechanics and Mining Sciences 144: 104582, https://doi.org/10.1016/j.ijrmms.2020.104582.

Shao J.-F., Yu Z., Liu Z., Vu M.-N., Armand G. 2024. Numerical analysis of thermo-hydromechanical process related to deep geological radioactive repository, Deep Resources Engineering, Volume 1, Issue 1, 100001, ISSN 2949-9305, https://doi.org/10.1016/j.deepre.2024.100001

Sillen, X., Marivoet, J. 2007. Thermal impact of a HLW repository in clay. Deep disposal of vitrified high-level waste and spent fuel. Mol, Belgium: SCK•CEN. 59 p. (External Report of the Belgian Nuclear Research Centre, ER-38, CCHO 2004-2470/00/01, DS 251.SAF). ISSN 1782-2335.

SKB 2010. Design, production and initial state of the buffer. TR-10-15. Svensk Kärnbränslehantering AB

SKB 2011. Long-term safety for the final repository for spent nuclear fuel at Forsmark. Main report of the SR-Site project – Volume I. TR-11-01. Svensk Kärnbränslehantering AB.

Song, H., Corman, G., Collin, F. 2023. Thermal Impact on the Excavation Damage Zone around a Supported Drift Using the 2nd Gradient Model. Rock Mechanics and Rock Engineering 56(10): 7575-7598. https://doi.org/10.1007/s00603-023-03440-x

Song F., Gens A., Collico S. Grgic D. 2024. Fully coupled THM constitutive model for clay rocks: formulation and application to laboratory tests. UNSAT-WASTE 2023, Shanghai, China.

Souley, M., Vu, M-N., de Lesquen C., Armand G. 2022. Effect of mechanical non-linearities on the thermal-hydraulic-mechanical response of a geological repository. 3rd International Conference on Coupled Processes in Fractured Geological Media: Observation, Modeling, and Application (CouFrac 2022), Nov 2022, Berkeley, United States.

Souley M., de Lesquen C., Vu M-N., Armand G. 2023. Effect of the temperature on the THM behaviour of the Callovo-Oxfordian claystone: Constitutive model. 2nd International Decovalex Coupled Processes Symposium. Troyes, France, 14-16 November 2023.

Souley M., de Lesquen C., Vu M.-N., Armand G. 2024. Effect of temperature on the short and long term THM behaviour of Callovo-Oxfordian claystone - Implications for a Radioactive Waste Repository. 4th International Conference on Coupled Processes in Fractured Geological Media: Observation, Modeling, and Application (CouFrac2024), Kyoto, Japan, November 13-15, 2024.

Spang, B. 2002. Excel Add-In for Properties of Water and Steam in SI-Units. http://www.cheresources.com/iapwsif97.shtml

Špinka, O., Grunwald, L., Zahradník, O., Veverka, A., Fiedler, F., Nohejl, J. 2018. Siting study – Březový potok FINAL report, SÚRAO 139/2017.

Šťástka, J., Hausmannová, L., Hanusová, I. 2017. The Mock-Up Josef In-Situ Physical Model after 4 Years of Operation. Abstract for the 7th International Conference on Clays in Natural and Engineered Barriers for Radioactive Waste Confinement, Davos.

Šťástka, J. 2014. MOCK-UP Josef demonstration experiment. Tunel 23(2) : 65-73. http://www.ita-aites.cz/files/tunel/2014/2/tunel_2_14-12.pdf

Stavropoulou, E., Andò, E., Roubin, E., Lenoir, N., Tengattini, A., Briffaut, M. Bésuelle, P. 2020. Dynamics of Water Absorption in Callovo-Oxfordian Claystone Revealed With Multimodal X-Ray and Neutron Tomography. Frontiers in Earth Science 8:6, doi: 10.3389/feart.2020.00006.

Sultan, N. 1997. Etude du comportement thermo-mécanique de l'Argile de Boom: Expériences et modélisation. PhD thesis, École Nationale des Ponts et Chaussées.

Sultan, N., Delage, P., Cui, Y.J. 2000. Comportement thermomécanique de l'Argile de Boom. C. R. Acad. Sci. Paris 328, Série II *b*: 457–463.

Sun, H., Mašín, D., Najser, J., Scaringi, G. 2020. Water retention of a bentonite for deep geological radioactive waste repositories: High-temperature experiments and thermodynamic modeling. Engineering Geology 269: 105549.

Svensson, D., 2015. The Bentonite barrier. Swelling properties, redox chemistry and mineral evolution. Doctoral thesis. Lund. ISBN 978-91-7422-385-9.

Svensson, D., Hansen, S. 2013. Redox chemistry in two iron-bentonite field experiments at Äspö hard rock laboratory, Sweden: An XRD and Fe-K edge XANES study. Clays and Clay Minerals 61: 566-579.

Svensson, D., Dueck, A., Nilsson, U., Olsson, S., Sandén, T., Lydmark, S., Jägerwall, S., Pedersen, K., Hansen, S. 2011. Alternative Buffer Material, Status of the ongoing laboratory investigation of reference materials and test package 1. SKB Technical Report TR-11-06. Svensk Kärnbränslehantering.

Svensson, D., Sellin, P, Kaufhold, S., Chaaya, R., Gaboreau, S., Tremosa, J., Villar, M.V., Melón, A.M, Zabala, A.B., Iglesias, R. J., Najser, J., Svoboda, J., Černochová, K., Sayenko, S., Zlobenko B., Bugera S., Fedorenko Y., Rozko A., Cuevas, J., Ortega, A., Ruiz, A.I., Kašpar, V., Šachlová, S., Pulkkanen, V.M., Rauhala, O.P. 2023a. HITEC technical report on Material characterisation. Final version as of 23.11.2023 of deliverable D7.7 of the HORIZON 2020 project EURAD. EC Grant agreement no: 847593.

Svensson, D., Bladström, T., Sandén T., Dueck, A., Nilsson, U., Jensen, V. 2023b. Alternative Buffer Material (ABM) experiment - Investigations of test packages ABM2 and ABM5. SKB Technical report.

Tang, A.M., Cui, Y.J. 2007. "Controlling suction by vapour equilibrium technique at different temperatures, application to the determination of the water retention properties of MX80 clay." Can. Geotech. J. 42(1): 287–296.

Tang, A.M., Cui, Y.J., Le, T.T. 2008a. A study on the thermal conductivity of compacted bentonites. Appl. Clay Sci. 41 (3): 181–189.

Tang, A.M., Cui, Y.J., Barnel, N. 2008b. Thermo-mechanical behaviour of a compacted swelling clay. Géotechnique 58(1): 45-54.

Teodori, S.P., Gaus, I. (Eds.) (2012): Report of the construction of the HE-E experiment. Deliverable D2.2-3 of the PEBS Project. EU report downloadable from http://www.pebseu.de/.

Terzaghi, K., Peck, R., Mesri, G. 1996. Soil Mechanics in Engineering Practice. Third edition, John Wiley & sons.

Thatcher, K.E., Newson, R.K., Watson, S.P., Norris, S. 2017. Review of data and models on the mechanical properties of bentonite available at the start of Beacon. Deliverable D2.2.

Thatcher, K. 2017. FEBEX-DP: THM modelling, Contractor Report to RWM no. QRS-1713A-R2, V1.8, March 2017.

TIMODAZ 2010. Deliverable D13 – Simulation of lab and in situ tests. European commission.

Toprak, E. 2018. Long term response of multi-barrier schemes for underground radioactive waste disposal. Doctoral thesis, Universitat Politècnica de Catalunya.

Toprak, E., Mokni, N., Olivella, S., Pintado, X. 2013. Thermo-hydraulic-mechanical modelling of buffer and backfill. Report POSIVA 2012-47, Posiva Oy. ISBN 978-951-652-230-5.

Tourchi, S., Vaunat, J., Gens, A. 2019. THM modelling of the ALC1604 experiment. Rapport Andra n°CGRPCMFS190016.

Tourchi S., Vaunat J., Gens A., Bumbieler F., Vu M.-N., Armand G. 2021. A full-scale in situ heating test in Callovo-Oxfordian claystone: observations, analysis and interpretation, Computers and Geotechnics, Vol 133, 104045, https://doi.org/10.1016/j.compgeo.2021.104045

Tourchi, S., Mánica, M.A., Gens, A., Vaunat, J., Vu, M.N., Armand, G. 2024. A thermomechanical model for argillaceous hard soils-weak rocks: application to THM simulation of deep excavations in claystone. Géotechnique, https://doi.org/10.1680/jgeot.23.00023

Traber, D., Blaser, P. 2013. Gesteinsparameter der Wirtgesteine Opalinuston, 'Brauner Dogger', Effinger Schichten und Helvetische Mergel als Grundlage für die Sorptionsdatenbank. NAGRA Arbeitsbericht NAB 12-039.

Tripathy, S., Thomas, H.R., Stratos, P. 2017. Response of Compacted Bentonites to Thermal and Thermo-Hydraulic Loadings at High Temperatures. Geosciences 7(53): 1 – 23.

Tsiampousi, A., Zdravković, L., Potts, D.M. 2013. A new Hvorslev surface for critical state type unsaturated and saturated constitutive models. Computers and Geotechnics 48: 156–166.

Tsitsopoulos, V., Baxter, S., Holton, D., Dodd, J., Williams, S., Thompson, S. 2018. Modelling the Prototype Repository. Geological Society Special Publications 482: 241-260, London, 7 December 2018.

Valter, M., Plötze, M. 2013. Characteristics of variably saturated granular bentonite after long-term storage at near-field relevant temperatures. Clay Minerals 48(2): 343-361.

Van Geet, M., Lalieux, P., Van Humbeek, H., Dierckx, A., De Preter, P., Gens, R., Bernier, F. 2007. PRACLAY success criteria. NIROND note 2007-1144 (internal report).

Van Geet, M., Bastiaens, W., Ortiz, L. 2008. Self-sealing capacity of argillaceous rocks: review of laboratory results obtained from the SELFRAC project. Physics and Chemistry of the Earth, Parts A/B/C 33 (Supplement 1): S396–S406. https://doi.org/10.1016/j.pce.2008.10.063

Van Humbeeck, H., Verstricht, J., Li, X.L., De Cannière, P., Bernier, F., Kursten, B. 2009. The OPHELIE mock-up. Final report. EURIDICE report 09-134. 197 pp. http://www.euridice.be/sites/default/files/scientific/OPHELIE%20mockup%20final%20report%20low%20resolution.pdf

Van Marcke, P., Li, X.L, Bastiaens W., Verstricht J., Chen G., Leysen J., Rypens J., 2013. The design and installation of the PRACLAY In-Situ Experiment. EURIDICE report 13-129.

Vandenberghe, N., De Craen, M., Wouters, L. 2014. The Boom Clay geology, from sedimentation to present-day occurrence, a review. Royal Belgian institute of natural sciences. Memoirs of the geological survey of Belgium, N.60-2014.

Vasconcelos, R.B. de, 2021. A double-porosity formulation for the THM behaviour of bentonite-based materials. PhD Thesis, Technical University of Catalonia. Barcelona, Spain.

Vasconcelos, R.B. de, Rodríguez C. E., Gens A., Krejčí T., Mašín D., Koudelka T., Kruis J., Pulkkanen V.M., Rauhala, O.P. 2023. HITEC modelling. Deliverable D7.10 of the HORIZON 2020 project EURAD. EC Grant agreement no: 847593. 81 pp.

Večerník, P., Trpkošová, D., Hofmanová, E. 2014. Vývoj aparatur pro charakterizaci materiálů inženýrských bariér hlubinného úložiště radioaktivních odpadů a vyhořelého jaderného paliva - TA04021378. Zpráva ÚJV Řež, a. s. číslo 14422.

Velde, B., Vasseur, G. 1992. Estimation of the diagenetic smectite to illite transformation in time-temperature space. American Mineralogist 77: 967–976.

Villar, M.V. 2002. Thermo-hydro-mechanical characterisation of a bentonite from Cabo de Gata. A study applied to the use of bentonite as sealing material in high level radioactive waste repositories. Publicación Técnica Enresa 01/2002, Madrid, 258 pp.

Villar, M.V. 2005. MX-80 bentonite. Thermo-hydro-mechanical characterisation performed at CIEMAT in the context of the Prototype Project. Informes Técnicos CIEMAT 1053. CIEMAT, Madrid, 39 pp. Febrero 2005.

Villar, M.V. (Ed.) 2006. FEBEX Project Final report. Post-mortem bentonite analysis. Publicación Técnica ENRESA 05-1/2006, Madrid, 183 pp.

Villar, M.V. 2007. Water retention of two natural compacted bentonites. Clays and Clay Minerals 55(3): 311-322.

Villar, M.V. 2013. Long-term THM tests reports: Isothermal infiltration tests with materials from the HE-E. PEBS Deliverable 2.2-7.2. CIEMAT Technical Report CIEMAT/DMA/2G210/07/2013. Madrid, 32 pp.

Villar, M.V. 2017. FEBEX-DP Postmortem THM/THC Analysis Report. Technical Report NAB 16-017. 147 pp.

Villar, M.V., Lloret, A. 2004. Influence of temperature on the hydro-mechanical behaviour of a compacted bentonite. Applied Clay Science 26(1–4): 337–350.

Villar, M.V., Gómez-Espina, R. 2008. Effect of temperature on the water retention capacity of FEBEX and MX-80 bentonites. In: Toll, D.G., Augarde, C.E., Gallipoli, D., Wheeler, S.J. (eds.). Unsaturated soils: Advances in Geo-engineering. Proceedings of the first European Conference on unsaturated soils, E-UNSAT 2008. Durham, UK, July 2-4 2008. CRC Press/Balkema. Taylor & Francis Group, London, 257-262.

Villar, M.V., Gómez-Espina, R. 2009. Report on thermo-hydro-mechanical laboratory tests performed by CIEMAT on FEBEX bentonite 2004 – 2008. Informes Técnicos CIEMAT 1178. Madrid, 67 pp. Agosto 2009.

Villar, M.V., Gómez-Espina, R., Martín, P.L. 2006. Behaviour of MX-80 bentonite at unsaturated conditions and under thermo-hydraulic gradient. Work performed by CIEMAT in the context of the TBT project. Informes Técnicos CIEMAT 1081. CIEMAT, Madrid, 45 pp. July 2006. DOI: 10.13140/RG.2.2.30062.92482

Villar, M.V., Sánchez, M., Gens, A. 2008. Behaviour of a bentonite barrier in the laboratory: Experimental results up to 8 years and numerical simulation. Physics and Chemistry of the Earth 33: S476–S485.

Villar, M.V., Gómez-Espina, R., Martín, P.L., Barcala, J.M. 2012. Tests in thermo-hydraulic cells to simulate the behaviour of engineered barriers. In: Laloui, L., Ferrari, A. (eds). Multiphysical Testing of Rocks and Shales. Springer Series in Geomechanics and Geoengineering, Springer, Berlin, 137-142. ISBN: 978-3-642-32491-8.

Villar, M.V., Iglesias, R.J., Abós, H., Martínez, V., de la Rosa, C., Manchón, M.A. 2016a. FEBEX-DP onsite analyses report. NAB 16-12. 106 pp.

Villar, M.V., Martín, P.L., Romero, F.J., Iglesias, R.J., Gutiérrez-Rodrigo, V. 2016b. Saturation of barrier materials under thermal gradient. Geomechanics for Energy and the Environment 8: 38-51. https://doi.org/10.1016/j.gete.2016.05.004

Villar, M.V., Armand, G., Conil, N., de Lesquen, Ch., Herold, Ph., Simo, E., Mayor, J.C., Dizier, A., Li, X., Chen, G., Leupin, O., Niskanen, M., Bailey, M., Thompson, S., Svensson, D., Sellin, P., Hausmannova, L. 2020. D7.1 HITEC. Initial State-of-the-Art on THM behaviour of i) Buffer clay materials and of ii) Host clay materials. Deliverable D7.1 HITEC. EURAD Project, Horizon 2020 No 847593. 214 pp.

Villar, M.V., Cuevas, J., Melón, A.M. Gutiérrez-Álvarez, C., Ruiz, A.I., Ortega, A., Iglesias, R.J., González, A.E., Brea, N., Fernández, R., Real, E. 2021. Project MINALBEN. Report on postmortem analyses of samples from cells running for 2.5 years (C3, C4 and C5). Technical Report CIEMAT/DMA/2G219/1/21. Madrid, 86 pp.

Villar, M.V., Iglesias, R.J., Gutiérrez-Álvarez, C. 2022. THM column cell with MX-80 pellets simulating the HE-E in situ experiment for 10 years: online results and final physical state. Informes Técnicos CIEMAT 1507. Madrid, 65 pp.

Villar, M.V., Svoboda, J., Černochová, K., Gutiérrez-Álvarez, C., Iglesias, R.J., García-Herrera, G. 2023a. HITEC Technical Report on small and mid-scale laboratory experiments. Final version as of 10.11.2023 of deliverable D7.9 of the HORIZON 2020 project EURAD. EC Grant agreement no: 847593.

Villar, M.V., Cuevas, J., Zabala, A.B., Ortega, A., Melón, A.M., Ruiz, A.I., Iglesias R.J. 2023b. Mineralogy and geochemistry of a bentonite pellets column heated for 10 years. Clays and Clay Minerals 71: 166-190. https://doi.org/10.1007/s42860-023-00238-4

Von Wolffersdorff, P.A. 1996. A hypoplastic relation for granular materials with a predefined limit state surface. Mechanics of Cohesive-Frictional Materials 1: 251–271.

Vuorinen, U., Snellman, M. 1998. Finnish reference waters for solubility, sorption and diffusion studies. Posiva Working Report

Wan, M., Ye, W.M., Chen, Y.G., Cui, Y.J. 2015. Influence of temperature on the water retention properties of compacted GMZ01 bentonite. Environmental Earth Science 73: 4053-4061.

Wang, L., Bornert, M., Chanchole, S. 2013. Micro-Scale Experimental Investigation of Deformation and Damage of Argillaceous Rocks under Hydric and Mechanical Loads. Poromechanics V: 1635-1643.

Wemaere, I., Marivoet, J., Labat, S. 2008. Hydraulic conductivity variability of the Boom Clay in the north-east Belgium based on four core drilled boreholes. Physics and Chemistry of the Earth 33(s1): 24-36.

Wersin, P., Johnson, L.H., McKinley, I.G. 2007. Performance of the bentonite barrier at temperatures beyond 100°C: A critical review. Physics and Chemistry of the Earth 32(8–14): 780–788.

Wigger, C., (Ed.), Hanusová, I., Hausmannová, L., Heino, V., Lavikainen, L., Leupin, O.X., Marshall, P., Mayor, J.C., Meleshyn, A., Pusch, R., Sellin, P., Swahn, J., Talandier, J., Wendling, J., Wieczorek, K. 2017. Beacon - Bentonite Mechanical Evolution. State-of-the-Art Report. Deliverable D1.1.

Wileveau, Y. 2005. THM behaviour of host rock (HE-D) experiment: Progress report. Part 1, Technical Report TR 2005-03. Mont Terri Project.

Wileveau, Y., Rothfuchs, T. 2007. THM behaviour of host rock (HE-D). Experiment: Study of Thermal effects on Opalinus Clay. Mont Terri Technical Report 2006-01.

Wilson, J. 2017. FEBEX-DP: Geochemical Modelling of Iron-Bentonite Interactions, Contractor Report to RWM no. QRS-1713A-R3, May 2017P.

Wilson, J., Savage, D., Bond, A., Watson, S., Push, R., Bennett, D. 2010. Bentonite: a review of key properties, processes and issues for consideration in the UK context. Quintessa 1.1: 145 pp. QRS-1378ZG-1.1.

Xu, Y., Sun, D., Zeng, Z., Lv, H. 2019. Temperature dependence of apparent thermal conductivity of compacted bentonites as buffer material for high-level radioactive waste repository. Applied Clay Science 174: 10-14.

Ye, W.M., Wan, M., Chen, B., Chen, Y.G., Cui, Y.J., Wang, J. 2012. Temperature effects on the unsaturated permeability of the densely compacted GMZ01 bentonite under confined conditions. Engineering Geology 126: 1–7.

Yoon, S., Lee, G.J., Park, T.J., Lee, C., Cho, D.K. 2023. Thermal conductivity evaluation for bentonite buffer materials under elevated temperature conditions. Case Studies in Thermal Engineering 30: 101792. https://doi.org/10.1016/j.csite.2022.101792

Yu, L., Weetjens, E., Vietor, T., Hart, J. 2010. TIMODAZ (Contract Number: FI6W-CT-2007-036449). Integration of TIMODAZ results within the safety case and recommendations for repository design (D14). Final report of WP6, 48 pp.

Yu, L., Rogiers, B., Gedeon, M., Marivoet, J., De Craen, M., Mallants, D. 2013. A critical review of laboratory and in-situ hydraulic conductivity measurements for the Boom Clay in Belgium. Applied Clay Science 75-76: 1-12.

Zlobenko, B., Fedorenko, Y., Olkhovyk, Y., Buhera, S., Rozko, A. 2023. Test on the Thermal-hydro-mechanical Behaviors of Cherkasy Bentonite as a Buffer Material of an HLW Repository. In: A. Zaporozhets and O. Popov (eds.): Systems, Decision and Control in Energy IV. Studies in Systems, Decision and Control 456: 185–196, https://doi.org/10.1007/978-3-031-22500-0_12

Zhang, C.L., Rothfuchs, T. 2007. Laboratory Experiments on the THM Behaviour of Clay Rocks, TIMODAZ, Report D.2.

Zhang, C.L., Rothfuchs, T., Jockwer, N., Wieczorek, K., Dittrich, J., Müller, J., Hartwig, L., Komischke, M. 2007. Thermal Effects on the Opalinus Clay. A Joint Heating Experiment of ANDRA and GRS at the Mont Terri URL (HE-D Project). Final Report. Mont Terri Project Technical Report TR 2007-02 and GRS Report 224, ISBN 3-931995-98-4. https://www.grs.de/sites/default/files/fue/grs_224_thermeff_clay.pdf.

Zhang, C.L., Czaikowski, O., Rothfuchs, T. 2010. Thermo-Hydro-Mechanical behaviour of the Callovo-Oxfordian clay rock, GRS – 266, 2010.

Zhang, F., Xie, S.Y., Shao, J.F. 2012. Groupement de Laboratoires-Géomécanique, Fiche GM6: Effets de la température sur le comportement des argilites. Etude expérimentale et modélisations des effets de la température sur le comportement des argilites. Rapport Andra n° C.RP.0LML.11.0004.

Zhang, C.L., Armand, G., Conil, N. 2015. Investigation on the Anisotropic Mechanical Behavior of the Callovo-Oxfordian Clay Rock. Final report GRS 360.

Zheng, L., Rutqvist, J., Birkholzer, J.T., Liu, H.H. 2015. On the impact of temperatures up to 200°C in clay repositories with bentonite engineer barrier systems: A study with coupled thermal, hydrological, chemical, and mechanical modeling. Engineering Geology 197: 278–295.

Zihms, S.G., Harrington, J.F. 2015. Thermal cycling: impact on bentonite permeability. Mineralogical Magazine 79(6): 1543–1550, November 2015.

Zlobenko, B., Fedorenko, Y., Olkhovyk, Y., Buhera, S., Rozko, A. 2023. Test on the Thermal-hydro-mechanical Behaviors of Cherkasy Bentonite as a Buffer Material of an HLW Repository. In: A. Zaporozhets and O. Popov (eds.): Systems, Decision and Control in Energy IV. Studies in Systems, Decision and Control 456: 185–196, https://doi.org/10.1007/978-3-031-22500-0_12